

# **Mitochondrial regulation of CD8<sup>+</sup> T cell cytotoxicity**



**Miriam Lisci**

Cambridge Institute for Medical Research – Department of Medicine

University of Cambridge

This thesis is submitted for the degree of

*Doctor of Philosophy*



## **Declaration**

I hereby declare that except where specific reference is made to the work of others, the contents of this dissertation are original and have not been submitted in whole or in part for consideration for any other degree or qualification in this or any other University. This dissertation is the result of my own work and includes nothing which is the outcome of work done in collaboration, except where specifically indicated in the text. This dissertation contains less than 60,000 words excluding bibliography, figure and table legends and has less than 150 figures.



# Abstract

## Mitochondrial regulation of CD8<sup>+</sup> T cell cytotoxicity

Miriam Lisci

Recent discoveries in the field of immunometabolism have emphasised the importance of mitochondria in the context of T cell development, differentiation, signalling and exhaustion. However, the question of whether mitochondria can actively participate to the killing activity of differentiated, cytotoxic CD8<sup>+</sup> T cells (CTLs) remains unanswered. In this work I analyse CTLs derived from USP30-deficient mice, which have been previously characterised as part of the Infection, Immunity and Immunophenotype Consortium and shown to display altered CTL killing. USP30 is a deubiquitinase localised on the outer mitochondrial membrane and on the peroxisomal membrane, where it counteracts mitophagy and pexophagy by cleaving ubiquitin chains from target proteins. Here I characterise T cell motility, signalling, energy requirements and cytotoxicity in CD8<sup>+</sup> T cells derived from splenocytes of *Usp30*<sup>-/-</sup> mice. Furthermore, I test different mitochondrial functions using both genetic and pharmacological manipulation of oxidative phosphorylation, mitochondrial calcium flux and mitochondrial translation. I highlight mitochondrial translation as a previously uncharacterised mitochondrial function that allows for optimal CTL cytotoxicity. Specifically, I show that both *Usp30*<sup>-/-</sup> CTLs and CTLs in which mitochondrial translation is inhibited display impaired cytosolic protein synthesis, which results in lower abundance of cytolytic molecules essential for killing. This requirement was especially evident when CTLs were limiting in numbers or when they needed to sustain killing for prolonged time, underscoring the importance of efficient mitochondrial translation during an immune challenge. Finally, I investigate mechanisms that could link mitochondrial translation to a loss of cytosolic protein synthesis, including mTOR signalling, mitochondrial reactive oxygen species generation and the integrated stress response. Overall, this work uncovers a novel role for mitochondrial translation in CTL cytotoxicity and adds to the growing body of evidence revealing the multifaceted and crucial roles of mitochondria in T cell function.



## Acknowledgements

I would like to thank all current and past members of the Griffiths lab for their support throughout my PhD. I thank my supervisor, Gillian Griffiths, for allowing me to join her lab and for letting me work on such an entertaining project. In addition, I am grateful to Gillian for helping me improve on my presentation and writing skills and for tolerating the long hours she had to spend with me in the lab while the rest of the Department was getting ready for lockdown.

I thank Katharina Strege and Sandra Ammann for teaching me how to work with human T cells; Christian Gawden-Bone, Lyra Randzavola and Arianne Richard for their support with mouse T cell work and for providing guidance throughout the course of my PhD. I thank Claire Ma for the CyTOF experiments and for all the chocolate she bought for the lab. I thank Jane Stinchcombe for providing EM experience and helpful discussion, but also for her encouragement in times of need and for making me a better lab member by pointing out when my coffee habit was out of place, or my music too loud. I thank Alex Davenport for providing support in times of distress and for teaching me how not to take myself too seriously. Thanks also to Yukako Asano and Gordon Frazer for their assistance, in particular with our spinning disk microscope. I am grateful to everyone who endured opera and Italian rap in the tissue culture room, and especially to Carla Vazquez Amos, Tiphaine Douanne and Anna Lippert for tolerating my singing (and for joining in). To Carla and Tiphaine, thank you for your assistance during one of the most significant achievement of my PhD: the Sweeney Todd lab video for the FEBS post-lockdown competition. In addition, I would like to thank Jonathan Gehrig, the kindest and most hardworking master student any PhD student would wish to work with.

I would also like to thank Julien Prudent and all members of the Prudent lab for offering a helping hand with all mitochondria-related matters. I thank all groups at the MBU and the CIMR who kindly provided reagents, mice and advice throughout the course of this work. I thank Carlo Viscomi and Massimo Zeviani for the *Ttc19<sup>-/-</sup>* and *Ndufs4<sup>-/-</sup>* mice, Stephen Burr and Patrick Chinnery for the *mt-tRNA<sup>Ala</sup>* mice, and Pedro Guiomar, Michal Minczuk and David Ron for helpful discussion on mitochondrial translation and the integrated stress response. In addition, I thank Julia Marchingo and Doreen Cantrell at the University of Dundee for contributing to this study with their experience on T cell proteomics.

I would also like to thank Margaret Robinson, David Rubinsztein, Folma Buss and Evan Reid for taking a chance on me by allowing me to join the CIMR PhD programme. A special thank you also goes to Claudia Allmendinger and Amanda Goldsmith for assisting me throughout the application

and PhD. It is not an overstatement to say that I would have not been able to join the CIMR if it had not been for Claudia Allmendinger. My first months at the CIMR were a steep learning curve, during which I learnt a tremendous amount and met wonderful people. I would like to thank Joe Chambers, Elke Malzer, Cansu Karabiyik, Claudia Puri, Stefan Marciniak and David Rubinsztein for welcoming me to the CIMR and providing help, support and supervision. I am grateful to Reiner Schulte, Chiara Cossetti and Gabriela Grondys-Kotarba for their continuous assistance with the flow cytometers, and to Mark Bowen and Matthew Gratian for their help with the LSM microscopes.

This thesis would have never been completed without the never-ending support provided by my friends. I thank everyone I lived with for their words of encouragements, but especially Marzia Munafò and Mara Sgroi for listening to every single complaint I had during my PhD, for our movie marathons and card games during the first lockdown, and for showing me that even I can learn how to cook. Furthermore, I thank Miriam Belmonte and Chiara Toschi for being my little corner of Italy in Cambridge, offering support, laughter, company and Prosecco when I needed it the most. I thank Can Aztekin for his harsh but fair scientific advice, but most importantly for being a true friend and always being there for me – I look forward to many more exciting times in Lausanne in the near future. I thank the community at Darwin College and my “DarMates” for making me feel at home in Cambridge. In particular, thanks to everyone at the Darwin Cuban Salsa Club for filling several unforgettable Monday evenings with joy. I am deeply grateful to the people who showed me that geographical distance does not matter when friendship is real: Cecilia Formiconi, Ludovica Iuè, Giulia Forconi, Alice Simonato, Sara Di Iorio, Sara Crescenzi and Nicoletta Romano. Thank you for being my safe haven and for always being there to share the good and bad times. Last but not least, I thank Gabriele Mangiavacchi for surprising me and comforting me with his unbelievable patience and encouragement, which helped me carry this work to completion.

Finally, I would like to thank my family. It takes a great deal of strength to learn how to live and love in three separate countries for a decade. I thank my parents for always urging me to aim higher and for teaching me the value of knowledge. “*Riempi il sacco*” (“fill the bag”) has been my father’s motto throughout the years – meaning one should keep collecting information and never stop learning. In addition, I thank my incredible siblings, Elena and Gabriele, for their unwavering support and faith in me. Thank you, *Panzini del mio cuore*, because your questions and curiosity remind me why I find my work interesting even when times are rough. It is because of you that I always have, and I always will, strive to be the best I can be.





# Table of Contents

<b>Declaration</b> .....	<b>i</b>
<b>Abstract</b> .....	<b>iii</b>
<b>Acknowledgements</b> .....	<b>v</b>
<b>Table of Contents</b> .....	<b>ix</b>
<b>List of Figures</b> .....	<b>xv</b>
<b>List of Tables</b> .....	<b>xix</b>
<b>Abbreviations</b> .....	<b>xxi</b>
<b>CHAPTER 1 Introduction</b> .....	<b>1</b>
<b>1.1 Overview of CD8<sup>+</sup> cytotoxic T lymphocytes (CTLs)</b> .....	<b>3</b>
1.1.1 CD8 <sup>+</sup> T cell priming: the journey from naïve to killers, and from killers to patrols .....	3
1.1.2 Signalling pathways triggered by TCR engagement in effector T cells .....	5
1.1.3 Morphological alterations triggered by TCR engagement.....	7
1.1.4 Trafficking and maturation of lytic granules .....	8
1.1.5 Granzymes and Perforin-dependent cytotoxic pathways.....	9
1.1.6 Additional pathways mediating cytotoxicity .....	11
1.1.7 Post-transcriptional regulation of CTL killing.....	12
1.1.8 CD8 <sup>+</sup> T cells are serial killers .....	13
<b>1.2 Mitochondria: dynamic organelles shaping T cell function</b> .....	<b>15</b>
1.2.1 Overview of mitochondrial function and architecture .....	15
1.2.2 Mitochondrial dynamics via fission and fusion .....	16
1.2.3 Mitochondrial clearance by mitophagy.....	18
1.2.4 Mitochondrial act as cellular stress sensors .....	19
1.2.5 Mitochondrial communicate with other organelles via membrane contact sites .....	21
1.2.6 Mitochondria influence T cell differentiation, signalling and metabolism.....	23
1.2.7 Mitochondria can modulate CTL effector functions.....	25
1.2.8 Metabolism at the centre of gene expression and cytotoxicity .....	26
<b>1.3 The role of USP30 in cellular homeostasis</b> .....	<b>29</b>
1.3.1 USP30: an inhibitor of pexophagy and mitophagy.....	29
1.3.2 USP30 as a therapeutic target .....	31
<b>1.4 Aims of this work</b> .....	<b>33</b>

## **CHAPTER 2 Materials and Methods..... 35**

2.1	Mouse strains.....	37
2.2	Cell culture and generation of stable cell lines.....	37
2.3	Pharmacological treatments.....	38
2.4	Nucleofection procedure and plasmids.....	39
2.5	Analysis of T cell populations in murine splenocytes.....	39
2.6	LDH cytotoxicity assays.....	40
2.7	IncuCyte® cytotoxicity assay.....	40
2.8	Degranulation assay.....	41
2.9	Calcium flux assay.....	41
2.10	SDS-PAGE and immunoblotting.....	42
2.11	RNA extraction and real-time qPCR.....	43
2.12	Measurement of mitochondrial mass, membrane potential and mtROS.....	44
2.13	Immunofluorescence staining and samples imaging.....	44
2.14	Live cell microscopy and quantitation of cell migration, mitophagy and pexophagy.....	46
2.15	Sample preparation and processing for transmission electron microscopy.....	47
2.16	Seahorse Mito Stress Assay.....	47
2.17	ATP assay.....	48
2.18	HPG protein synthesis assay.....	48
2.19	Intracellular cytokine staining.....	49
2.20	CyTOF sample processing and analysis.....	50
2.21	Mass spectrometry processing and analysis.....	52
2.22	CRISPR/Cas9-mediated gene knockouts.....	54
2.23	Data acquisition and analysis.....	55

## **CHAPTER 3 Analysis of *Usp30*<sup>-/-</sup> CTLs: impaired cytosolic translation prevents synthesis of cytolytic proteins and sustained killing ..... 57**

3.1	Background.....	59
3.2	Loss of USP30 does not impair T cell development.....	59
3.3	T cell stimulation induces loss of mitochondrial markers in <i>Usp30</i> <sup>-/-</sup> CTLs.....	63
3.4	TCR activation results in a decrease in peroxisomal markers in <i>Usp30</i> <sup>-/-</sup> CTLs.....	71
3.5	Analysis of autophagic flux in USP30-depleted CTLs.....	73
3.6	Loss of USP30 impairs CTL cytotoxicity.....	74
3.7	ATP generation and CTL migration are not affected by lack of USP30.....	75

3.8	<i>Usp30</i> <sup>-/-</sup> CTLs can trigger the signalling cascade associated with killing.....	77
3.9	Target cell recognition and granule polarisation are not affected by loss of USP30 .....	80
3.10	Lytic granule content and size are reduced in <i>Usp30</i> <sup>-/-</sup> CTLs .....	83
3.11	Cytosolic translation is impaired in <i>Usp30</i> <sup>-/-</sup> CTLs .....	85
3.12	Inhibition of <i>de novo</i> protein synthesis impairs killing by preventing the replenishment of cytolytic proteins .....	86
3.13	Proteomic analysis of <i>Usp30</i> <sup>-/-</sup> CTLs.....	88
3.14	Evidence for selectivity in the downregulation of protein expression in <i>Usp30</i> <sup>-/-</sup> CTLs	92
3.15	Analysis of PINK1/PARKIN expression in CTLs .....	95
3.16	Preventing mitophagy in <i>Usp30</i> <sup>-/-</sup> rescues killing and translation defect .....	97
3.17	Summary.....	102

## **CHAPTER 4 Examination of mitochondrial and peroxisomal functions reveals a requirement for mitochondrial translation in CTL cytotoxicity ..... 105**

4.1	Background.....	107
4.2	Metabolic defects in peroxisomes alter mitochondrial function.....	107
4.3	Mitochondrial oxidative phosphorylation: <i>Ndufs4</i> <sup>-/-</sup> and <i>Ttc19</i> <sup>-/-</sup> mice .....	110
4.4	Mitochondrial calcium flux: MCU CRISPR knockout CTLs .....	116
4.5	Analysis of mitochondrial protein synthesis in WT and <i>Usp30</i> <sup>-/-</sup> CTLs .....	118
4.6	Genetic inhibition of mitochondrial translation: <i>mt-tRNA<sup>Ala</sup></i> mice .....	120
4.7	Genetic inhibition of mitochondrial translation: mito-ribosome CRISPR knockouts...	127
4.8	Pharmacological inhibition of mitochondrial translation: CAM and DOX.....	139
4.9	Mass spectrometry of doxycycline-treated CTLs.....	145
4.10	Additive effect of doxycycline and chloramphenicol on USP30-depleted CTLs .....	148
4.11	Comparison of DOX-treated and USP30-depleted CTL proteomes .....	150
4.12	Summary.....	153

## **CHAPTER 5 Evaluation of mechanisms determining the inhibition of cytosolic protein synthesis and cytotoxicity in *Usp30*<sup>-/-</sup> CTL ..... 155**

5.1	Background.....	157
5.2	Measurement of mitochondrial reactive oxygen species in <i>Usp30</i> <sup>-/-</sup> CTLs.....	157
5.3	Examination of mTOR signalling in USP30-depleted CTLs .....	159
5.4	The ISR does not cause translation and cytotoxicity defects in <i>Usp30</i> <sup>-/-</sup> CTLs .....	161
5.5	Nucleofection alters CTL cytotoxicity and cytosolic protein synthesis .....	167

5.6	Metabolic enzyme expression is dysregulated in <i>Usp30</i> <sup>-/-</sup> CTLs .....	170
5.7	Summary.....	174

**CHAPTER 6 Discussion ..... 177**

6.1	Summary of Results.....	179
6.2	The <i>Usp30</i> <sup>-/-</sup> mouse as a model for studying mitochondria in CTL .....	180
6.3	Mitochondria participate to calcium flux in TCR-stimulated CTLs .....	181
6.4	Mitochondrial fitness impacts cytosolic translation .....	182
6.5	A focus on mitochondrial translation as a requirement for CTL killing .....	183
6.6	The balance between mitochondrial homeostasis and cytosolic protein synthesis .....	185
6.7	The role of additional mitochondrial functions in <i>Usp30</i> <sup>-/-</sup> CTLs .....	186
6.8	The crosstalk between mitochondria and peroxisomes .....	187
6.9	CTL nucleofection: altering T cell proteome, metabolism and beyond? .....	188
6.10	Outlook and concluding remarks.....	189

**References ..... 193**





## List of Figures

Figure 1.1. CTLs trigger apoptosis of target cells by secretion of cytolytic proteins.....	11
Figure 1.2. Mitochondrial morphology and dynamics. ....	17
Figure 1.3. USP30 negatively regulates mitophagy and pexophagy.....	31
Figure 3.1. Analysis of WT and <i>Usp30</i> <sup>-/-</sup> splenocytes. ....	60
Figure 3.2. Analysis of activation markers in naïve and effector <i>Usp30</i> <sup>-/-</sup> CTLs.....	62
Figure 3.3. Mitochondrial mass and membrane potential are lost in activated <i>Usp30</i> <sup>-/-</sup> CTLs.	63
Figure 3.4. Mitochondrial membrane and matrix markers are reduced in activated <i>Usp30</i> <sup>-/-</sup> CTLs.....	66
Figure 3.5. Mitochondria in <i>Usp30</i> <sup>-/-</sup> show loss of inner cristae structure. ....	67
Figure 3.6. Lack of USP30 results in loss of OXPHOS and increased glycolysis.....	68
Figure 3.7. <i>Usp30</i> <sup>-/-</sup> CTLs show increased mitophagy. ....	70
Figure 3.8. Activated <i>Usp30</i> <sup>-/-</sup> CTLs show reduction in peroxisomal markers and increased pexophagy. ....	72
Figure 3.9. Increased autophagic flux in day 5 <i>Usp30</i> <sup>-/-</sup> CTLs.....	74
Figure 3.10. Loss of USP30 impairs CTL killing. ....	75
Figure 3.11. Migration speed and ATP production are not affected by loss of USP30. ....	77
Figure 3.12. Proximal and distal TCR signalling is not inhibited by mitochondrial depletion.	80
Figure 3.13. <i>Usp30</i> <sup>-/-</sup> CTLs can induce organelle polarization at the IS. ....	82
Figure 3.14. Lytic granules are smaller in <i>Usp30</i> <sup>-/-</sup> CTLs. ....	83
Figure 3.15. Loss of USP30 results in reduced abundance of cytolytic proteins.....	84
Figure 3.16. <i>Usp30</i> <sup>-/-</sup> CTLs show profound reduction in protein synthesis. ....	86
Figure 3.17. <i>De novo</i> protein synthesis is required for sustained CTL killing and it is inhibited in <i>Usp30</i> <sup>-/-</sup> CTL.....	88
Figure 3.18. Proteomic analysis of USP30-depleted CTLs.....	90
Figure 3.19. Cytokine synthesis is impaired in <i>Usp30</i> <sup>-/-</sup> CTLs. ....	92
Figure 3.20. Comparison of protein expression in USP30-depleted and CHX-treated CTLs. .	94
Figure 3.21. PINK1 expression in day 5 CTLs.....	96
Figure 3.22. mDIVI-1+M1 treatment rescues mitochondrial depletion in <i>Usp30</i> <sup>-/-</sup> CTLs. ....	98
Figure 3.23. mDIVI-1+M1 treatment rescues cytotoxicity in <i>Usp30</i> <sup>-/-</sup> CTLs. ....	99
Figure 3.24. mDIVI-1+M1 treatment enhances translation but does not upregulate cytolytic protein synthesis.....	100

<b>Figure 3.25. mDIVI-1+M1 treatment promotes CTL proliferation.</b>	101
<b>Figure 4.1. Testing depletion of peroxisomal function in CTLs.</b>	109
<b>Figure 4.2. Analysis of <i>Ndufs4</i><sup>-/-</sup> and <i>Ttc19</i><sup>-/-</sup> splenocytes.</b>	112
<b>Figure 4.3. Loss of NDUFS4 or TTC19 does not affect mitochondrial mass and membrane potential.</b>	113
<b>Figure 4.4. Efficient OXPHOS is not required for CTL killing.</b>	115
<b>Figure 4.5. Optimal MCU expression is not required for CTL calcium flux nor killing.</b>	117
<b>Figure 4.6. Mitochondrial translation is inhibited in <i>Usp30</i><sup>-/-</sup> CTLs.</b>	119
<b>Figure 4.7. Analysis of WT and <i>mt-tRNA<sup>Ala</sup></i> splenocytes.</b>	121
<b>Figure 4.8. <i>mt-tRNA<sup>Ala</sup></i> mutation does not affect mitochondrial mass nor mitochondrial membrane potential.</b>	122
<b>Figure 4.9. Analysis of degranulation and cytotoxicity in <i>mt-tRNA<sup>Ala</sup></i> CTLs.</b>	122
<b>Figure 4.10. <i>mt-tRNA<sup>Ala</sup></i> mutation decreases cytosolic translation and granzyme B expression.</b>	123
<b>Figure 4.11. Mutational burden decreases upon activation in <i>mt-tRNA<sup>Ala</sup></i> CTLs.</b>	125
<b>Figure 4.12. <i>mt-tRNA<sup>Ala</sup></i> CTLs show efficient mitochondrial protein synthesis.</b>	126
<b>Figure 4.13. Testing the role of mitochondrial ribosome assembly factors in CTL cytotoxicity.</b>	128
<b>Figure 4.14. <i>Gfm1</i> CRISPR KO fails to reduce GFM1 protein expression and mitochondrial translation.</b>	129
<b>Figure 4.15. Protein expression of small and large mitochondrial ribosome subunits after CRISPR KO.</b>	131
<b>Figure 4.16. Loss of MRPS16, MRPL22 and MRPL37 decreases mitochondrial protein synthesis.</b>	133
<b>Figure 4.17. Flow cytometry analysis of <i>Mrps16</i> and <i>Mrpl37</i> CRISPR KO CTLs.</b>	134
<b>Figure 4.18. Granzyme B expression in <i>Mrps16</i> and <i>Mrpl37</i> CRISPR KO samples.</b>	135
<b>Figure 4.19. Cytokine synthesis and cytotoxicity in <i>Mrps16</i> and <i>Mrpl37</i> CRISPR KO samples.</b>	136
<b>Figure 4.20. CRISPR KO in naïve T cells results in poor KO efficiency.</b>	138
<b>Figure 4.21. Chloramphenicol and doxycycline inhibit mitochondrial protein synthesis.</b>	140
<b>Figure 4.22. Mitochondrial translation inhibition reduces CTL killing.</b>	141
<b>Figure 4.23. Inhibition of mitochondrial translation impairs cytosolic protein synthesis.</b>	142
<b>Figure 4.24. Loss of mitochondrial translation impairs synthesis of granzyme B and perforin.</b>	143

<b>Figure 4.25. CAM and DOX reduce degranulation and intracellular calcium flux upon TCR triggering.....</b>	<b>145</b>
<b>Figure 4.26. Mass spectrometry analysis of unstimulated and TCR-triggered DOX-treated CTLs.....</b>	<b>147</b>
<b>Figure 4.27. Cytotoxicity of <i>Usp30</i><sup>-/-</sup> treated with CAM and DOX CTLs.....</b>	<b>148</b>
<b>Figure 4.28. CAM and DOX decrease cytokine synthesis in <i>Usp30</i><sup>-/-</sup> CTLs.....</b>	<b>150</b>
<b>Figure 4.29. Comparison of proteomic changes in DOX-treated and USP30-depleted CTLs. ....</b>	<b>152</b>
<b>Figure 5.1. <i>Usp30</i><sup>-/-</sup> CTLs show low MitoSOX fluorescence and are insensitive to antimycin A treatment.....</b>	<b>158</b>
<b>Figure 5.2. mTOR signalling is unperturbed in WT and <i>Usp30</i><sup>-/-</sup> CTLs.....</b>	<b>161</b>
<b>Figure 5.3. The ISR is upregulated by loss of USP30 and inhibition of mitochondrial translation. ....</b>	<b>163</b>
<b>Figure 5.4. ISR inhibition does not rescue translation and cytotoxicity in day 5 <i>Usp30</i><sup>-/-</sup> CTLs. ....</b>	<b>166</b>
<b>Figure 5.5. Nucleofection is sufficient to rescue granzyme B expression and cytotoxicity in <i>Usp30</i><sup>-/-</sup> CTLs.....</b>	<b>168</b>
<b>Figure 5.6. Nucleofected CTLs show enhanced mitochondrial mass and membrane potential. ....</b>	<b>169</b>
<b>Figure 5.7. Enzymes moonlighting as RBPs show altered expression in <i>Usp30</i><sup>-/-</sup> and DOX-treated CTLs.....</b>	<b>173</b>



## List of Tables

<b>Table 2.1. Mouse T cell media.....</b>	<b>37</b>
<b>Table 2.2. List of primary and secondary antibodies used for immunoblotting.....</b>	<b>43</b>
<b>Table 2.3. List of primary and secondary antibodies used for immunofluorescence. ....</b>	<b>45</b>
<b>Table 2.4. List of antibodies used for mass cytometry.....</b>	<b>51</b>
<b>Table 2.5. List of Dharmacon crRNA guides for CRISPR/Cas9-mediated gene knockouts. ...</b>	<b>54</b>



## Abbreviations

2-DG	2-deoxy-D-glucose
4EBP1, 4EBP2	eIF4E binding protein 1, eIF4E binding protein 2
ACLY	ATP-citrate synthase
AP3	adaptor-related protein complex 3
APC	antigen-presenting cells
ARE	AU-rich elements
ARP2/3	actin-related protein 2/3 complex
ATP	adenosine triphosphate
BAF	bafilomycin A
BSA	bovine serum albumin
Ca <sup>2+</sup>	calcium
CAM	chloramphenicol
CHX	cycloheximide
CRAC	calcium-release activated channels
CTL	cytotoxic T lymphocyte
DAG	diacylglycerol
DOX	doxycycline
DRP1	dynammin-related protein 1
DSS	dextran sulfate sodium
DUB	deubiquitinase
ECAR	extracellular acidification rate
eIF	eukaryotic initiation factor
EOMES	eomesodermin
ER	endoplasmic reticulum
ETC	electron transport chain
F-actin	filamentous actin
FADD	FAS-associating protein with death domain
FAR1	fatty acyl-CoA reductase 1
FASL	FAS ligand
FASN	fatty acid synthase
FBS	foetal bovine serum
FC	fold change
FCCP	trifluoromethoxy carbonylcyanide phenylhydrazone
FDR	false discover rate
FHL	familial haemophagocytic lymphohistiocytosis
GAPDH	glyceraldehyde 3-phosphate dehydrogenase
GEF	guanine exchange factor
GO	gene ontology
GZMB	granzyme B
HK1, HK2	hexokinase 1, hexokinase 2
HPG	homopropargylglycine
HPS	Hermasky-Pudlack syndrome
IFN $\gamma$	interferon gamma
IL-2	interleukin-2

IMM	inner mitochondrial membrane
IP3	inositol 1,4,5-triphosphate
IP3R	inositol 1,4,5-triphosphate receptor
IS	immunological synapse
ISR	integrated stress response
ISRmt	mitochondrial ISR
ITAMs	immunoreceptor tyrosine-based activation motif
KO	knockout
LAMP1, LAMP2	lysosomal-associated membrane protein 1 and 2
LT $\alpha$	lymphotoxin alpha
LYST	lysosomal trafficking regulator
M6PR	mannose-6-phosphate receptors
MAM	mitochondria-associated membrane
MAPK	mitogen activated protein kinase
MCU	mitochondrial calcium uniport
MFN1, MFN2	mitofusin 1 and 2
MHC-I	major histocompatibility complex class I
MPP	mitochondrial processing peptidase
mtDNA	mitochondrial DNA
mtROS	mitochondrial reactive oxygen species
mTOR	mammalian target of rapamycin complex
mtUPR	mitochondrial unfolded protein response
NCLX	Na <sup>+</sup> /Ca <sup>2+</sup> exchanger protein
NFAT	nuclear factor of activated T cells
NF $\kappa$ B	nuclear factor of kappa light polypeptide gene enhancer in B-cells
NK	natural-killer cells
No nuc	no nucleofection / not nucleofected control
No stain	unstained control
No stim	unstimulated control
ns/n.s	not statistically significant
N.t	non targeting control
OCR	oxygen consumption rate
OMM	outer mitochondrial membrane
OPA1	optic atrophy 1
OXPHOS	oxidative phosphorylation
PARL	presenilin-associated rhomboid-like protease
PDH	pyruvate dehydrogenase
PFA	paraformaldehyde
PHB2	prohibitin 2
PI(4)P	phosphatidylinositol 4-phosphate
PI3K	phosphatidylinositol 3-kinase
PINK1	PTEN-induced putative kinase 1
PIP2	phosphatidylinositol biphosphate
PRF1	perforin
RAB27A	Ras-related protein 27a
RBP	RNA-binding protein
S6K1, S6K2	ribosomal protein S6 kinase 2, ribosomal protein S6 kinase 2
SLP1, SLP2	synaptotagmin-like protein 1 and 2

TACE	TNF- $\alpha$ -associated converting enzyme
TCA cycle	tricarboxylic acid cycle
TCR	T cell receptor
TEM	transmission electron microscopy
TIM	translocase of inner membrane
TMRE	tetramethylrhodamine, ethyl ester
TNF $\alpha$ , TNF $\beta$	tumour necrosis factor alpha/beta
TOM	translocase of outer membrane
TRAIL	TNF-related apoptosis-inducing ligand
UPRam	UPR induced by mitochondrial protein mistargeting
USP30	ubiquitin-specific protease 30
V-ATPase	vacuolar-type H <sup>+</sup> -ATPase
VDAC	voltage-dependent ion channel
WASp	Wiskott-Aldrich syndrome protein
WT	wild-type



# **CHAPTER 1**

## **Introduction**



## 1.1 Overview of CD8<sup>+</sup> cytotoxic T lymphocytes (CTLs)

Cytotoxic T lymphocytes (CTLs) are specialised white blood cells mediating adaptive immunity by killing tumours and virally infected cells (Dieckmann et al., 2016; Golstein and Griffiths, 2018). CTLs are referred to as “serial killers” due to the ability of each single CTL to trigger apoptosis in several targets in a sequential manner. CTL cytotoxicity is being exploited as a strategy for immunotherapy (Madden and Rathmell, 2021), and seminal work in this field was highlighted by the 2018 Nobel Prize in Medicine (Freeman et al., 2000; Leach et al., 1996). The exact molecular mechanisms that regulate CTL killing are a topic of intense investigation as they offer insights into the mechanisms regulating both adaptive immunity and basic cell biology processes.

### 1.1.1 CD8<sup>+</sup> T cell priming: the journey from naïve to killers, and from killers to patrols

Early studies in mixed cell cultures showed that lymphoid cells were able to recognise non-self targets and trigger cell lysis, characterised by aggregation of multiple lymphoid cells around vacuolated targets (Vainio et al., 1964). These thymus-derived cells (“T” lymphocytes) are part of the CD8<sup>+</sup> lineage, which commits to develop into cytotoxic cells, able to spearhead the immune system defence against virally infected cells and cancers (Zhang and Bevan, 2011). Another major T cell lineage includes various subsets of CD4<sup>+</sup> T cells, which modulate the immune response by both promoting and preventing (the latter via regulatory T cells) activation of the innate and adaptive branches of the immune system (Luckheeram et al., 2012).

T cells mature in the thymus, following a process that involves both negative and positive selection stages. Autoreactive T cells (which would attack the host organism) and T cells that have failed to produce a functional T cell receptor (TCR) (essential for T cell stimulation) are both eliminated from the developing T cell pool (Klein et al., 2014). It is estimated that about 95% of T cells are lost during the selection process in the thymus, while the remaining 5% preferentially migrate to lymph nodes, the spleen and in the lymphoid regions in the small intestine known as Peyer’s patches (Scollay et al., 1980). Lymphocyte retention or egress in lymphoid tissues is determined by chemokine gradients (Schulz et al., 2016) and by the expression of surface receptors that regulate adhesion and arrest in a specific tissue, also known as homing (Fu et al., 2016). Additional selection against autoreactive T cells can occur in lymphoid organs, resulting in further selection (Kurts et al., 1998).

Each T cell displays a virtually unique TCR, which increases the likelihood of recognition of molecular patterns pertaining to cancerous or virally infected cells (Murphy and Weaver, 2017). This

recognition is referred to as T cell activation. Prior to target recognition, T cells are defined as naïve and have no intrinsic capability to kill upon TCR triggering. Naïve T cells are characterised by a quiescent state, which is actively maintained by high transcription factor turnover and mRNA repression (Wolf et al., 2020). Naïve T cell priming occurs upon stimulation by professional antigen presenting cells (APCs), such as dendritic cells (Joffre et al., 2012). APCs process peptides from cancerous and virally infected cells and load them onto a class I major histocompatibility complex (MHC-I), which is exposed on the APC surface. T cell activation occurs when a naïve T cell encounters an APCs displaying a peptide recognized by the T cell receptor (Townsend et al., 1986). Once this interaction occurs, the naïve CD8<sup>+</sup> T cell is activated to become a full effector, cytolytic T cell, which initiates rapid clonal expansion (Sprent, 1976). Further interaction between the activated T cell and the antigen-presenting target cell is again mediated by the TCR and the MHC-I, and results in apoptosis of the target.

It is important to note that TCR stimulation is insufficient for naïve T cell commitment to growth and differentiation. T cells stimulated uniquely through the T cell receptor enter an unresponsive and non-proliferative state (anergy) (Jenkins and Schwartz, 1987; Lamb et al., 1983). Engagement of co-stimulatory surface proteins such as CD28 is required for proper naïve CD8<sup>+</sup> T and CD4<sup>+</sup> cells maturation by inducing the secretion of interleukin 2 (IL-2) (Harding and Allison, 1993; Harding et al., 1992). Co-stimulatory molecules on the T cell surface (CD8, CD28) participate in the activation process by prolonging TCR-MHC I interaction and promoting downstream signalling and proliferation (June et al., 1987; Kane et al., 1989). This phenomenon is referred to as the two-signal model, which suggests that naïve T cells need stimulation both by a MHC-I-bound antigen and by the APC itself, engaging surface molecules on the APC (McAdam et al., 1998). By contributing to signal transduction upon antigen recognition, CD28 co-stimulation modulates a vast array of pathways involving transcriptional, metabolic and cytoskeletal regulation (Esensten et al., 2016).

Naïve T cell activation results in differential expression of surface cell receptors involved in T cell signalling and migration to malignant tissues. Several of these receptors are used as markers to discriminate naïve and differentiated T cells. T cell activation upregulates CD44, a transmembrane protein that can influence intracellular signal transduction (Ponta et al., 2003). In addition, CD44 expression aids cell adhesion by binding to hyaluronic acid, a polysaccharide located on the extracellular matrix (Gallatin et al., 1983). By contrast, CD62L is a membrane protein regulating T cell homing (Lasky et al., 1989; Siegelman et al., 1989), and it is rapidly downregulated in activated T cells (Jung et al., 1988) as CD62L shedding promotes migration out of the lymph nodes and into

the bloodstream (Galkina et al., 2003). Therefore, increased CD44 expression is linked to T cell activation, while high CD62L expression is used as a marker of T cell quiescence.

The effector T cell population is short-lived, and as such it undergoes a contraction phase which leads to the survival of only a small fraction of antigen-specific T cells (Sprent, 1976). The surviving cells are referred to as memory T cells, which can be maintained for years after antigen encounter. Memory T cells can be distinguished from their naïve and effector counterparts on the basis of changes in gene expression and metabolism (Kaech et al., 2002; Pearce, 2010). In addition, memory T cells display a lower activation threshold than naïve T cells, allowing them to quickly respond to a previously encountered antigen and facilitate its clearance (de Jong et al., 1991; Sallusto et al., 1999). This characteristic is broadly referred to as immunological memory and underlies the rationale for vaccine development.

Memory T cells can be divided into further subsets: central memory, effector memory and tissue-resident memory T cells, which vary in their homing, effector and proliferative capacities (Sallusto et al., 2004). Central memory T cells circulate in secondary lymphoid organs (such as the lymph nodes and the spleen), while effector memory T cells migrate between blood and non-lymphoid peripheral tissues (Sallusto et al., 2004). By contrast, tissue-resident memory T cells stably reside in non-lymphoid peripheral tissues (Schenkel and Masopust, 2014). Effector memory T cells have a higher cytolytic capability than central memory T cells, thus providing a more immediate response to antigen encounter (Sallusto et al., 1999). Rapid response is also mediated by tissue-resident memory T cells, which are ideally located to respond to first signs of infection in peripheral tissues (Schenkel and Masopust, 2014). How specific T cells are selected to become memory T cells is still a subject of investigation, and it is thought to involve modulation of gene expression via transcriptional and epigenetic regulation (Gray et al., 2014). Interestingly, transcriptome analysis indicated that effector and central memory T cells are more similar to each other than to tissue-resident memory T cells, which are characterised by a distinct transcriptional signature (Mackay et al., 2013).

### **1.1.2 Signalling pathways triggered by TCR engagement in effector T cells**

Target cell recognition and killing rely on the initiation of a complex signalling cascade which includes the activation of mitogenic pathways (Cantrell, 2015), calcium flux and calcium-dependent signalling (Schwarz et al., 2013) and cytoskeletal rearrangements (Douanne and Griffiths, 2021). This culminates in the formation of the immunological synapse (IS), a highly organised interface between the CTL and the target cell (Paul and Seder, 1994). Of note, while naïve CD8<sup>+</sup> T cell stimulation

requires signalling from both the TCR and co-stimulatory molecules such as CD28, TCR-mediated signal transduction is sufficient to mediate the killing response in mature, effector T cells (Harding and Allison, 1993).

Initial studies of TCR structure identified commonalities in the cytoplasmic tail of the T and B cell receptors, thought to be essential to couple antigen recognition to intracellular transduction of signalling (Reth, 1989). These intracellular regions, known as immunoreceptor tyrosine-based activation motifs (ITAMs) form a scaffold mediating the assembly of kinases responding to the early phase of TCR activation. Proximal TCR signalling is mediated by the Src-family kinases ZAP70, LCK and FYN, which trigger ITAM phosphorylation (Cantrell, 2015). A major node of TCR signalling relies on phosphorylation of the integral protein LAT by ZAP70, which results in the formation of a complex (LAT signalosome) mediating the branching of the TCR cascade (Zhang et al., 1998).

Phosphorylated LAT activates PLC $\gamma$  (Finco et al., 1998), which catalyses the conversion of phosphatidylinositol biphosphate (PIP<sub>2</sub>) into diacylglycerol (DAG) and inositol triphosphate (IP<sub>3</sub>) (Treves et al., 1987). DAG affects transcription through the mitogen activated protein kinase (MAPK) signalling cascade (Ebinu et al., 2000), IP<sub>3</sub> is released in the cytosol and causes the opening of intracellular calcium stores by binding to the IP<sub>3</sub> receptors on the endoplasmic reticulum (ER) (Imboden and Stobo, 1985). Depletion of ER calcium stores induces in the opening of calcium-release activated channels (CRAC) on the plasma membrane (Zweifach and Lewis, 1993) causing a surge in intracellular calcium. High Ca<sup>2+</sup> concentration results in the Ca<sup>2+</sup>/calmodulin-dependent activation of calcineurin (Kincaid et al., 1987), whose phosphatase activity allows for translocation of the nuclear factor of activated T cells (NFAT) into the nucleus (Jain et al., 1993). NFAT controls the expression of several key proteins, including the cytokine IL-2, required for T cell proliferation (Shaw et al., 1988).

Notably, both DAG generation and assembly of the LAT signalosome can control transcription by regulating the localisation and phosphorylation of the guanine exchange factor (GEF) for Ras proteins (Dower et al., 2000). Ras-mediated signalling activates the MAPK proteins ERK1 and ERK2, which regulate both thymic T cell development and mature T cell function by modulating gene transcription, cytokine synthesis and expression of surface receptors involved in T cell homing (Cantrell, 2015). Thus, ERK activation induces further branching of the TCR signalling cascade, modulating both intracellular and extracellular T cell functions.

Both TCR- and CD28-dependent signalling induce recruitment of phosphatidylinositol 3-kinase

(PI3K) (Ueda et al., 1995). PI3K activation results in AKT phosphorylation (Franke et al., 1995). AKT phosphorylation triggers a signalling cascade promoting the expression of cytokines and chemokine receptors (Cantrell, 2015). Moreover, AKT phosphorylation induces activation of the mechanistic target of rapamycin (mTOR), thus sustaining the metabolic needs of activated cells by boosting nutrient uptake, mitochondrial biogenesis and protein synthesis (Saxton and Sabatini, 2017). The CD28-PI3K-AKT axis stimulates glycolysis, a hallmark metabolic shift in activated effector CTLs (Pearce, 2010).

TCR activation can also promote cytoskeletal reorganisation. The assembly of the LAT signalosome induces SLP76-mediated recruitment of the the Wiskott-Aldrich syndrome protein (WASp) which allows for its activation by the Rho GTPase protein CDC42 (Zeng et al., 2003). Activated WASp interacts with the actin-related protein 2/3 complex (ARP2/3), enhancing actin polymerization and cytoskeletal reorganisation in activated T cells (Machesky and Insall, 1998). Mutations in this pathway are detrimental not only for migration capacity, but they also extend to metabolism by impairing surface receptor recycling, including the glucose transporter GLUT1 (Randzavola et al., 2019).

### **1.1.3 Morphological alterations triggered by TCR engagement**

Activated T cells migrate to peripheral tissues and scan the membrane of neighbouring cells until they find a cognate antigen. During migration a distinct morphology can be observed, characterised by a leading edge, rich in filamentous actin (F-actin) and a trailing edge, rich in filopodia (Dupre et al., 2015). The actin dynamics mediating migration are governed by a complex interplay of signals, ranging from external stimuli (e.g. chemokines), adhesion receptors, and intracellular signalling events triggered by the engagement of the TCR (Dupre et al., 2015). During migration the nucleus is often found in the cell leading edge, while most other organelles are localised in either the cell midbody or in the uropod. Target recognition induces organelle polarisation towards the IS (Martin-Cofreces et al., 2014).

Target cell recognition is initiated by F-actin protrusions and leads to the polarisation of the entire T cell body alongside the formation of IS (Ritter et al., 2015). The IS is a highly organized structure that can be segregated into three regions: the central, peripheral and distal supramolecular activation clusters (referred to as cSMAC, pSMAC, dSMAC respectively) (Freiberg et al., 2002; Monks et al., 1998). These clusters are characterised by the recruitment of different proteins that allow for sustained

interaction between the T cell and the target: T cells receptors interacting with MCH-I cluster in the cSMAC (Monks et al., 1998), integrins mediating cell adhesion between the T cell and the target are found in the pSMAC (Monks et al., 1998) and filamentous actin, localised in the dSMAC (Sims et al., 2007). The delivery of cytotoxic proteins triggering target cell apoptosis occurs in a specialised region known as the secretory domain (Stinchcombe et al., 2001b).

TCR engagement and IS formation are accompanied by microtubule-dependent organelle polarisation (Kupfer and Dennert, 1984) as directed by the centrosome, whose docking at the cSMAC is needed for optimal target killing to occur (Tsun et al., 2011). Simultaneously, changes in the cell membrane allow for lipid specialisation (Gawden-Bone et al., 2018) and actin depletion clearance (Ritter et al., 2015). Centrosome docking and alterations in membrane composition ultimately enable the fusion of specialised lysosomes (lytic granules) at the secretory domain within the IS (Stinchcombe et al., 2001b; Stinchcombe et al., 2006; Stinchcombe et al., 2015). This process is referred to as degranulation, and it depends on increases in intracellular calcium concentration induced by TCR stimulation (Lancki et al., 1987; Takayama and Sitkovsky, 1987).

#### **1.1.4 Trafficking and maturation of lytic granules**

Lytic granules are found in T cells and natural killer (NK) cells, and they are marked by the late-endosome/lysosomal proteins LAMP1, LAMP2 and CD63 and characterised by an acidic pH (Peters et al., 1991). These specialized organelles contain hydrolases mediating degradation, which exert their function at low pH, and other components that participate in the cytotoxic response, which are active at neutral pH (Burkhardt et al., 1990).

Positive and negative regulators of granule maturation, trafficking and fusion are all thought to determine the cytotoxic capacity of CTLs, finely balancing the number of granules that will fuse with the plasma membrane during each killing event. Lytic granule maturation involves trafficking via mannose-6-phosphate receptors (M6PR) (Griffiths and Isaaz, 1993) and the adaptor-related protein complex AP3 (Rous et al., 2002) together with fusion events via the lysosomal trafficking regulator LYST (Stinchcombe et al., 2000). Defects in protein sorting and maturation of the lytic granules are associated with the development of immunodeficiency, such as Hermansky-Pudlack syndrome, Chediak-Higashi syndrome and familial haemophagocytic lymphohistiocytosis (FHL) (de Saint Basile et al., 2010).

Lytic granules are anchored to microtubules, and impairing microtubule formation by nocodazole treatment is sufficient to reduce granule polarisation at the IS (Tamzalit et al., 2020). The docking of lytic granules at the plasma membrane is mediated by the Ras-related protein RAB27A, which tethers granules to the plasma membrane by interacting with synaptotagmin-like proteins 1 and 2 (SLP1 and SLP2) (Holt et al., 2008). Lack of RAB27A results in a type of immunodeficiency known as Griscelli syndrome type 2, characterised by defective exocytosis (Menasche et al., 2000). Downstream of docking, the lysosomal membrane MUNC proteins interact with vesicle and plasma membrane-tethered SNAREs (v-SNAREs and t-SNAREs), which mediate the fusion process. Mutations in MUNC13-4 (Feldmann et al., 2003) and MUNC18-2 (zur Stadt et al., 2009) are both known to cause FHL, as well as mutations in the MUNC18-2 t-SNARE partner syntaxin-11 (zur Stadt et al., 2005). AP3 deficiency also results in defective lytic granule polarisation, suggesting that it regulates sorting of proteins involved in lytic granule motility (Clark et al., 2003).

Lytic granule fusion allows for the release of cytolytic proteins, which trigger target cell death by activation of caspase signalling (Adrain et al., 2005) (**Figure 1.1**). Secretion of the lytic granule content occurs within a small cleft formed between the CTL and the target cell, preventing damage to neighbouring cells (Stinchcombe et al., 2001b). Interestingly, only the target cell is affected by the activity of these proteins, while the T cell is immune to their action. This immunity is thought to be aided by different cell membrane composition, but the subject is still under intense investigation (Krawczyk et al., 2020; Rudd-Schmidt et al., 2019). Actin recovery terminates secretion (Ritter et al., 2017), allowing the CTL to detach from the dying target.

### **1.1.5 Granzymes and Perforin-dependent cytotoxic pathways**

The main components of lytic granules are serine esterase known as granzymes (Masson et al., 1986). Granzyme B is one of the most highly synthesised proteins in CTLs, and it the most abundant effector molecule, followed by granzyme A, C and perforin (Howden et al., 2019; Hukelmann et al., 2016).

Granzyme B is produced as a proenzyme that undergoes two rounds of proteolytic cleavage before maturing into an active enzyme: the first event occurs in the ER, where the signalling peptide is removed, and the second happens within the lytic granules, with the cleavage of an amino-terminal dipeptide (Caputo et al., 1993). Inactive granzyme B is trafficked to the granules by a M6PR-mediated pathway (Griffiths and Isaaz, 1993). Within the granules, granzyme B is cleaved by cathepsin C (Pham and Ley, 1999) and by cathepsin H (D'Angelo et al., 2010). Upon secretion of the lytic

granules, granzyme B enters the target cell and cleaves caspase-3 (Quan et al., 1996), generating a signalling cascade that results in apoptosis (Adrain et al., 2005) (**Figure 1.1**).

The pore-forming protein perforin is also stored within lytic granules and it is crucial to their cytotoxicity (Blumenthal et al., 1984). Perforin is synthesised as an inactive precursor that undergoes proteolytic cleavage removing a short C-terminal peptide including asparagine-linked glycans (Uellner et al., 1997). Although the trafficking and proteolytic cleavage of perforin have not been elucidated as extensively as with granzyme B, studies have suggested that perforin can be cleaved by cathepsin L *in vitro* (Konjar et al., 2010) and that the acidic environment within granules promotes perforin stability (Kataoka et al., 1994). C-terminal cleavage exposes a C2 phospholipid-binding domain, which allows calcium-dependent insertion of perforin into the target membrane (Uellner et al., 1997). Upon membrane insertion, perforin is able to oligomerize and create pores (Podack and Konigsberg, 1984) which allows for granzyme-mediated cytotoxicity to occur (Shiver and Henkart, 1991) (**Figure 1.1**). Recent work suggest that the mechanical force exerted by CTLs during synapse formation might enhance perforin activity by increasing the membrane tension of the target, facilitating the insertion of perforin oligomers (Basu et al., 2016).

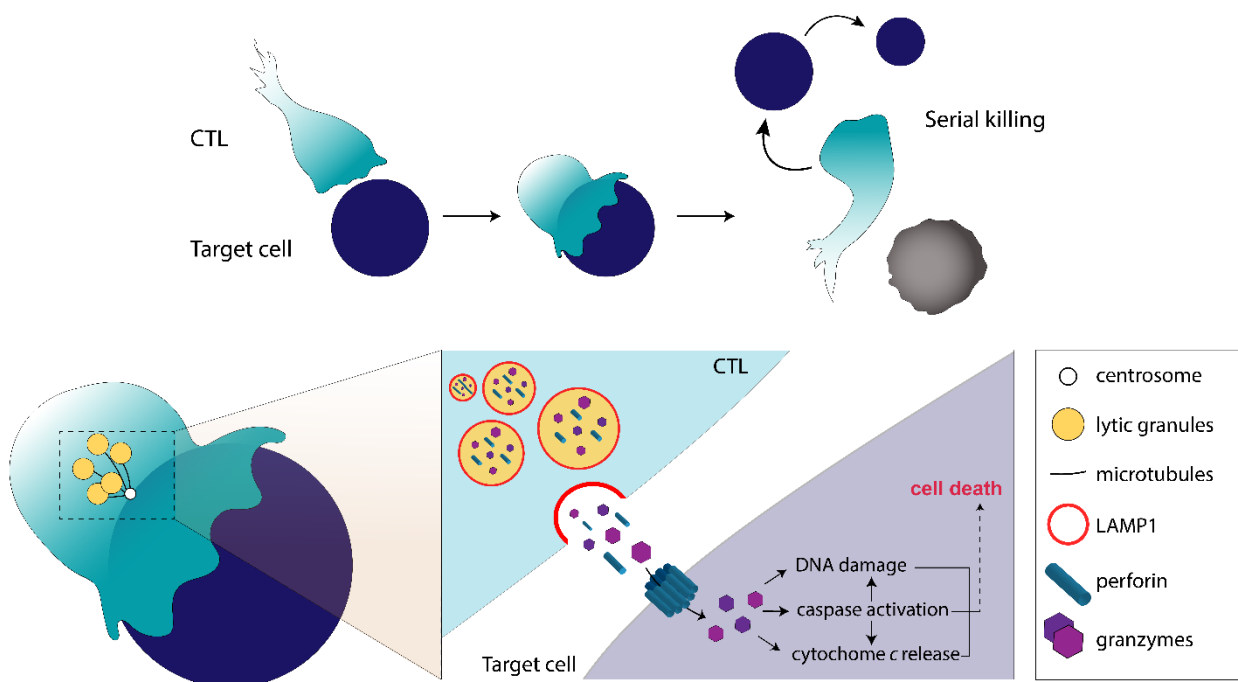


**Figure 1.1. CTLs trigger apoptosis of target cells by secretion of cytolytic proteins.**

Migrating CTLs recognise the target cell and tightly bind to it to selectively trigger cell death. The centrosome and lytic granules polarise at the interface between the CTL and the target cell, where the content of lytic granules is secreted. Perforin monomers oligomerise and form pores on the target cell membrane. Granzymes enter the target cell through these pores, triggering caspase activation and caspase-dependent and independent DNA fragmentation and cytochrome *c* release from mitochondria, leading to target cell lysis.

### 1.1.6 Additional pathways mediating cytotoxicity

Although perforin and granzyme B activity accounts for a large portion of the events leading to CTL-mediated killing, additional pathways can result in target apoptosis. This discovery originated from observing that while  $\text{Ca}^{2+}$ -depleted media prevented CTL degranulation, this only resulted in a partial decrease in target cell death (Ostergaard et al., 1987; Trenn et al., 1987). In addition to lytic granule polarisation, observations of organelle polarisation upon TCR engagement suggested that Golgi reorientation at the IS could facilitate the exocytosis of secretory vesicles containing cytotoxic substances (Kupfer and Dennert, 1984).

CTL can induce FAS-mediated death triggered by the FAS ligand (FASL). FAS is a surface receptor involved in the induction of apoptosis (Trauth et al., 1989; Yonehara et al., 1989), which was found to bind to a single protein identified in a CTL hybridoma line, named FASL (Suda and Nagata, 1994). Upon FASL binding, FAS cytoplasmic region binds FADD (Fas-associating protein with death

domain) (Chinnaiyan et al., 1995), which results in caspase activation and mitochondrial damage-mediated apoptosis (Barry and Bleackley, 2002). FASL-mediated apoptosis is thought to be one of the processes mediating effector CTL death after activation, which results in the contraction of the effector T cell pool after the antigen has been cleared (Owen-Schaub et al., 1992). FAS-mediated death also contributes to negative selection in the thymus, triggering apoptosis in immature autoreactive T cells (Castro et al., 1996).

Perforin-deficient and FASL-deficient mice still exhibit T cell killing, indicating the existence of additional mediators of cytotoxicity (Braun et al., 1996). Tumour necrosis factor alpha (TNF $\alpha$ ) was first identified as a serum component capable of inducing tumour necrosis (Carswell et al., 1975). Newly synthesised TNF $\alpha$  has been shown to accumulate in the Golgi and to be re-routed to the plasma membrane through the recycling endosome (Murray et al., 2005). Membrane-bound TNF $\alpha$  can be cleaved by the TNF- $\alpha$ -converting enzyme (TACE) also known as ADAM17 (Black et al., 1997; Moss et al., 1997) and by ADAM10 (Rosendahl et al., 1997), generating a soluble factor. TNF $\alpha$  binds the TNF-receptors 1 and 2 (TNFR1 and TNFR2) on the target cell membrane, both of which are required to trigger apoptosis (Vandenabeele et al., 1995). As with FASL, TNF $\alpha$  can induce death of activated T cells (Zheng et al., 1995).

TNF $\alpha$ -induced apoptosis can be potentiated by the presence of the cytokine interferon-gamma (IFN $\gamma$ ) (Fransen et al., 1986). IFN $\gamma$  has pleiotropic role in the immune system, upregulating MHC-I and regulating signalling cascades involved in both antiviral and antitumour immunity (Castro et al., 2018). An additional cytokine able to induce apoptosis in tumour cell lines is APO-2L, or TNF-related apoptosis-inducing factor (TRAIL) (Pitti et al., 1996; Wiley et al., 1995). TRAIL can bind to several receptors on the target cell membrane (Diaz Arguello and Haisma, 2021). Similarly to TNF $\alpha$  and FASL, TRAIL can lead to apoptosis through caspase signalling (Mariani et al., 1997) and it is also implicated in activation-induced death in lymphocytes (Martinez-Lorenzo et al., 1998)

### **1.1.7 Post-transcriptional regulation of CTL killing**

Stimulation of T cells via the TCR and co-stimulatory receptors can upregulate cytokine expression via a post-transcriptional mechanism linked to mRNA stability (Lindstein et al., 1989). Despite evidence for transcriptional regulator of granzyme A (Philip et al., 2017), chromatin accessibility for key cytolytic proteins such as TNF $\alpha$  and perforin is not altered during the transition from naïve to effector T cells (Philip et al., 2017). Instead, TCR engagement in CTLs promotes the

temporally specific protein expression of several mediators of T cell cytotoxicity, such as TNF $\alpha$  and IFN $\gamma$  (Lindstein et al., 1989; Salerno et al., 2017).

This phenomenon is thought to be aided by post-transcriptional regulation by RNA-binding proteins (RBPs). These complexes were first described with the name of informosomes (Spirin, 1969). Since then, RBPs have been suggested to both promote and decrease mRNA stability in lymphocytes, depending on the type of RBP, mRNA species and cell type analysed (Salerno et al., 2020; Turner and Diaz-Munoz, 2018). This additional layer of post-transcriptional regulation presents several benefits. On one hand, it allows for rapid effector molecule synthesis without the need of *de novo* transcription, which prevents delays from target cell encounter to the onset of killing. On the other, RBP also allow for rapid downregulation of pro-inflammatory molecules, thus precluding immunopathology related to excessive inflammation. This rapid fine-tuning of effector molecules has been well-described in the context of cytokine regulation (Salerno et al., 2020).

Measurements of the correlation between the transcriptome and proteome of naïve and activated CD4<sup>+</sup> and CD8<sup>+</sup> T cells revealed that the T cell transcriptome is a poor predictor of protein expression (Hukelmann et al., 2016; Tan et al., 2017a; Wolf et al., 2020). Thus, CTL activation relies more on selective translation of pre-existing mRNA species rather than on a specialised transcriptional programme occurring after TCR crosslinking, highlighting the significance of post-transcriptional regulation in CTLs.

### **1.1.8 CD8<sup>+</sup> T cells are serial killers**

A crucial characteristic that allows for CTL efficient clearing of tumours and viral infection is the ability to engage in subsequent killing events, described as serial killing. This phenomenon was observed in co-cultures of effector CTLs and target cells seeded at variable effector to target ratios (Berke et al., 1972). These studies showed that CTLs could achieve target cell lysis even when targets were seeded in excess, and that lysis continued over time (>5h). This observation led to the conclusion that “the lymphoid cell kills and continues to kill” (Berke et al., 1972).

Early microcinematography studies showed that a CTL can trigger cell death, detach itself from the dying target and quickly induce apoptosis in a different, nearby cell (Sanderson, 1976). While CTLs respond to TCR engagement by rapidly polarising lytic granules at the plasma membrane, only a few granules are released during a single killing event (Ritter et al., 2015). Strong stimulation in media containing abundant calcium results in only half of the total lytic granule pool being released after

one hour of sustained stimulation (Pores-Fernando et al., 2005). Taken together, these findings indicate that the cytotoxic ability of a single T cell greatly surpasses the threshold for apoptosis of a single target, and that the same T cell can perform sustained killing over time.

Of note, chronically stimulated T cells can lose their ability to proliferate and kill. This phenotype is referred to as T cell exhaustion, and it involves alterations in gene expression, signalling and metabolism (Franco et al., 2020; Sen et al., 2016). Chronic stimulation leading to T cell exhaustion has been described upon both viral infection and tumorigenesis. Exhaustion is correlated with the expression of surface markers that inhibit T cell signalling, such as PD-1, CTLA-4, TIM-3, LAG-3 and TIGIT (Wherry and Kurachi, 2015). While intense investigation has focused on preventing or reversing exhaustion, it is not clear if the epigenetics modifications in exhausted T cells can be fully reversed (Abdel-Hakeem et al., 2021).

## 1.2 Mitochondria: dynamic organelles shaping T cell function

The rise of the immunometabolism field has unravelled the multifaceted roles of mitochondria in both the innate and adaptive immune system (O'Neill et al., 2016). Mitochondrial morphology, position and function can potentiate an effective immune response, just as their dysfunction can result in immunodeficiencies. These findings highlight the complex metabolic rewiring that occurs during T cell differentiation, and bring the field closer to optimising immunotherapy strategies to better cater for the metabolic microenvironment found within tumours (Madden and Rathmell, 2021).

### 1.2.1 Overview of mitochondrial function and architecture

Mitochondria display a highly organised structure characterised by an outer mitochondrial membrane (OMM) and an inner mitochondrial membrane (IMM), separated by an intermembrane space (Palade, 1952). The IMM encloses the innermost part of the organelle, known as the mitochondrial matrix (**Figure 1.2A**). The IMM folds are referred to as cristae, and their architecture is crucial for the assembly of the complexes mediating oxidative phosphorylation (OXPHOS) (Cogliati et al., 2016). Complexes I-IV of the ETC generate a proton gradient across the IMM, which is harnessed by the ATP synthase (complex V) to produce ATP (Mitchell and Moyle, 1965) (**Figure 1.2B**). This gradient creates a difference in proton concentration across the IMM referred to as mitochondrial membrane potential.

Maintenance of the mitochondrial membrane potential is not only necessary for ATP generation, but also for mitochondrial import (Gasser et al., 1982). It is in fact estimated that over 90% of the mitochondrial proteome is encoded by nuclear genes, with only 13 subunits of the electron transport chain (ETC), 2 rRNA and 22 tRNAs retained in the mitochondrial genome (D'Souza and Minczuk, 2018). Mitochondrial proteins encoded by nuclear genes are synthesised in the cytosol and later imported into mitochondria. Mitochondrial import is determined by the presence of an N-terminal targeting sequence, directing proteins to the translocase of outer membrane (TOM) complex (Schmidt et al., 2010). Further protein import inside the organelle is mediated by the translocase of inner membrane (TIM) complexes, allowing entrance into the mitochondrial matrix (Schmidt et al., 2010).

The transport of ions and metabolites into the mitochondria is also tightly regulated. The voltage-dependent anion channel (VDAC) allows entrance via the OMM, and multiple dedicated channels act as gates in the IMM (Chandel, 2015b). Metabolites crossing the IMM can participate in several biosynthetic processes occurring in the mitochondrial matrix. These include pyruvate oxidation

through the tricarboxylic (TCA) cycle, fatty acid catabolism through  $\beta$ -oxidation, iron metabolism via heme biosynthesis and reactive oxygen species (ROS) scavenging (Chandel, 2015b). In addition, the mitochondrial matrix hosts enzymes involved in one-carbon metabolism, required for amino acids and nucleotide biosynthesis. Altogether, OXPHOS and the metabolic processes occurring in the mitochondrial matrix are crucial to sustain cellular homeostasis and proliferation.

The mitochondrial matrix is the site for mitochondrial DNA (mtDNA) replication, transcription and translation (Gustafsson et al., 2016). Of note, different mtDNA genotypes can co-exist within the same cell or organism. This phenomenon is known as heteroplasmy and it is due to *de novo* mutations occurring during mtDNA replication (Craven et al., 2017; Rossignol et al., 2003). mtDNA mutations can be pathogenic and result in a vast array of clinical manifestations, depending on both the pervasiveness of heteroplasmy and the affected tissue. The effect of pathogenic mutations is often most evident in highly metabolic tissues, such as skeletal muscle and cardiac tissue (Rossignol et al., 2003).

### 1.2.2 Mitochondrial dynamics via fission and fusion

Mitochondria display remarkable functional and morphological differences within the same cell (Collins et al., 2002) and between different cell types (Palade, 1952). Furthermore, mitochondrial morphology can adapt to fluctuations in cellular metabolism (Hackenbrock, 1966). These alterations occur through processes of fission and fusion of the mitochondrial membrane, disruption of which can result in human pathologies (Adebayo et al., 2021), emphasising the importance of plasticity of the mitochondrial network in homeostasis.

The classical mitochondrial morphology presents as an interconnected network of elongated mitochondria (**Figure 1.2C**). The proteins mitofusin 1 (MFN1) and mitofusin 2 (MFN2) are required for OMM fusion (Santel et al., 2003; Santel and Fuller, 2001). MFN1 and MFN2 promote fusion by oligomerisation on membranes of adjacent mitochondria (Koshiba et al., 2004). This process is completed after IMM fusion by the protein optic atrophy 1 (OPA1) (Cipolat et al., 2004). In addition, OPA1 has fusion-independent roles, modulating cristae morphology and cytochrome *c* release, thereby mediating mitochondrial architecture and apoptosis (Frezza et al., 2006).

Mitochondria can also exhibit a rounder and less interconnected shape, which is driven by fission (**Figure 1.2C**). The main player in mitochondrial fission is the dynamin-related protein 1 (DRP1). DRP1 shuttles between the OMM and the cytosol, accumulating on mitochondria ahead of a division

event (Smirnova et al., 2001). Actin filaments drive the initial membrane constriction via INF2-mediated polymerisation, thought to enable DRP1 association with the mitochondrial membrane (Korobova et al., 2013). Several proteins, including FIS1 and MFF, can act as receptors for DRP1 on the OMM (Gandre-Babbe and van der Blik, 2008; Yoon et al., 2003).

Mitochondrial fragmentation is a required step in mitosis (Christiansen, 1949). During metaphase, waves of actin assembly and disassembly on mitochondria ensure an equal and random distribution of mitochondria in dividing cells (Moore et al., 2021). This phenomenon is thought to occur to ensure equal inheritance of mitochondria in daughter cells.

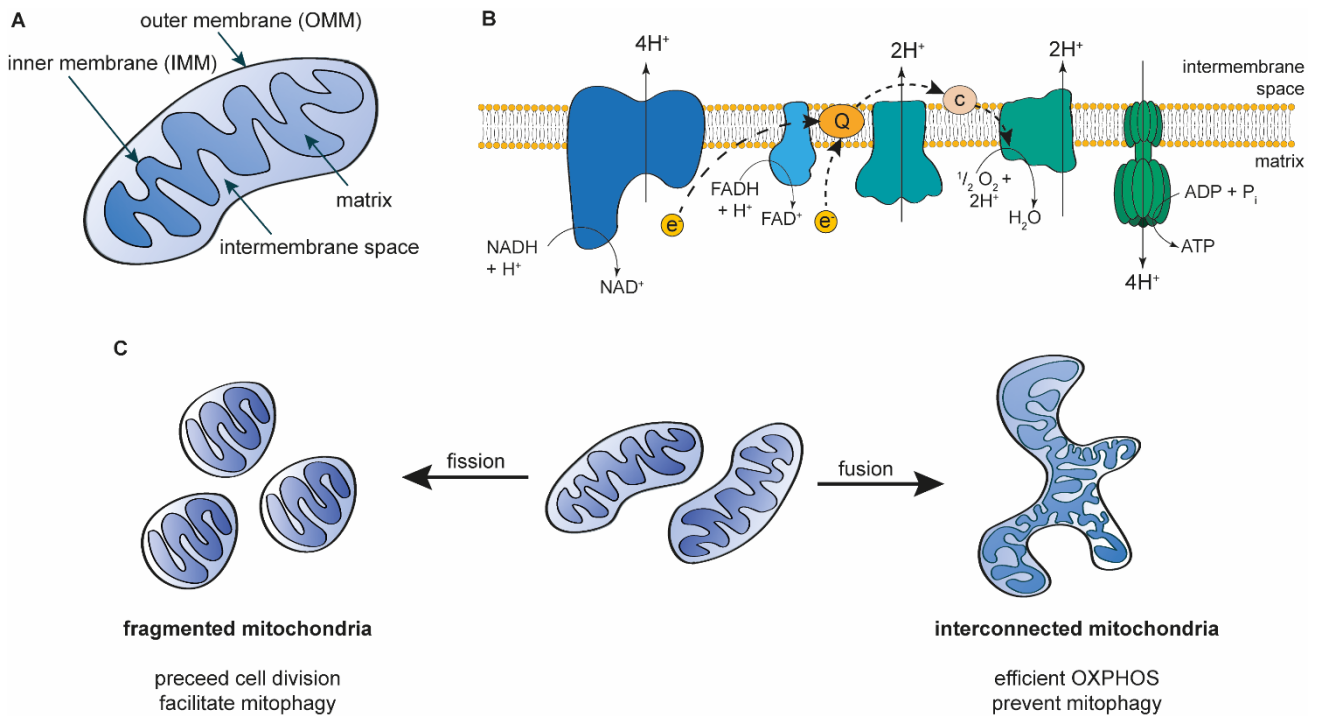


**Figure 1.2. Mitochondrial morphology and dynamics.**

(A) Mitochondrial architecture. Mitochondrial outer membrane (OMM), inner membrane (IMM), intermembrane space and matrix are labelled. (B) Mitochondrial electron transport chain (ETC). Complexes I, III and IV mediate proton transport across the IMM. Complex V harnesses the proton gradient for ATP synthesis. (C) Mitochondrial dynamics involve both mitochondrial fragmentation (fission) and mitochondrial elongation (fusion). Elongated mitochondria create an interconnected network throughout the cell.

### 1.2.3 Mitochondrial clearance by mitophagy

Mitochondrial fission is depicted as a process that facilitates the removal of damaged mitochondria (mitophagy), while mitochondrial fusion is thought to be protective against mitophagy (**Figure 1.2C**) (Twig et al., 2008).

Mitophagy investigation has focused on the role of the PTEN-induced putative kinase 1 (PINK1) and the E3 ligase PARKIN in promoting mitochondrial degradation. Despite most cases of Parkinson's disease being sporadic (Poewe et al., 2017), familial cases of hereditary Parkinson's have highlighted the role of PARKIN (Kitada et al., 1998) and PINK1 (Valente et al., 2004) in this neurodegenerative condition. The PTEN-induced putative kinase PINK1 bears a mitochondrial localisation motif allowing for PINK1 targeting to the mitochondria (Beilina et al., 2005; Silvestri et al., 2005). Mitochondrial membrane potential drives the translocation of PINK1 (Lin and Kang, 2008) into the mitochondrial matrix, where PINK1 can be cleaved by presenilin-associated rhomboid-like protease (PARL) (Jin et al., 2010), the mitochondria processing peptidase MPP (Greene et al., 2012) and additional proteases. Cleaved forms of PINK1 are exported back to the cytosol, where they are degraded by the proteasome (Yamano and Youle, 2013). Disruption of mitochondrial membrane potential allows for PINK1 accumulation on the OMM (Lin and Kang, 2008). PINK1 then promotes recruitment of the E3 ubiquitin ligase PARKIN to damaged mitochondria (Geisler et al., 2010; Matsuda et al., 2010; Narendra et al., 2008; Narendra et al., 2010; Vives-Bauza et al., 2010) by phosphorylation of both PARKIN and ubiquitin, which activates PARKIN E3 ligases function (Kondapalli et al., 2012; Koyano et al., 2014; Shiba-Fukushima et al., 2012). Ubiquitinated proteins can interact with autophagy adaptors and recruit LC3-rich autophagosomal membranes (Geisler et al., 2010; Narendra et al., 2008), or proceed to proteasomal-dependent degradation (Chan et al., 2011)

Some studies of mitophagy have relied on the overexpression of PINK1 and/or PARKIN, often coupled to drug-induced mitochondrial depolarisation (loss of the mitochondrial membrane potential). These highly artificial models have called into question the role of PINK1 and PARKIN in mitophagy, particularly as mouse and *Drosophila* models lacking PINK1 or PARKIN expression still show efficient mitophagy (Lee et al., 2018; McWilliams et al., 2018). Furthermore, PINK1 can mediate mitophagy via E3 ligases other than PARKIN, such as MUL1 and ARIH1, and the autophagosome can also be recruited by proteins localised on the OMM (e.g. BNIP3, NIX, FUNDC1, AMBRA1) (Villa et al., 2018). OMM rupture can also induce mitophagy by exposing the LC3 receptor prohibitin 2 (PHB2), increasing autophagosome recruitment (Wei et al., 2017). In addition, mitochondrial stress promotes translocation of the IMM lipid cardiolipin to the OMM, where it can act as an autophagy receptor (Chu et al., 2013).

#### 1.2.4 Mitochondrial act as cellular stress sensors

Mitochondria are able to both receive and send signals concerning homeostasis within cells (Chandel, 2015a). For instance, loss of homeostasis can result in apoptosis, which is mediated by the pro-apoptotic proteins BAX and BAK. Upon cellular insult, BH3-containing proteins activate BAK and BAX both directly and indirectly via inhibition of BCL-2 family members (Dadsena et al., 2021; Kim et al., 2006a). Activated BAX and BAK redistribute on the OMM, where they oligomerise (Dai et al., 2011; Wolter et al., 1997), creating pores that allow for release of pro-apoptotic cytochrome *c* (Liu et al., 1996), resulting in caspase-mediated cell death (Li et al., 1997).

Just as cellular homeostasis or lack thereof can be communicated to mitochondria, mitochondria can also communicate lack of fitness to the rest of the cell (Anderson and Haynes, 2020; Battersby and Richter, 2013; Boos et al., 2020; Topf et al., 2016). As indicated earlier, most mitochondrial proteins are encoded in the nuclear genome and synthesised in the cytosol (D'Souza and Minczuk, 2018) and the import of these proteins into the mitochondrion depends on mitochondrial membrane potential (Schleyer et al., 1982). Mitochondrial fitness is therefore the product of a carefully balanced stoichiometry between nuclear-encoded and mitochondrial-encoded components, which can be assembled as subunits of the same structure, such as the mitochondrial ribosome and complexes of the electron transport chain (Battersby and Richter, 2013). While work in *Saccharomyces cerevisiae* has suggested that this stoichiometry is communicated unidirectionally from the nucleus to the mitochondria (Couvillion et al., 2016), other studies in *Caenorhabditis elegans* have shown that imbalance in mitochondrial ribosome abundance can feed back to the cytosol and reduce the abundance of cytosolic ribosome in order to maintain homeostasis (Molenaars et al., 2020).

Lack of protein import into the mitochondria results in the accumulation of mitochondrial protein precursors into the cytosol and increased protein mistargeting. This type of mitochondrial stress is referred to as unfolded protein response activated by protein mistargeting (UPRam) (Wrobel et al., 2015). The UPRam results in the inhibition of cytosolic protein synthesis and in enhanced proteasome activation (Wrobel et al., 2015), thought to be triggered by protein aggregates in the cytosol (Nowicka et al., 2021). A different form of communication, termed the mitochondrial unfolded protein response (mtUPR) is canonically triggered by defective mitochondrial translation or defective folding of mitochondrial proteins, and it upregulates the expression of mitochondrial chaperonins (Zhao et al., 2002). While additional mitochondrial insults (such as impaired fusion) can trigger the mtUPR, only inhibition of mitochondrial protein synthesis was shown to affect cytosolic translation (Molenaars et al., 2020). Notably, the mtUPR can be beneficial, as both worms and mice with deficiency in

mitochondrial translation since early development display longer lifespan in adulthood (Houtkooper et al., 2013).

How is mitochondrial dysfunction communicated to the cytosol? The transcription factor ATFS-1 has been described as a key player in *C. elegans*. ATFS-1 bears both a mitochondrial localisation sequence and a weak nuclear localisation sequence, and it is usually imported into the mitochondria, where it is targeted for degradation (Nargund et al., 2012). Upon mitochondrial distress, lack of membrane potential abolishes ATFS-1 mitochondrial localisation and results in its translocation to the nucleus, where it can induce transcription of genes associated with promotion of cellular homeostasis (Nargund et al., 2012). It is currently unclear whether a similar event occurs in mammalian cells, although a similar regulatory mechanism has been proposed for ATF5 in HeLa and HEK293T cells (Fiorese et al., 2016). In addition, lack of mitochondrial precursor import has been suggested to impair cytosolic protein synthesis and recruit chaperones via the transcription factor HFS-1 (Boos et al., 2020). HFS-1 is usually kept in an inactive state by cytosolic chaperone binding. However, increases in mitochondrial precursor aggregation can recruit chaperones to aggregates, allowing free HFS-1 to translocate to the nucleus and induce transcription of genes associated with pro-survival response. Furthermore, as mitochondrial dysfunction could lead to morphological alterations, lipid signalling has also been highlighted as a potential pathway that relays stress signals back to the cytosol (Kim et al., 2016).

Another key event occurring upon mitochondrial dysfunction is triggering of the integrated stress response (ISR), which differs from the mtUPR. The ISR is induced by activation of one or more main kinases (HRI, PERK, GCN and PKR) which respond to different cellular insults, such as ER stress, amino acid deficiency, viral infection, oxidative stress, iron depletion, proteasome inhibition and hypoxia (Pakos-Zebrucka et al., 2016). Kinase engagement triggers phosphorylation of the eukaryotic initiation factor eIF2 $\alpha$ , which prevents the formation of the GTP-bound active form required for translation initiation (Safer et al., 1975; Siekierka et al., 1982). This event results in downregulation of protein synthesis and in the preferential translation of mRNAs with short open reading frames in their 5' UTR (Harding et al., 2000). One of the transcription factors preferentially translated upon ISR triggering is ATF4, which promotes the restoration of cellular homeostasis (Harding et al., 2000; Harding et al., 2003). It is important to note that acute ISR aims to restore cellular fitness, but chronic ISR is damaging and can lead to apoptosis (Pakos-Zebrucka et al., 2016).

While the mtUPR results in increased expression of ATF5 and chaperones, mitochondrial stress triggering the ISR results in upregulation of ATF4 target genes (Quiros et al., 2017). Inhibition of mitochondrial translation was shown to trigger an ATF4-dependent decrease in cytosolic protein

synthesis (Molenaars et al., 2020; Quiros et al., 2017). In addition, two recent studies revealed a direct link between mitochondrial dysfunction and cytosolic translation via the DELE1-HRI pathway (Fessler et al., 2020; Guo et al., 2020). Mitochondrial stress allows for DELE1 to be released from mitochondria and to bind HRI, one of the ISR kinases, resulting in ISR triggering and impaired cytosolic translation. While these results highlight that mitochondrial dysfunction can induce the canonical ISR, kinase depletion does not always result in an interruption of the ISR triggered by mitochondrial insult (Quiros et al., 2017). In addition, eIF2 $\alpha$ -independent upregulation of ATF4 has been observed (Ben-Sahra et al., 2016; Quiros et al., 2017). Taken together, these findings suggest the existence of a non-canonical activation of the ISR upon loss of mitochondrial homeostasis.

Furthermore, mitochondrial stress can impair mTOR signalling and inhibit cytosolic translation. This has been observed as part of the mitochondrial ISR response (ISRmt), triggered by defects in mtDNA replication (Khan et al., 2017). Mitochondrial ROS (mtROS) signalling has also been involved in the impairment of protein synthesis upon mitochondrial damage. According to this model, mitochondrial damage leads to leakage of reactive oxygen species, which can decrease the affinity of the ribosome for RNA by oxidizing ribosomal subunits (Topf et al., 2018). In addition, mtROS can inhibit cytosolic translation by inducing the formation of stress granules, ribonucleotide complexes characterised by the presence of translationally inactive mRNA and initiation factors. In CTLs, aberrant mtROS release causes tRNA fragmentation, impairing cytosolic protein synthesis (Yue et al., 2021).

### **1.2.5 Mitochondrial communicate with other organelles via membrane contact sites**

Mitochondria can directly interact with other organelles through the formation of membrane contact sites (Prinz et al., 2020). Observations of a contiguous membrane juxtaposition between the ER and mitochondria (Bernhard et al., 1952) were supported by findings revealing the enrichment of specific enzymes mediating lipid biosynthesis at these sites (Vance, 1990), named mitochondria-associated membranes (MAMs) (Rusinol et al., 1994) or contact sites (Ardail et al., 1993). These observations led to the hypothesis that MAMs could be functionally relevant for lipid transfer between the two organelles. While the definition and the study of contact sites poses numerous semantic and technical challenges (Scorrano et al., 2019), mitochondria have been shown to form morphologically and functionally relevant juxtaposition with several organelles.

The most frequent mitochondrial contact sites occur with the ER, followed by the Golgi and lipid droplets (Valm et al., 2017). Membrane juxtaposition between the ER and mitochondria is mediated by several proteins, indicating the importance of MAMs in cellular homeostasis (Gordaliza-Alaguero

et al., 2019). The frequency of contact sites between the ER and mitochondria increases upon ER stress, and this has been suggested to serve cytoprotective functions (Bravo et al., 2011). However, the connection between ER and mitochondria can also result in calcium fluxes ultimately leading to apoptosis by promoting cytochrome *c* release (Breckenridge et al., 2003; Szalai et al., 1999). The chaperone protein GRP75 physically links the voltage-dependent ion channel VDAC on the OMM and the inositol 1,4,5-triphosphate receptor (IP3R) on the ER (Szabadkai et al., 2006). This and other close appositions allow for the local surge in calcium concentration upon IP3-mediated stimulation (Rizzuto et al., 1993), which can be more than twenty times higher than the concurrent concentration of calcium in the cytoplasm (Csordas et al., 1999). Mitochondrial depolarisation results in the loss of locally controlled  $\text{Ca}^{2+}$  oscillations upon stimulation and induces a broad propagation of calcium in the cytosol (Tinel et al., 1999). Mitochondria-ER contact sites are also used for ROS signalling, which can both induce and be induced by calcium flux, creating a feed-forward loop (Booth et al., 2016).

Some contact sites can specify regions that will undergo mitochondrial fission: this is the case with the ER, forming a platform for DRP1 assembly (Friedman et al., 2011), lysosomes, via RAB7 GTP hydrolysis (Wong et al., 2018) and Golgi-derived vesicles containing phosphatidylinositol 4-phosphate [PI(4)P] (Nagashima et al., 2020). Interestingly, a recent study has proposed that these contact sites could discriminate between fission leading to mitochondrial proliferation and fission leading to mitophagy (Kleele et al., 2021). Lysosome-mitochondria contacts have also been implicated in mitochondrial function in axons. Late endosomes were found to associate with both mitochondria and RNA granules encoding mitochondrial proteins, promoting mitochondrial homeostasis by allowing for locally targeted translation (Cioni et al., 2019).

Mitochondria have been observed to form contacts with a multitude of different proposed functions. Stable contacts between the Golgi and mitochondria have also been observed, and they might provide  $\text{Ca}^{2+}$  gradients and ATP supply across the Golgi (Dolman et al., 2005). In addition, mitochondria can make membrane contacts with lipid droplets, supporting their expansion (Benador et al., 2018). Starvation increases contact sites between mitochondria and lipid droplets, which is thought to enhance fatty acid oxidation in the mitochondria, further indicating that these membrane associations are crucial in responding to alteration in cellular homeostasis (Valm et al., 2017). Mitochondria can also form juxtapositions with the nucleus to communicate loss of homeostasis (Desai et al., 2020). Furthermore, mitochondria and peroxisomes have also been shown to interact via membrane contact sites, thought to promote the exchange of metabolites supporting fatty acid oxidation and steroid synthesis (Fan et al., 2016).

Mutations in proteins mediating contact sites can result in diabetes, cancer and neurodegeneration (Prinz et al., 2020). It is important to note that the prevalence and functionality of contact sites in lymphocytes has been understudied. A recent preprint pointed out that the protein TCAIM was needed for cholesterol biosynthesis at ER-mitochondria contact site. Loss of TCAIM resulted in altered function in CD8<sup>+</sup> T cells by reducing the expression of the transcription factor HIF1 $\alpha$ , which modulates metabolism and the expression of effector genes (Iwert et al 2021; <https://doi.org/10.1101/2021.04.20.440500>). This interesting observation calls for more studies to investigate the role of contact sites in lymphocytes and in specifically in CTL-mediated cytotoxicity.

### **1.2.6 Mitochondria influence T cell differentiation, signalling and metabolism.**

Mitochondria can contribute to both innate and adaptive immunity with a variety of roles extending beyond energy requirements and intertwining with TCR-dependent signalling (Mehta et al., 2017). Mitochondrial function, architecture and clearance can all affect T cell metabolism, thus modulating T cell development, differentiation and effector functions (Zhang and Romero, 2018).

Manipulating mitochondrial dynamics and metabolism by deleting the fusion protein OPA1 (Corrado et al., 2021), the division promoter DRP1 (Simula et al., 2018) or the mitochondrial pyruvate carrier, essential for pyruvate entry into the TCA cycle (Ramstead et al., 2020) can affect thymic development, skewing T cell differentiation and altering TCR-dependent signalling. These defects are pervasive and can lead to autoimmune phenotypes (Ramstead et al., 2020). Interestingly, while OPA1 depletion results in the inability to generate a competent pool of long-lived memory T cells (Corrado et al., 2021), DRP1-deficient mice show an enhanced propensity for T cell differentiation towards a memory phenotype (Simula et al., 2018). Impairing mitochondrial transcription by TFAM knockout can also affect T cell development and results in fewer CD4<sup>+</sup> and CD8<sup>+</sup> T cells in peripheral tissues, and in a higher prevalence of pro-inflammatory CD4<sup>+</sup> T cells (Desdin-Mico et al., 2020). Similarly, genetic deletion of the ETC complex III (Sena et al., 2013), ablation of complex IV assembly factors (Tan et al., 2017a) and DRP1 depletion (Simula et al., 2018) can reduce the amount of CD4<sup>+</sup> and CD8<sup>+</sup> T cells in peripheral tissues. Pharmacological inhibition of complex I can also impair naïve CD8<sup>+</sup> T cell expansion upon stimulation (Yi et al., 2006).

Naïve T lymphocytes are metabolically quiescent cells that rely on both mitochondrial metabolism and glycolysis for their survival (Pearce, 2010). TCR stimulation dramatically alters the metabolic profile of T cells, triggering an initial burst of both OXPHOS and glycolysis (Levine et al., 2021), which is supported by the high availability of glycolytic enzymes even in quiescent naïve cells (Wolf

et al., 2020). CD28 stimulation promotes expression and trafficking of the glucose transporter GLUT1, which enhances glucose metabolism, T cell proliferation and cytokine production (Jacobs et al., 2008). In addition, CD28-mediated signalling increases glutamine uptake upon activation, which is essential for T cell proliferation (Carr et al., 2010).

OXPHOS is essential for naïve T cell proliferation and activation (Chang et al., 2013; Sena et al., 2013; Tan et al., 2017a; Yi et al., 2006). OXPHOS inhibition in newly activated naïve T cells reduces ATP and ROS production, ERK1/2 phosphorylation and calcium flux (Yi et al., 2006). TCR crosslinking rapidly generates mtROS (Devadas et al., 2002) required for activation and expansion of both CD4<sup>+</sup> (Sena et al., 2013) and CD8<sup>+</sup> (Fischer et al., 2018) T cells. Conversely, deprivation of mtROS prevents TCR-dependent proliferation and NFAT translocation to the nucleus, independently of calcium signalling (Sena et al., 2013). Furthermore, absence of mtROS signalling impairs IL-2-dependent production of cytokines and cytotoxic molecules in newly activated CD8<sup>+</sup> T cells (Fischer et al., 2018).

Ultimately, mature CTLs show enhanced reliance on glycolysis instead of OXPHOS even when oxygen is available (Menk et al., 2018; Pearce, 2010). This phenomenon is common to both T lymphocytes and tumorigenic cells, and it is referred to as the Warburg effect (Warburg, 1956). Despite being less efficient in terms of ATP production, glycolysis is thought to be favoured over OXPHOS to sustain biosynthetic needs, as glycolytic intermediates can fuel the synthesis of amino acids, nucleotides and lipids (Lunt and Vander Heiden, 2011). mtROS generation in CTLs seems to serve different purposes than in naïve T cells. In mature CTLs, both NFAT translocation and IL-2 transcription are independent from mtROS production, while ERK1/2 signalling requires it (Devadas et al., 2002; Fischer et al., 2018). While OXPHOS inhibition prevents naïve T cell development, OXPHOS-impaired CTLs can survive and develop into effectors, showing remarkable metabolic plasticity (Chang et al., 2013). This plasticity is thought to allow T cells to proliferate and function efficiently both in oxygen-replete (lymphoid organs) and oxygen-depleted (tumour) environments.

Remarkably, the ability of T cells to undergo further differentiation depends on mitochondria. Effector T cells tend to have smaller and round mitochondria, which is thought to be less OXPHOS-efficient, while memory T cells have long and interconnected mitochondria, thought to facilitate OXPHOS by increased juxtaposition of ETC complexes (Buck et al., 2016). Indeed, mitochondrial fusion is required for memory T cell production but not for CTL survival. Forcing mitochondrial fusion can skew T cell differentiation into a memory phenotype, highlighting the importance of mitochondrial dynamics in T cell development (Buck et al., 2016). Impairment of mitochondrial

division via *Drp1* silencing skews T cell differentiation towards a memory phenotype by inhibiting glycolysis and promoting OXPHOS, fatty acid oxidation and the TCA cycle (Simula et al., 2018).

Memory T cells show augmented mitochondrial mass and mitochondrial respiration compared to both naïve and effector CTLs (van der Windt et al., 2012), and engagement of glycolysis, fatty acid oxidation, mitochondrial-derived ATP and mtROS are all thought to sustain memory T cell proliferation during the recall response (Gubser et al., 2013; Sena et al., 2013; van der Windt et al., 2013). Both metabolic pathways are sustained by CD28 signalling. CD28 can enhance glycolysis by boosting PI3K/AKT signalling (Frauwirth et al., 2002) but it can also trigger a signalling cascade resulting in cristae reorganisation, increased respiratory capacity and upregulated expression of fatty acid oxidation enzymes (Klein Geltink et al., 2017)

Mitochondria in memory T cells can form membrane contact sites with the ER, which improves their respiratory and metabolic capacity, thought to be key to the rapid recall response (Bantug et al., 2018). Interestingly, terminally differentiated effector CTLs and memory T cells are also characterised by a different percentage of damaged mitochondria, with the anabolic effector T cell population displaying less mitochondrial degradation than the catabolic memory T cell population. This discrepancy is thought to originate during cytokinesis, where one daughter cell acquires more aged mitochondria despite an initial homogeneous distribution during metaphase (Adams et al., 2016). The molecular machinery involved in asymmetric mitochondrial distribution are not clear. Moreover, this notion is at odds with recent work describing a “shuffling” model for equivalent mitochondrial inheritance (Moore et al., 2021), and could suggest that different mechanisms are at a play in cells where asymmetrical division is used as a tool to affect differentiation.

### **1.2.7 Mitochondria can modulate CTL effector functions**

Despite the well-known shift to glycolysis following T cell receptor engagement, AMPK and mTOR signalling coordinate an increase in both mitochondrial mass and mtDNA in newly activated CD8<sup>+</sup> T cell (D'Souza et al., 2007), resulting in a profound alteration of the T cell proteome (Howden et al., 2019). Mitochondrial mass positively correlates with CTL anti-tumour function (Scharping et al., 2016). Tumours unresponsive to PD-1 therapy were shown to escape T cell-mediated immunosurveillance by either downregulating MHC-I expression, or by directly decreasing mitochondrial function through a soluble factor and independently from signalling events relying on transcription or translation (Kumar et al., 2020). This evidence alludes to a role for mitochondria in

T cell cytotoxicity. However, whether mitochondria play a direct role in killing has not been elucidated.

Mitochondria can support lymphocyte migration by ATP generation (Campello et al., 2006). Mitochondria have also been suggested to participate in calcium flux in CD4<sup>+</sup> T cells by acting as a mitochondrial membrane potential-dependent calcium store (Hoth et al., 1997). Engagement of either the TCR or the integrin LFA-1 induces mitochondrial migration towards the IS in CD4<sup>+</sup> T cells (Contento et al., 2010; Quintana et al., 2007). Polarised mitochondria are thought to sustain TCR signalling (Baixauli et al., 2011) and calcium flux by promoting CRAC channel activation (Hoth et al., 2000; Quintana et al., 2006; Schwindling et al., 2010). Sustained increases in intracellular calcium induces NFAT translocation to the nucleus, thus providing a role for mitochondria in regulating T cell transcription during the killing response (Contento et al., 2010; Hoth et al., 2000). Mitochondrial translocation to the IS depends on the fission factor DRP1 (Baixauli et al., 2011). Interestingly, *Drp1* silencing not only impairs mitochondrial polarisation at the IS, but also potentiates calcium flux (Baixauli et al., 2011; Simula et al., 2018).

A role for mitochondrial respiration in killing was also suggested by complex I inhibition, which precluded cytokine synthesis and degranulation in memory and effector T cells (Yi et al., 2006). Interestingly, impaired complex I activity affected TNF $\alpha$  production more than IFN $\gamma$  in CTLs. By contrast, the expression of both cytokines was dramatically downregulated in memory T cells (Yi et al., 2006). This highlights differences in cytokine regulation in effector and memory T cells, adding another layer of complexity to the role of mitochondrial function in different T cell populations.

### **1.2.8 Metabolism at the centre of gene expression and cytotoxicity**

An increasing amount of research has been devoted to the metabolic pathways employed by different subtypes of T cells, and how they might influence their effector function (Pearce et al., 2013). CTL metabolic plasticity is not only remarkable per se, but it also offers insights into potential anti-tumoral treatments. In the tumour microenvironment, CTLs preferentially uptake glucose, while cancer cells rely on glutamine uptake and only outcompete neighbouring T lymphocytes for glucose when glutamine is scarce (Reinfeld et al., 2021). Treating murine tumours with glutamine antagonists leads to decreased tumour proliferation by TCA cycle and glycolysis suppression. The effect of glutamine blockage on tumour-infiltrating lymphocytes seem to vary in different experimental setups (Leone et al., 2019; Reinfeld et al., 2021), but it appears to lead to augmented expression of cytokines and granzyme B, and increased expression of memory T cell markers, suggesting improved tumour

clearance ability (Leone et al., 2019). Thus, immunotherapeutic treatment could exploit the ability of T cells to re-route their metabolism while conserving efficient effector functions.

As detailed earlier, the expression of cytolytic proteins often relies on post-transcriptional regulation. Several metabolic enzymes are known to moonlight as RNA-binding proteins, altering both mRNA turnover and their recruitment to ribosome for translation initiation (Castello et al., 2015). A well-described member of these metabolic regulators is the enzyme glyceraldehyde 3-phosphate dehydrogenase (GAPDH), which canonically catalyses the formation of 1,3-biphosphoglycerate from glyceraldehyde 3-phosphate during the process of glycolysis (Chandel, 2015b). However, GAPDH can also act as a RBP by binding both tRNA (Singh and Green, 1993) and mRNA (Nagy and Rigby, 1995). mRNA binding occurs through the recognition of AU-rich elements (ARE) in the 3' UTR, often found in cytokine mRNA (Nagy and Rigby, 1995). Enforcing mitochondrial respiration disengages GAPDH from glycolysis and increases its activity as a RBP, resulting in decreased IFN $\gamma$  production (Chang et al., 2013). Additional metabolic enzymes that can act as RBPs include the glycolytic enzymes aldolase, enolase, pyruvate kinase and triosephosphate isomerase, together with enzymes catalysing fatty acid oxidation, TCA cycle and even nucleoside and amino acid metabolism (Castello et al., 2015). Thus, metabolic rewiring can play a role in post-transcriptional regulation by repurposing RBP to modulate the lymphocyte proteomic landscape (Turner and Diaz-Munoz, 2018).

Metabolic pathways also influence chromatin structure and accessibility by regulating histone methylation, acetylation, and lactylation (Franco et al., 2020). Strategies aimed at regulating the metabolic milieu in the tumour microenvironment are therefore focusing on exploiting metabolic regulation of epigenetics for therapeutic purposes (Van Acker et al., 2021). Mitochondrial dysfunction can lead to changes in metabolite abundances, which can in turn modify chromatin accessibility, leading to dysregulated gene expression and diminished T cell function. These chromatin modifications are crucial in CD8<sup>+</sup> T cells, as fixed chromatin accessibility (defined as a lack of amenability to modification) correlates with exhaustion in human CD8<sup>+</sup> T cells (Philip et al., 2017). Accumulation of depolarised mitochondria in tumour-infiltrating lymphocytes is associated with a transcriptomic signature and anergy typical of exhausted T cells (Yu et al., 2020). The hypoxic and stimulatory conditions found in the tumour microenvironment are thought to contribute to mitochondrial dysfunction, generating high levels of mtROS that upregulate exhaustion marker expression and impair cytokine synthesis (Scharping et al., 2021). Furthermore, dysfunctional mitochondria in CD4<sup>+</sup> T cells can induce cytokine storms and premature senescence in peripheral tissue, as it is occurs with T cells lacking the mitochondrial transcription factor TFAM (Desdin-Mico et al., 2020).

The exhaustion markers PD-1, CTLA-4 and TIM-3 all impair glucose uptake and glycolysis. In addition, the receptors LAG-3, 4-1BB and OX40 downregulate mitochondrial metabolism, compromising CTL functions and memory T cell survival (Madden and Rathmell, 2021). Modulating T cell metabolism might promote longer-term protection, as shown by studies where glycolysis inhibition was sufficient to skew T cell differentiation towards a memory phenotype and antitumour functions (Geiger et al., 2016; Sukumar et al., 2013). By understanding how metabolic choices affect T cell exhaustion and vice versa, it may be possible to improve on existing immunotherapeutic strategies (Zhang and Romero, 2018).

Evidence suggests that *in vivo* metabolism might be quite different from *in vitro* studies (Ma et al., 2019). This is partially caused by the unphysiological concentration of metabolites in standard tissue culture media, which poorly recapitulate *in vivo* conditions and might therefore alter the activation of metabolic and proliferation pathways (Cantor et al., 2017; Vande Voorde et al., 2019). Modulating glucose concentration in media is sufficient to alter the expression of activation markers, cytokines and proliferation in virus-specific CD8<sup>+</sup> T cells (Sanchez et al., 2020). Further research is therefore needed to clarify which metabolic pathways are utilised *in vivo* to better potentiate T cell response to virally infected cells and cancers.

## 1.3 The role of USP30 in cellular homeostasis

### 1.3.1 USP30: an inhibitor of pexophagy and mitophagy

The ubiquitin-specific protease 30 (USP30) is a transmembrane protein anchored to the outer membrane of mitochondria (Nakamura and Hirose, 2008) and peroxisomes (Marcassa et al., 2018) (**Figure 1.3**). In mitochondria, the N-terminus of USP30 is localised in the intermembrane space, and it is followed by an intermembrane domain flanked by positively charged residues, which is inserted in the OMM. The cytoplasmic portion of the protein mediates the enzymatic activity (Nakamura and Hirose, 2008). Expression of truncated USP30 bearing only the N-terminal and transmembrane sequence is sufficient for localisation to peroxisomes, while the addition of the positively charged residues results in expression in both peroxisomes and mitochondria (Marcassa et al., 2018).

USP30 was identified as a mitophagy inhibitor, as it cleaves ubiquitin chains on specific substrates on the OMM (Bingol et al., 2014). USP30 preferentially cleaves Lys6 and Lys11-linked ubiquitin (Cunningham et al., 2015; Deol et al., 2020; Gersch et al., 2017; Sato et al., 2017). In addition, USP30 delays PARKIN recruitment to mitochondria upon loss of mitochondrial membrane potential (Wang et al., 2015). Distally phosphorylated ubiquitin inhibits USP30, suggesting that prolonged PINK1-mediated phosphorylation could ultimately prevent deubiquitinase activity (Deol et al., 2020; Gersch et al., 2017; Sato et al., 2017). USP30 depletion results in enhanced ubiquitylation of OMM proteins and sensitises cells to apoptosis (Liang et al., 2015).

In addition to PARKIN, the E3 ubiquitin ligase MARCH5 has also been identified as a positive regulator of mitophagy counteracting the activity of USP30. MARCH5 is localised close to the TOM complex, and targets proteins entering the TOM channel for degradation (Phu et al., 2020). Loss of USP30 results in preferential ubiquitination of components of the TOM complex (TOM20, TOM5, TOM40, TOM70), and the anion channel proteins VDAC1, VDAC2 and VDAC3 in neurons (Ordureau et al., 2020). Taken together, these results support a role for USP30 in regulating mitochondrial protein import. These studies indicated the existence of mitophagy-inducing proteins in addition to PARKIN and MARCH5 (Ordureau et al., 2020), suggesting that the full picture of USP30-mediated quality control of mitochondria has not been fully elucidated yet.

Additional targets of USP30 include proteins interacting with the OMM, such as the fusion promoter MFN2 and the fission protein FIS1 (Ordureau et al., 2020). Interestingly, both overexpression (Chen et al., 2021) and downregulation (Nakamura and Hirose, 2008; Yue et al., 2014) of USP30 have been

linked to mitochondrial elongation, raising the possibility that modulating ubiquitination might affect mitochondrial dynamics. Furthermore, USP30 inhibition leads to the ubiquitination of the glycolytic enzyme hexokinase 1 (HK1) (Ordureau et al., 2020). HK1 can associate with the outer mitochondrial membrane (Craven and Basford, 1969; Kropp and Wilson, 1970) by interacting with VDAC1 (Fiek et al., 1982; Linden et al., 1982). This interaction is thought to couple the ATP-dependent enzymatic activity of HK1 to the site of ATP production (Gots and Bessman, 1974). The enzymes fatty acid synthase (FASN) and ATP-citrate synthase (ACLY) were also downregulated upon loss of USP30 (Ordureau et al., 2020). Therefore, USP30 can play a role in mitophagy flux, mitochondrial morphology and metabolism.

The localisation of USP30 on peroxisomes allows it to inhibit PEX2-induced ubiquitination and peroxisomal degradation (pexophagy) (Marcassa et al., 2018; Riccio et al., 2019) (**Figure 1.3**). It is currently unknown whether other E3 ligases counteract USP30 action on peroxisomes, or indeed if other deubiquitinases in addition to USP30 are directly responsible for modulating pexophagy. The only other well-characterised mammalian peroxisomal deubiquitinase, USP9X, seems to have a more general role in mediating protein import into the organelle by acting on the PEX5 shuttling receptor (Grou et al., 2012).

USP30 is not the only protein showing a promiscuous localisation or function in both mitochondria and peroxisomes. A few proteins regulating biogenesis (PGC-1 $\alpha$ ) (Bagattin et al., 2010; Wu et al., 1999) and fission (FIS1, DRP1, MFF) (Gandre-Babbe and van der Bliek, 2008; Koch et al., 2003; Koch et al., 2005) are common to both mitochondria and peroxisomes. The complex interplay between the two organelles is likely wider than previously appreciated. Patients exhibiting defects in peroxisome biogenesis (Zellweger's syndrome) display altered mitochondrial morphology and impaired mitochondrial respiration (Goldfischer et al., 1973). These phenotypes have also been described in mouse models of peroxisomal biogenesis or metabolism defects (Baes and Van Veldhoven, 2012). The molecular mechanisms responsible for the crosstalk between defective peroxisome and mitochondria are unknown, but they have been suggested to depend on the shared handling of ROS and lipid metabolism by mitochondria and peroxisomes (Fransen et al., 2017).

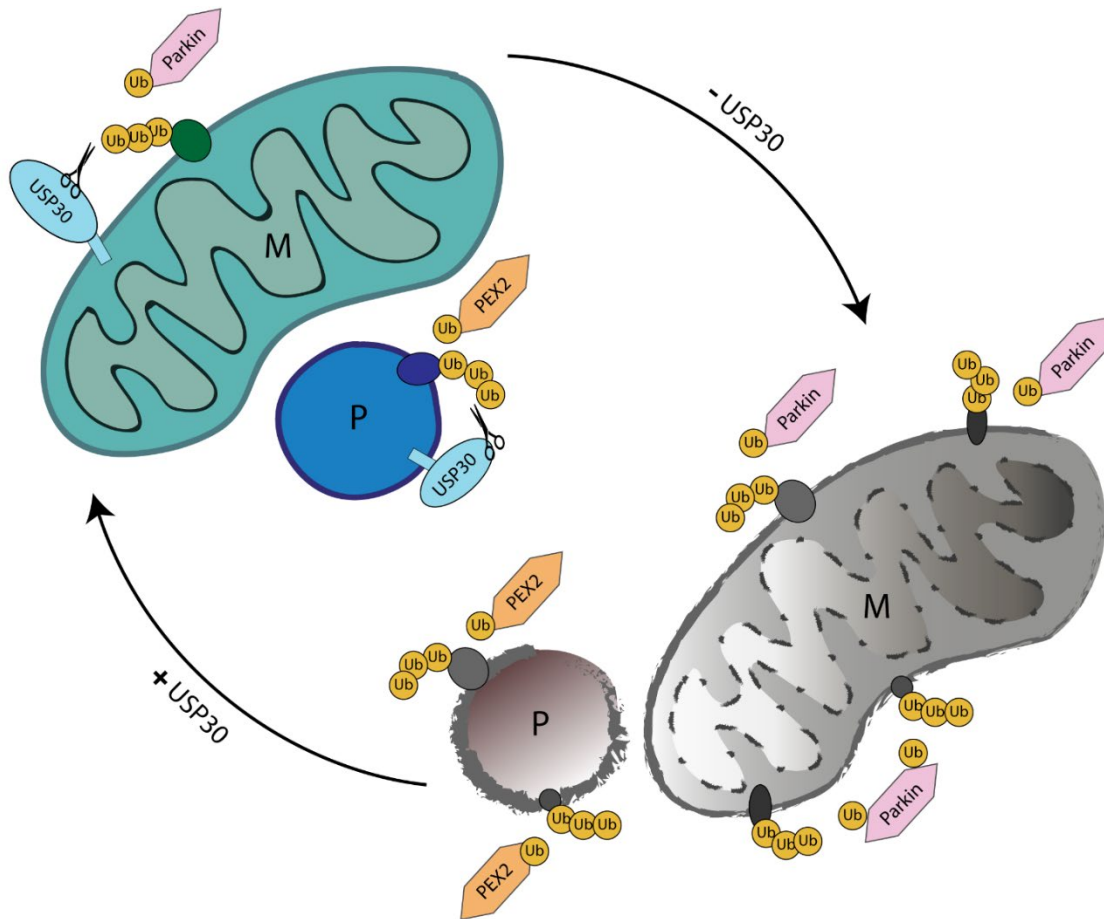


**Figure 1.3. USP30 negatively regulates mitophagy and pexophagy.**

USP30 cleaves ubiquitin chains from substrates on the outer mitochondrial (M) and peroxisomal (P) membrane, counteracting the E3 ligases PARKIN on mitochondria and PEX2 on peroxisomes. Loss of USP30 results in ubiquitin accumulation on the outer mitochondrial and peroxisomal membrane, triggering mitophagy and pexophagy.

### 1.3.2 USP30 as a therapeutic target

The role of USP30 as a mitophagy inhibitor has been under study as a potential therapeutic target for Parkinson's disease (Thobois, 2015). Cellular degeneration observed in Parkinson's patients is thought to be partially caused by a disruption in mitochondria quality control pathways. Hereditary Parkinson's is often linked to loss of function mutations in *Pink1* and *Parkin* (Pickrell and Youle, 2015). As previously described, PINK1 and PARKIN trigger mitophagy initiation, while downregulation of their activity prevents the clearance of damaged mitochondria. Based on this model, USP30 depletion is supposed to restore cellular homeostasis by removing the break on mitophagy and therefore facilitating the degradation of mitochondria.

The development of pharmacological treatments for Parkinson's disease has focused on activators of PINK1 and PARKIN and on inhibitors of mitochondrial deubiquitinases (DUBs) (Miller and Muqit, 2019). In addition to USP30, other mitophagy regulators include USP8 (Durcan et al., 2014), USP14 (Chakraborty et al., 2018), USP15 (Cornelissen et al., 2014), USP35 (Wang et al., 2015) and ATXN3 (Durcan et al., 2011). Interestingly, USP14 has been shown to counteract mitophagy via a PINK1/PARKIN-independent pathway (Chakraborty et al., 2018). Not all DUBs negatively regulate mitophagy: for example, ATXN3 and USP8 do not affect PARKIN substrates but rather PARKIN itself, affecting its stability and its recruitment to mitochondria (Durcan et al., 2011; Durcan et al., 2014). Finally, some DUBs are known to be involved in the development of Parkinson's related phenotype by alternative pathways. This is the case for USP9X, which acts on  $\alpha$ -synuclein, whose aggregation is thought to be toxic in neurons (Rott et al., 2011).

USP30 is the only deubiquitinase known to be anchored to the OMM (Urbe et al., 2012). Its role is specific to mitophagy and pexophagy regulation, while other DUBs are involved in additional processes such as modulating proteasome-mediated degradation and endosomal trafficking (Chakraborty and Ziviani, 2020). Because of its well-characterised and restricted mode of action, USP30 has been chosen as a target for the development of inhibitors that could be used as therapeutic solutions for Parkinson's disease patients (Kluge et al., 2018; Rusilowicz-Jones et al., 2020; Yue et al., 2014). It is currently unknown whether USP30 downregulation could be beneficial or detrimental in tissues other than the neuronal system. A recent report characterised the *in vivo* effects of USP30 by measuring mitophagy in the heart, brain and liver tissue of mice treated with a USP30 inhibitor (Luo et al., 2021). Interestingly, only the cardiac tissue showed a detectable increase in mitophagy, suggesting that the role of USP30 could be either tissue-specific or subject to different rates of metabolic breakdown in different tissues (Luo et al., 2021).

*In vitro* studies have investigated the role of USP30 in a variety of immortalised cell lines, such as HeLa, HEK293T, MEFs, SH-SY5Y, U2OS, RPE1 and COS7 (Bingol et al., 2014; Cunningham et al., 2015; Marcassa et al., 2018; Nakamura and Hirose, 2008; Phu et al., 2020; Riccio et al., 2019) and in neurons derived from human embryonic stem cells (Ordureau et al., 2020). To date, the role of USP30 has not been investigated in primary cell lines. The lack of studies in additional models prevents a full understanding of the role of USP30 in other tissues. Specifically, the effects of USP30 depletion in the immune system have not been explored.

## 1.4 Aims of this work

USP30 was recently identified as a novel regulator of T cell cytotoxicity in a large screen aimed at uncovering new regulators of the immune response (Abeler-Dörner et al., 2020). This work showed that *Usp30*<sup>-/-</sup> mice had no apparent morphological or developmental defect but exhibited diminished CD8<sup>+</sup> T cell cytotoxicity and altered susceptibility to dextran sulfate sodium (DSS)-induced colitis (Abeler-Dörner et al., 2020). While the role of mitochondria has been described in T cell differentiation and metabolism, little is known about the way that mitochondria affect the ability of CD8<sup>+</sup> effector T cells to kill, and specifically which mitochondrial functions might mediate cytotoxicity.

The aim of this thesis is to understand how USP30 depletion leads to a loss of CTL killing. First, I will provide a characterisation of mitochondria and peroxisomes in *Usp30*<sup>-/-</sup> CTLs, followed by a morphological and functional analysis of the mitochondrial population in USP30-depleted CTLs. Next, I will investigate the cytotoxicity defect in a stepwise manner focusing on cell migration, target cell recognition, T cell signalling and lytic granule polarisation at the immunological synapse.

I will then explore T cell development and cytotoxicity in different murine and CRISPR knockout models to probe for the requirement for specific mitochondrial functions in CTL killing. Finally, I will examine pathways known to link mitochondrial fitness to cellular homeostasis to understand how optimal mitochondrial function regulates T cell-mediated immunosurveillance.



## **CHAPTER 2**

### **Materials and Methods**



## 2.1 Mouse strains

Wild-type (WT), *Usp30*<sup>-/-</sup> mice (C57BL/6N background) and *mt-tRNA<sup>Ala</sup>* mice (C57BL/6J background) were bred and housed in a specific-pathogen-free (SPF) mouse facility at the Anne McLaren Building on the Cambridge Biomedical Campus. *mt-tRNA<sup>Ala</sup>* mice were a kind gift from Stephen Burr and Patrick Chinnery (Mitochondrial Biology Unit, University of Cambridge). *Ttc19*<sup>-/-</sup> and *Ndufs4*<sup>-/-</sup> mice were a generous gift from Carlo Viscomi and Massimo Zeviani (Department of Neuroscience, University of Padova). Splens were extracted from 3-6 months (*Usp30*<sup>-/-</sup>), 4-weeks (*Ndufs4*<sup>-/-</sup>), 3-5 months (*Ttc19*<sup>-/-</sup>) and 2-3 months old (*mt-tRNA<sup>Ala</sup>*) mice. All animals were age and gender-matched with control (WT) animals housed in the same mouse facility.

This research has been regulated under the Animals (Scientific Procedures) Act 1986 Amendment Regulations 2012 following ethical review by the University of Cambridge Animal Welfare and Ethical Review Body (AWERB).

## 2.2 Cell culture and generation of stable cell lines

Splenocytes were activated as a single cell suspension on plate-bound 0.5 µg/ml hamster α-mouse CD3ε (clone eBio500A2) (eBioscience, 16-0033-86) and 1 µg/ml hamster α-mouse α-CD28 (clone 37.51) (eBioscience, 16-0281-82) for 48h at 37°C. CTLs were cultured in RPMI supplemented as indicated in **Table 2.1**. CD8<sup>+</sup> T cells were purified 3 days after stimulation (unless otherwise indicated in the text) using the mouse CD8a<sup>+</sup> T Cell Isolation Kit (MACS Miltenyi Biotec, 130-104-075) following manufacturer's instructions.

**Table 2.1. Mouse T cell media.**

Reagent	Concentration	Supplier
RPMI with L-glutamine and sodium bicarbonate	–	Sigma-Aldrich, 1640
Foetal bovine serum (FBS)	10%	LabTech, FBS-Sa
L-glutamine	2 mM	Sigma-Aldrich, G7513
Murine IL-2	100 U/ml	Peptotech, 212-12
β-mercaptoethanol	50 µM	Thermo Fisher Scientific, 31350010
Sodium pyruvate	1 mM	Thermo Fisher Scientific, 11360070
Penicillin	100 U/ml	Sigma-Aldrich, P0781
Streptomycin	0.1 mg/ml	Sigma-Aldrich, P0781

P815 mouse mastocytoma cells (ATCC, TIB-64) were used as target cells in cytotoxicity assays, degranulation assays and for conjugate immunofluorescence staining. P815 cells were grown in DMEM (Thermo Fisher Scientific, 41966052) supplemented with 10% FBS (LabTech, FBS-Sa), 100U/ml penicillin and 0.1 mg/ml streptomycin (Sigma-Aldrich, P0781), hereafter referred to as target cell media. P815 used in the IncuCyte-based cytotoxicity assay were transduced with the NucLight lentiviral vector by Katharina Strege, enabling mKate2 nuclear expression (Essen Bioscience, 4625). NucLight-expressing P815 were grown in target cell media under 1  $\mu$ g/ml puromycin selection (Thermo Fisher Scientific, A1113803). Blue P815 used for conjugate immunofluorescence were generated by Alex Ritter and Yukako Asano by retroviral transduction. pMig-rThy1.1 was used stably express tagBFP2 fused to a farnesylation sequence (Farnesyl-5-TagBFP2) to drive BFP2 expression on the P815 plasma membrane (Ritter et al., 2013). Blue P815 were grown in target cell media as indicated above.

### **2.3 Pharmacological treatments**

Mitochondrial translation was inhibited by supplementing cell culture media with 100 nM-10  $\mu$ g/ml doxycycline (Merck, D9891) or 50-500  $\mu$ g/ml chloramphenicol (Sigma-Aldrich, R4408) as indicated in the text for the entire duration of the killing and translation assays. CTLs used for immunoblots were treated with 10  $\mu$ g/ml doxycycline or 500  $\mu$ g/ml chloramphenicol for 4h before cell lysis. To monitor autophagic flux, CTLs were either left untreated or treated with 400 nM bafilomycin A (Enzo Life Sciences, BML-CM110) for 4h at 37°C. The integrated stress response was inhibited using 100 nM ISRIB (Sigma-Aldrich, SML0843) for the entire duration of killing and translation assay as above, and for 4h in CTLs used for immunoblots.

Mitochondrial fission was inhibited using 10  $\mu$ M mDIVI-1 (Sigma-Aldrich, 475856) and mitochondrial fusion was promoted using 20  $\mu$ M M1 (Sigma-Aldrich, 475859) as previously described (Buck et al., 2016). CTLs were treated for 6h, 24h and 48h as indicated in the text. mDIVI-1 and M1 were supplemented to the cell culture media for the entire duration of the killing and translation assays.

## 2.4 Nucleofection procedure and plasmids

Primary CTLs were nucleofected using the 4D-Nucleofector System (Lonza).  $5 \times 10^6$  CTLs were resuspended in P3 Primary Cell Nucleofector™ Solution (Lonza, V4XP-3024) containing 5 µg of plasmid DNA and they were nucleofected in the Nucleocuvette™ Vessel (Lonza, V4XP-3024) using the primary mouse T cell programme. Post-nucleofection, cells were incubated for 4h at 37°C in mouse T Cell Nucleofector™ Medium (Lonza, VZB-1001) supplemented with 10% FBS (LabTech, FBS-Sa) and 2mM L-glutamine (Sigma-Aldrich, G7513) to promote recovery. CTLs were split after 4h in mouse T cell media and used for assays 16-24h after nucleofection, unless otherwise indicated.

CTLs were nucleofected with Lifeact-mApple for migration analysis via live cell microscopy. Lifeact-mApple was a gift from Michael Davidson (Addgene, plasmid 54747). Mitophagy and pexophagy were analysed via nucleofection with plasmids expressing the coral-derived protein Keima targeted to either the mitochondrial inner membrane (mt-Keima) or to the peroxisome lumen (Keima-SKL). The mt-Keima construct was originally a gift from Martin Bennet (University of Cambridge), and it was cloned in the pEGFP-C1 vector in place of the EGFP tag by Christian Gawden-Bone (University of Cambridge). The Keima-SKL construct was a kind gift from Sylvie Urbé (University of Liverpool) (Marcassa *et al.*, 2018).

## 2.5 Analysis of T cell populations in murine splenocytes

Single cell suspension splenocytes (day 0 T cells,  $1 \times 10^6$  cells/sample) were washed in FACS buffer (PBS, 1% FBS) and surface markers were labelled using the following antibodies: 2.5 µg/ml Alexa Fluor 488 α-CD4 (clone RM4-5) (BioLegend, 100532), 1 µg/ml Brilliant Violet 711 α-CD8 (clone 53-6.7) (BioLegend, 100748), 1 µg/ml APC α-CD44 (clone IM7) (BioLegend, 103012), 1 µg/ml PE α-CD62L (clone MEL-14) (eBioscience, 12-0621-81). Surface labelling was performed at 4°C for 30 min. CTLs were washed, then fixed and permeabilised using the Foxp3 nuclear staining kit (Thermo Fisher Scientific, 00-5523-00) following the instructions provided by the manufacturer. All samples were treated with 1 µg/ml FCR block (α-CD16/32) (BioLegend, 101302) for 5 min at room temperature to block unspecific staining. Intracellular staining was performed using 1 µg/ml eFluor450 α-FOXP3 (clone FJK-16s) (eBioscience, 48-5773-80) or 1 µg/ml Rat IgG2aκ isotype control (clone eBR2a) (Thermo Fisher Scientific, 48-4321-80) for 30 min at room temperature. Cells were rinsed in permeabilization buffer and PBS and resuspended in PBS for analysis. Samples were analysed on an Attune NxT Acousting Focusing Cytometer (Thermo Fisher Scientific) using the Attune NxT Software (Invitrogen).

## 2.6 LDH cytotoxicity assays

P815 target cells and day 5 CTLs were resuspended in RPMI with no phenol red (Thermo Fisher Scientific, 32404014) supplemented with 2% FBS (LabTech, FBS-Sa), 100 U/ml penicillin and 0.1 mg/ml streptomycin (Sigma-Aldrich, P0781) at  $10^5$  cells/ml ( $10^4$  target cells per sample). P815 target cells were coated with 0.5  $\mu$ g/ml hamster  $\alpha$ -mouse CD3 $\epsilon$  (clone eBio500A2) (eBioscience, 16-0033-86) to allow for CTL killing by re-directed lysis. CTLs were resuspended in RPMI with no phenol red (supplemented as described above) at  $10^6$  cells/ml. CTLs were serially diluted to test multiple CTL to target ratios (25:1, 12.5:1, 6.25:1, 3.1:1, 1.5:1, 0.75:1 ratios, corresponding to  $2.5 \times 10^5$ ,  $1.25 \times 10^5$ ,  $6.25 \times 10^4$ ,  $3.1 \times 10^4$ ,  $1.5 \times 10^4$  and  $7.5 \times 10^3$  CTLs). CTLs were incubated with P815 targets for 2.5h. Target cell apoptosis resulted in the release of LDH in the cell culture media, which was quantified by colorimetric measurement using the CytoTox 96 non-radioactive cytotoxicity assay (Promega, G1780). Cell culture supernatant was mixed with substrate buffer and incubated at room temperature for 30 min. LDH concentration was calculated by measuring absorbance at 490 nm with a SpectraMax M5 spectrophotometer (Molecular Devices) using the SoftMaxPro 5.4.1 software (Molecular Devices). Percentage of target cell lysis was computed by assessing non-specific cell death (P815 in culture media) and complete cell death (P815 incubated with lysis buffer) as reference values.

## 2.7 IncuCyte® cytotoxicity assay

P815-NucLight were resuspended at  $4 \times 10^4$  cells/ml (effector:target ratio=10:1) or  $4 \times 10^5$  cells/ml (effector:target ratio=1:1) cells/ml and incubated with 1  $\mu$ g/ml hamster  $\alpha$ -mouse CD3 $\epsilon$  (clone eBio500A2) (eBioscience, 16-0033-86) to allow for CTL recognition by TCR crosslinking.  $4 \times 10^3$  (effector:target ratio=10:1) or  $4 \times 10^4$  (effector:target ratio=1:1) target cells per sample were seeded in an ultra-low attachment round-bottom 96-well plate (Corning, 7007) and pelleted by centrifugation. Day 5 CTLs were resuspended at  $4 \times 10^5$  cells/ml and  $4 \times 10^4$  CTLs per sample were seeded on top of target cells at the effector:target ratios indicated in the text. Samples were imaged using the IncuCyte® S3 Live Cell Analysis System (Essen Bioscience). Vessels were scanned using a 4 X objective lens in both the brightfield and red (excitation: 655 nm; emission: 681 nm) channels. Analysis of IncuCyte® data was performed using the IncuCyte® S3 2018-2021 software (Essen BioScience). Spheroid quantification in the red channel was set up using a top-hat segmentation specifying particle radius and RCU threshold. High background was excluded by filtering on particles

eccentricity and mean integrated intensity. Loss of red fluorescence intensity was used as an indicator of target cell apoptosis.

## 2.8 Degranulation assay

P815 target cells were resuspended at  $2 \times 10^6$  cells/ml in mouse T cell media and coated with 1  $\mu\text{g/ml}$  hamster  $\alpha$ -mouse CD3 $\epsilon$  (clone eBio500A2) (eBioscience, 16-0033-86) to induce TCR crosslinking on CTLs. Day 5 CTLs were resuspended at  $2 \times 10^6$  cells/ml in mouse T cell media. 2  $\mu\text{g/ml}$  PE  $\alpha$ -mouse CD107a (LAMP1) (BioLegend, 12-1071-83) was added to day 5 CTLs to label lytic granule delivery to the plasma membrane. CTLs were either left unstimulated or stimulated with 0.5  $\mu\text{g/ml}$  hamster  $\alpha$ -mouse CD3 $\epsilon$  (clone eBio500A2) (eBioscience, 16-0033-86)-coated P815.  $2 \times 10^5$  CTLs and targets were co-incubated for 2.5h at 37°C.

Surface staining was performed with 1  $\mu\text{g/ml}$   $\alpha$ -CD8 Brilliant Violet 711 (clone 53-6.7) (BioLegend, 100748) and 1:200 Zombie Yellow (BioLegend, 423103) for 20 min at 4°C. Samples were resuspended in PBS and degranulation was quantified by measuring LAMP1 signal on cell surface using an Attune NxT Acousting Focusing Cytometer (Life Technologies).

## 2.9 Calcium flux assay

Day 5 CTLs were resuspended at  $10^6$  cells/ml in mouse T cell media.  $0.5-1 \times 10^6$  cells were incubated with 1  $\mu\text{M}$  INDO-1, AM (Thermo Fisher, I1223) for 30 min at 37°C. Surface staining was performed by incubating the cells with 1  $\mu\text{g/ml}$  APC  $\alpha$ -mouse CD8 (clone 53-6.7), (BioLegend, 100712) and 5  $\mu\text{g/ml}$  hamster  $\alpha$ -mouse CD3 $\epsilon$  (clone eBio500A2) (eBioscience, 16-0033-86) for 15 min at RT. CTLs were resuspended in complete mouse T cell media and basal INDO-1 MFI was recorded for 1 min. TCR crosslinking was achieved by adding 50  $\mu\text{g/ml}$  goat  $\alpha$ -hamster (Thermo Fisher Scientific, 31115) to the sample and immediately recording subsequent calcium fluxes for up to 5 min after stimulation. After 5min of INDO-1 fluorescence recording, 1  $\mu\text{g/ml}$  ionomycin was added to CTLs to measure maximal calcium flux for 2 min.

All data was acquired on an LSR Fortessa (Becton Dickinson) using the BD FACSDIVA software (BD Biosciences). For ratiometric analysis, INDO-1 was excited at 355 nm and emission was collected at 450 nm (Ca<sup>2+</sup>-unbound) and at 379 nm (Ca<sup>2+</sup>-bound). The MFI ratio ( $379/450 = \text{Ca}^{2+}\text{-bound} / \text{Ca}^{2+}\text{-unbound}$ ) was plotted against time to display calcium flux.

## 2.10 SDS-PAGE and immunoblotting

Cells were lysed in RIPA buffer (50mM Tris HCl pH 8.0, 150mM NaCl, 1% NP-40, 0.5% sodium deoxycholate, 0.1% SDS) at  $2 \times 10^7$  cells/ml. Prior to loading on 4-12% Bis-Tris protein gel (NuPAGE, NP0322BOX), lysates were denatured at 95°C for 5 min in NuPAGE 10X Sample Reducing Agent (500mM DTT) (Thermo Fisher Scientific, NP0009) and NuPAGE 4X LDS Sample Buffer, pH 8.4 (Thermo Fisher Scientific, NP0007). Samples run on 7.5% non-reducing gels were mixed with 4X LDS Sample Buffer only and they were not boiled.

Reducing gels were run at 120 V constant voltage in NuPAGE MES running buffer (Thermo Fisher Scientific, NP0002). Non-reducing gels were run at 100 V in Tris-Glycine running buffer (25mM Tris, 192 mM glycine, 0.1% SDS). Reduced samples were transferred to an Amersham Protran 0.45  $\mu$ m nitrocellulose membrane (GE Healthcare Life science, 10600002) using a Power Blotter Semi-Dry Transfer System (Thermo Fisher Scientific). Samples run on non-reducing 7.5% gels were transferred in Novex Tris-Glycine Transfer Buffer (Thermo Fisher Scientific, LC3675) using a wet-transfer system at 300 mA for 90 min.

Membranes were blocked in 5% milk powder or 5% BSA (as indicated by the antibody manufacturer) for 45-60 min at room temperature before overnight incubation at 4°C with primary antibodies (**Table 2.2**). Membranes were washed in TBS + 0.1% Tween and then incubated for 1h at room temperature with HRP-conjugated secondary antibodies (**Table 2.2**). HRP signal was detected using Amersham ECL prime detection reagents (GE Healthcare, RPN2232) and a ChemiDoc MP Imaging System (Bio-Rad). Images were acquired using Image Lab 4.1 (Bio-Rad). Western blot images were labelled for presentation purposes using Illustrator 2020 (Adobe).

**Table 2.2. List of primary and secondary antibodies used for immunoblotting.**

Target	Species	Supplier	Dilution
<b>Primary antibodies</b>			
β-actin (clone AC-15)	Mouse	Sigma-Aldrich, A1978	1:5000
Calnexin	Rabbit	Sigma-Aldrich, C4731	1:5000
Granzyme B	Rabbit	Abcam, ab4059	1:500
Perforin	Rat	Enzo Life Sciences, ALX-804-057-C100	1:500
TOM20	Mouse	Abcam, ab56783	1:100
PMP70	Mouse	Sigma-Aldrich, SAB4200181	1:1000
PEX16	Rabbit	Atlas Antibodies, HPA043286	1:500
4EBP1	Rabbit	Cell Signaling Technology, 9452S	1:500
Phospho-4EBP1 (Thr37/46)	Rabbit	Cell Signaling Technology, 9459S	1:500
eIF2a	Rabbit	Cell Signaling Technology, 9722S	1:500
Phospho-eIF2a (Ser51, clone D9G8)	Rabbit	Cell Signaling Technology, 3398S	1:500
Phospho-S6 (Ser240/244)	Rabbit	Cell Signaling Technology, 5364S	1:500
S6 ribosomal protein (clone 54D2)	Rabbit	Cell Signaling Technology, 2317S	1:500
ATF4 (clone D4B8)	Rabbit	Cell Signaling Technology, 11815S	1:500
PINK1	Rabbit	Novus, BC100-494	1:500
PINK1	Rabbit	Abcam, ab23707	1:500
<b>Secondary antibodies</b>			
HRP α-rabbit	Goat	Thermo Fisher Scientific, A16110	1:10,000
HRP α-mouse	Goat	Thermo Fisher Scientific, A16078	1:10,000
HRP α-rat	Goat	Thermo Fisher Scientific, 31470	1:10,000

## 2.11 RNA extraction and real-time qPCR

Total RNA was extracted 5 days after stimulation from  $5 \times 10^6$  CTLs using the RNeasy mini kit (Qiagen, 74104) and QIAshredder columns (Qiagen, 79654) following manufacturer's instructions. RNA yield was quantified using NanoPore OneC spectrophotometer (Thermo Fisher Scientific) and 100 ng per sample were used to synthesise cDNA using the Accuscript high fidelity 1<sup>st</sup> strand cDNA synthesis kit (Agilent, 200820). Granzyme B and perforin gene expression was measured using the TaqMan Gene Expression Master Mix (Thermo Fisher Scientific, 4369016) and the relevant qPCR probes (Thermo Fischer Scientific, 4331182) for mouse transcripts: granzyme B (Mm00442837\_m1), perforin (Mm00812512\_m1) and TATA-binding protein (*Tbp*) (Mm01277042\_m1) as a control. Data was acquired using the 7500 Real-Time PCR System (Thermo Fisher Scientific). mRNA abundance was quantified by calculating the  $C_T$  of the target of interest and normalising it to *Tbp* ( $\Delta C_T$ ).

## 2.12 Measurement of mitochondrial mass, membrane potential and mtROS

Day 0 (splenocytes) and day 3, 5 and 7 CTLs were resuspended at  $10^6$  cells/ml in mouse T cell media.  $10^6$  cells (splenocytes) and  $10^5$  CTLs (day 3-7 post-stimulation) per sample were stained using 1:400 Zombie Yellow Fixable Viability Kit (BioLegend, 423103) and 1  $\mu$ g/ml Brilliant Violet 711  $\alpha$ -mouse CD8a antibody (clone 53-6.7) (BioLegend, 100748) for 15 min at room temperature. Cells were then incubated with 100 nM Mitotracker Green (Thermo Fisher Scientific, M7514) or 100nM MitoTracker Deep Red (Thermo Fisher Scientific, M22426) and 100 nM TMRE (Abcam, ab113852) for 30 min at 37°C to label mitochondrial mass and membrane potential, respectively. Samples were run on an LSR Fortessa (Becton Dickinson). All data was acquired using the BD FACSDIVA software (BD Biosciences).

mtROS were measured in day 5 CTLs. Cells were resuspended at  $10^6$  cells/ml and  $10^5$  CTLs were stained with 1  $\mu$ g/ml Brilliant Violet 711  $\alpha$ -mouse CD8a antibody (clone 53-6.7) (BioLegend, 100748) for 15 min at room temperature. CTLs were then incubated with 5 $\mu$ M MitoSOX (Thermo Fisher Scientific, M36008) for 5 min at 37°C. Control samples were treated with 10 $\mu$ M antimycin A during MitoSOX incubation. Cells were analysed on an Attune NxT Acousting Focusing Cytometer (Thermo Fisher Scientific) using the Attune NxT Software (Invitrogen).

## 2.13 Immunofluorescence staining and samples imaging

For mitochondrial staining, day 5 CTLs were washed and resuspended at  $1.5 \times 10^6$  cells/ml in serum-free RPMI (Sigma-Aldrich, 1640) to promote adherence to multispot microscope slides (Hendley-Essex, PH005).  $4.5 \times 10^4$  CTLs per well were incubated at 37°C for 10 min. For TOM20 and PDH staining, cells were fixed with 5% paraformaldehyde (PFA) (Electron Microscopy Sciences, 3025-89-4) for 15 min at 37°C. All steps after fixation were performed at room temperature. Excess PFA was quenched in 50mM ammonium chloride and cells were permeabilized for 10 min in either 0.1% Triton X-100 (Sigma-Aldrich, T878) for PDH staining, or 0.1% saponin (Sigma-Aldrich, S7900) for TOM20 staining. For catalase staining, cells were fixed and permeabilised in methanol for 5 min at -20°C. Non-specific antibody binding was minimized using 1% BSA as a blocking agent (Sigma-Aldrich, A7906) for PDH and catalase staining, or 1% BSA + 0.1% saponin for TOM20 staining. The outer mitochondrial membrane (TOM20), inner mitochondrial matrix (PDH), and peroxisomes (catalase) were labelled by incubating samples with primary antibodies (**Table 2.3**) for 2h at room temperature. Cells were then incubated with fluorescently conjugated secondary antibodies (**Table 2.3**) for 1h at room temperature. Samples were washed in PBS containing 1:10,000

Hoechst 33342 (Thermo Fisher Scientific, H3570) and mounted in ProLong Diamond Antifade Mounting medium (Thermo Fisher Scientific, P36961) using 22x64 mm No.1.5 cover slips (Scientific Laboratory Supplies LTD., MIC3248).

Conjugate formation was achieved by washing day 5 CTLs and BFP2-expressing P815 target cells in serum-free RPMI (Sigma-Aldrich, 1640) and resuspending cells at  $2 \times 10^6$  cells/ml. Target cells were coated with  $1 \mu\text{g/ml}$   $\alpha\text{-CD3}\epsilon$  (clone eBio500A2) (eBioscience, 16-0033-86). CTLs and P815 were then mixed at a 1:1 ratio (final concentration= $10^6$  cells/ml) and incubated on multisport microscope slides for 20 min at  $37^\circ\text{C}$  ( $3 \times 10^4$  CTLs and  $3 \times 10^4$  target cells per well). Cells were supplemented with complete mouse T cell media after settling to prevent side-effects due to starvation. Samples were then mixed and permeabilised in methanol for 5 min at  $-20^\circ\text{C}$ . Non-specific staining was minimised by blocking in 1% BSA. Cells were incubated for 2h at room temperature with primary antibodies against LAMP1,  $\gamma$ -tubulin and CD8 (**Table 2.3**). Secondary antibody staining was performed at room temperature for 1h (**Table 2.3**). Samples were mounted as described above.

Mitochondria were imaged on a Laser Scanning Microscope 880 (Zeiss) using the Zen Black software (Zeiss) for image acquisition of mitochondrial structures. Increased spatial resolution and decreased signal-to-noise ratio were achieved through Airyscan mode image acquisition and processing using the Zen Black software. Fluorophores were excited at 405, 488, and 561 nm and single planes were imaged for each sample using a 63 X objective. Peroxisomes and conjugate formation were imaged as a z-stack at  $0.5 \mu\text{m}$  intervals using an Andor Revolution spinning disk microscope (Andor Technology, Oxford instruments). Fluorophores were excited at 405, 488, 561 and 633 nm. Z-stacks were imaged for each sample using a 63 X or 100 X objective.

**Table 2.3. List of primary and secondary antibodies used for immunofluorescence.**

Target	Species	Supplier	Dilution
<b>Primary antibodies</b>			
TOM20	Mouse	Abcam, ab56783	1:100
PDH	Mouse	Abcam, ab110330	1:2000
$\gamma$ -tubulin	Rabbit	Sigma-Aldrich, T5192	1:1000
LAMP1 (clone 1D4B)	Rat	Supernatant (laboratory stock)	1:100
Alexa Fluor 488-conjugated $\alpha\text{-CD8a}$	Mouse	eBioscience, 53-0081-82	1:100
Catalase	Mouse	Abcam, ab16771	1:400
<b>Secondary antibodies</b>			
Alexa Fluor 546 $\alpha$ -mouse	Goat	Thermo Fisher Scientific, A-11030	1:400
Alexa Fluor 633 $\alpha$ -rabbit	Donkey	Thermo Fisher Scientific, A-21071	1:400

## **2.14 Live cell microscopy and quantitation of cell migration, mitophagy and pexophagy**

For all live imaging experiments, 3.5 cm dishes (MatTek) were coated with 0.5 µg/mL recombinant mouse ICAM-1/CD45 Fc chimera protein (R&D Systems, 796-IC) overnight at 4°C to promote CTL adherence. On the day of the assay, cells were resuspended at  $1.5 \times 10^6$  cells/ml in CO<sub>2</sub>-independent media with no phenol red (Gibco, 18045-054) supplemented with 10% FBS (LabTech, FBS-SA) and 2mM L-glutamine (Sigma-Aldrich, G7513).  $2 \times 10^6$  CTLs per sample were transferred to the dish and allowed to settle for 10 min. Single planes were imaged for 5 min using a 63 X objective. All data was acquired with a Laser Scanning Microscope 780 (Zeiss) using the Zen Black software (Zeiss).

$5 \times 10^6$  CTLs were nucleofected with 5 µg mt-Keima on day 4 post-stimulation and imaged on day 5 post-stimulation for mitophagy analysis. Pexophagy was detected by nucleofecting  $5 \times 10^6$  CTLs with 5 µg Keima-SKL on day 4 and 6 post-stimulation and by imaging samples on day 5 and 7, respectively. Mitophagy and pexophagy events were detected by exciting the Keima probe with either a 488 nm laser (optimal excitation at pH=8) or a 561 nm laser (optimal excitation at pH=4.5). Keima fluorescence was assessed by using the Imaris spot tracking function to filter mitochondria (mt-Keima) and peroxisome (Keima-SKL) signal. The median fluorescence intensity (MFI) was then calculated for each object, and spots were defined as “red” if the red channel MFI was more than two-folds higher than the green channel MFI. The percentage of red spots per image was quantified to display percentage of mitophagy (mt-Keima) and pexophagy (Keima-SKL) events.

Cell migration was quantified in day 5 CTLs.  $5 \times 10^6$  day 4 CTLs were nucleofected with 5 µg Lifeact-mApple and stained on the day of the assay (day 5 post-stimulation) with 1:50,000 Hoechst (5 min, room temperature) to label cell nuclei. Lifeact-mApple signal was detected using the 561 nm laser, while Hoechst signal was detected using the 405 nm laser. The speed of CTL migration was quantified using ImageJ v1.52 (NIH). The TrackMate plugin was used to filter nuclei of live cells to track their motion as an indicator of cell migration. The average track speed was then exported for each cell and plotted to display CTL migration speed.

## **2.15 Sample preparation and processing for transmission electron microscopy**

For TEM experiments, day 4 CD8<sup>+</sup> T cells were FACS sorted by labelling with 1:400 Zombie Aqua (BioLegend, 423102) and 1 µg/ml APC α-mouse CD8, (BioLegend, 100712) then incubated at 37°C in 10% CO<sub>2</sub> for 16-24h to promote recovery after sorting. Day 5 CTLs were washed in serum-free RPMI (Sigma-Aldrich, 1640), and plated onto 4-well plastic tissue culture plates (Nunc) at 1-2x10<sup>6</sup> cells/well. Samples were incubated 37°C for 20 min to allow cells to adhere to the plates, then fixed in 2% PFA (Electron Microscopy Sciences, 15710-S) / 1.5% glutaraldehyde (Agar Scientific) and, after washing, post-fixed in 1% osmium then 0.5% uranyl acetate after which the samples were processed for EPON embedding as previously described (Jenkins et al., 2009). Thin sections (60-80 nm) were post-stained with lead citrate and imaged using a FEI Tecnai G2 Spirit BioTWIN transmission EM (Eindhoven) with a Gatan 4K US1000 CCD camera and FEI TIA software. For quantitation studies, images were collected of every individual cell profile within 4-5 grid squares of a single section for each WT and KO CTL sample. Mitochondrial phenotype was analysed in 128 WT and 154 KO cells and scored as follows: “none” (no mitochondria), “normal” (normal mitochondria) and “disrupted” (mitochondria with disrupted cristae), All phenotypes refer to mitochondrial morphology as observed in a single cell profile. Lytic granule number and cross-sectional area was analysed in 139 WT and 164 KO cell profiles, with the Photoshop lasso tool (Adobe) used to calculate granule cross sectional area (nm<sup>2</sup>). Cell profiles were scored for markers of sectioning plane to ensure a similar range of cell section depths was sampled for both CTL populations.

## **2.16 Seahorse Mito Stress Assay**

Analysis of mitochondrial respiration and glycolytic rate was performed using a Seahorse XFe96 extracellular flux analyser with a Seahorse XF Cell Mito Stress Test Kit (Agilent, 103015-100) following manufacturer’s instructions. The Seahorse XFe96 FluxPak cartridge (Agilent, 102416-100) was hydrated with distilled water overnight at 37°C (no CO<sub>2</sub>) and equilibrated for 1h on the day of the assay in Seahorse XF Calibrant solution (Agilent, 103059-000). Vessels were pre-coated with 22.4 µg/ml Cell-Tak (Corning, 354240) for 20 min at 37°C to ensure continued CTL adhesion on the plate during the assay. Day 5 CTLs were resuspended at 1.6x10<sup>6</sup> cells/ml in DMEM media (Sigma-Aldrich D5030), which was supplemented with 10 mM glucose (Thermo Fisher Scientific, A2494001), 1 mM sodium pyruvate (Thermo Fisher Scientific, 11360070) and 2 mM L-glutamine (Sigma-Aldrich, G7513) and pH was adjusted to 7.4 using a SevenEasy pH meter (Mettler Toledo). 3x10<sup>5</sup> CTLs were seeded in each well of the XFe96 FluxPak plate. 1 µM oligomycin A

(Sigma-Aldrich, 75351), 1  $\mu$ M FCCP (Sigma-Aldrich, C2920) and 0.5  $\mu$ M rotenone (Sigma-Aldrich, R8875) mixed with 0.5  $\mu$ M antimycin A (Sigma-Aldrich, A8674) were loaded to test oxygen consumption rate (OCR) and extracellular acidification rate (ECAR) at the indicated time points. Seahorse data was collected using Wave Controller 2.6 (Agilent).

### 2.17 ATP assay

Intracellular ATP concentration was measured using the ATP Determination Kit (Thermo Fisher Scientific, A22066).  $5 \times 10^6$  day 5 post-stimulation CTLs were either left unstimulated or stimulated on 2  $\mu$ g/ml plate-bound  $\alpha$ -CD3 $\epsilon$  (clone eBio500A2) (eBioscience, 16-0033-86) for 4.5h at 37°C in 10% CO<sub>2</sub>. CTL culture media was supplemented with 25  $\mu$ M oligomycin (Sigma-Aldrich, 75351) and 100 mM 2-deoxy-D-glucose (2-DG) (Sigma-Aldrich, D6134) to respectively distinguish mitochondria-derived ATP and glycolysis-derived ATP.  $2 \times 10^6$  CTLs per sample were counted and washed in ice-cold PBS and lysed by boiling in distilled water at 90°C for 5 min as previously described (Garewal et al., 1986). Samples were centrifuged to clear supernatant (14,000rpm, 10 min, 4°C). ATP standards and ATP reaction buffer were prepared as indicated by manufacturer, and ATP concentration was quantified by measuring luminescence at 560 nm using a SpectraMax M5 spectrophotometer (Molecular Devices) and the SoftMaxPro 5.4.1 software (Molecular Devices).

### 2.18 HPG protein synthesis assay

Protein synthesis was assayed using the Click-iT HPG Alexa Fluor 488 Protein Synthesis Assay Kit (Thermo Fisher Scientific, C10428). Day 5 CTLs were washed and resuspended at  $2 \times 10^6$  cells/ml in methionine-free RPMI (Thermo Fisher Scientific, A1451701) enriched with the same supplements as complete mouse T cell media (**Table 2.1**). CTLs were deprived of methionine via incubation in methionine-free RPMI, supplemented as indicated above, for 30 min at 37°C. The rate of protein peptide synthesis was monitored by adding 100  $\mu$ M Click-IT L-homopropargylglycine (HPG) (Thermo Fisher Technologies, C10186) to the culture media. 100  $\mu$ g/ml cycloheximide (Sigma-Aldrich, C4859) was added to control samples to inhibit cytosolic translation in the presence of 100 $\mu$ M HPG.  $2 \times 10^5$  CTLs were seeded on uncoated plate or on a plate coated with 2  $\mu$ g/ml  $\alpha$ -CD3 $\epsilon$  (clone eBio500A2) (eBioscience, 16-0033-86) and incubated at 37°C for the indicated time (1-4.5h) to allow for HPG incorporation.

Cell surface staining was performed with 1:400 Zombie Violet Fixable Viability Kit (BioLegend, 423114) and 1 µg/ml Brilliant Violet 711 α-mouse CD8a antibody (clone 53-6.7) (BioLegend, 100748) for 20 min at 4°C. Samples were fixed in 3.7% PFA (Electron Microscopy Sciences, 15710-S) for 15 min at room temperature. Cells were then washed in 3% BSA (Sigma-Aldrich, A7906) and permeabilised in 0.5% Triton X-100 (Sigma-Aldrich, T8787). Samples were washed in 3% BSA again before HPG labelling through click-chemistry using azide-conjugated Alexa-Fluor 488 as indicated in manufacturer's protocol. Upon staining completion, cells were washed in rinse buffer (provided by the manufacturer) and resuspended in PBS. Samples were analysed on an Attune NxT Acoustic Focusing Cytometer (Thermo Fisher Scientific) using the Attune NxT Software (Invitrogen).

Mitochondrial protein synthesis was assayed by washing and incubating 10<sup>6</sup> day 5 post-activation CTLs in methionine-free RPMI supplemented as above, with the exception of FBS, which was dialysed against PBS (cellulose dialysis tubing: MWCO 8 kDa; Thermo Fisher, D104) to further remove any additional source of methionine. CTLs were incubated at 10<sup>6</sup> cells/ml in methionine-free media for 30 min at 37°C, then 100 µg/ml cycloheximide (Sigma-Aldrich, C4859) was added to all samples to inhibit cytosolic ribosomes. 100 µM Click-IT L-homopropargylglycine (HPG) (Thermo Fisher Technologies, C10186) was supplemented for 1-1.5h at 37°C to label mitochondrial protein synthesis.

CTLs were then washed in serum-free RPMI (Sigma-Aldrich, 1640) and allowed to adhere to slides at 37°C in 10% CO<sub>2</sub> for 10-15 min (3x10<sup>4</sup> CTLs/well) before fixation with 3.7% paraformaldehyde (PFA) (Electron Microscopy Sciences, 15710-S) for 15 min at 37°C. Cells were permeabilized for 20 min in 0.5% Triton X-100 (Sigma-Aldrich, T8787) and HPG was labelled through click-chemistry using azide-conjugated Alexa-Fluor 488 (Thermo Fisher Scientific, C10428). Samples were then washed in PBS and mitochondria were labelled using 1 µg/ml mouse α-mouse PDH (Abcam, ab110330) (2h, room temperature) and 5 µg/ml goat α-mouse 546 Alexa Fluor secondary antibody (Thermo Fisher Scientific, A-11030) for 1h at room temperature. Nuclei staining was performed using 1:50,000 Hoechst 33342 (Thermo Fisher Scientific, H3570) and samples were mounted in ProLong Diamond Antifade Mounting medium (Life Technologies, P36961).

## **2.19 Intracellular cytokine staining**

Day 5 CTLs were washed and resuspended at 2x10<sup>6</sup> cells/ml in mouse T cell media. 2x10<sup>5</sup> CTLs per sample were either left unstimulated or stimulated on 2 µg/ml α-CD3ε-coated plates (clone

eBio500A2) (eBioscience, 16-0033-86) for 4.5h. Golgi stop (BD Biosciences, 554714) was added to cell culture media to prevent secretion and investigate total cytokine production. After incubation the cell culture media was removed and CTLs were washed in PBS at 4°C, then stained using 1:400 Zombie Violet Fixable Viability Kit (BioLegend, 423114) and 1 µg/ml Brilliant Violet 711 α-mouse CD8a antibody (clone 53-6.7) (BioLegend, 100748) for 20 min at 4°C. After washing in FACS buffer (PBS, 1% FBS), samples were fixed and permeabilised using the Foxp3 nuclear staining kit (Thermo Fisher Scientific, 00-5523-00) as indicated in the manufacturer's protocol. All samples were treated with 1 µg/ml FCR block (α-CD16/32) (BioLegend, 101302) for 5 min at room temperature to block unspecific staining. Intracellular staining was performed using 1 µg/ml PE α-IFNγ (clone XMG1.2) (BioLegend, 505808) and 1 µg/ml Alexa Fluor 488 α-TNFα (clone MP6-XT22) (BioLegend, 506313) for 30 min at room temperature. Control samples were intracellularly labelled with 2 µg/ml Alexa Fluor PE IgG1 (clone EBRG1) (eBioscience, 12-4301-81) and 5 µg/ml Alexa Fluor 488 IgG1κ (clone RTK2071) (BioLegend, 400417) as isotype controls. Cells were rinsed in permeabilization buffer and PBS and resuspended in PBS for analysis. Samples were analysed on an Attune NxT Acousting Focusing Cytometer (Thermo Fisher Scientific) using the Attune NxT Software (Invitrogen).

## 2.20 CyTOF sample processing and analysis

Staining for CyTOF sample processing was performed using MaxPar reagents (Fluidigm). Day 5-7 post-stimulation CTLs were resuspended at  $10^6$  cells/ml incubated with 5 µM Cell-ID Cisplatin (Fluidigm, 201064) for 5 min at 37°C in 10% CO<sub>2</sub> to discriminate live cells. CTLs were either left unstimulated or stimulated on 1 µg/ml α-CD3ε (clone 145-2C11) (BD Biosciences, 553058) for 1h at 37°C ( $1.6 \times 10^5$  cells/sample). Samples were fixed for 10 min at room temperature in Maxpar Fix I Buffer (Fluidigm, 201065) and barcoded using the Cell-ID 20-Plex Pd Barcoding Kit (Fluidigm, 201060) before being pooled for staining ( $9.6 \times 10^5$  cells/pooled sample). Unspecific labelling was blocked with FCR blocking reagent (clone 93) (Biolegend, 101302) ahead of staining with metal-conjugated surface antibodies (**Table 2.4**). Intracellular staining with metal-conjugated antibodies was performed after methanol permeabilisation (**Table 2.4**). All antibodies were diluted in Maxpar Cell Staining Buffer (Fluidigm, 201068). CTLs were fixed with 1.6% PFA (Electron Microscopy Sciences, 15710-S) and stained overnight with 125 nM Cell-ID Intercalator-Ir (Fluidigm, 201192B) in Maxpar Fix and Perm Buffer (Fluidigm, 201067). All samples were analysed on a Helios CyTOF system (Fluidigm). Data normalisation and de-barcoding was performed using the Fluidigm CyTOF software.

**Table 2.4. List of antibodies used for mass cytometry.**

Supplier	Custom conjugation	Label	Target	Antibody clone	Working concentration (ng/μl)
<b>Surface staining</b>					
Fluidigm	0	89Y	CD45	30-F11	5
Fluidigm	0	146Nd	CD8α	53-6.7	1
Fluidigm	0	150Nd	CD44	IM7	0.75
Fluidigm	0	151Eu	CD25	3C7	5
Fluidigm	0	169Tm	TCRβ	H57-597	1.5
Fluidigm	0	143Nd	CD69	H1.2F3	2
<b>Intracellular staining – Phosphosignalling nodes</b>					
Fluidigm	0	147Sm	pSTAT5 [Y694]	47	2.5
Fluidigm	0	152Sm	pAKT [S473]	D9E	2.5
Fluidigm	0	156 Gd	pSLP76 [Y128]	J141-668.36.58	2.5
Fluidigm	0	162Dy	pLCK [Y505]	4/LCK-Y505	2
Fluidigm	0	164Dy	IκBα	L35A5	1.25
CST Custom	1	165 Ho	pPLCγ1 [Y783]	D6M9S	5
Fluidigm	0	167Er	pERK 1/2 [T202/Y204]	D13.14.4E	5
Fluidigm	0	171Yb	pZAP70 [Y319]/Syk [Y352]	17a	1
Fluidigm	0	175Lu	pS6 [S235/S236]	N7-548	2
<b>Intracellular staining - Total protein</b>					
CST Custom	1	149 Sm	ERK1/2	137F5	5
CST Custom	1	153 Eu	S6	54D2	2.5
Merck Millipore	1	154 Sm	Lck	3A5	10
Novus	1	158 Gd	PLCγ1	3H1C10	5
Thermo Fisher Scientific	1	159 Tb	ZAP70	1E7.2	5
Biologend	1	170 Er	SLP76	H76	10
Thermo Fisher Scientific	1	173 Yb	Stat 5	ST5-8F7	10
CST Custom	1	176 Yb	AKT	C67E7	5

## 2.21 Mass spectrometry processing and analysis

CTLs (5 days post-activation) were resuspended at  $10^6$  cells/ml in mouse T cell media and either left unstimulated or stimulated with 2  $\mu\text{g/ml}$   $\alpha\text{-CD3}\epsilon$  (clone eBio500A2) (eBioscience, 16-0033-86) for 4.5h at 37°C. Cytosolic translation was inhibited where indicated by supplementing the cell culture media of stimulated samples (4.5h  $\alpha\text{-CD3}$ ) with 100  $\mu\text{g/ml}$  cycloheximide (Sigma, C4859). Doxycycline-treated CTLs were incubated in the presence of 10  $\mu\text{g/ml}$  doxycycline for 4-4.5h. Samples were prepared for mass spectrometry analysis by counting  $5 \times 10^6$  CTLs per sample, washing cells twice in ice-cold PBS and flash-freezing samples on dry-ice.

Cell pellets were lysed by agitating samples at room temperature for 5 min in 5% SDS, 50 mM TEAB pH 8.5, 10 mM TCEP, and protein concentration was determined after boiling and sonification using the EZQ protein quantification kit (Invitrogen, R33200) following the manufacturer's instructions. Lysates alkylation was performed in 20 mM iodoacetamide for 1h, with subsequent protein clean up using the S-Trap method (Protifi) as previously described (Zougman et al., 2014). Quantitation of peptide concentration was performed using the CBQCA protein quantitation kit (Invitrogen, C6667). Samples were vacuum-dried then dissolved in 5% formic acid ahead of LC-ES-MS/MS analysis.

2  $\mu\text{g}$  peptide/sample were analysed for WT/KO and CHX-treated samples. Samples were injected onto a nanoscale C18 reverse-phase chromatography system (UltiMate 3000 RSLC nano, Thermo Fischer Scientific), electrosprayed into an Q Exactive HF-X Mass Spectrometer (Thermo Fischer Scientific) and loaded on a trap column (Thermo Fischer Scientific, 100  $\mu\text{m} \times 2$  cm, PepMap nanoViper C18 column, 5  $\mu\text{m}$ , 100 Å) at 15  $\mu\text{L/min}$ , and equilibrated in 0.1% trifluoroacetic acid. The column was kept at constant temperature (50°C) and utilised as follows: after washing the trap column in TFA and switching to a resolving C18 column (75  $\mu\text{m} \times 50$  cm, PepMap RSLC C18 column, 2  $\mu\text{m}$ , 100Å), the peptides were eluted at a constant flow rate (300 nl/min) with an increasing gradient of 80% acetonitrile and 0.1% formic acid in Milli-Q water (v/v). The column was then washed, re-equilibrated and used to run two blanks in-between each experimental sample to avoid carry over.

Data acquisition was performed using an easy spray source (positive mode, 1.9 kV, capillary temperature=250°C, funnel RF=60) in a data-independent acquisition (DIA) mode as previously reported (Muntel et al., 2019) with the following modifications. Full mass spectrometry survey scan ( $m/z$  range=350-1650, maximum ion injection time=20 ms, resolution=120,000, automatic gain control= $5 \times 10^6$ ) was followed by MS/MS DIA scan (default charge state=3, resolution=30,000, maximum ion injection time=55 ms, AGC= $3 \times 10^6$ , stepped normalized collision energy=25.5, 27,30,

fixed first mass=200 m/z). Profile mode acquisition was used for both MS and MS/MS scans. Mass accuracy was checked for all samples.

Samples were analysed as described in the previous paragraphs for doxycycline treated samples except for the following differences: 1.5 µg peptide was injected per sample, analysis was performed on Orbitrap Exploris 480 Mass Spectrometer (Thermo Fisher Scientific), sample were loaded at 10 µL/min onto trap column and the easy spray source operated in positive mode with spray voltage at 2.445 kV, and the ion transfer tube temperature at 250°C.

The Spectronaut 14 software (Bruderer et al., 2015) was used for data processing using the directDIA settings with the following adjustments: cleavage rules=Trypsin/P, peptide maximum length=52 amino acids, peptide minimum length=7 amino acids, missed cleavages=2, calibration mode=automatic. Modifications included in the search criteria were carbamidomethylation of cysteine (fixed modification), and oxidation of methionine, deamidation of asparagine and glutamine and acetylation (protein N-terminus) (variable modifications). The false discovery rate (FDR) threshold was set to 1% (Q-value) for both the Precursor and Protein level data. The single hit definition was to stripped sequence. Mass spectrometry DIA data was searched against the July 2019 Uniprot database release, which includes manually annotated mouse SwissProt entries, mouse TrEMBL entries (protein level evidence available) and manually annotated homologues from the human SwissProt database, as previously described (Marchingo et al., 2020). Additional parameters included the following: major group quantity=sum of peptide quantity, minor group quantity=sum of precursor quantity, cross run normalization=disabled. The Template Correlation Profiling setting was switched on.

Protein copy number quantification was performed using Perseus, version 1.6.6.0. The proteomics ruler plugin was used to calculate mean copy number/cell, as previously described (Wisniewski et al., 2014). All mass spectrometry data have been deposited to the ProteomeXchange Consortium via the PRIDE partner repository (Perez-Riverol et al., 2019). Dataset identifiers: PXD021508 (*Usp30<sup>-/-</sup>*, cycloheximide), PXD026948 (doxycycline).

## 2.22 CRISPR/Cas9-mediated gene knockouts

The CRISPR/Cas9 system was used for gene deletion as previously described (Jinek et al., 2012). TrueCut Cas9 Protein v2 (Thermo Fisher, A36499), tracrRNA (Dharmacon, U-002005) and either non-targeting crRNA (Dharmacon, U-007501-01) or 3 guide crRNA per gene (Dharmacon, see **Table 2.5**) were mixed at a 1:1:1 ratio in Nucleofector Solution (Lonza, V4XP-3024) (total volume=100  $\mu$ l).  $5 \times 10^6$  day 0 CD8<sup>+</sup> T cells or day 2-4 post-stimulation CTLs (as indicated in the text) were resuspended in the solution mix and nucleofected in a nucleocuvette (Lonza, V4XP-3024) using the unstimulated mouse T cell programme on the Amaxa 4D-Nucleofector (Lonza). Cells were transferred to pre-warmed Mouse T Cell Nucleofector Medium (Lonza, VZB-1001) and incubated for 4h at 37°C before splitting in mouse T cell media (**Table 2.1**). CRISPR components were removed the following day by centrifugation. Protein expression was assessed 4 days after nucleofection unless otherwise indicated.

**Table 2.5. List of Dharmacon crRNA guides for CRISPR/Cas9-mediated gene knockouts.**

Gene target	Catalogue number
<i>Atf4</i>	CM-042737-01-0002, CM-042737-02-0002, CM-042737-03-0002
<i>Mcu</i>	CM-062849-01-0005, CM-062849-02-0005, CM-062849-03-0005
<i>Pex16</i>	CM-052798-01-0002, CM-052798-02-0002, CM-052798-03-0002
<i>Gtpbp10</i>	CM-054341-01-0002, CM-054341-02-0002, CM-054341-04-0002
<i>Ftsj2/Mrm2</i>	CM-046522-01-0002, CM-046522-02-0002, CM-046522-03-0002
<i>Rnm11/Mrm3</i>	CM-049414-01-0002, CM-049414-02-0002, CM-049414-03-0002
<i>Slc8b1/NclX</i>	CM-065138-01-0002, CM-065138-02-0002, CM-065138-03-0002
<i>Gfm1</i>	CM-052774-01-0002, CM-052774-02-0002, CM-052774-03-0002
<i>Mrps16</i>	CM-044973-01-0002, CM-044973-02-0002, CM-044973-03-0002
<i>Mrps22</i>	CM-046221-01-0002, CM-046221-02-0002, CM-046221-03-0002
<i>Mrpl49</i>	CM-050402-01-0002, CM-050402-02-0002, CM-050402-03-0002
<i>Mrpl48</i>	CM-054957-01-0002, CM-054957-02-0002, CM-054957-03-0002
<i>Mrps35</i>	CM-053467-01-0002, CM-053467-02-0002, CM-053467-03-0002
<i>Mrpl28</i>	CM-044386-01-0002, CM-044386-02-0002, CM-044386-03-0002
<i>Mrpl37</i>	CM-046399-01-0002, CM-046399-02-0002, CM-046399-03-0002
<i>Mrpl12</i>	CM-054164-03-0002, CM-054164-03-0002, CM-054164-03-0002

## 2.23 Data acquisition and analysis

All flow cytometry data was acquired using the BD FACSDIVA software (BD Biosciences) or the Attune NxT software (Thermo Fisher Scientific) and analysed using FlowJo v10. MFI refers to mean fluorescence intensity of the fluorophore specified in the text. Microscopy images were analysed using the Imaris 9 software (Bitplane). Student's t-test was used to determine statistical significance as indicated in the figure legends. Graphs were generated using Prism 8 (GraphPad Software).

For mass spectrometry data, copy number values were used to calculate fold change (FC). P values were calculated using a two-tailed paired Students' t-test and applying a false discovery rate (FDR) correction based on the Benjamini-Hochberg method (Benjamini and Hochberg, 1995). Analysis was performed in Excel (Microsoft) and RStudio (R Studio Team). Copy number values were displayed as a heat map using Morpheus (Broad), while pie charts indicating cellular compartments were visualised using Prism 8 (GraphPad). Volcano plots were generated by plotting fold change and p values for all peptides on Tableau Interactive Dashboard 2020-2021 (Tableau) and highlighting FDR based on the Benjamini-Hochberg method or protein class and localisation as detailed below.

Protein cellular localisation was manually curated based on UniProt annotations (<https://www.uniprot.org/>) and KEGG terms. Mass contribution of proteins (g/cell) was calculated as (protein copy number/cell) \* (molecular weight(Daltons))/(Avogadro's constant). Percentage of mitochondrial protein content of mitochondrial ribosomes was calculated by defining total mitochondrial proteins as the proteins from in the Mouse MitoCarta 2.0 database (Calvo et al., 2016) and mitochondrial ribosomal proteins on the protein description terms "ribosomal protein" and "mitochondrial". Cytosolic ribosomal proteins were defined by the KEGG term "ribosome". Moonlighting metabolic enzymes were labelled based on their ability to bind RNA, as previously reported (Beckmann et al., 2015; Castello et al., 2015; Ciesla, 2006; Garcin, 2019; Turner and Diaz-Munoz, 2018).

For gene ontology (GO) enrichment analysis, values for FC and FDR correction were compared for proteins detected in the mass spectrometry of both KO vs WT and DOX-treated vs untreated CTLs (all unstimulated). GO enrichment (<http://geneontology.org/>) (Ashburner et al., 2000; Gene Ontology, 2021) was analysed by detecting overrepresented "biological process" in the list of commonly downregulated proteins in KO and DOX-treated CTLs with FDR<10%.



## CHAPTER 3

**Analysis of *Usp30*<sup>-/-</sup> CTLs: impaired cytosolic translation prevents synthesis of cytolytic proteins and sustained killing**



### 3.1 Background

The *Usp30*<sup>-/-</sup> mice were identified as part of the Infection, Immunity and Immunophenotyping (3i) project, which aimed to characterise genes with previously unknown immune cell functions (<https://www.immunophenotype.org/>). This screen highlighted USP30 as a potential regulator of CTL killing, with no effect on viability or development of the mice (Abeler-Dörner et al., 2020). USP30 is a transmembrane deubiquitinase localised on the OMM and on the peroxisomal membrane, where it inhibits mitophagy and pexophagy by counteracting PINK1/PARKIN and PEX2-mediated ubiquitination (Bingol et al., 2014; Marcassa et al., 2018; Nakamura and Hirose, 2008; Riccio et al., 2019). Lack of USP30 is associated with increased mitochondrial and peroxisomal degradation. The role of USP30 in the immune system, and specifically its role in mediating cytotoxicity in CTLs, is currently unknown.

### 3.2 Loss of USP30 does not impair T cell development

Impairment of mitochondrial function is linked to defects in T cell development in the thymus and in peripheral tissues (Corrado et al., 2021; Ramstead et al., 2020; Sena et al., 2013; Simula et al., 2018). To examine whether loss of USP30 affected T cell development, I characterised splenocyte populations in wild-type (WT) and *Usp30*<sup>-/-</sup> mice (**Figure 3.1**). WT and *Usp30*<sup>-/-</sup> mice were generated by crossing heterozygous *Usp30*<sup>+/-</sup> mice (C57BL/6N background). The derived WT and *Usp30*<sup>-/-</sup> mice were housed and bred separately in a SPF facility. Genotyping was carried out routinely by the facility personnel on newly weaned animals. Splenocyte populations were characterised in 10-25 weeks old male and female mice (three per genotype). WT and *Usp30*<sup>-/-</sup> mice were age- and gender-matched for all experiments.

Antibodies against the transmembrane proteins CD4 and CD8 were used to characterise the prevalence of these two T cell populations in the spleen. CD44 expression was used as an indicator of T cell activation (Ponta et al., 2003) and CD62L was used as a marker of increased T cell homing, which inversely correlates with activation (Jung et al., 1988). Detection of CD44 and CD62L surface markers allowed the identification of naïve (CD44<sup>low</sup>, CD62L<sup>high</sup>), central memory (CD44<sup>high</sup>, CD62L<sup>high</sup>) and effector memory (CD44<sup>high</sup>, CD62L<sup>low</sup>) T cell populations.

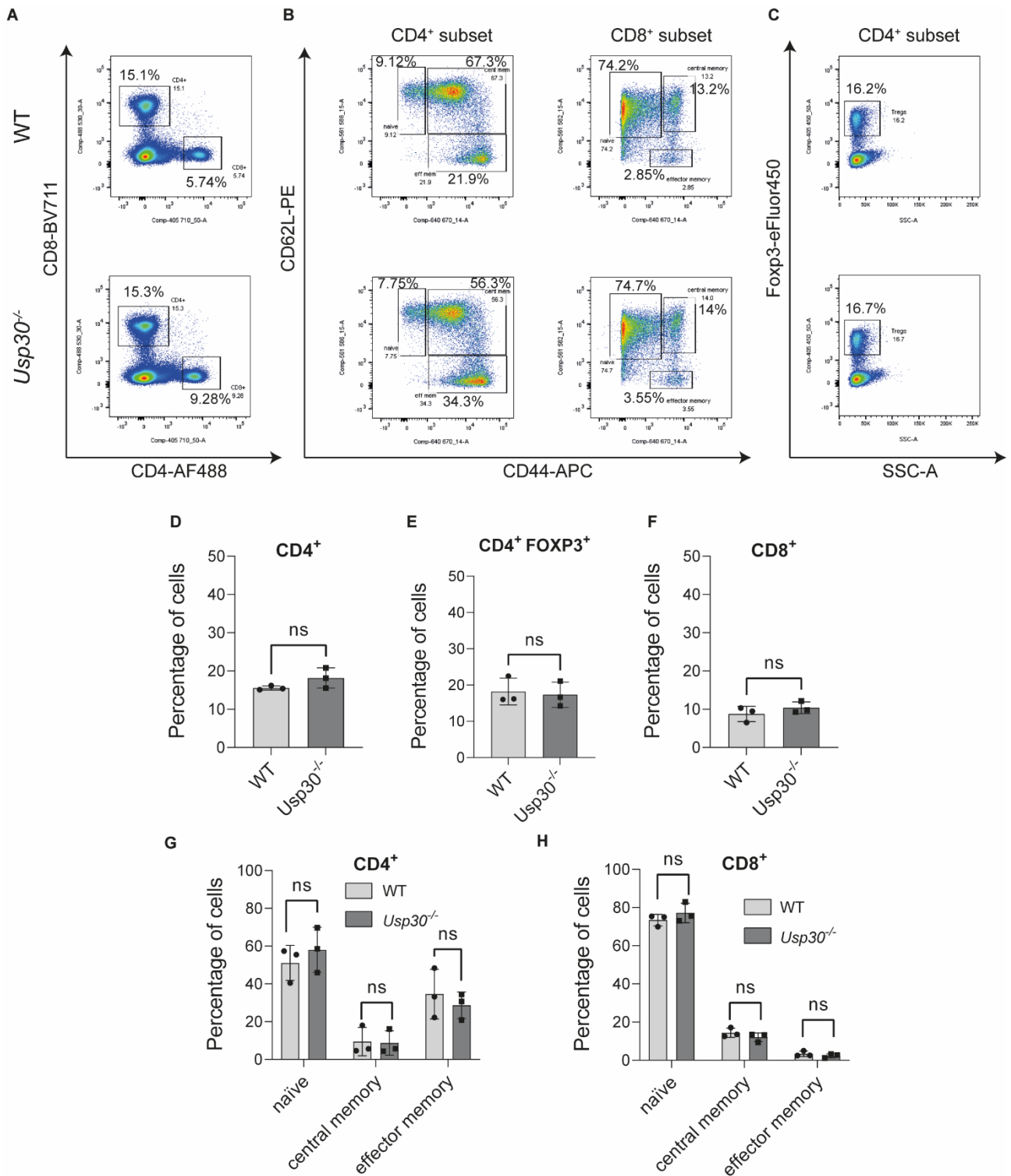


**Figure 3.1. Analysis of WT and *Usp30*<sup>-/-</sup> splenocytes.**

(A) CD4<sup>+</sup>/CD8<sup>+</sup> ratio in WT and *Usp30*<sup>-/-</sup> splenocytes. (B) CD4<sup>+</sup> and CD8<sup>+</sup> naïve (CD62L<sup>high</sup>, CD44<sup>low</sup>), central memory (CD62L<sup>high</sup>, CD44<sup>high</sup>) and effector memory (CD62L<sup>low</sup>, CD44<sup>high</sup>) T cell populations in WT and *Usp30*<sup>-/-</sup> splenocytes. (C) Regulatory T cells (CD4<sup>+</sup>, FOXP3<sup>+</sup>) in WT and *Usp30*<sup>-/-</sup> splenocytes. (D-H) Quantitation of (D) CD4<sup>+</sup>, (E) regulatory T cells, (F) CD8<sup>+</sup>, (G) total CD4<sup>+</sup> and (H) CD8<sup>+</sup> populations (naïve, central memory, effector memory). Plots show the average of three biological replicates (10<sup>6</sup> splenocytes per sample) ±SD. ns = not significant (two-tailed paired Student's t-test).

Lack of USP30 did not alter in the proportions of CD4<sup>+</sup> and CD8<sup>+</sup> T cells in the spleen (**Figure 3.1**). On average, the percentage of CD4<sup>+</sup> and CD8<sup>+</sup> T cells was 15% and 9% in WT and 18% and 10% in *Usp30*<sup>-/-</sup> splenocytes. The percentage of regulatory T cells (CD4<sup>+</sup> FOXP3<sup>+</sup>) was 18% and 17% in WT and *Usp30*<sup>-/-</sup>, respectively. Naïve, central memory and effector memory T cells were also not affected in *Usp30*<sup>-/-</sup> splenocytes compared to their WT counterparts. Within the CD4<sup>+</sup> populations, 51% were naïve, 9% central memory and 35% effector memory T cells in the WT, while 59%, 9% and 27% were respectively naïve, central memory and effector memory in *Usp30*<sup>-/-</sup> T cells. The CD8<sup>+</sup> population was made of 73% naïve, 14% central memory and 3% effector memory T cells in WT splenocytes and 77%, 12% and 3% naïve, central memory and effector memory T cells in *Usp30*<sup>-/-</sup>. None of the observed variations were statistically significant. Overall, T cell development and differentiation in murine splenocytes was not affected by the lack of USP30.

I next asked whether there were any differences in T cell differentiation after *in vitro* activation of naïve *Usp30*<sup>-/-</sup> or WT T cells. Naïve T cells were activated by TCR and co-stimulatory receptor stimulation, mimicked by plate-bound  $\alpha$ -CD3 and  $\alpha$ -CD28 antibodies (**Figure 3.2A**). Expression of CD44, CD62L and CD25 was used as a marker of T cell activation. CD25 (IL-2 receptor chain  $\alpha$ ) promotes uptake of the stimulatory cytokine IL-2, which induces proliferation in activated T cells (Meuer et al., 1984). I labelled CD8<sup>+</sup> T cells on day 0 (unstimulated splenocytes), 3, 5 and 7 post-stimulation and followed the surface expression of these activation markers by flow cytometry (**Figure 3.2 B-G**). The increase in CD44 and CD25 was comparable in WT and *Usp30*<sup>-/-</sup> CTLs, demonstrating that *Usp30*<sup>-/-</sup> could upregulate the expression of markers consistent with normal T cell activation (**Figure 3.2B, E**). Notably, while CD62L expression decreased upon stimulation in both samples, a percentage of *Usp30*<sup>-/-</sup> CTLs retained high CD62L signal on day 5 and 7 after stimulation (**Figure 3.2 F-I**). These results indicated that *Usp30*<sup>-/-</sup> T cells were similar to WT before activation and they appeared to initiate a WT-like activation programme upon stimulation. The expression of activation markers appeared altered only 5 days post-stimulation.

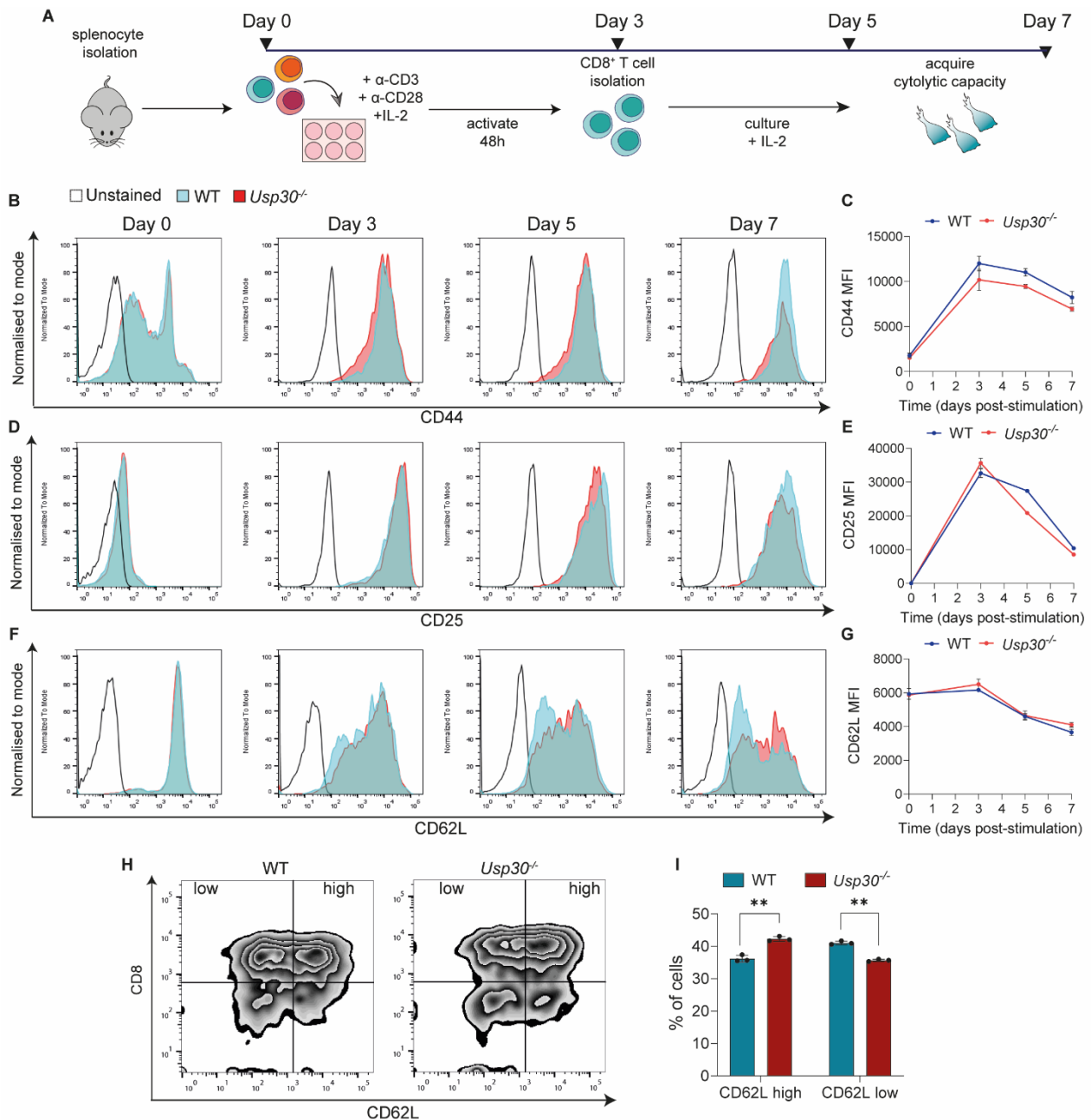


**Figure 3.2. Analysis of activation markers in naïve and effector *Usp30*<sup>-/-</sup> CTLs.**

(A) Activation, stimulation and isolation of CD8<sup>+</sup> T cells from WT and *Usp30*<sup>-/-</sup> mice. (B) Time course of CD44 expression in WT and *Usp30*<sup>-/-</sup> T cells from naïve CD8<sup>+</sup> T cells (day 0) as they mature into CTLs after stimulation (day 3-7). (C) Quantitation of CD44 MFI in day 0-7 CTLs. (D) Time course of CD25 expression in WT and *Usp30*<sup>-/-</sup> T cells naïve CD8<sup>+</sup> T cells (day 0) and CTLs (days 3-7). (E) Quantitation of CD25 MFI in day 0-7 CTLs. (F) Time course of CD62L expression in WT and *Usp30*<sup>-/-</sup> T cells naïve CD8<sup>+</sup> T cells (day 0) and CTLs (days 3-7). (G) Quantitation of CD62L MFI in day 0-7 CTLs. (H) CD8 and CD62L expression in day 5 WT and *Usp30*<sup>-/-</sup> CTLs. (I) Percentage of CD8<sup>+</sup> cells displaying high and low CD62L signal in day 5 WT and *Usp30*<sup>-/-</sup> CTLs, based on gating strategy outlined in (H). Error bars show average of technical replicates  $\pm$ SD (day 0: 10<sup>6</sup> splenocytes/sample; days 3-7: 10<sup>5</sup> CTLs/sample). \*\*= $p < 0.01$  (two-tailed unpaired Student's t-test). Data representative of at least two independent biological replicates.

### 3.3 T cell stimulation induces loss of mitochondrial markers in *Usp30*<sup>-/-</sup> CTLs

The role of USP30 as a deubiquitinase has been highlighted in the context of mitophagy and pexophagy. USP30 cleaves ubiquitin chains from proteins localised on the outer membrane of mitochondria and peroxisomes, protecting them from degradation (Bingol et al., 2014; Marcassa et al., 2018; Nakamura and Hirose, 2008; Riccio et al., 2019). While several studies have described USP30 DUB activity in a variety of immortalised cell lines, whether USP30 plays the same role in primary immune cells was not known.

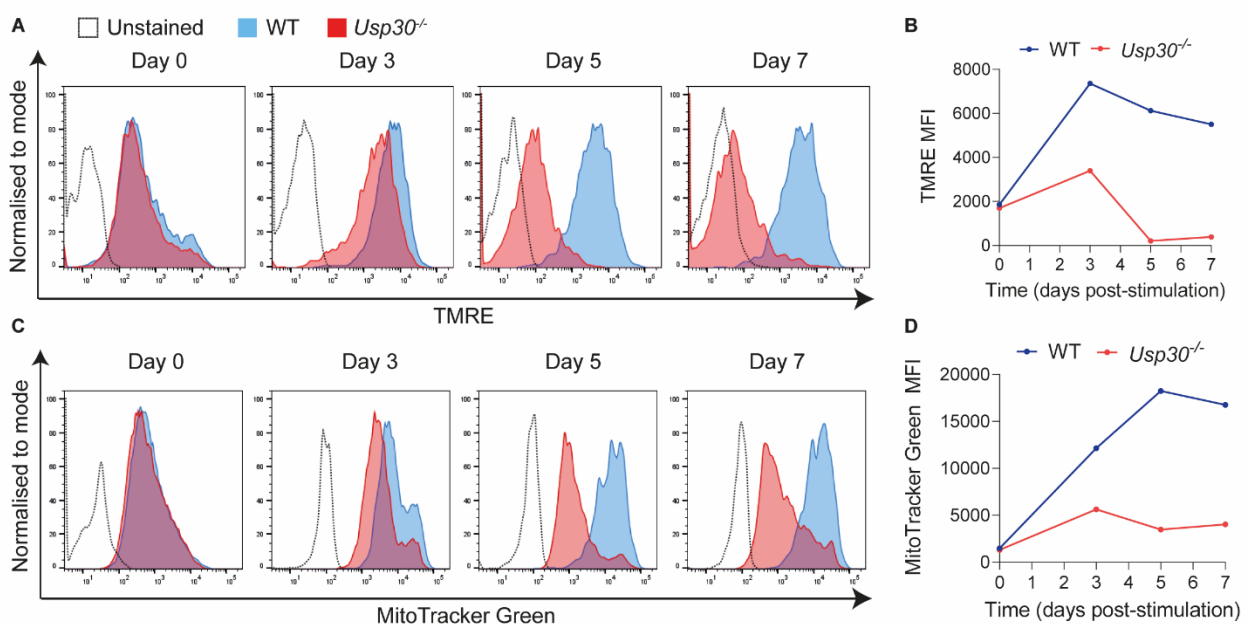


**Figure 3.3. Mitochondrial mass and membrane potential are lost in activated *Usp30*<sup>-/-</sup> CTLs.**

(A) Time course of mitochondria labelled with TMRE in WT and *Usp30*<sup>-/-</sup> naïve CD8<sup>+</sup> T cells (day 0) as they mature into CTLs after stimulation (day 3-7). (B) Quantitation of TMRE MFI corresponding to histograms shown in (A). (C) Time course of mitochondria labelled with MitoTracker Green in WT and *Usp30*<sup>-/-</sup> naïve CD8<sup>+</sup> T cells (day 0) as they mature into CTLs after stimulation (day 3-7). (D) Quantitation of MitoTracker MFI corresponding to histograms shown in (C). All data representative of at least three independent biological replicates (day 0: 10<sup>6</sup> splenocytes/sample; days 3-7: 10<sup>5</sup> CTLs/sample).

To address this question, I analysed mitochondrial mass and membrane potential on day 0 (splenocytes) and day 3, 5 and 7 CD8<sup>+</sup> T cells post-activation. I used MitoTracker Green as a measure of mitochondrial mass and the dye tetramethylrhodamine, ethyl ester (TMRE) as an indicator of mitochondrial membrane potential (**Figure 3.3**). MitoTracker Green and TMRE fluorescence were equivalent in day 0 WT and *Usp30*<sup>-/-</sup> CD8<sup>+</sup> T cells, implying that mitochondrial mass and membrane potential were not affected in USP30-deficient splenocytes. As previously reported (D'Souza et al., 2007; Grayson et al., 2003; Howden et al., 2019), I observed a surge in both mitochondrial mass and membrane potential in stimulated WT CTLs, peaking on day 3-5 after stimulation. *Usp30*<sup>-/-</sup> T cells also showed an increase in mitochondrial mass and membrane potential, although to a lesser extent than WT CTLs. TMRE and MitoTracker Green signal were furtherly decreased in day 5 *Usp30*<sup>-/-</sup> CTLs, suggesting a loss of mitochondrial abundance and membrane potential. Mitochondria remained defective after day 5, despite an apparent partial regain of WT-like mitochondrial mass (MitoTracker Green signal) in a minority of *Usp30*<sup>-/-</sup> CTLs.

The ability of MitoTracker Green to accumulate within mitochondria independently of mitochondrial membrane potential has been debated (Buckman et al., 2001; Keij et al., 2000; Pendergrass et al., 2004). Therefore, I used immunoblotting together with fluorescence and electron microscopy to investigate the mitochondrial defect observed by flow cytometry in day 5 CD8<sup>+</sup> *Usp30*<sup>-/-</sup> CTLs. Expression of TOM20, a known target of USP30 (Phu et al., 2020), was analysed from day 3 to day 9 post-activation by Western blot (**Figure 3.4A**). TOM20 abundance was moderately reduced in day 3 *Usp30*<sup>-/-</sup> CTLs compared to their WT counterparts, and it was almost completely lost in subsequent days in activated USP30-deficient cells. This result was consistent with the loss of MitoTracker Green observed by flow cytometry (**Figure 3.3A, B**). Interestingly, TOM20 expression showed a progressive decrease also in stimulated WT CTLs, albeit not to the extent observed in *Usp30*<sup>-/-</sup> CTLs.

For immunofluorescence staining I used antibodies raised against TOM20 and the mitochondrial matrix protein pyruvate dehydrogenase (PDH) (**Figure 3.4B, C**). Phalloidin staining was used to label F-actin. Immunofluorescent detection of both TOM20 and PDH highlighted an abundance of mitochondria in WT CTLs, mostly displaying the classic round morphology that distinguishes mitochondria in effector T cells from mitochondria in memory T cells (Buck et al., 2016). By contrast, the signal from these mitochondrial markers was reduced in *Usp30*<sup>-/-</sup> CTLs, with an average of only 47% and 56% of USP30-deficient CTLs displaying any TOM20 and PDH fluorescence, respectively (**Figure 3.4 D-G**). *Usp30*<sup>-/-</sup> CTLs retaining TOM20 or PDH signal showed a dramatic decrease in the fluorescence intensity of these markers, indicating that even the cells that had not fully lost TOM20 and PDH were expressing lower levels of these proteins compared to WT CTLs (**Figure 3.4 D-G**).

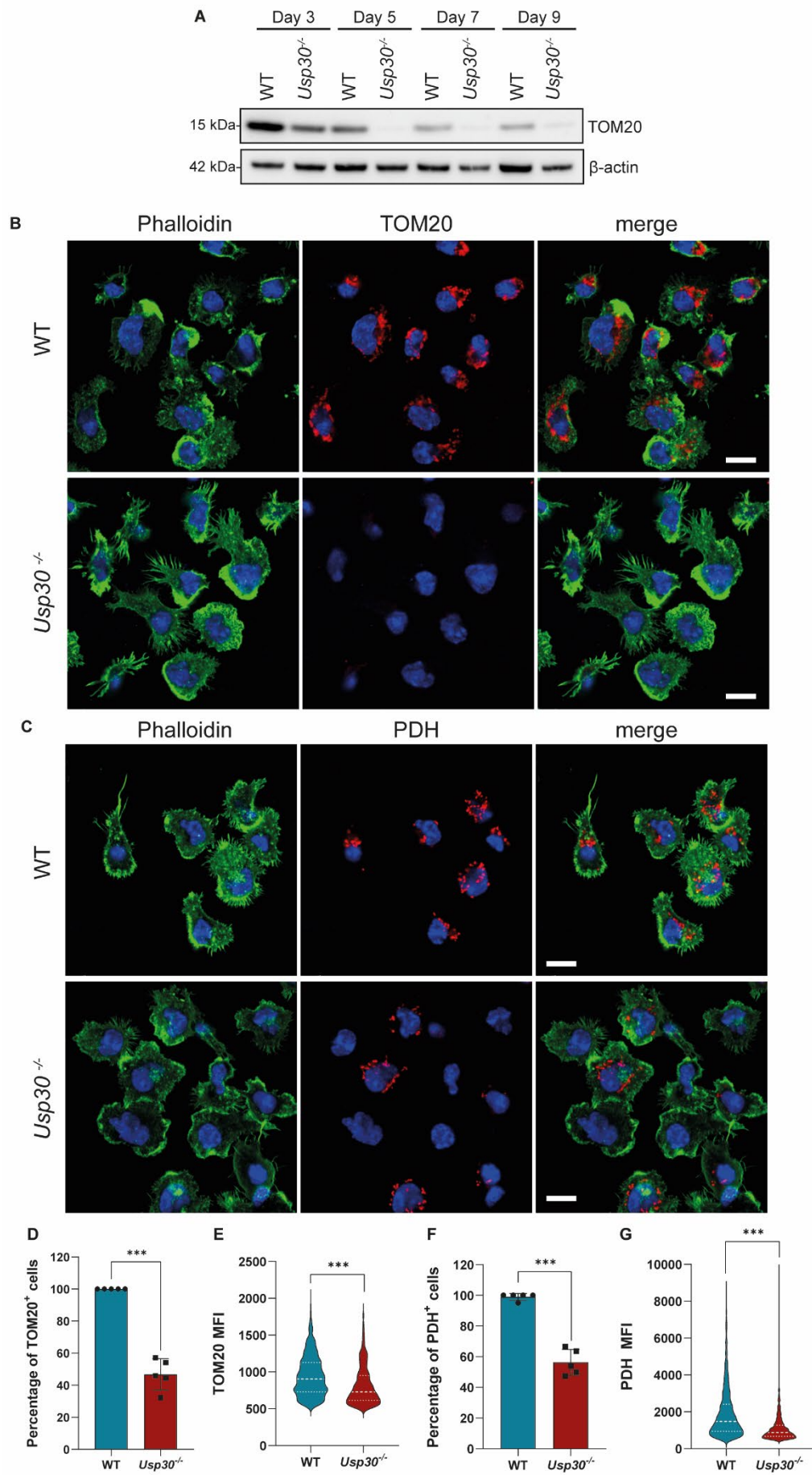


**Figure 3.4. Mitochondrial membrane and matrix markers are reduced in activated *Usp30*<sup>-/-</sup> CTLs.**

(A) Immunoblot showing time course of TOM20 expression in activated (day 3-9 post-stimulation) WT and *Usp30*<sup>-/-</sup> CTLs (3.33 µg lysate/sample). (B, C) Immunofluorescence staining of (B) TOM20 and (C) PDH in day 5 WT and *Usp30*<sup>-/-</sup> CTLs (4.5x10<sup>4</sup> CTLs/sample). Phalloidin labels F-actin. Scale bars=10 µm. (D, E) Quantitation of day 5 CTLs expressing (D) TOM20 and (E) TOM20 MFI by immunofluorescence (>65 cells per genotype in each independent repeat). (F, G) Quantitation of day 5 CTLs expressing (F) PDH and (G) PDH MFI by immunofluorescence (>60 cells per genotype in each repeat). Error bars (D, F) indicate mean values ±SD of technical replicates in one representative experiment. \*\*\* = p<0.001 (two-tailed unpaired Student's t-test). Dashed lines=median; dotted lines=quartiles in (E, G). Data representative of at least three independent biological replicates.

Transmission electron microscopy (TEM) on day 5 CD8<sup>+</sup> purified WT and *Usp30*<sup>-/-</sup> CTLs showed differences in mitochondrial morphology (**Figure 3.5**). Most mitochondria observed in WT CTLs appeared as electron-dense structures characterised by tightly packed cristae (**Figure 3.5A**). TEM analysis indicated that 23% of WT and 57% of *Usp30*<sup>-/-</sup> CTLs sections did not contain any visible mitochondria, suggesting a decrease in mitochondrial abundance in USP30-depleted CTLs. Examination of mitochondrial phenotypes, divided into “normal” (normal mitochondrial morphology), “disrupted” (disrupted mitochondrial morphology) and “none” (no mitochondria observed in the cross-section) confirmed both a reduction in mitochondria and a higher prevalence of defective mitochondrial structures in *Usp30*<sup>-/-</sup> CTLs, defined by disrupted cristae (**Figure 3.5B**). The results of this quantitation were consistent with the data obtained by fluorescent microscopy: only 47% (“TOM20<sup>+</sup>” by immunofluorescence, **Figure 3.4D**) or 43% (“normal/disrupted” by TEM, **Figure 3.5B**) of *Usp30*<sup>-/-</sup> CTLs retained partial mitochondrial structures. Overall, these results supported the hypothesis that mitochondria were lost or disrupted after activation in *Usp30*<sup>-/-</sup> CTLs.

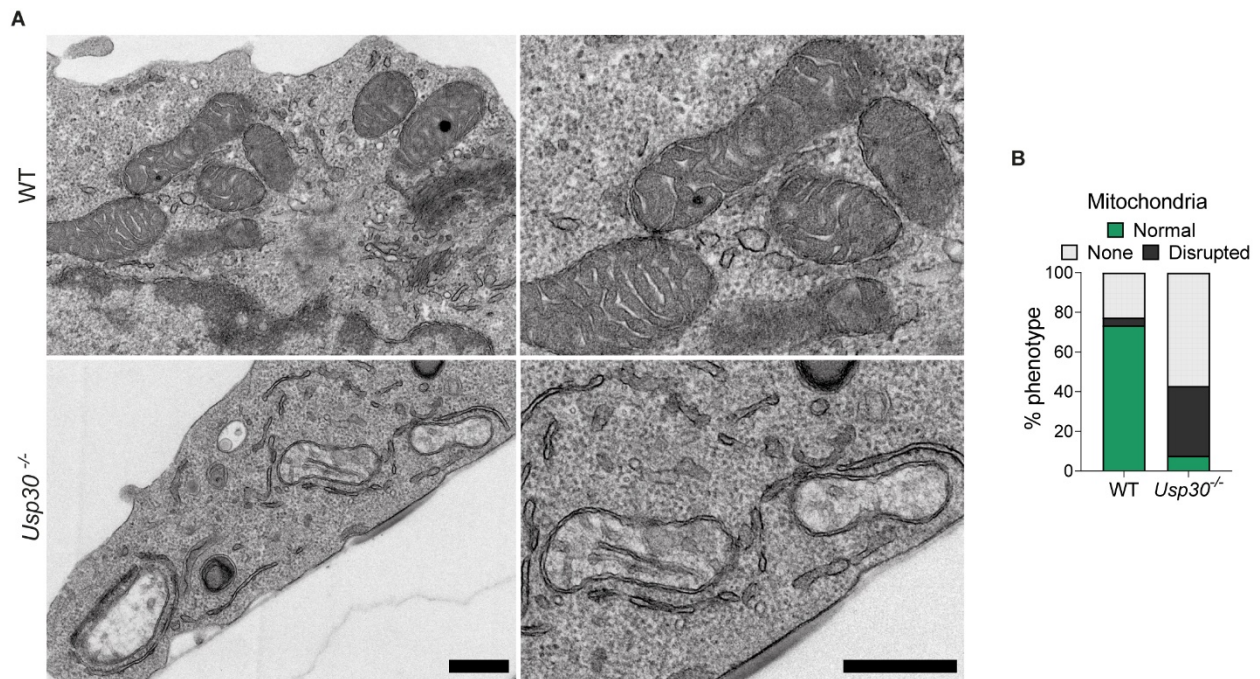


**Figure 3.5. Mitochondria in *Usp30*<sup>-/-</sup> show loss of inner cristae structure.**

(A) Transmission electron microscopy (TEM) sections (70 nm) of mitochondria in day 5 WT and *Usp30*<sup>-/-</sup> CTLs ( $2 \times 10^6$  CTLs/sample). Scale bars=500 nm. (B) Quantitation of mitochondrial phenotypes (normal = normal mitochondria, disrupted = disrupted mitochondrial morphology, none = no mitochondria in the section) in TEM images from 128 WT and 154 *Usp30*<sup>-/-</sup> cell profiles. TEM samples were prepared, processed and analysed by Jane Stinchcombe. Data representative of two independent biological replicates.

Given the striking disruption in mitochondrial cristae organisation (**Figure 3.5A**) and in mitochondrial membrane potential (**Figure 3.3**), I assayed mitochondrial respiration in day 5 WT and *Usp30*<sup>-/-</sup> CTLs using a Seahorse XF Cell Mito Stress Test assay (**Figure 3.6**). The Seahorse assay calculates oxygen consumption rate (OCR) as a measure of OXPHOS, and extracellular acidification rate (ECAR) as an indicator of glycolysis. Media acidification is due to the secretion of lactate as a product of glycolysis (Ferrick et al., 2008). OXPHOS is modulated by the addition of oligomycin, FCCP (the protonophore trifluoromethoxy carbonylcyanide phenylhydrazone) and a combination of rotenone and antimycin A. These drugs impair ATP synthesis (Lardy et al., 1958), uncouple ATP production from electron transport (Cunarro and Weiner, 1975; Heytler and Prichard, 1962) and inhibit complex I and III of the ETC (Lindahl and Oberg, 1961; Potter and Reif, 1952), respectively. These pharmacological treatments allow for quantitation of both basal and maximal oxygen consumption rate.

Basal OCR was higher in WT CTLs compared to *Usp30*<sup>-/-</sup> CTLs. WT OCR increased further upon FCCP addition, demonstrating that day 5 WT CTLs had ample spare respiratory capacity (**Figure 3.6A**). By contrast, *Usp30*<sup>-/-</sup> CTLs showed little OCR at resting state, with values only slightly higher than the signal associated with proton leak, measured as the difference between OCR after oligomycin addition and OCR after rotenone/antimycin A treatment. FCCP addition could not enhance OCR in *Usp30*<sup>-/-</sup> CTLs, indicating that the mitochondria in these cells were operating at their maximal respiratory capacity. These results suggested that despite the marked reduction in mitochondrial abundance, a small number of mitochondria were still able to engage OXPHOS in *Usp30*<sup>-/-</sup> CTLs.

Simultaneous analysis of ECAR highlighted dynamic responses of glycolysis upon pharmacological treatment in both WT and *Usp30*<sup>-/-</sup> CTLs. ECAR increased in WT CTLs when mitochondrial respiration was impaired (oligomycin addition) and decreased in both WT and *Usp30*<sup>-/-</sup> CTLs when OCR was maximised (FCCP addition) (**Figure 3.6B**). Basal ECAR was upregulated in untreated *Usp30*<sup>-/-</sup> CTLs compared to WT, implying that USP30 depletion resulted in an enhanced reliance on glycolysis (**Figure 3.6B, C**). Notably, there was little upregulation in *Usp30*<sup>-/-</sup> ECAR upon oligomycin addition, denoting that the increased reliance on glycolysis in untreated *Usp30*<sup>-/-</sup> was likely to represent the maximal glycolytic capacity of day 5 CTLs.

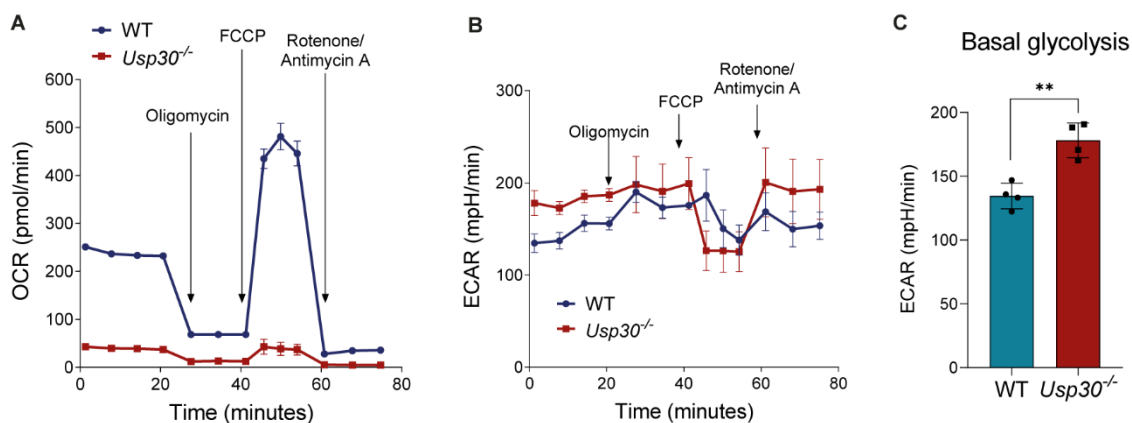


**Figure 3.6. Lack of USP30 results in loss of OXPHOS and increased glycolysis.**

(A) Mitochondrial respiratory capacity measured by oxygen consumption rate (OCR) in day 5 WT and *Usp30*<sup>-/-</sup> CTLs treated with 1 $\mu$ M oligomycin A, 1 $\mu$ M FCCP, 0.5 $\mu$ M rotenone and 0.5 $\mu$ M antimycin A. (B) Glycolytic flux as indicated by extracellular acidification rate (ECAR) in day 5 WT and *Usp30*<sup>-/-</sup> CTLs treated as in (A). (C) Basal glycolysis in day 5 WT and *Usp30*<sup>-/-</sup> CTLs quantitated by ECAR values at resting state. \*\*= $p < 0.01$  (two-tailed unpaired Student's t-test). Error bars show mean values  $\pm$ SD of technical replicates in one representative experiment ( $3 \times 10^5$  CTLs/sample). Data representative of three independent biological replicates.

As USP30 has been described as a negative regulator of mitophagy (Bingol et al., 2014; Liang et al., 2015), I asked whether the loss of mitochondrial in USP30-deficient CTLs could be attributed to an increase in mitophagy. To this end, I used the fluorescent probe Keima, a coral-derived protein whose fluorescence profile change on the basis of pH (Sun et al., 2017a; Sun et al., 2015). Upon excitation, Keima emission can be detected at 633 nm. Keima excitation changes according to the pH of the cellular compartment in which the probe is localised: while maximum excitation in a neutral or slightly basic environment (pH=7-8) can be obtained by exciting the compound at 488 nm, excitation at 561 nm is required for an optimal signal in an acidic environment (pH=4-5). Thus, Keima can be used to distinguish the pH of the organelles in which it is localised, and it has been employed to measure mitophagy upon targeting to the inner mitochondrial membrane (Sun et al., 2017b; Sun et al., 2015).

Mitochondria-targeted Keima (mt-Keima) exhibits maximal fluorescence when excited at 488 nm (hereafter defined as “green signal”) in healthy mitochondria. By contrast, mt-Keima displays maximal fluorescence when excited with the 561 nm laser (hereafter referred to as “red signal”) upon mitochondrial damage, when unhealthy mitochondria are degraded within acidic lysosomal compartments. The mt-Keima construct was introduced in WT and *Usp30*<sup>-/-</sup> CTLs by nucleofection and fluorescence was assessed by live microscopy. Most mitochondria in day 5 WT CTLs displayed green mt-Keima fluorescence, indicative of a healthy mitochondrial network (**Figure 3.7A**). By contrast, I observed a marked decrease in green signal and a higher proportion of red mt-Keima signal in USP30-deficient CTLs (**Figure 3.7A**). An average of 10% of mitochondria were undergoing degradation in day 5 WT CTLs against 52% in USP30-deficient CTLs (**Figure 3.7B**). These results demonstrated that mitophagy was upregulated in *Usp30*<sup>-/-</sup> CTLs, consistent with previously published work describing the role of USP30 in other cell types (Bingol et al., 2014; Liang et al., 2015).

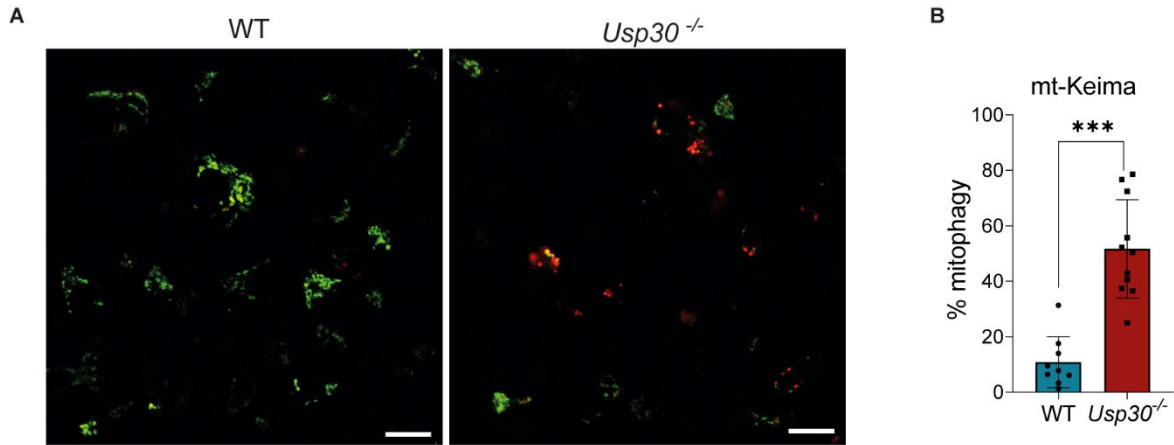


**Figure 3.7. *Usp30*<sup>-/-</sup> CTLs show increased mitophagy.**

(A) Representative images of mt-Keima signal in day 5 WT and *Usp30*<sup>-/-</sup> CTLs. Scale bars=15  $\mu$ m. (B) Quantitation of live cell imaging of day 5 WT and *Usp30*<sup>-/-</sup> CTLs expressing mt-Keima. Each data point shows percentage of mitolysosomes (red mt-Keima signal) in a 63 X field, indicative of mitophagy (>40 cells per genotype in each independent repeat). Error bars display mean values  $\pm$ SD of technical replicates in one representative experiment ( $2 \times 10^6$  CTLs/sample). \*\*\*= $p < 0.001$  (two-tailed unpaired Student's t-test). Data representative of three independent biological replicates.

### 3.4 TCR activation results in a decrease in peroxisomal markers in *Usp30*<sup>-/-</sup> CTLs

In addition to playing a role in mitophagy, USP30 counteracts the peroxisomal E3 ubiquitin ligase PEX2, thus acting as a negative regulator of pexophagy (Marcassa et al., 2018; Riccio et al., 2019). Therefore, I asked whether peroxisomes were degraded in *Usp30*<sup>-/-</sup> CTLs. First, I assessed the expression of the peroxisomal membrane protein PMP70 by immunoblot on day 3, 5, 7 and 9 post-stimulation (**Figure 3.8A**). While PMP70 expression was comparable in WT and USP30-deficient CTLs on day 3, PMP70 appeared downregulated in *Usp30*<sup>-/-</sup> CTLs from day 5 post-stimulation, with the most noticeable difference compared to WT CTLs appearing on day 7-9. Notably, PMP70 expression was not completely lost as observed with TOM20 (**Figure 3.4A**). However, PMP70 expression also did not decrease over time in WT CTLs, as opposed to the downregulation in TOM20 levels observed in activated WT CTLs (**Figure 3.4A**). This suggested different dynamics for either the regulation of mitophagy and pexophagy or specifically for TOM20 and PMP70 expression.

Next, I used immunofluorescence to detect the peroxisomal matrix enzyme catalase to further characterise peroxisomes in WT and *Usp30*<sup>-/-</sup> CTLs (**Figure 3.8B**). Immunostaining was performed on day 7 post-activation to examine peroxisomal morphology at a time point where the difference between WT and *Usp30*<sup>-/-</sup> CTL appeared most significant. Immunofluorescent detection of peroxisomes proved to be technically challenging, as catalase staining was difficult to distinguish above background signal, a feature that prevented the systematic quantitation of peroxisomes. Despite this, the fluorescence intensity of catalase staining suggested diminished protein abundance in USP30-deficient CTLs, supporting the results obtained by PMP70 immunoblotting.

To better examine whether the loss of USP30 resulted in peroxisome degradation, I employed the Keima probe by using a peroxisome-targeted construct based on the SKL peroxisomal localising motif (Keima-SKL) (Cunningham et al., 2015; Marcassa et al., 2018). WT and *Usp30*<sup>-/-</sup> CD8<sup>+</sup> T cells were nucleofected with Keima-SKL and analysed by live imaging to monitor peroxisome degradation. As with the mt-Keima probe, healthy peroxisomes could be detected by green Keima-SKL signal, while peroxisomal membranes undergoing degradation within lysosomes (pexophagy) could be detected by red Keima-SKL signal (**Figure 3.8C**). In agreement with the PMP70 Western blot data, pexophagy was not significantly upregulated in day 5 CTLs (**Figure 3.8D**). By contrast, day 7 *Usp30*<sup>-/-</sup> CTLs displayed an average surge in pexophagy from 28% (WT) to 43% (*Usp30*<sup>-/-</sup>) (**Figure 3.8D**), confirming that lack of USP30 resulted in increased peroxisome degradation, although not to the same extent as observed with mitophagy (**Figure 3.7**).

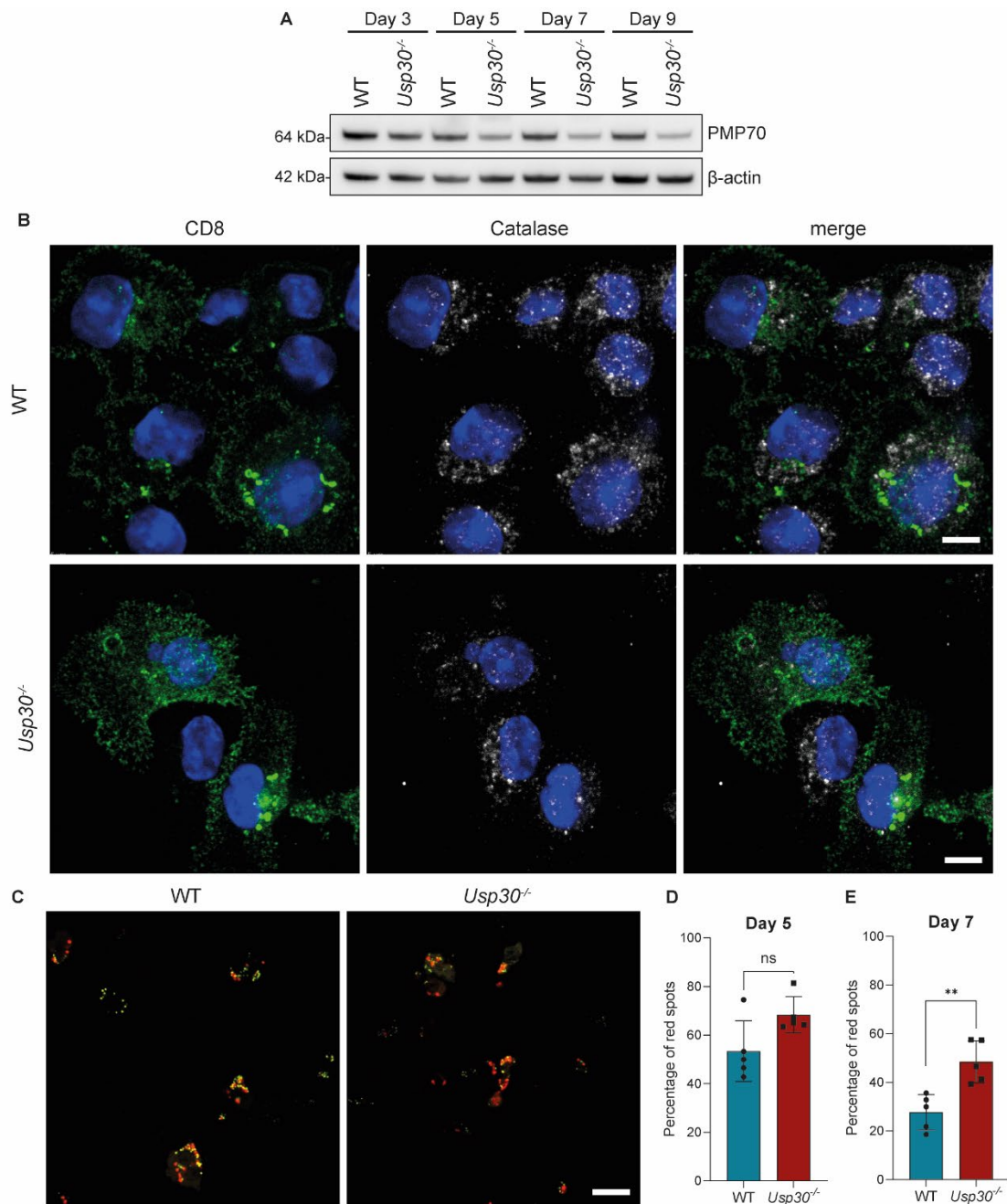


**Figure 3.8. Activated *Usp30<sup>-/-</sup>* CTLs show reduction in peroxisomal markers and increased pexophagy.**

(A) Immunoblot showing time course of PMP70 expression in activated (day 3-9 post-stimulation) WT and *Usp30<sup>-/-</sup>* CTLs (3.33  $\mu$ g lysate/sample). (B) Immunofluorescence staining of catalase in day 7 WT and *Usp30<sup>-/-</sup>* CTLs ( $3 \times 10^4$  CTLs/sample). Scale bars=10  $\mu$ m. (C) Representative images of Keima-SKL signal in day 7 WT and *Usp30<sup>-/-</sup>* CTLs ( $2 \times 10^6$  CTLs/sample). Scale bars=15  $\mu$ m. (D, E) Quantitation of live cell imaging of (D) day 5, and (E) day 7 WT and *Usp30<sup>-/-</sup>* CTLs expressing Keima-SKL. Each data point displays percentage of pexophagy (red Keima-SKL signal) in a randomly chosen 63 X field (>40 cells per genotype in each independent repeat). Error bars indicate mean values  $\pm$ SD of technical replicates in one representative experiment. \*\* =  $p < 0.01$ , ns=not significant (two-tailed unpaired Student's t-test). Data representative of at least two independent biological replicates.

### 3.5 Analysis of autophagic flux in USP30-depleted CTLs

The higher rate of mitophagy and pexophagy observed in USP30-deficient CTLs prompted the analysis of overall autophagic flux. LC3 protein expression is detected in two forms by Western blot, with the lower molecular weight band representing LC3B (or LC3-II), the mature form of LC3 that is conjugated to the autophagosome (Klionsky et al., 2021). LC3B is degraded upon fusion of the autophagosome with lysosomes (autolysosomes). Therefore, decreased LC3B expression can either indicate a defect in autophagosome formation or increased formation of autolysosomes. To distinguish between these two scenarios, I treated WT and *Usp30*<sup>-/-</sup> CTLs with Bafilomycin A (BAF). BAF is a potent inhibitor of the vacuolar-type H<sup>+</sup>-ATPase (V-ATPase) that couples ATP hydrolysis to cation transfer, allowing for the acidification of cellular organelles, including lysosomes (Bowman et al., 1988). In addition, BAF treatment prevents autophagosome fusion with lysosomes (Yamamoto et al., 1998). By hindering lysosomal acidification and autolysosome formation, LC3B is not degraded and its total expression can be measured.

LC3B expression was reduced in day 5 *Usp30*<sup>-/-</sup> CTLs (**Figure 3.9A**), suggesting either an increase in autophagic flux (and therefore enhanced degradation of LC3B) or defective autophagosome formation (thus lower abundance of LC3B due to fewer autophagosomal structures). To understand the cause of LC3B decrease, I treated both day 5 WT and *Usp30*<sup>-/-</sup> CTLs with BAF and analysed LC3B expression in untreated and treated CTLs by Western blot. I found a marked upregulation in LC3B in both WT and *Usp30*<sup>-/-</sup> CTLs after a short term (4h) BAF treatment (**Figure 3.9B**). These data indicated that the downregulation in LC3B expression observed upon loss of USP30 depends on higher autophagic flux and not on defective autophagosome formation. Taken together with the mt-Keima and Keima-SKL live imaging data, these results support the hypothesis that loss of USP30 relieves the break on autophagy and targets mitochondria and peroxisomes for engulfment by the autophagosome and degradation within lysosomes.

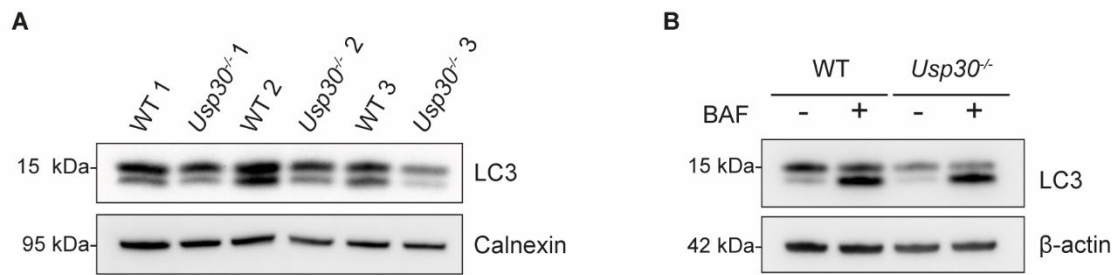


**Figure 3.9. Increased autophagic flux in day 5 *Usp30*<sup>-/-</sup> CTLs.**

(A) LC3 expression in three biological replicates of day 5 WT and *Usp30*<sup>-/-</sup> CTLs. (B) LC3 expression in untreated and bafilomycin A (BAF)-treated (400nM, 4h) day 5 WT and *Usp30*<sup>-/-</sup> CTLs. Data in (B) representative of two independent biological replicates (3.33 μg lysate/sample).

### 3.6 Loss of USP30 impairs CTL cytotoxicity

As USP30 was identified as a regulator of CTL cytotoxicity in a mixed T cell population (>70% CD8<sup>+</sup> T cells) (Abeler-Dörner et al., 2020), I aimed to confirm these results by using CD8<sup>+</sup> purified day 5 CTLs.

Using a short-term (2.5h) assay, I incubated effector T cells and target P815 mastocytoma cells at different CTL:target ratios. Target lysis was achieved by incubating the P815 target cells with α-CD3 in order to trigger TCR crosslinking upon T cell-target contact. Target cell death was quantitated based on LDH release from dying cells. This short-term killing assay showed that *Usp30*<sup>-/-</sup> CTLs had diminished killing potential at all tested CTL:target ratios (**Figure 3.10A**), confirming previous observations in the 3i screen (Abeler-Dörner et al., 2020).

Next, I aimed to characterise T cell cytotoxicity over time in a long-term (>10h) killing assay. For this experiment, I used the IncuCyte system, together with P815 targets transduced with the NuLight Red lentiviral construct and coated with α-CD3 as described above. Target cell lysis was measured by loss of red fluorescent nuclei. I first used the 10:1 CTL:target ratio, which allowed WT CTLs to kill all target cells within 7h from the start of the assay. While USP30-deficient CTLs were still able to kill, they needed at least 10h to achieve complete target cell death (**Figure 3.10B**). Next, I performed a long term IncuCyte-based killing assay by seeding the cells at a 1:1 CTL:target ratio to further challenge T cell-mediated killing. Interestingly, WT CTLs were able to kill rapidly for the first 4h, after which killing slowed down (**Figure 3.10C**). WT T cells required 14-16h to achieve complete target cell lysis. The killing capacity of *Usp30*<sup>-/-</sup> CTLs was strikingly different at the 1:1

CTL:target ratio. While USP30-deficient CTLs were able to induce target cell apoptosis for the first 4h, killing was ablated at later time points. These results indicated that loss of USP30 significantly prolongs killing time when T cells were in excess compared to target cells, and it caused a loss of cytotoxicity after 4h when T cells and target cells were found in equal numbers.

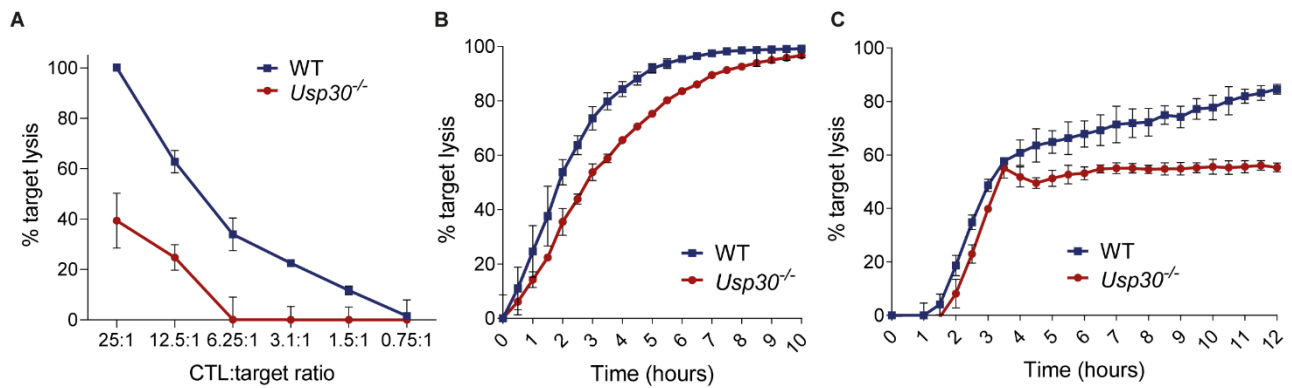


**Figure 3.10. Loss of USP30 impairs CTL killing.**

(A) Short-term (2.5h) killing assay with day 5 WT and *Usp30*<sup>-/-</sup> CTLs, varying CTL:target ratio.  $10^4$  targets/sample. CTLs numbers varying according to ratio:  $2.5 \times 10^5$  (25:1),  $1.25 \times 10^5$  (12.5:1),  $6.25 \times 10^4$  (6.25:1),  $3.1 \times 10^4$  (3.1:1),  $1.5 \times 10^4$  (1.5:1) and  $7.5 \times 10^3$  (0.75:1) CTLs/sample. (B) Long-term (10h) killing assay showing percentage of target cell lysis over time (CTL:target ratio, 10:1) with day 5 WT and *Usp30*<sup>-/-</sup> CTLs ( $4 \times 10^3$  targets and  $4 \times 10^4$  CTLs per sample). (C) Long-term (12h) killing assay displaying percentage of target cell lysis over time (CTL:target ratio, 1:1) with day 5 WT and *Usp30*<sup>-/-</sup> CTLs ( $4 \times 10^4$  targets and  $4 \times 10^4$  CTLs per sample). Errors bars in (A-C) indicate mean values  $\pm$ SD of technical replicates in one representative experiment. Data representative of at least three independent biological replicates.

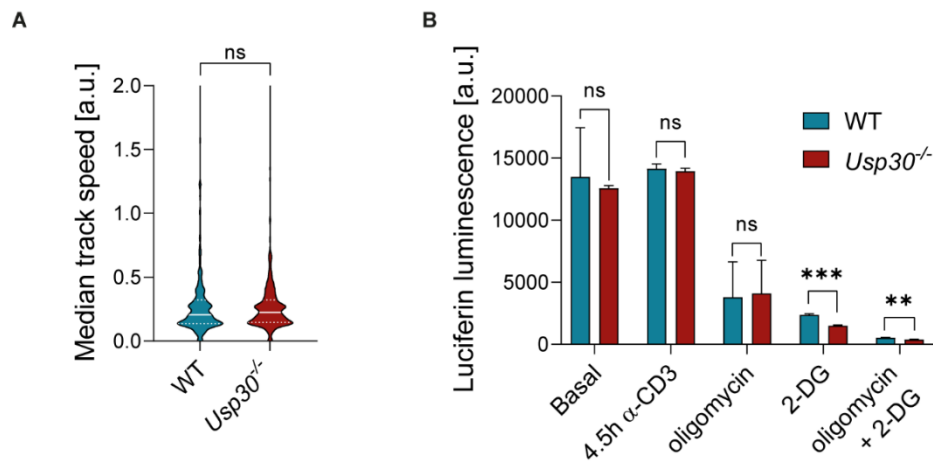
### 3.7 ATP generation and CTL migration are not affected by lack of USP30

To elucidate the cytotoxicity defect in *Usp30*<sup>-/-</sup> CTLs, I asked which aspect of killing could be impaired by the loss of USP30. The first step in T cell-mediated cytotoxicity is migration towards the site of infection or tumorigenesis. Mitochondria play a role in lymphocyte migration (Campello et al., 2006). Therefore, I measured migration of WT and USP30-deficient CTLs by live microscopy. Cell nuclei were stained with the cell-permeable dye Hoechst to monitor cell migration based on nuclei displacement. CTLs were nucleofected with the LifeAct-mApple construct to label F-actin and observe qualitative changes in actin dynamics during migration. Track speed per cell was quantitated and showed no deficiency in migration speed upon loss of USP30 (**Figure 3.11A**). Migratory characteristics such as an enrichment in F-actin at the leading edge and the presence of filopodia at the cell uropod were observed in both WT and *Usp30*<sup>-/-</sup>, indicating that USP30-deficient CTLs were not experiencing gross defects in actin dynamics during cell migration.

As lymphocyte migration can be propelled by mitochondria-derived ATP (Campello et al., 2006), I next measured cellular ATP in WT and *Usp30*<sup>-/-</sup> CTLs. I used a luminescence-based assay, which takes advantage of the ATP requirement for the activity of the enzyme luciferase. Upon addition of equal concentrations of D-luciferin substrate to cell lysates, luciferin luminescence can be used to estimate the ATP present in the samples. ATP concentration showed variability in both WT and *Usp30*<sup>-/-</sup> unstimulated CTLs, likely dependent on fluctuations in energy demands (**Figure 3.11B**). However, no reproducible difference in ATP concentration could be detected, implying that energy levels are met in USP30-deficient CTLs despite the loss of mitochondria. ATP concentration was also quantitated after stimulation to mimic T cell activation upon TCR crosslinking with  $\alpha$ -CD3. Measurements were taken 4.5h after stimulation to assess ATP concentration when sustained CTL killing was challenged (**Figure 3.10C**). No difference in ATP generation was found between WT and *Usp30*<sup>-/-</sup> CTLs, confirming that even during TCR triggering, ATP production is not limiting for *Usp30*<sup>-/-</sup> CTL function. Interestingly, ATP concentration did not significantly increase upon TCR crosslinking, indicating that either the reaction substrate was limiting, or that maximal ATP synthesis occurs in resting day 5 CTLs even without re-stimulation.

As glycolysis can also be a source of ATP, and glycolytic flux was found to be upregulated upon loss of USP30 (**Figure 3.6B, C**), I hypothesised that *Usp30*<sup>-/-</sup> CTLs could be sustaining ATP levels via glycolysis. To assess the contribution of OXPHOS and glycolysis to ATP production, I treated WT and *Usp30*<sup>-/-</sup> CTLs with the ATP synthase inhibitor oligomycin and the glycolysis inhibitor 2-deoxyglucose (2-DG). 2-DG can enter glycolysis but cannot be fully metabolised, thus limiting glycolytic flux (Wick et al., 1957). Incubation of WT and *Usp30*<sup>-/-</sup> CTLs with both oligomycin and 2-DG almost completely abolished generation of ATP. Separate treatments with either oligomycin or 2-DG lowered ATP levels in both WT and *Usp30*<sup>-/-</sup> CTLs, with the largest and most reproducible decrease obtained with 2-DG treatment. This was consistent with the idea that effector T cells are highly glycolytic (Buck et al., 2016; Hedeskov, 1968), and that *Usp30*<sup>-/-</sup> CTLs had a higher reliance on glycolysis than WT CTLs, as shown by the increased reduction in ATP levels in 2-DG-treated *Usp30*<sup>-/-</sup> CTLs. Interestingly, oligomycin caused a marked decline in ATP levels not only in WT but also in *Usp30*<sup>-/-</sup> CTLs, despite the loss in mitochondrial abundance and function observed in these cells. While this result was surprising, TEM analysis highlighted the presence of ~10% WT-like mitochondria in *Usp30*<sup>-/-</sup> CTLs (**Figure 3.5B**). In addition, while OCR values were lower in *Usp30*<sup>-/-</sup> CTLs compared to their WT counterparts, oligomycin treatment could still induce a small decrease in OCR in *Usp30*<sup>-/-</sup> CTLs (**Figure 3.6A**), suggesting a detectable presence of mitochondrial

respiration despite loss of USP30. Taken together, these results indicated that a small population of WT-like mitochondria were retained in *Usp30*<sup>-/-</sup> CTLs, and that these mitochondria were able to engage OXPHOS and produce mitochondria-derived ATP.



### 3.8 *Usp30*<sup>-/-</sup> CTLs can trigger the signalling cascade associated with killing

Mitochondria have been suggested to participate to TCR signalling upon target cell encounter (Hoth et al., 2000). Given the loss of mitochondrial abundance and function, I asked whether day 5 *Usp30*<sup>-/-</sup> CTLs could recognise target cells. TCR crosslinking in effector T cells generates a signalling cascade propagated by phosphorylation events, leading to transcriptional, translational, metabolic and cytoskeletal changes (Cantrell, 2015; Courtney et al., 2018). Mass cytometry was used to monitor phosphorylation of both proximal (ZAP70, SLP76, PLC $\gamma$ 1, LCK) and distal (ERK1/2, AKT, STAT5, I $\kappa$ B, S6) markers of TCR signalling, as described previously (Ma et al., 2020). TCR signal transduction was not perturbed by loss of USP30, suggesting that *Usp30*<sup>-/-</sup> CTLs were able to

recognise target cells and to initiate the signalling cascade leading to target cell apoptosis (**Figure 3.12 A-I**).

To complement this analysis, I measured calcium flux in WT and *Usp30*<sup>-/-</sup> CTLs. TCR engagement leads to a surge in intracellular calcium concentration, modulating signalling and promoting lytic granule polarisation and secretion (Cantrell, 2015; Lancki et al., 1987; Takayama and Sitkovsky, 1987). Mitochondria participate in calcium flux by interacting with the ER (Rizzuto et al., 1993), and they can influence intracellular calcium concentration in T cells upon TCR triggering (Hoth et al., 1997; Quintana et al., 2006).

To ask whether the mitochondrial depletion observed in *Usp30*<sup>-/-</sup> CTLs would affect calcium flux, I used the ratiometric calcium dye INDO-1 to detect changes in intracellular calcium concentration. While INDO-1 is fluorescent even when not bound to calcium (excitation: 355 nm, emission: 450 nm), its fluorescence spectrum changes upon calcium binding (excitation: 355 nm, emission: 375 nm). By calculating the ratio of calcium-bound INDO-1 to calcium-unbound INDO-1, it is possible to measure changes in intracellular calcium levels while controlling for potential differences in dye uptake. Physiological calcium flux was mimicked by TCR crosslinking with  $\alpha$ -CD3, while maximal calcium flux was assessed using the ionophore ionomycin to trigger calcium influx across T cell plasma membrane (Lyll et al., 1980).

Basal intracellular calcium levels (time=0-60s) were equivalent in WT and *Usp30*<sup>-/-</sup> CTLs (**Figure 3.12J**). Calcium flux in *Usp30*<sup>-/-</sup> was not diminished in the absence of mitochondria. TCR crosslinking (t=60s) induced an increase in intracellular calcium that followed similar temporal dynamics in WT and *Usp30*<sup>-/-</sup> CTLs. However, intracellular calcium reached a higher concentration in USP30-deficient CTLs, and it was sustained for longer than in their WT counterparts. Ionomycin addition (t=300s) induced an instantaneous surge in calcium concentration, which was equivalent in WT and *Usp30*<sup>-/-</sup> CTLs and higher than the peak observed in *Usp30*<sup>-/-</sup> CTLs upon TCR crosslinking. The increase in intracellular calcium after ionomycin treatment was also sustained for longer in *Usp30*<sup>-/-</sup> CTLs. These results indicated that calcium flux was not inhibited, but potentiated, by loss of USP30.

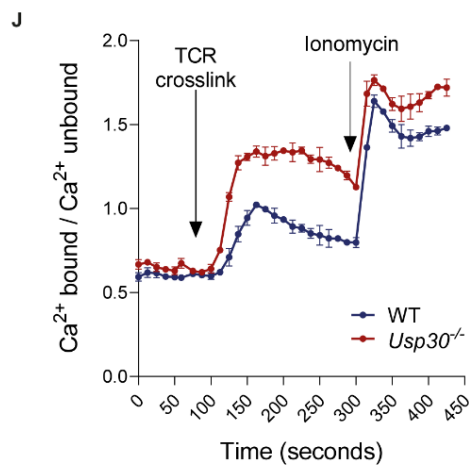
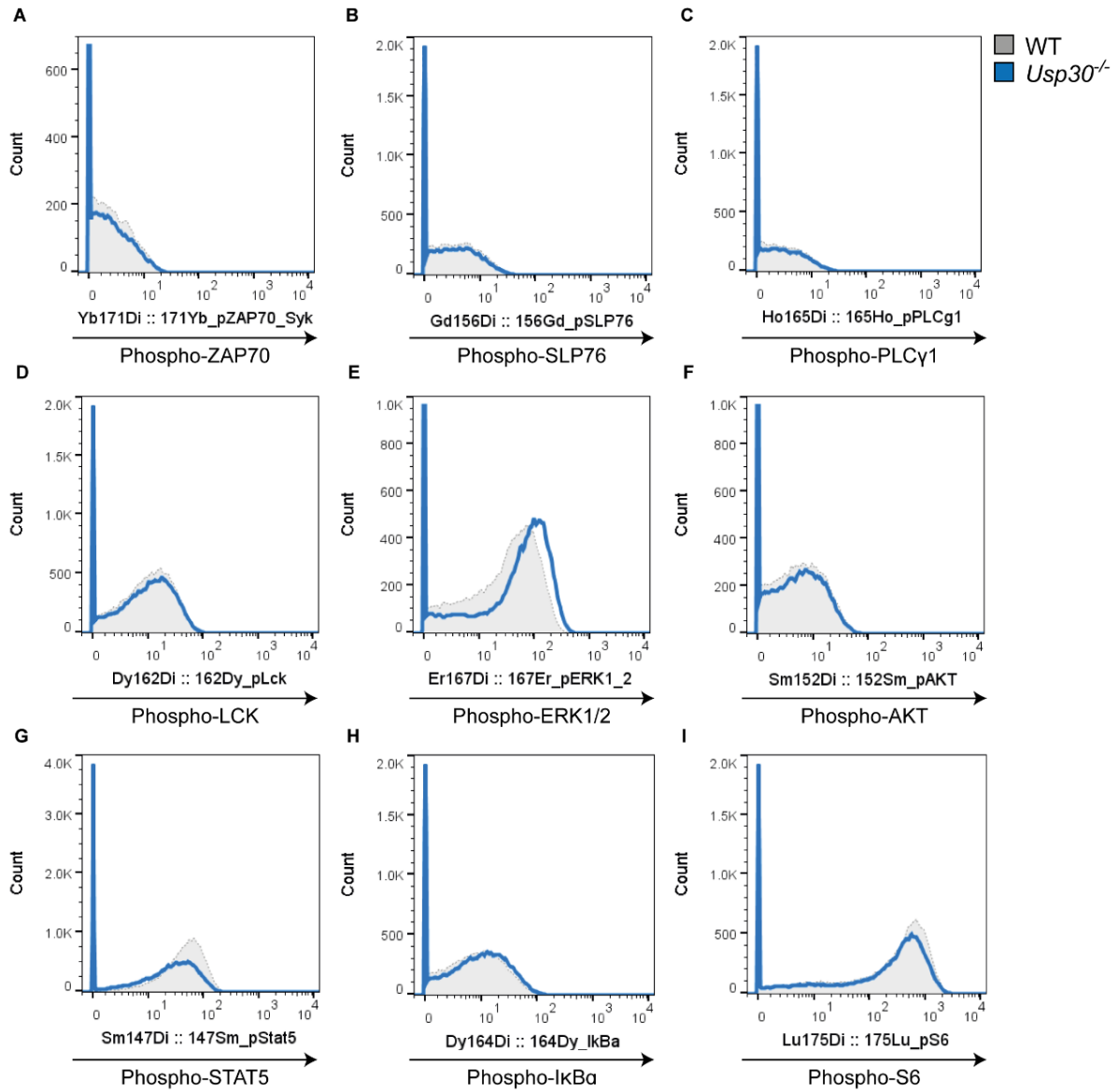


### Figure 3.12. Proximal and distal TCR signalling is not inhibited by mitochondrial depletion.

(A-I) TCR signal transduction in TCR activated WT and *Usp30*<sup>-/-</sup> CTLs (1.6x10<sup>5</sup> CTLs/sample) measured by phosphorylation of distal and proximal markers via mass cytometry. Histograms showing fluorescence intensity for (A) pZAP70, (B) pSLP76, (C) pPLC $\gamma$ 1, (D) pLCK, (E) pERK1/2, (F) pAKT, (G) pSTAT5, (H) pI $\kappa$ B $\alpha$  and (I) pS6. (J) INDO-1 calcium assay displaying changes in intracellular calcium concentration in day 5 WT and *Usp30*<sup>-/-</sup> CTLs before (t=0-60s) and after TCR crosslinking (t=60s) or ionomycin addition (t=300s). Error bars indicate mean values  $\pm$ SD of technical replicates in one representative experiment (0.5-1x10<sup>6</sup> CTLs/sample). Samples for mass cytometry were prepared and analysed by Claire Ma. Data representative of (A-I) two and (J) three independent biological replicates.

### 3.9 Target cell recognition and granule polarisation are not affected by loss of USP30

TCR crosslinking in effector CTLs leads to the polarisation of the centrosome and lytic granules at the IS (Stinchcombe et al., 2001b). Polarisation is followed by the fusion of lytic granules at the CTL plasma membrane (degranulation), allowing for the release of cytolytic proteins such as perforin and granzymes. Degranulation depends on TCR-triggered calcium influx (Lancki et al., 1987; Takayama and Sitkovsky, 1987). As the signalling cascade triggered by TCR crosslinking was not perturbed and calcium flux was potentiated, I asked whether a defect in lytic granule polarisation or secretion could cause the loss of cytotoxicity observed in *Usp30*<sup>-/-</sup> CTLs.

To analyse lytic granule polarisation at the IS, I co-incubated day 5 WT and *Usp30*<sup>-/-</sup> with  $\alpha$ -CD3-coated P815 target cells expressing FarnesylTag-BFP on their plasma membrane (Ritter et al., 2015). I determined the frequency of IS formation between a single CTL and a target cell by immunofluorescence (**Figure 3.13A, B**). Antibodies against the membrane protein CD8 were used to distinguish the T cell from the blue target cell, while LAMP1 identified granules and  $\gamma$ -tubulin the centrosome. CTLs displaying complete polarisation of the centrosome and lytic granules at the IS were scored as “conjugates” and the percentage of conjugated versus unconjugated CTLs was examined by microscopy in multiple, randomly chosen fields with a 63 X objective.

*Usp30*<sup>-/-</sup> CTLs did not display any defect in conjugate formation: not only were they able to polarise the centrosome and the lytic granules at the IS (**Figure 3.13A**), but they also formed conjugates with target cells as frequently as WT CTLs. On average, 20 minutes of co-incubation between CTLs and P815 targets allowed for 83% of WT and 77% of *Usp30*<sup>-/-</sup> to form conjugates, with no statistically significant difference (p=0.35) (**Figure 3.13B**). These results confirmed that loss of USP30 does not impair target cell recognition nor the formation of an IS.

Lytic granule polarisation at the IS is not always indicative of a successful degranulation event, as shown by investigation of CTLs derived from patients or murine models lacking the protein RAB27A (Menasche et al., 2000; Wilson et al., 2000), which mediates lytic granule fusion at the plasma membrane (Haddad et al., 2001; Stinchcombe et al., 2001a). To assess whether lytic granule polarisation was followed by granule fusion, we used a flow cytometry-based assay to determine LAMP1 surface expression on unstimulated and TCR-triggered CTLs. LAMP1 surface expression increases as lytic granules fuse with the plasma membrane and release their cytolytic content. Degranulation is measured by monitoring LAMP1 appearance on the cell surface in TCR-triggered CTLs and comparing it to LAMP1 surface expression before stimulation.

To this end, WT and *Usp30*<sup>-/-</sup> CTLs were either incubated alone or with  $\alpha$ -CD3-coated P815 target cells, and LAMP1 surface expression was analysed by flow cytometry (**Figure 3.13C, D**). Interestingly, LAMP1 signal intensity appeared decreased in both unstimulated and TCR-triggered *Usp30*<sup>-/-</sup> CTLs. This suggested either a defect in LAMP1 trafficking or lower total LAMP1 abundance. Nevertheless, LAMP1 surface expression increased in both WT and *Usp30*<sup>-/-</sup> CTLs upon target cell encounter. This result indicated that loss of USP30 did not prevent lytic granule fusion at the plasma membrane.

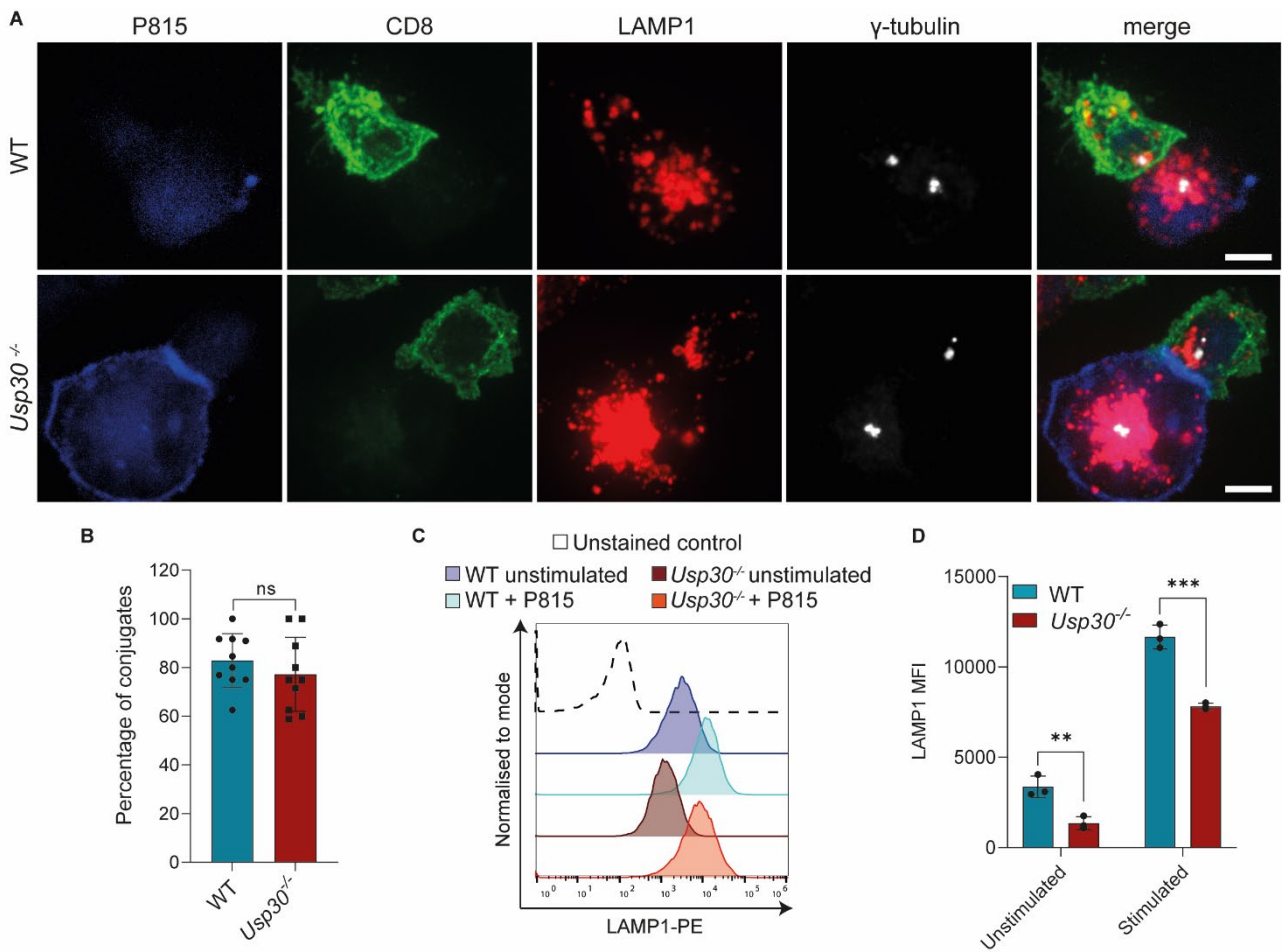


**Figure 3.13. *Usp30*<sup>-/-</sup> CTLs can induce organelle polarization at the IS.**

(A) Conjugates formed by  $3 \times 10^4$  day 5 WT or *Usp30*<sup>-/-</sup> CTLs (green) incubated with  $3 \times 10^4$  P815 targets (blue) showing polarization of cytolytic granules (red) and centrosome (white). Scale bars=5  $\mu$ m. (B) Quantitation of conjugate formation between day 5 WT and *Usp30*<sup>-/-</sup> CTLs and P815 target cells (>70 cells per genotype analysed in each independent repeat). Each dot displays the average % conjugates in a randomly chosen field, imaged with a 63 X objective. (C) Histograms representing surface LAMP1-PE fluorescence intensity in  $2 \times 10^5$  day 5 WT and *Usp30*<sup>-/-</sup> CTLs before and after incubation with  $2 \times 10^5$  P815 target cells. (D) Quantitation of LAMP1 MFI in unstimulated and TCR-triggered CTLs. Error bars in (B, D) indicate mean values  $\pm$ SD of technical replicates in one representative experiment. \*\*\*= $p < 0.001$ , \*\*= $p < 0.01$ , ns=not significant (two-tailed unpaired Student's t-test). Data representative of at least three independent biological replicates.

### 3.10 Lytic granule content and size are reduced in *Usp30*<sup>-/-</sup> CTLs

This stepwise analysis of the killing process indicated that *Usp30*<sup>-/-</sup> CTLs were able to migrate, recognise target cells, and trigger the signalling events that lead to target cell apoptosis, from TCR-dependent phosphorylation events and calcium fluxes, up to secretion of lytic granule content. Given the cytotoxicity defect observed in *Usp30*<sup>-/-</sup> CTLs, I asked whether the lytic granules themselves were perturbed by loss of USP30. TEM sections from day 5 WT and *Usp30*<sup>-/-</sup> CTLs revealed no changes in lytic granule inner morphology, as demonstrated by the presence of a dense core (**Figure 3.14A**), or in lytic granule number (**Figure 3.14B**). However, the size of the granules appeared smaller in *Usp30*<sup>-/-</sup> (**Figure 3.14A, C**), prompting the analysis of lytic granule content.

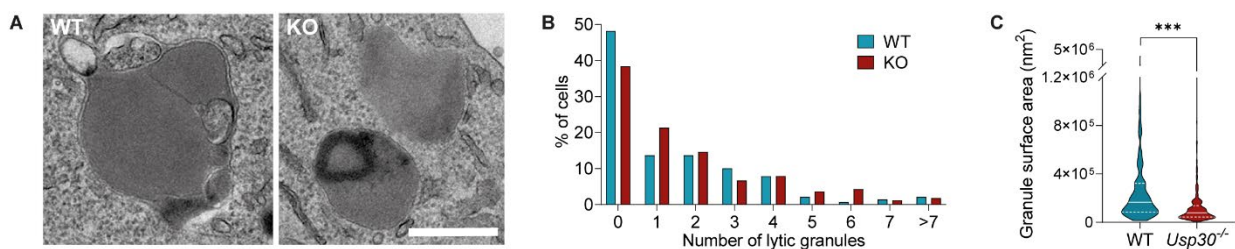


**Figure 3.14. Lytic granules are smaller in *Usp30*<sup>-/-</sup> CTLs.**

(A) TEM sections (70 nm) of lytic granules in day 5 WT and *Usp30*<sup>-/-</sup> (KO) CTLs (2x10<sup>6</sup> CTLs/sample). Scale bar=500 nm. (B, C) Quantitation of (B) lytic granule number (solid line=median; dotted lines=quartiles) and (C) cross-sectional surface areas from 139 (WT) and 164 (*Usp30*<sup>-/-</sup>) profiles. \*\*\*=p<0.001 (two-tailed unpaired Student's t-test). TEM samples were processed and analysed by Jane Stinchcombe. Data representative of two independent biological replicates.

I used immunoblotting to assess the protein abundance of two of the main players of the killing response: the pore-forming protein perforin and the pro-apoptotic granzyme B (**Figure 1.1**). Granzyme B expression steadily increased after T cell stimulation, peaking between day 7 and 9 after stimulation in WT CTLs (**Figure 3.15A**). While granzyme B abundance was similar in day 3 WT and *Usp30*<sup>-/-</sup> CTLs, it was reduced in USP30-depleted CTLs on day 5. Granzyme B expression was not upregulated in subsequent days as observed in WT CTLs. This result indicated that the main component of lytic granules (Howden et al., 2019; Hukelmann et al., 2016) was present in lower abundance in *Usp30*<sup>-/-</sup> CTLs.

Immature forms of perforin can be distinguished by their molecular weight, as newly synthesised perforin is conjugated to a mannose-6-phosphate group, to which complex glycans are added in the Golgi (Uellner et al., 1997). This causes immature forms of perforin to run as two higher molecular weight bands (ER and Golgi forms). Proteolytic cleavage prior to storage in lytic granules generates the mature, lowest molecular weight band (Uellner et al., 1997).

Perforin expression increased in WT CTLs as they acquired cytolytic capacity, reaching a peak on day 9 after stimulation (**Figure 3.15B**). Perforin expression was downregulated in *Usp30*<sup>-/-</sup> CTLs at all time points tested. In addition, immunoblotting showed the appearance of higher molecular weight bands, indicative of delayed perforin synthesis. As the abundance of perforin on day 9 prevented an accurate analysis by Western blot in day 5 and day 7 CTLs, day 5 samples were also run separately to assess whether the defect in perforin production was present at the same time point in which the decrease in granzyme B could be observed (**Figure 3.15C**). As in day 9 samples, the prevalent form of perforin in day 5 WT CTLs was the mature one. The two immature forms of perforin were detected in day 5 *Usp30*<sup>-/-</sup> CTLs, whereas the mature product was less abundant. Taken together, these results demonstrated that while lytic granule secretion was largely unperturbed in USP30-depleted CTLs, the granule size and content were diminished, likely inhibiting the efficacy of the killing response.

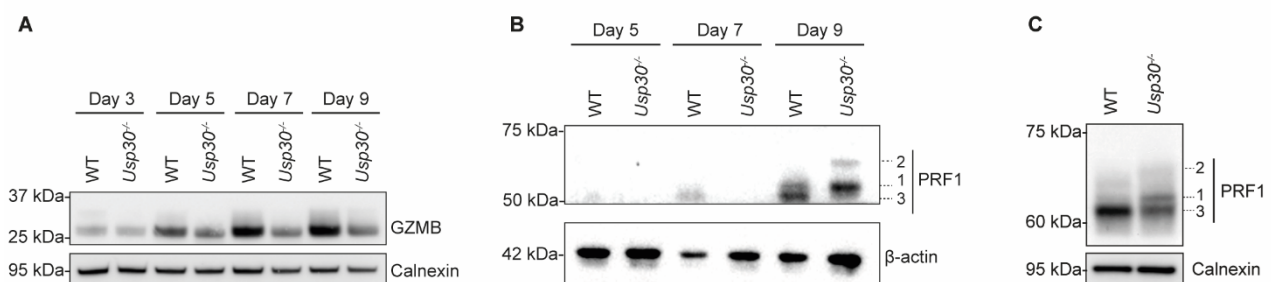


**Figure 3.15. Loss of USP30 results in reduced abundance of cytolytic proteins.**

(A-C) Immunoblots for (A) granzyme B (GZMB) and (B, C) perforin (PRF1) in WT and *Usp30*<sup>-/-</sup> CTLs (3.33  $\mu$ g lysate/sample). Western blots in (A, B) display time course of granzyme B and perforin expression in activated CTLs, while (C) shows perforin expression in day 5 CTLs only. Immature (1), intermediate (2) and mature (3) forms of perforin are labelled. Data representative of at least three independent biological replicates.

### 3.11 Cytosolic translation is impaired in *Usp30*<sup>-/-</sup> CTLs

Mitochondrial dysfunction in naïve CD8<sup>+</sup> T cells can cause defective IL-2 signalling, which leads to a downstream inhibition of granzyme B and perforin transcription (Fischer et al., 2018). Our *in vitro* cell culture provides high concentration of murine IL-2 (100U/ml), and I did not observe substantial defects in the expression of the IL-2  $\alpha$  chain receptor (CD25) upon T cell stimulation (**Figure 3.2D, E**).

To further interrogate this mechanism as a potential cause for diminished cytolytic protein expression, I quantitated mRNA abundance of perforin and granzyme B, and I found it to be similar in WT and *Usp30*<sup>-/-</sup> CTLs (**Figure 3.16A**). This analysis indicated that the reduced lytic granule content was not a consequence of a transcription defect of the *Gzmb* and *Prfl* genes, and pointed to either a defect in translation or increased degradation as potential causes of diminished protein abundance.

I monitored translation by depriving CTLs of methionine and supplementing the cell culture media with HPG, a methionine analogue, to measure *de novo* protein synthesis. Cells deprived of methionine rapidly incorporate HPG, which can be fluorescently labelled via click chemistry; this assay has also been used in CTLs (Araki et al., 2017). By analysing HPG fluorescence via flow cytometry, I observed a decrease in *de novo* protein synthesis in unstimulated day 5 *Usp30*<sup>-/-</sup> CTLs (**Figure 3.16B, C**). HPG incorporation marginally increased when prolonging the incubation of unstimulated *Usp30*<sup>-/-</sup> CTLs with HPG (4.5h), although it did not reach the levels observed in WT CTLs. Therefore, loss of USP30 was correlated with a dramatic inhibition of protein synthesis, which was likely to affect the expression of cytolytic proteins.

TCR crosslinking induces preferential translation of mRNA species of proteins involved in killing, such as TNF $\alpha$  and IFN $\gamma$  (Anderson, 2008). To ask whether the reduced protein synthesis observed in *Usp30*<sup>-/-</sup> CTLs could be enhanced by TCR engagement, I used HPG to measure cytosolic translation in  $\alpha$ -CD3-stimulated CTLs. No substantial increase in protein synthesis was observed in WT CTLs, regardless of the length of the stimulation (1h and 4.5h TCR activation) (**Figure 3.16B, C**). This suggested that either HPG concentration was limiting, or that while selectivity for specific mRNA species might vary, WT CTLs operate at their maximum translational capacity even in the absence of TCR-mediated stimulation (**Figure 3.16B, C**). This is consistent with previous observations indicating that day 5 post-activation CD8<sup>+</sup> CTLs are especially translationally active compared to both naïve CD8<sup>+</sup> T cells and to CTL at later stages after restimulation (Araki et al., 2017). On the other hand, while short-term TCR crosslinking had little effect on *Usp30*<sup>-/-</sup> CTLs, prolonged TCR stimulation (4.5h) increased the percentage of *Usp30*<sup>-/-</sup> CTLs showing efficiently translation.

Nevertheless, even after 4.5h of stimulation, CTL lacking USP30 could not reach the same protein synthesis efficiency as WT CTLs.

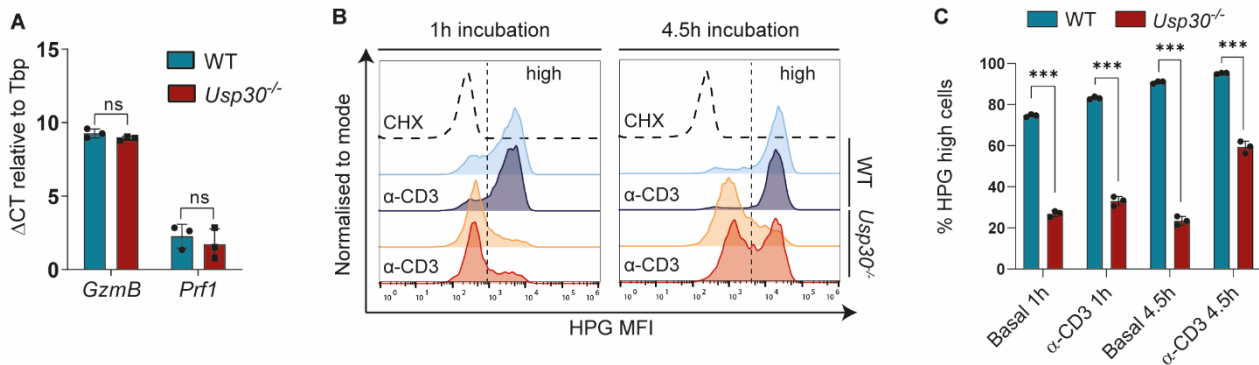


**Figure 3.16. *Usp30*<sup>-/-</sup> CTLs show profound reduction in protein synthesis.**

(A) Granzyme B (*Gzmb*) and perforin (*Prf1*) mRNA in day 5 WT and *Usp30*<sup>-/-</sup> CTLs (starting material: 100 ng cDNA/sample); ΔCT normalised to TATA-binding protein (Tbp). Error bars indicate mean values ±SD of three biological replicates. ns=not significant (two-tailed paired Student's t-test). (B) HPG-AF488 incorporation into day 5 WT and *Usp30*<sup>-/-</sup> CTLs (2x10<sup>5</sup> CTLs/sample), stimulated with α-CD3 (TCR triggering) where shown, compared with CTLs treated with 100μg/ml cycloheximide (CHX) in which cytosolic translation is inhibited (control). Samples were treated for 1h or 4.5h as indicated in the figure. Vertical line denotes position of the gate used to quantitate high HPG incorporation. (C) Percentage of CTLs displaying high HPG signal, as determined by vertical dashed line in (B). Error bars indicate mean values ±SD of technical replicates within one representative experiment. \*\*\*=p<0.001 (two-tailed unpaired Student's t-test). Data representative of at least three independent biological replicates.

### 3.12 Inhibition of *de novo* protein synthesis impairs killing by preventing the replenishment of cytolytic proteins

The long-term killing assay performed at the 1:1 CTL:target ratio showed that target cell killing slowed down in WT CTLs and was halted in *Usp30*<sup>-/-</sup> CTLs after 4h of incubation (**Figure 3.10C**). Given the impaired cytosolic translation observed in *Usp30*<sup>-/-</sup> CTLs, I asked whether the abundance of cytolytic proteins could be depleted after prolonged killing. I stimulated day 5 WT and *Usp30*<sup>-/-</sup> CTLs with α-CD3 for 4.5h and then compared perforin and granzyme B expression in unstimulated and stimulated CTLs.

Mature granzyme B decreased in stimulated WT CTLs. This was likely to be caused by granzyme B secretion occurring after TCR engagement (**Figure 3.17A**). A novel, higher molecular weight band

appeared, consistent with the molecular weight of newly synthesised glycosylated granzyme B (Caputo et al., 1993; Isaaz et al., 1995). Inhibition of cytosolic translation by cycloheximide (Obrig et al., 1971; Schneider-Poetsch et al., 2010) prevented the appearance of this band. These results suggested that granzyme B was synthesised *de novo* to fuel sustained killing. Mature granzyme B expression was low before stimulation and was further diminished upon TCR triggering in *Usp30<sup>-/-</sup>* CTLs. *De novo* synthesis of granzyme B was almost undetectable in  $\alpha$ -CD3-stimulated *Usp30<sup>-/-</sup>* CTLs.

Similarly, most perforin was found in the mature form in unstimulated WT CTLs. Mature perforin expression diminished in TCR-triggered WT CTLs, indicative of perforin secretion (**Figure 3.17B**). An increase in newly synthesised perforin could be observed in WT cells stimulated with  $\alpha$ -CD3, shown by the appearance of immature forms of perforin displaying a higher molecular weight. Most perforin in day 5 *Usp30<sup>-/-</sup>* CTLs was found in immature forms, as previously observed (**Figure 3.4B**). Despite the enhancement in protein translation detected upon prolonged stimulation (**Figure 3.16B, C**), *de novo* perforin synthesis was reduced in USP30-depleted CTLs compared to their WT counterparts. Altogether, repeated killing decreased the abundance of mature granzyme B and perforin in both WT and *Usp30<sup>-/-</sup>* CTLs. However, while efficient translation could allow for *de novo* synthesis of cytolytic proteins in the WT, granzyme B and perforin production was impaired in *Usp30<sup>-/-</sup>* CTLs.

These results suggested a requirement for *de novo* protein synthesis to sustain CTL killing. To address this question directly, I treated day 5 WT and USP30-depleted CTLs with CHX. WT and *Usp30<sup>-/-</sup>* CTLs could kill for the first 4h of the assay, regardless of CHX treatment (**Figure 3.17C**). However, CHX-treated WT CTLs showed a dramatic loss of killing after 4h. This result indicates that loss of cytosolic translation is sufficient to hinder sustained CTL killing.

Notably, cycloheximide had an additive effect on *Usp30<sup>-/-</sup>* CTLs. Cycloheximide-treated *Usp30<sup>-/-</sup>* CTLs killed more slowly for the first 6h, after which cytotoxicity was inhibited. Although USP30-deficient CTLs displayed reduced protein synthesis, translation was not completely halted (**Figure 3.16B, C**), possibly enabling CTL survival and sustaining initial killing events. Therefore, CHX treatment likely abolished the remaining cytosolic translation in *Usp30<sup>-/-</sup>* CTLs, further impairing killing (**Figure 3.17C**). Overall, these results demonstrated that *de novo* protein synthesis was essential to maintain cytotoxicity, and specifically pointed to a requirement for sustained translation of cytolytic proteins to promote CTL killing.

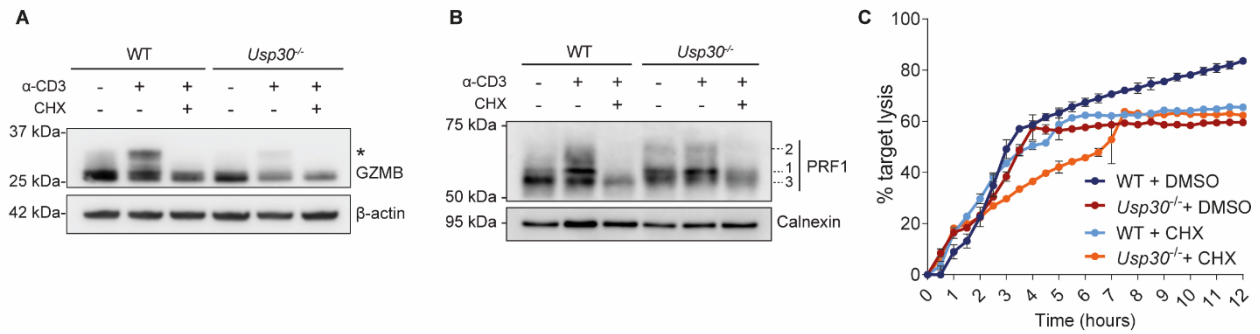


**Figure 3.17. *De novo* protein synthesis is required for sustained CTL killing and it is inhibited in *Usp30*<sup>-/-</sup> CTL**

(A, B) Immunoblots showing (A) granzyme B (GZMB) and (B) perforin (PRF1) in day 5 WT and *Usp30*<sup>-/-</sup> CTLs (3.33 μg lysate/sample) before and after 4.5h TCR activation with α-CD3 and/or treated with 100μg/ml CHX. Newly synthesised GZMB labelled by (\*); PRF1 forms labelled as (1) immature, (2) intermediate and (3) mature perforin products. (C) Long-term (12h) killing assay with day 5 WT and *Usp30*<sup>-/-</sup> CTLs (CTL:target, 1:1), treated with carrier (DMSO) or 100μg/ml CHX. Error bars indicate mean values ±SD of technical replicates in one representative experiment (4x10<sup>4</sup> targets and 4x10<sup>4</sup> CTLs per sample). Data representative of at least three independent biological replicates.

### 3.13 Proteomic analysis of *Usp30*<sup>-/-</sup> CTLs

To gain further insight into the impaired cytosolic translation observed upon USP30 depletion, we performed mass spectrometry analysis in day 5 WT and *Usp30*<sup>-/-</sup> CTLs. Samples were analysed in both the unstimulated (basal) and TCR-triggered (4.5h α-CD3) state. We observed that the decrease in protein synthesis did not affect all proteins equally, as only a subset of peptides was found to have a statistically significant (FDR<10%) lower expression in *Usp30*<sup>-/-</sup> CTLs under basal conditions (**Figure 3.18 A-C**). As expected, several downregulated proteins were found to be either mitochondrial (72%) or peroxisomal (3%), which is consistent with the role of USP30 as an inhibitor of mitophagy and pexophagy (**Figure 3.18B, C**).

Surprisingly, the glucose transporter SLC2A3/GLUT3 and the glycolysis enzymes HK1, HK2 and ALDOC were also found to be downregulated in *Usp30*<sup>-/-</sup> CTLs. These results could be due to HK1 and HK2 association with the mitochondrial membrane (Wilson, 2003). Given the enhanced glycolytic flux in *Usp30*<sup>-/-</sup> CTLs (**Figure 3.6B, C**), the presence of glycolytic enzymes in the downregulated dataset was surprising. This could highlight either a redundant role for these proteins, or a high expression that exceeds the glycolytic demand of the cell (Mehta et al., 2018).

Our analysis showed that the transcription factor eomesodermin (EOMES) and the cytotoxic protein granzyme B were found among the most highly downregulated proteins in unstimulated *Usp30*<sup>-/-</sup> CTLs (**Figure 3.18B**). EOMES regulates the expression of IFN $\gamma$ , granzyme B and perforin in CD8<sup>+</sup> T cells (Pearce et al., 2003), while granzyme B is both one of the main cytotoxic components of lytic granules and one of the most highly expressed proteins in CTLs (Howden et al., 2019; Hukelmann et al., 2016). These data point to a previously unknown T cell-specific defect in USP30-deficient cells, where lack of USP30 affects key regulators of CTL cytotoxicity.

We also observed a downregulation of acetylation/methylation factors mediating chromatin accessibility (OGSH, CSRP2, DLST, PHB2, ACSS2, TET2, BCL3, ALKBH1) and enzymes regulating the cholesterol biosynthetic pathway (LSS, LDLR, HMGCS1, RNF145, SREBF2, SC2D, SC5D, CYP51A1). Cholesterol biosynthesis is essential during CD8<sup>+</sup> T cell activation due to the membrane biosynthesis requirement for proliferation (Kidani et al., 2013). In addition, cholesterol availability influences membrane composition and TCR clustering, thus mediating TCR-dependent signalling (Bietz et al., 2017). These data suggested that in addition to the loss of mitochondrial and peroxisomal proteins, lack of USP30 was likely to affect cell proliferation, transcriptional regulation and cytotoxic potential, decreasing the ability of CTLs to mount an effective response upon antigen recognition.

Notably, a smaller set of proteins was upregulated in unstimulated *Usp30*<sup>-/-</sup> CTLs (**Figure 3.18A, B**). Within this set, we found the autophagy adaptor p62/SQSTM1, the lysosomal amino acid transporter and mTOR activator SLC38A9, and mediators of lipid droplets formation (BSCL2, PLIN2). In addition, several upregulated proteins in unstimulated *Usp30*<sup>-/-</sup> CTLs were found to be markers of ER stress and involved the integrated stress response. This list included CEBPB, HMOX1, AVIL/DOC6, BCL2L11, SLC6A9, NIBAN1, IFRD1, CTH and BBC3.

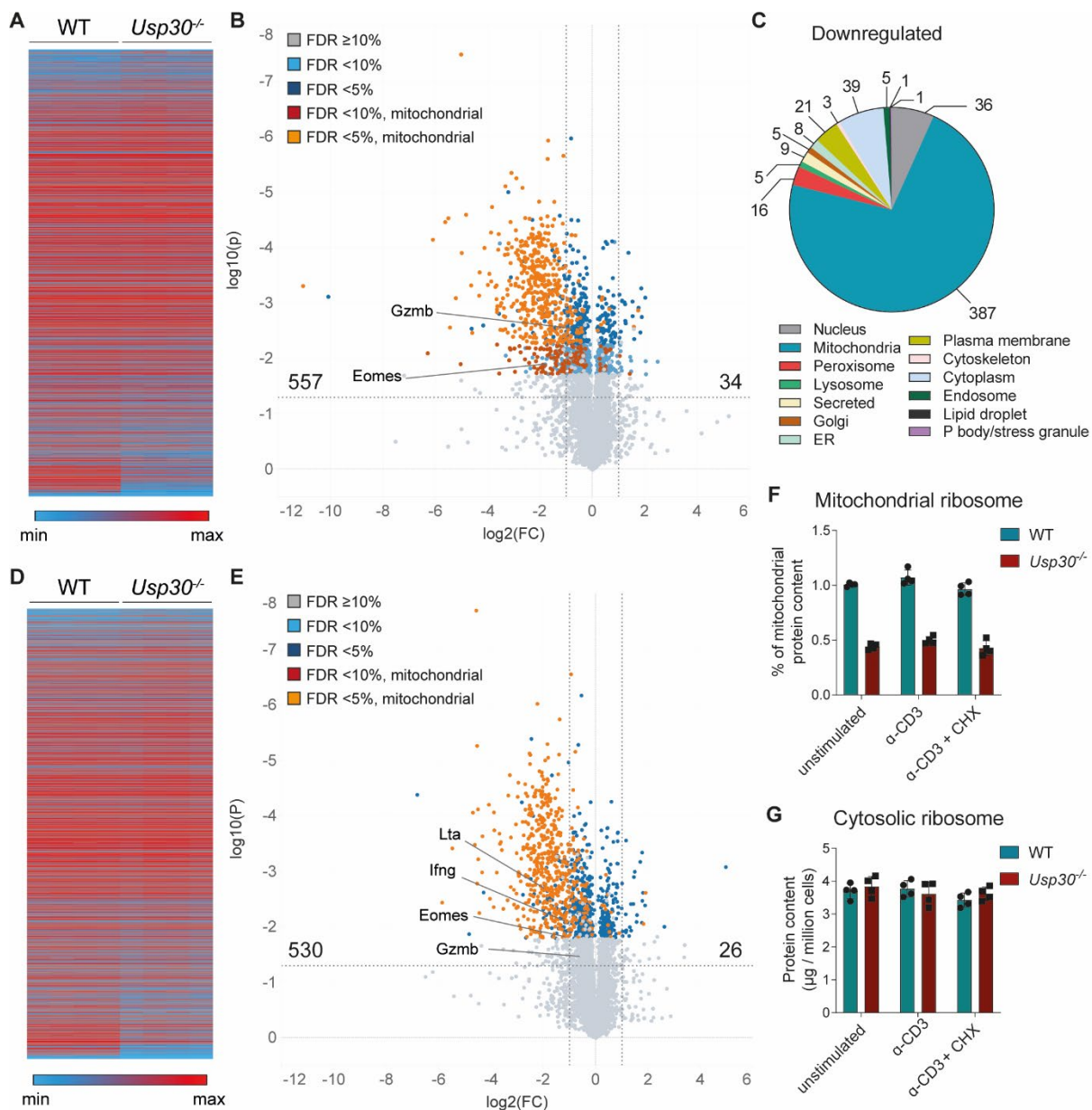


**Figure 3.18. Proteomic analysis of USP30-depleted CTLs.**

(A) Heat map displaying protein copy number in WT and *Usp30*<sup>-/-</sup> CTLs. (B) Volcano plot of upregulated (right quadrant) and downregulated (left quadrant) proteins in *Usp30*<sup>-/-</sup> CTLs compared to WT. Quadrants denote  $\log_2(\text{FC})=1, -1$  (vertical lines) and uncorrected  $p=0.05$  threshold (horizontal lines). Coloured dots show mitochondrial proteins and other hits within the 5% and 10% false discovery rate (FDR) range. The number of proteins with  $\text{FDR}<10\%$  and  $\log_2(\text{FC})>1$  or  $\log_2(\text{FC})<-1$  is indicated in each quadrant. (C) Localisation of downregulated proteins within <5% FDR in *Usp30*<sup>-/-</sup> CTLs. The number of proteins in each subcellular compartment is indicated on the pie chart. (D) Heat map for TCR activated WT and *Usp30*<sup>-/-</sup> CTLs. (E) Volcano plot of upregulated and downregulated proteins in stimulated *Usp30*<sup>-/-</sup> CTLs. Quadrants and colour scheme as in (B). Highlighted proteins are referenced by gene names in (B) and (E). (F, G) Percentage of mitochondrial ribosomal protein out of total mitochondrial peptides (F) and cytosolic ribosome protein expression (G) in unstimulated,  $\alpha$ -CD3 and 100 $\mu\text{g}/\text{ml}$  CHX-treated day 5 CTLs. Error bars=mean  $\pm$ SD from four independent biological replicates (2  $\mu\text{g}$  protein/sample). Julia M. Marchingo oversaw the sample processing and conducted the initial peptide analysis and protein copy number quantitation.

To investigate whether the translational profile of *Usp30*<sup>-/-</sup> CTLs could be altered upon TCR stimulation, we analysed protein expression in day 5 WT and *Usp30*<sup>-/-</sup> CTLs stimulated for 4.5h with  $\alpha$ -CD3. As in the unstimulated samples, we observed that the translation defect did not affect all proteins equally (**Figure 3.18D**). Many of the additional proteins showing a statistically significant reduction in expression upon stimulation (FDR<10%) were identified as mitochondrial (75%) and peroxisomal (2%) proteins (**Figure 3.18E**) as in the unstimulated samples. Mitochondrial ribosomal proteins were one of the most depleted subgroups (**Figure 3.18F**), while cytosolic ribosomes were not affected by the lack of USP30, indicating that the defect in cytosolic translation in *Usp30*<sup>-/-</sup> CTLs was not due to defective ribosomal content (**Figure 3.18G**).

EOMES and granzyme B were still downregulated in stimulated *Usp30*<sup>-/-</sup> CTLs, together with the cytokines IFN $\gamma$  and TNF $\beta$ /LT $\alpha$ , suggesting a further decrease in cytotoxic potential. The polyamine biosynthesis rate-limiting enzyme ODC1 was also downregulated upon stimulation. Polyamine biosynthesis is essential for cell proliferation and cytokine production (Puleston et al., 2019) and its reduction could be mediating the lower abundance of IFN $\gamma$  and TNF $\beta$ , together with additional cytokines and chemokines that were found to be significantly downregulated in stimulated *Usp30*<sup>-/-</sup> CTLs (IL-10, IL-4, TNFSF9, CCL1, CCL4). Interestingly, while granzyme B expression was reduced in both basal and TCR-triggered *Usp30*<sup>-/-</sup> CTLs, granzymes G, E, D and F were all significantly upregulated in the stimulated dataset. This result pointed to an altered regulation of granzyme expression in *Usp30*<sup>-/-</sup> CTLs upon activation.

TCR-triggered *Usp30*<sup>-/-</sup> CTLs displayed a highly significant upregulation of the exhaustion marker NR4A1/NUR77. NR4A1 has been described as a crucial player in T cell dysfunction, as it represses AP-1-mediated transcription and it leads to enhanced expression of exhaustion-associated genes (Liu et al., 2019). Notably, the NR4A1 repressor GADD45GIP1 was downregulated in both unstimulated and stimulated USP30-depleted CTLs.

Taken together, these results suggested that *Usp30*<sup>-/-</sup> CTLs were subject to an increase in inhibitory signals (NR4A1 upregulation) and a decrease in cytotoxic molecules (granzyme B, perforin, cytokines) upon stimulation, which were likely to mediate the killing defect observed in USP30-depleted CTLs. To confirm the defect in cytotoxic potential in *Usp30*<sup>-/-</sup> CTLs, we independently assessed the protein expression of TNF $\alpha$  and IFN $\gamma$  in day 5 CTLs before and after stimulation with  $\alpha$ -CD3 (4.5h). Our results showed that cytokine expression was reduced in stimulated *Usp30*<sup>-/-</sup> CTLs compared to stimulated WT CTLs, therefore confirming the mass spectrometry data (**Figure 3.19**).

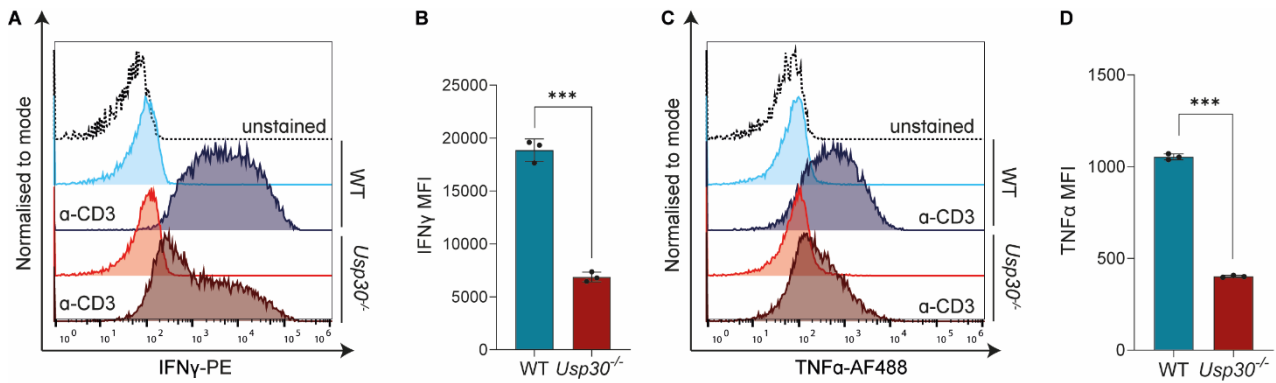


**Figure 3.19. Cytokine synthesis is impaired in *Usp30*<sup>-/-</sup> CTLs.**

(A) IFN $\gamma$  synthesis in  $2 \times 10^5$  day 5 WT and *Usp30*<sup>-/-</sup> CTLs before and after 4.5h  $\alpha$ -CD3 stimulation (TCR activation). (B) Quantitation of IFN $\gamma$  MFI in stimulated CTLs. (C) TNF $\alpha$  synthesis in  $2 \times 10^5$  day 5 WT and *Usp30*<sup>-/-</sup> CTLs before and after 4.5h  $\alpha$ -CD3 stimulation (TCR activation). (D) Quantitation of TNF $\alpha$  MFI in stimulated CTLs. \*\*\*= $p < 0.001$  (two-tailed unpaired Student's t-test). Data representative of at least three independent biological replicates.

### 3.14 Evidence for selectivity in the downregulation of protein expression in *Usp30*<sup>-/-</sup> CTLs

734 proteins with a statistically significant different expression (FDR<10%) in *Usp30*<sup>-/-</sup> CTLs were not known targets of USP30 deubiquitination. These additional proteins could be characterised by a short half-life and could be more susceptible to a decrease in protein synthesis. Therefore, I analysed the proteome of CTLs treated with CHX to ask which proteins would be affected by inhibition of translation. Next, I compared the mass spectrometry data from CHX-treated CTLs to the dataset obtained from *Usp30*<sup>-/-</sup> CTLs to examine whether USP30 depletion affected protein expression in a similar way as CHX treatment. Both datasets examined day 5 TCR-triggered CTLs.

Little correlation was observed between CHX treatment and USP30 depletion (**Figure 3.20A**). Only 9% of all proteins showing a statistically significant different expression (FDR<10%) were either upregulated or downregulated by both USP30 depletion and CHX treatment.

135 proteins were significantly downregulated in both datasets. Several were mitochondrial proteins, consistent with a requirement for cytosolic translation for their synthesis (D'Souza and Minczuk, 2018). These proteins included subunits of the electron transport chain (NDUFA4, NDUFA8, NDUFA11, NDUFAF7, NDUFS5, NDUFB5, NDUFB7, UQCRC1, UQCRC2) but also subunits of the mitochondrial ribosome and proteins involved in mitochondrial translation (MRPL4, MRPL9,

MRPL15, MRPL23, MRPL32, MRPS22, MRPS23, MRPS26, MRPS30, CHCHD1, GFM1). This result highlighted how inhibition of cytosolic protein synthesis could have a downstream effect on mitochondrial function and specifically translation, as previously reported (Couvillion et al., 2016).

Several cytokines and chemokines showed reduced expression upon both USP30 depletion and CHX treatment, consistent with their known post-transcriptional regulation (**Figure 3.20B**) (Salerno et al., 2017). Among these, 10 were statistically significant in both datasets (FDR<10%) (IL-10, IL-3, CCL4, CSF2, LT $\alpha$ , LIF, SPP1, TNFSF9, XCL1 and IFN $\gamma$ ). In addition, receptors involved in CTL signalling showed reduced expression in both datasets (IL4R, CD27, CD166, HAVCR2, ICOS, SLAMF7 and notably CD3 $\gamma$ ). LAG3, a cell surface protein associated with T cell exhaustion, was downregulated in both conditions, together with proteins participating to downstream TCR signalling, including JAK3 and NDFIP1. The expression of the transcription factors GATA3 and NOTCH1 (involved in T cell differentiation) was also reduced in both *Usp30*<sup>-/-</sup> and CHX-treated CTLs.

The only statistically significant protein upregulated by both USP30 depletion and CHX treatment was PTSS2 (**Figure 3.20A**). PTSS2 is a phosphatidylserine synthase protein enriched at the membrane contact sites between the ER and mitochondria (Stone and Vance, 2000). Increased phosphatidylserine expression on the plasma membrane is common in apoptotic lymphocytes (Fadok et al., 1992), and it might have been caused by loss of homeostasis in *Usp30*<sup>-/-</sup> and CHX-treated CTLs.

Despite these interestingly similarities, most of the proteomic changes observed in CHX-treated CTLs did not recapitulate the differences in protein expression detected in *Usp30*<sup>-/-</sup> CTLs. 961 proteins in USP30-depleted CTLs showed a statistically significant change in expression that was not recapitulated by CHX treatment, and 383 proteins were significantly affected by CHX treatment but not by USP30 depletion. As USP30 specifically inhibits mitophagy and pexophagy, it remained possible that the differentially affected proteins were mitochondrial and peroxisomal proteins that were selectively impacted by USP30 depletion but not by cycloheximide treatment. However, even upon exclusion of proteins with a known mitochondrial or peroxisomal localisation (as determined by KEGG terms), there were still 459 differentially affected proteins in *Usp30*<sup>-/-</sup> CTLs and 360 in CHX-treated CTLs. Overall, these results suggest that the protein synthesis defect observed in *Usp30*<sup>-/-</sup> CTLs was not equivalent to the acute, non-specific inhibition of translation induced by cycloheximide treatment. Reduction in cytosolic protein synthesis in USP30-depleted CTLs had a more selective effect than CHX on protein expression, and encompassed additional proteins beyond USP30's canonical mitochondrial and peroxisomal targets.

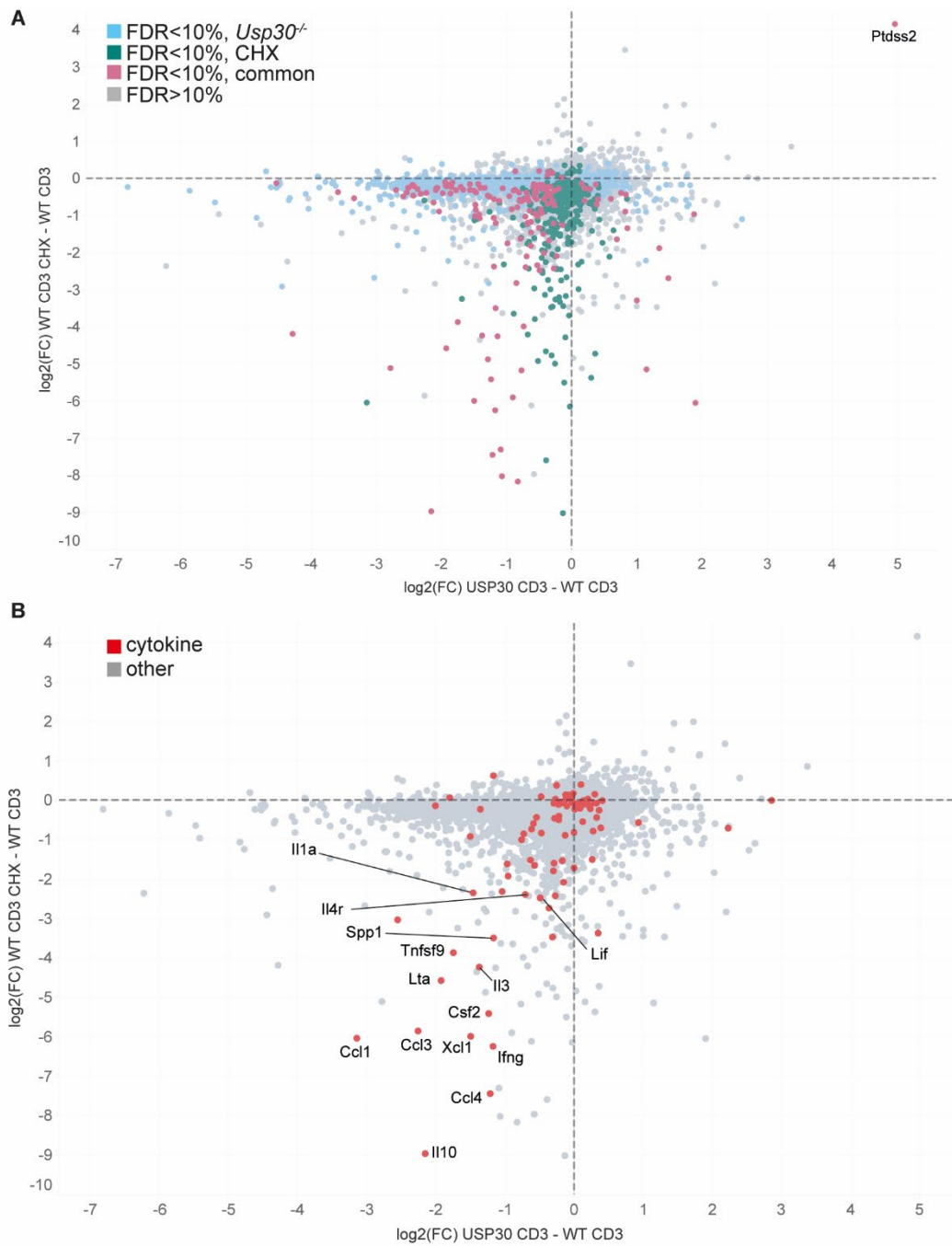


**Figure 3.20. Comparison of protein expression in USP30-depleted and CHX-treated CTLs.**

(A, B) Proteomes of stimulated (4h  $\alpha$ -CD3) day 5 CTLs from *Usp30*<sup>-/-</sup> CTLs compared with WT CTLs, and WT CTLs in which cytosolic translation was inhibited by 100 $\mu$ g/ml CHX compared with untreated CTLs. Comparison of effect sizes emphasises a selective downregulation of protein synthesis in *Usp30*<sup>-/-</sup> CTLs, with only partial overlap with the effects of CHX treatment. Dashed lines correspond to  $\log_2(\text{FC})=0$ . Coloured dots show proteins within the 10% false discovery rate (FDR) in the *Usp30*<sup>-/-</sup> vs WT dataset (light blue) and in the CHX vs untreated dataset (green). Magenta-labelled dots indicate proteins within the 10% FDR common to both datasets. (B) displays the same dataset as in (A), with cytokines highlighted in red and labelled by gene name. Data representative of four independent biological replicates (2  $\mu$ g protein/sample).

### 3.15 Analysis of PINK1/PARKIN expression in CTLs

USP30 has been described as a negative regulator of both PINK1/PARKIN-induced mitophagy and PEX2-induced pexophagy (Bingol et al., 2014; Riccio et al., 2019). The results presented in this Chapter indicated that *Usp30*<sup>-/-</sup> CTLs showed increased degradation of both mitochondria and peroxisomes. Loss of mitochondria was the most prominent defect on day 5 post-stimulation, when killing and translation also exhibited a marked reduction. To test whether the immunodeficiency observed in USP30-depleted CTLs was caused by mitochondria or peroxisomes, I aimed to downregulate mitophagy by inhibiting PINK1 expression. The kinase PINK1 bears a mitochondrial localisation signal that induces its translocation into the mitochondrial matrix, where PINK1 is cleaved by mitochondrial proteases and then released in the cytosol for proteasomal degradation (Greene et al., 2012; Jin et al., 2010; Yamano and Youle, 2013). Loss of mitochondrial membrane potential prevents PINK1 translocation and results in its stabilisation on the OMM. Here, PINK1 recruits the E3 ligase PARKIN, which promotes ubiquitylation of substrates on the OMM, thus triggering mitophagy (Geisler et al., 2010; Matsuda et al., 2010; Narendra et al., 2008; Narendra et al., 2010; Vives-Bauza et al., 2010).

As *Usp30*<sup>-/-</sup> CTLs show loss of mitochondrial membrane potential and increased mitophagy, I asked whether this also induced PINK1 upregulation, as observed in other cell types after mitochondrial membrane potential dissipation (Lin and Kang, 2008). Neither PINK1 nor PARKIN peptides were detected in the mass spectrometry of either unstimulated or TCR-activated WT and *Usp30*<sup>-/-</sup> CTLs. This suggested that either these proteins were present at a very low copy number and fell below the mass spectrometry detection threshold, or that they were not expressed in CTLs.

Next, I interrogated the database provided by the Immunological Proteome Resource (ImmPres, <http://immpres.co.uk/>), a comprehensive dataset of the murine cell proteome including CD4<sup>+</sup> T cells, CD8<sup>+</sup> T cells and NK cells. Neither PINK1 nor PARKIN expression were listed in the lymphocyte proteomes provided by this dataset. Therefore, PINK1 is unlikely to be easily detectable by mass spectrometry in CTLs.

To rule out a technical limitation of the mass spectrometry peptide analysis, I aimed to measure PINK1 protein levels by immunoblot to compare its expression between WT and *Usp30*<sup>-/-</sup> CTLs. Antibodies against mouse and human PINK1 could not detect any specific band with altered expression in *Usp30*<sup>-/-</sup> CTLs (**Figure 3.21A, B**). As PINK1 accumulation occurs on mitochondria (Lin and Kang, 2008), the lack of PINK1 upregulation could be caused by the reduction in mitochondrial structures observed in day 5 *Usp30*<sup>-/-</sup> CTLs (**Figure 3.3-3.5**). To test this further, I

treated both WT and *Usp30*<sup>-/-</sup> CTLs with FCCP to induce mitochondrial depolarisation and allow for PINK1 stabilisation. FCCP treatment did not upregulate the expression of any of the bands observed in untreated CTLs (**Figure 3.21C**), regardless of the presence (WT) or absence (*Usp30*<sup>-/-</sup>) of mitochondrial structures.

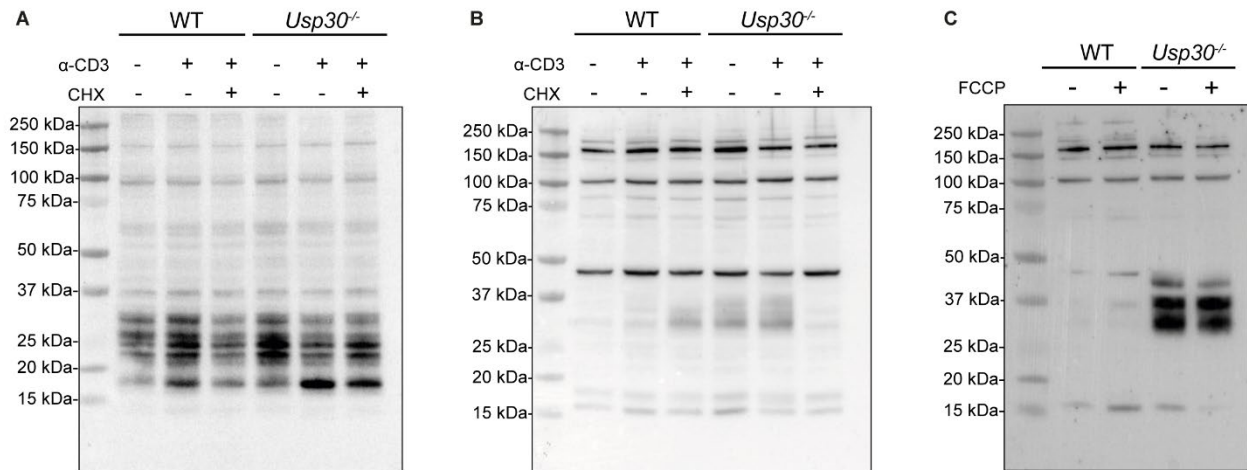


**Figure 3.21. PINK1 expression in day 5 CTLs.**

(A, B) Immunoblots of day 5 WT and *Usp30*<sup>-/-</sup> CTLs (3.33 µg lysate/sample) in basal, stimulated (α-CD3) and cycloheximide-treated (100µg/ml) conditions. PINK1 expression was probed using two different antibodies (A=Novus, B=Abcam) raised against human PINK1. (C) PINK expression analysed by Western blot in day 5 WT and *Usp30*<sup>-/-</sup> CTLs (3.33 µg lysate/sample) either left untreated or treated with 10 µM FCCP for 2h (Abcam antibody). Data representative of two independent biological replicates.

While these results could indicate that PINK1 peptides are not easily detected by CTL mass spectrometry or that the antibodies I used were not specific to mouse PINK1, it is also possible that PINK1 is not expressed in CTLs. Early studies of PINK1 and PARKIN showed little to no mRNA detection by Northern blot analysis of human samples from the spleen and the thymus (Kitada et al., 1998; Unoki and Nakamura, 2001).

Next, I focused on the E3 ligase PEX2, whose ubiquitinating activity is counteracted by USP30 on peroxisomes (Riccio et al., 2019). PEX2 peptides were not found in our mass spectrometry datasets. Furthermore, PEX2 expression was also not detected in neither naïve T cells nor in TCR-triggered activated CD8<sup>+</sup> T cells in the ImmPres database. Taken together with the lack of PINK1 and

PARKIN detection by mass spectrometry and immunoblot, these results argued against the feasibility of targeting PINK1 and PEX2 expression to inhibit mitophagy and pexophagy in *Usp30*<sup>-/-</sup> CTLs.

### 3.16 Preventing mitophagy in *Usp30*<sup>-/-</sup> rescues killing and translation defect

To circumvent the lack of reliable targets to oppose mitophagy and pexophagy in USP30-depleted CTLs, I targeted mitochondrial fission to modulate mitophagy. Fission of mitochondrial membranes is a required step for their engulfment by the autophagosome (Twig et al., 2008), and impairing fission precludes mitochondrial degradation. I used the fission inhibitor mDIVI-1 and the fusion promoter M1 to induce mitochondrial elongation and prevent fission in *Usp30*<sup>-/-</sup> CTLs, as previously done in CD8<sup>+</sup> T cells (Buck et al., 2016). WT cells were treated in parallel to observe the effects of mitophagy depletion in effector CTLs in order to account for any toxic effect that could be caused by the lack of removal of damaged mitochondria.

WT and *Usp30*<sup>-/-</sup> CTLs were treated for 6h, 24h or 48h (treatment started on day 5, 4 and 3 post-stimulation, respectively). TOM20 expression was analysed by Western blot as a marker of mitochondrial abundance (**Figure 3.22A**). While the 6h incubation had no effect, mDIVI-1 and M1 increased TOM20 expression in WT CTLs treated for 24h and 48h. Inhibiting mitochondrial fission for 6h or 24h did not rescue TOM20 expression in day 3 *Usp30*<sup>-/-</sup> CTLs. By contrast, a moderate yet reproducible upregulation in TOM20 abundance was observed in *Usp30*<sup>-/-</sup> CTLs treated for 48h. This result indicated that while lost mitochondrial mass could not be retrieved in USP30-depleted CTL, the loss itself could be prevented by treating *Usp30*<sup>-/-</sup> CTLs on day 3, before the onset of mitochondria degradation.

To test whether the mDIVI-1+M1 treatment affected TOM20 expression without resulting in increased mitochondrial abundance, I used immunofluorescence to detect the expression of the mitochondrial matrix marker PDH. Day 5 WT and *Usp30*<sup>-/-</sup> CTLs were treated with mDIVI-1 and M1 for 6h, 24h and 48h as detailed above. Similarly to TOM20 expression, PDH signal was rescued in day 5 and *Usp30*<sup>-/-</sup> CTLs that had been treated with mDIVI-1 and M1 before the onset of mitophagy (day 3, 48h treatment) (**Figure 3.22B**). Overall, these results validated the use of the mDIVI-1+M1 pharmacological treatment to rescue the loss of mitochondrial mass in *Usp30*<sup>-/-</sup> CTLs.

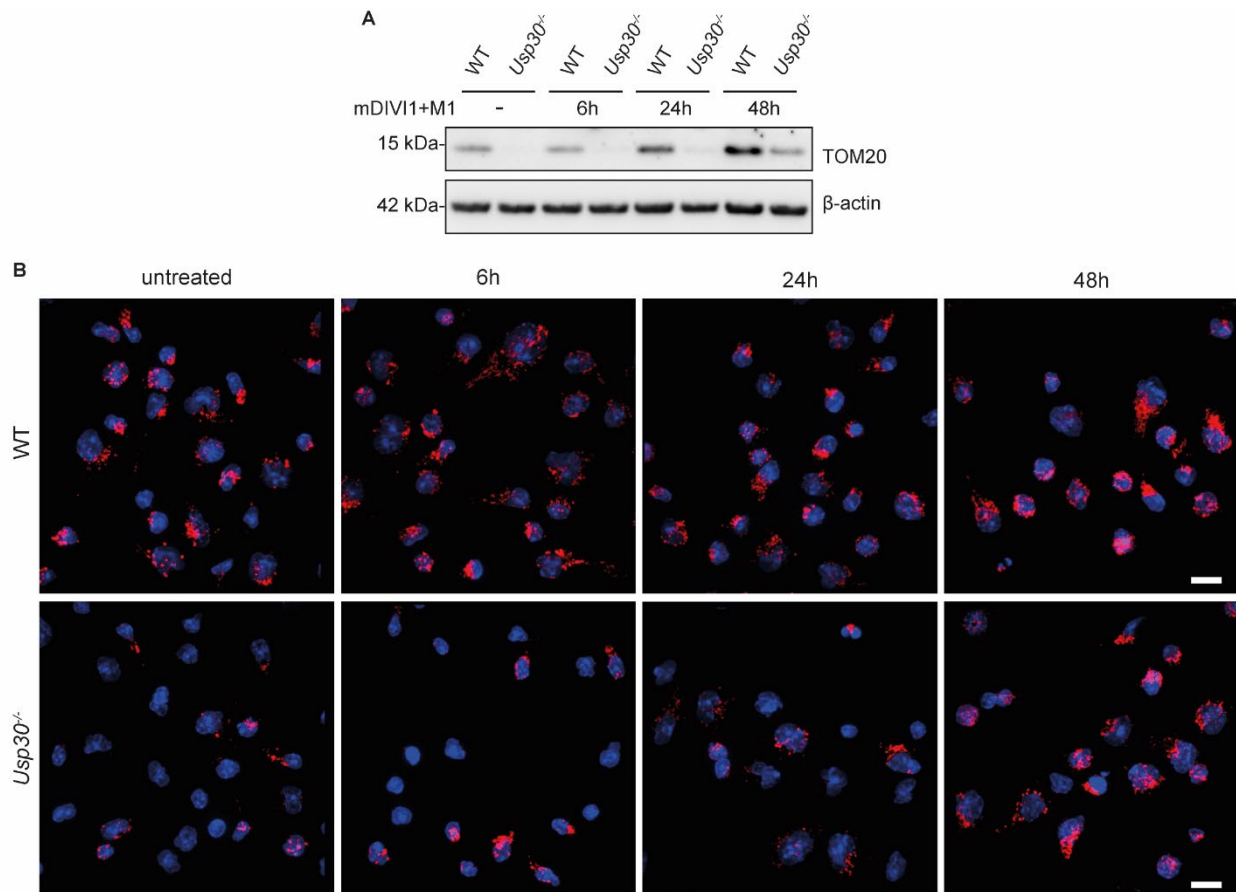


**Figure 3.22. mDIVI-1+M1 treatment rescues mitochondrial depletion in *Usp30<sup>-/-</sup>* CTLs.**

(A) Immunoblot showing TOM20 expression in day 5 WT and *Usp30<sup>-/-</sup>* CTLs (3.33 μg lysate/sample) upon treatment with 10 μM mDIVI-1 (mitochondrial fission inhibitor) and 20 μM M1 (mitochondrial fusion promoter) for 6h, 24h and 48h. Treatment started on day 5 (6h), day 4 (24h) and day 3 (48h) post-stimulation. (B) Immunofluorescence in day 5 WT and *Usp30<sup>-/-</sup>* CTLs treated as in (A) (4.5x10<sup>4</sup> CTLs/sample). Red fluorescence indicates PHD expression (mitochondrial matrix) in all samples. Scale bars = 10 μm. Data representative of three independent biological replicates.

As inhibiting mitochondrial fission prevented mitophagy, I tested whether the restored mitochondrial abundance in *Usp30<sup>-/-</sup>* would affect CTL killing. CTLs were treated with mDIVI+M1 for 6h, 24h and 48h and incubated with target cells. WT CTL killing was improved after all treatments (**Figure 3.23**). Inhibiting mitochondrial fission for 6h did not affect killing in *Usp30<sup>-/-</sup>* CTLs. However, prolonged treatment improved *Usp30<sup>-/-</sup>* CTL killing, with USP30-depleted CTLs killing as efficiently as treated WT CTLs after 48h of mDIVI and M1 treatment.

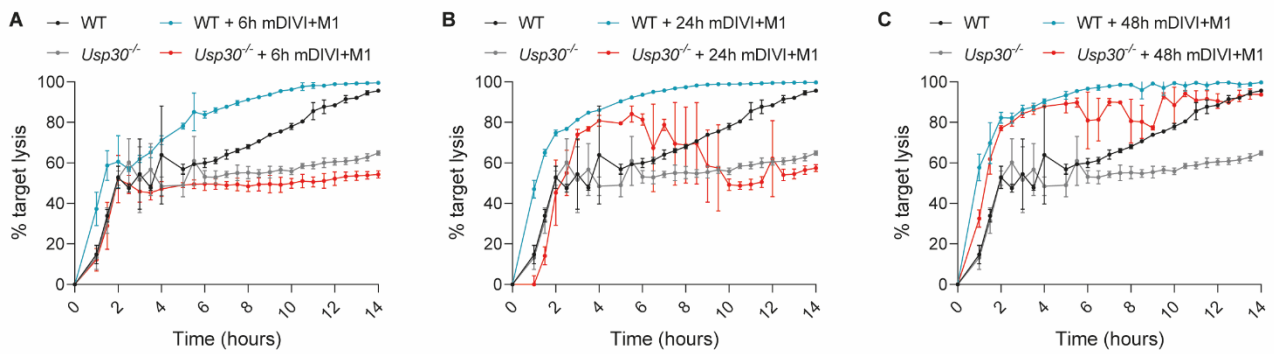


**Figure 3.23. mDIVI-1+M1 treatment rescues cytotoxicity in *Usp30*<sup>-/-</sup> CTLs.**

(A-C) Long-term (14h) killing assays with day 5 WT and *Usp30*<sup>-/-</sup> CTLs treated with 10  $\mu$ M mDIVI-1 and 20  $\mu$ M M1 for (A) 6h, (B) 24h and (C) 48h. Treatment started on (A) day 5, (B) day 4 and (C) day 3 post-stimulation. CTL:target ratio=1:1 ( $4 \times 10^4$  targets and  $4 \times 10^4$  CTLs per sample). Error bars represent mean values  $\pm$ SD of one representative experiment. Data representative of at least three independent biological replicates.

Given the requirement for cytosolic translation to sustain CTL killing (**Figure 3.17C**), I asked whether the restored killing in *Usp30*<sup>-/-</sup> CTLs could be due to enhanced protein synthesis. I supplemented CTL culture media with HPG to monitor *de novo* protein synthesis in unstimulated and stimulated ( $\alpha$ -CD3) CTLs treated with mDIVI-1 and M1 for 6h, 24h and 48h (**Figure 3.24 A-C**). Short-term treatment (6h) did not affect cytosolic translation in day 5 WT or *Usp30*<sup>-/-</sup> CTLs. Prolonged inhibition of mitochondrial fission in WT CTLs only modestly increased the percentage of highly translating CTLs. By contrast, blocking mitochondrial fission in *Usp30*<sup>-/-</sup> CTLs for 48h dramatically improved translation efficiency, indicating that preventing unrestricted mitochondrial degradation can restore cytosolic protein synthesis. TCR activation in day 5 USP30-depleted CTLs treated with mDIVI+M1 for 48h further enhanced HPG incorporation.

Prolonged treatment with inhibitors of mitochondrial fission increased killing and translation in both WT and *Usp30*<sup>-/-</sup> CTLs, suggesting that these cells might have a higher cytotoxic potential. Forcing mitochondrial fusion skews T cells towards a memory phenotype, altering T cell longevity and metabolism (Buck et al., 2016). I assessed granzyme B and perforin expression in day 5 WT and *Usp30*<sup>-/-</sup> treated with mDIVI-1+M1 to ask whether the enhanced cytotoxicity was due to upregulation of these proteins. Although mDIVI-1+M1 treatment allowed for granzyme B and perforin abundance to be equivalent in 48h-treated WT and *Usp30*<sup>-/-</sup> CTLs, the expression of these cytolytic proteins was downregulated in both samples compared to untreated WT CTLs (**Figure 3.24 D, E**). These results could be consistent with differentiation towards a memory T cell phenotype. In fact, while memory

T cells are still able to exert cytotoxic activity, reduced expression of granzyme B and perforin in memory versus effector T cells has been previously observed (Kaech et al., 2002; Sallusto et al., 1999).

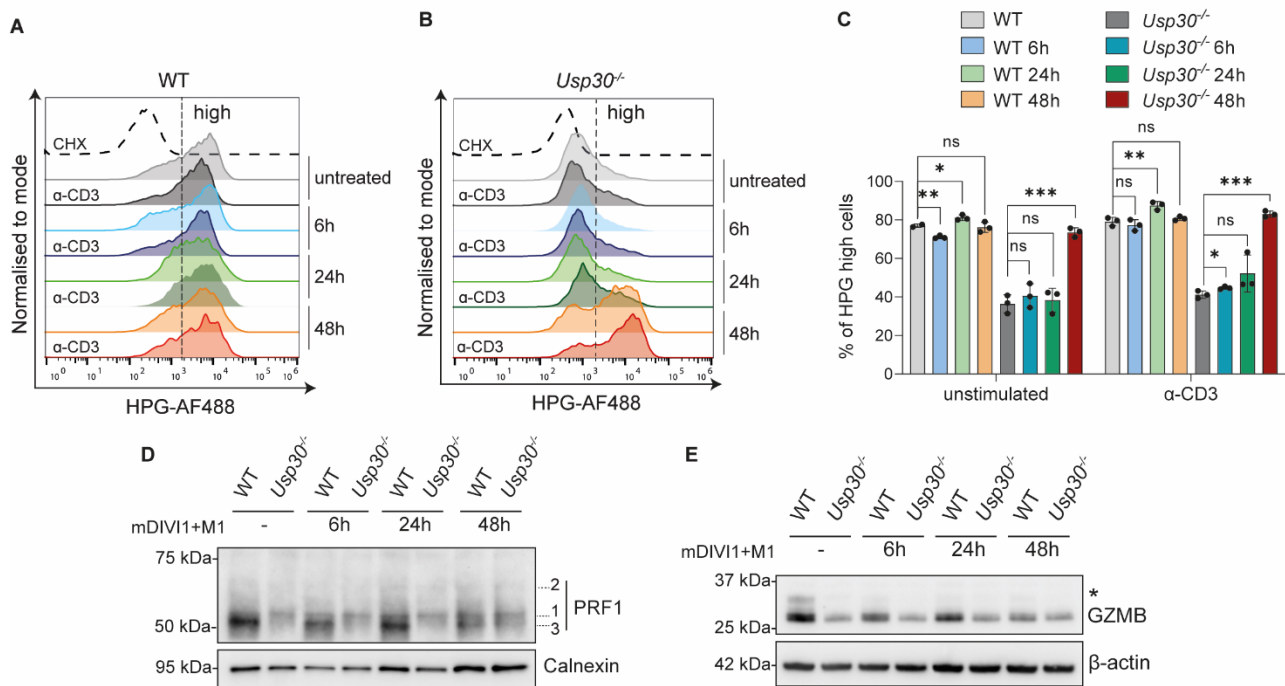


**Figure 3.24. mDIVI-1+M1 treatment enhances translation but does not upregulate cytolytic protein synthesis.**

(A-B) HPG incorporation measuring *de novo* protein synthesis in  $2 \times 10^5$  day 5 (A) WT and (B) *Usp30*<sup>-/-</sup> CTLs treated with 10  $\mu$ M mDIVI-1 and 20  $\mu$ M M1 for 6h, 24h and 48h (treatment started on day 5, 4 and 3 post-stimulation, respectively). CTLs were stimulated with  $\alpha$ -CD3 for 1h to mimic TCR triggering. Control samples were treated with cycloheximide (CHX) to inhibit cytosolic translation. Vertical dashed line shows the position of the gate used to quantify high HPG incorporation. (C) Quantitation of CTLs displaying high HPG incorporation as determined by the vertical dashed lines in (A, B). Error bars represent mean values  $\pm$ SD of one representative experiment. \*\*\*= $p < 0.001$ , \*\*= $p < 0.01$ , \*= $p < 0.05$ , ns=not significant. (D, E) Immunoblots for (D) perforin (PRF1) and (E) granzyme B (GZMB) in day 5 WT and *Usp30*<sup>-/-</sup> CTLs treated as in (A-C) (3.33  $\mu$ g lysate/sample). Immature (1), intermediate (2) and mature (3) forms of perforin are indicated. Newly synthesised granzyme B is labelled by (\*). Data representative of at least three independent biological replicates.

The increase in cytotoxicity observed in mDIVI+M1-treated WT and *Usp30*<sup>-/-</sup> CTLs was not due to upregulation of either granzyme B or perforin. This observation suggested that a granzyme B/perforin-independent killing pathway could be at play in CTLs in which mitochondrial fission was inhibited. To account for potential off-target effects that might influence the readings of the cytotoxicity assay, I measured proliferation of untreated CTLs compared to WT and *Usp30*<sup>-/-</sup> CTLs treated with mDIVI-1 and M1 for 6h, 24h and 48h. In addition, I analysed proliferation of target cells that were either left untreated or treated with mDIVI-1+M1 for the duration of the killing assays. Prolonged treatment promoted T cell proliferation in both WT and *Usp30*<sup>-/-</sup> CTLs (**Figure 3.25A**), while target cell proliferation was unaffected (**Figure 3.25B**). Taken together, these results indicated that enhanced killing upon mDIVI+M1 treatment might have occurred as a consequence of increased T cell numbers, and therefore overall cytotoxic potential, rather than to upregulation of cytolytic molecules within individual CTLs.

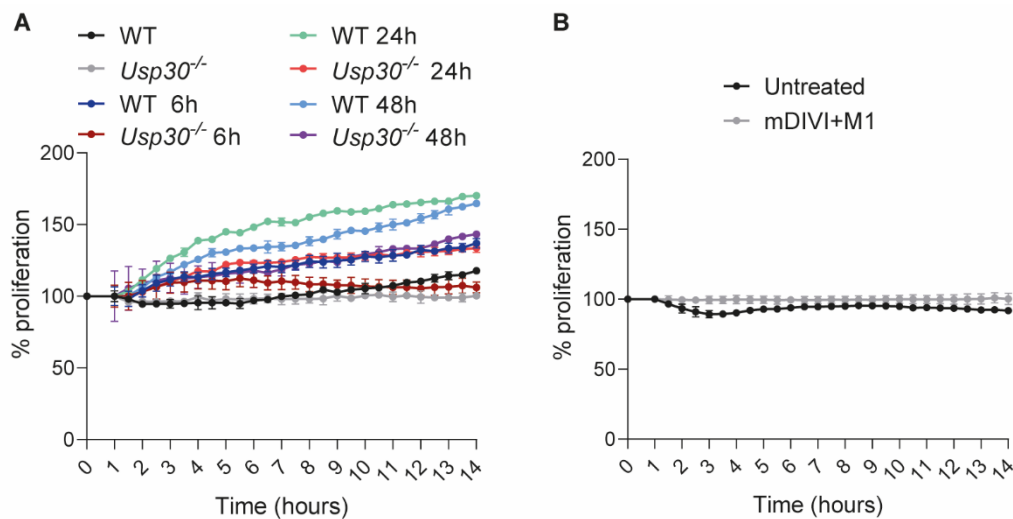


**Figure 3.25. mDIVI-1+M1 treatment promotes CTL proliferation.**

(A) Day 5 WT and *Usp30*<sup>-/-</sup> CTL proliferation during killing assays as in (A-C) upon treatment with 10  $\mu$ M mDIVI-1 and 20  $\mu$ M M1 for 6h, 24h and 48h (treatment started on day 5, 4 and 3 post-stimulation, respectively). (B) P815 target cell proliferation in untreated and treated (mDIVI-1+M1) conditions. Error bars represent mean values  $\pm$ SD of one representative experiment ( $4 \times 10^4$  targets and  $4 \times 10^4$  CTLs per sample). Data representative of at least three independent biological replicates.

### 3.17 Summary

The analysis of *Usp30*<sup>-/-</sup> murine splenocytes revealed that despite the role of USP30 in mitochondrial maintenance, USP30-deficient T cells developed normally and were found in WT-like ratios in the spleen. Naïve *Usp30*<sup>-/-</sup> CTLs could undergo normal activation upon TCR crosslinking. USP30 was only required in T cells after activation, as *Usp30*<sup>-/-</sup> CTLs lost mitochondria and peroxisomes 5-7 days after stimulation.

I found that loss of USP30 did not impair T cell migration nor TCR-derived signalling, but it affected translation efficiency and the cytolytic potential of CTLs. *De novo* protein synthesis was shown to be required to sustain prolonged killing. Lack of efficient translation negatively affected the production of granzymes, perforin and cytokines, which impaired killing after the existing reserves of these proteins had been exhausted. Intriguingly, acute inhibition of cytosolic translation with cycloheximide only partially recapitulated the differences in protein expression observed in *Usp30*<sup>-/-</sup> CTLs. This suggested that lack of USP30 resulted in selective protein downregulation, which was not restricted to mitochondrial and peroxisomal proteins.

Treatment with inhibitors of mitochondrial fission (mDIVI-1 and M1) showed that preventing mitochondrial degradation was sufficient to improve killing and translation in *Usp30*<sup>-/-</sup> CTLs. Restored killing was not due to upregulation of granzyme B and perforin, suggesting that the increase in translation affects other proteins. Interestingly, mDIVI-1+M1 treatment promoted CTL proliferation, which could contribute to augmented cytotoxicity.

Overall, these data pointed to a requirement for USP30 and mitochondria in CTL homeostasis by allowing for efficient cytosolic protein synthesis, which supported sustained cytotoxicity by ensuring adequate expression of cytolytic proteins.





## **CHAPTER 4**

**Examination of mitochondrial and peroxisomal functions reveals a requirement for mitochondrial translation in CTL cytotoxicity**



## 4.1 Background

USP30 is a negative regulator of mitophagy and pexophagy, and loss of USP30 results in aberrant degradation of mitochondria and peroxisomes (Bingol et al., 2014; Marcassa et al., 2018; Nakamura and Hirose, 2008; Riccio et al., 2019). In Chapter 3 I showed that naïve *Usp30*<sup>-/-</sup> CD8<sup>+</sup> T cells exhibited similar mitochondrial mass and membrane potential as WT CD8<sup>+</sup> T cells. Activation by TCR triggering allows for differentiation into effector CD8<sup>+</sup> T cells with cytotoxic capacity. *Usp30*<sup>-/-</sup> CTLs showed a marked loss of mitochondria by day 5 and a reduction in peroxisomes by day 7 post-stimulation, consistent with increased mitophagy and pexophagy. The onset of mitophagy by day 5 post-stimulation correlated with a defect in cytosolic protein synthesis, which ultimately impaired sustained killing by depriving *Usp30*<sup>-/-</sup> CTLs of key cytolytic proteins. Pharmacological inhibition of mitochondrial fission prevented mitophagy and rescued killing capacity and translation in day 5 *Usp30*<sup>-/-</sup> CTLs. Taken together, these results suggested that precluding mitochondrial degradation was sufficient to rescue the defect in cytotoxicity caused by USP30 depletion. Nevertheless, the involvement of peroxisomes was not entirely ruled out. In addition, it remained unclear whether the loss of cytotoxicity was due to the complete degradation of mitochondria, or whether a specific mitochondrial function was required to sustain cytosolic translation and CTL killing.

## 4.2 Metabolic defects in peroxisomes alter mitochondrial function

As both mitophagy and pexophagy are upregulated in *Usp30*<sup>-/-</sup> CTLs, I aimed to test whether a decrease in peroxisomal mass could affect CTL function without the simultaneous loss in mitochondrial content observed in *Usp30*<sup>-/-</sup> CTLs. PEX16 is a membrane protein localised on peroxisomes and involved in their biogenesis (Honsho et al., 1998; Kim et al., 2006b). Immunoblotting showed a band for PEX16 running slightly above 25 kDa in lysates from murine CTLs, consistent with the indications provided by the antibody manufacturer (**Figure 4.1A**). To test whether it would be possible to manipulate PEX16 expression, I performed CRISPR/Cas9-mediated gene knockout (KO). The Cas9 protein, tracrRNA and guide crRNAs were introduced in CTLs by nucleofection, an electroporation-based method which allows for efficient gene deletion in primary human T cells (Schumann et al., 2015). Control samples were either nucleofected in the absence of CRISPR reagents (nucleofection control) or with Cas9, tracrRNA and non-targeting guide crRNA (non-targeting control) to evaluate potential off-target effects caused by the nucleofection procedure or by the introduction of CRISPR reagents in CTLs. PEX16 protein abundance was assessed in day

7 CTLs, four days after the CRISPR KO was performed. Genetic deletion of *Pex16* in activated CTLs was unsuccessful (**Figure 4.1A**).

Next, I focused on fatty acyl-CoA reductase 1 (FAR1), which was highlighted as a potential regulator of CTL killing in a separate screen performed as an extension of the 3i project by Philippa Barton (Abeler-Dörner et al., 2020). FAR1 is a peroxisomal protein that catalyses fatty acid reduction, thus playing a role in lipid biosynthesis (Cheng and Russell, 2004). It is important to note that lipid oxidation takes place in both peroxisomes and mitochondria, thus metabolically coupling these two organelles (Wanders et al., 2015). Furthermore, defects in peroxisome assembly and functionality can result in altered mitochondrial morphology and function (Baes and Van Veldhoven, 2012; Goldfischer et al., 1973).

Given this metabolic crosstalk between mitochondria and peroxisomes, I investigated whether deletion of *Far1* could affect mitochondria. To this end I isolated WT and *Far1*<sup>-/-</sup> naïve T cells and I activated them *in vitro* as previously described (**Figure 3.2A; Material and Methods**). Differentiated CTLs were stained with MitoTracker Deep Red and TMRE on day 5 post-activation to quantitate mitochondrial mass and mitochondrial membrane potential. Interestingly, both of these parameters showed alterations in *Far1*<sup>-/-</sup> CTLs (**Figure 4.1 B-E**). FAR1 depletion reproducibly resulted in mitochondria displaying a bimodal distribution of mitochondrial mass (**Figure 4.1B**) although quantitation of CTLs displaying either low or high Mitotracker Deep Red signal did not reveal significant differences in the percentage of cells found in each population (**Figure 4.1C**). Furthermore, mitochondrial membrane potential was increased in *Far1*<sup>-/-</sup> CTLs as measured by TMRE (**Figure 4.1D, E**). These results suggested that alterations in peroxisomal metabolic processes can perturb mitochondrial function and indicated that *Far1*<sup>-/-</sup> mice were not suitable to selectively study the impact of peroxisomal defects in CTLs.

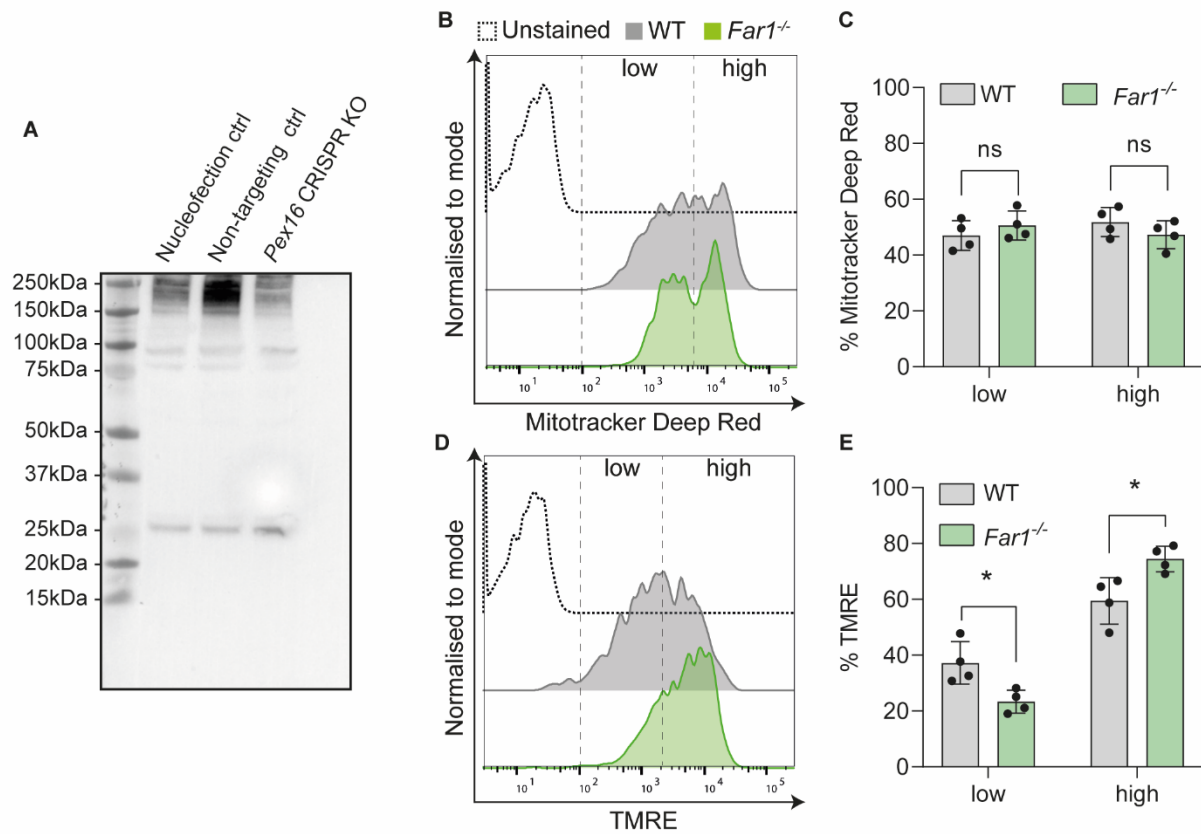


**Figure 4.1. Testing depletion of peroxisomal function in CTLs.**

(A) Immunoblot showing PEX16 protein expression in controls (nucleofection and non-targeting controls) and in CTLs nucleofected with guide crRNA for *Pex16*. Data representative of two independent biological replicates (3.33  $\mu$ g lysate/sample). (B) Flow cytometry analysis of mitochondrial mass in day 5 WT and *Far1*<sup>-/-</sup> CTLs (10<sup>5</sup> CTLs per sample). Vertical dashed lines denote the position of the gates used to calculate the percentages of CTLs expressing low or high MitoTracker signal. (C) Quantitation of Mitotracker Deep Red low and high populations as shown in (B). (D) Flow cytometry analysis of mitochondrial membrane potential in day 5 WT and *Far1*<sup>-/-</sup> CTLs (10<sup>5</sup> CTLs per sample). Vertical dashed lines denote the position of the gates used to calculate the percentages of CTLs expressing low or high TMRE signal. (E) Quantitation of TMRE low and high populations as shown in (D). Plots show the average of four biological replicates  $\pm$ SD. \*= $p$ <0.05, ns=not significant (two-tailed unpaired Student's t-test).

### 4.3 Mitochondrial oxidative phosphorylation: *Ndufs4*<sup>-/-</sup> and *Ttc19*<sup>-/-</sup> mice

The protein synthesis and killing defects observed in *Usp30*<sup>-/-</sup> CTLs occurred as mitochondria were lost after T cell activation, and preventing mitochondrial degradation was sufficient to rescue translation and cytotoxicity (**Figure 3.22-24**). However, it remained unclear whether this was merely due to a surge in mitochondrial mass or whether a specific mitochondrial function was required to sustain CTL killing. USP30-depleted CTLs showed a marked reduction in OXPHOS (**Figure 3.6A**). While oligomycin treatment does not impair CTL proliferation (Chang et al., 2013), it is not known whether OXPHOS deficiency can affect translation and killing capacity. Therefore, I analysed CD8<sup>+</sup> T cells derived from two murine models of deficient OXPHOS: the *Ndufs4*<sup>-/-</sup> and *Ttc19*<sup>-/-</sup> mice. NDUFS4 is a subunit of complex I required for its stability (Petruzzella et al., 2001), while TTC19 is an assembly factor participating in complex III biogenesis (Bottani et al., 2017). Genetic deletion and mutations in *Ndufs4* and *Ttc19* can decrease OXPHOS by inhibiting the activity of the ETC (Ghezzi et al., 2011; Kruse et al., 2008).

Mitochondrial dysfunction has been linked to defects in T cell development (Corrado et al., 2021; Ramstead et al., 2020; Sena et al., 2013; Simula et al., 2018). Therefore, I first tested whether lack of NDUFS4 or TTC19 could lead to alterations in the T cell populations found in the spleen. To this end, I measured the percentages of CD4<sup>+</sup> and CD8<sup>+</sup> T cells, regulatory T cells (CD4<sup>+</sup>, FOXP3<sup>+</sup>), and naïve (CD44<sup>low</sup>, CD62L<sup>high</sup>), central memory (CD44<sup>high</sup>, CD62L<sup>high</sup>) and effector memory (CD44<sup>high</sup>, CD62L<sup>low</sup>) T cells in both the CD4<sup>+</sup> and CD8<sup>+</sup> populations (**Figure 4.2**). Neither NDUFS4 nor TTC19 depletion affected the percentages of CD4<sup>+</sup> and CD8<sup>+</sup> T cells in the spleen. Regulatory, naïve, central memory and effector memory T cells within both the CD4<sup>+</sup> and CD8<sup>+</sup> populations were also found in similar percentages in *Ndufs4*<sup>-/-</sup> and *Ttc19*<sup>-/-</sup> splenocytes when compared to their WT counterparts. Overall, these results indicated that depletion of neither NDUFS4 nor TTC19 resulted in alterations in T cell populations in murine spleens.

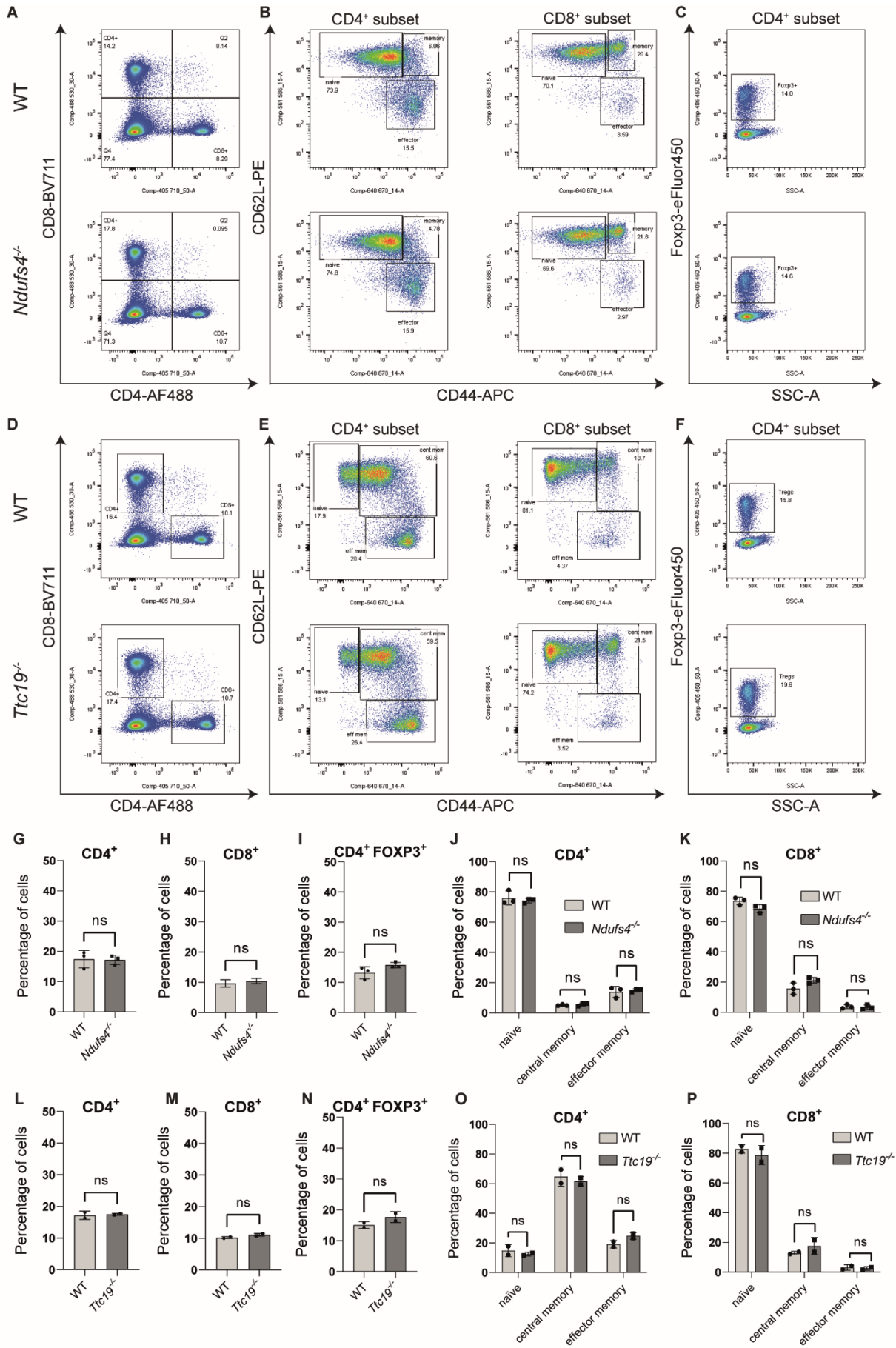


**Figure 4.2. Analysis of *Ndufs4*<sup>-/-</sup> and *Ttc19*<sup>-/-</sup> splenocytes.**

(A) CD4<sup>+</sup>/CD8<sup>+</sup> ratio in WT and *Ndufs4*<sup>-/-</sup> splenocytes. (B) CD4<sup>+</sup> and CD8<sup>+</sup> naïve (CD62L<sup>high</sup>, CD44<sup>low</sup>), central memory (CD62L<sup>high</sup>, CD44<sup>high</sup>) and effector memory (CD62L<sup>low</sup>, CD44<sup>high</sup>) T cell populations in WT and *Ndufs4*<sup>-/-</sup> splenocytes. (C) Regulatory T cells (CD4<sup>+</sup>, FOXP3<sup>+</sup>) in WT and *Ndufs4*<sup>-/-</sup> splenocytes. (D) CD4<sup>+</sup>/CD8<sup>+</sup> ratio in WT and *Ttc19*<sup>-/-</sup> splenocytes. (E) CD4<sup>+</sup> and CD8<sup>+</sup> naïve (CD62L<sup>high</sup>, CD44<sup>low</sup>), central memory (CD62L<sup>high</sup>, CD44<sup>high</sup>) and effector memory (CD62L<sup>low</sup>, CD44<sup>high</sup>) T cell populations in WT and *Ttc19*<sup>-/-</sup> splenocytes. (F) Regulatory T cells (CD4<sup>+</sup>, FOXP3<sup>+</sup>) in WT and *Ttc19*<sup>-/-</sup> splenocytes. (G-K) Quantitation of (G) CD4<sup>+</sup>, (H) CD8<sup>+</sup>, (I) regulatory T cells, (J) total CD4<sup>+</sup> and (K) CD8<sup>+</sup> populations (naïve, central memory, effector memory) in WT and *Ndufs4*<sup>-/-</sup> splenocytes. (L-P) Quantitation of (L) CD4<sup>+</sup>, (M) CD8<sup>+</sup>, (N) regulatory T cells, (O) total CD4<sup>+</sup> and (P) CD8<sup>+</sup> populations (naïve, central memory, effector memory) in WT and *Ttc19*<sup>-/-</sup> splenocytes. Note the different gating strategy in B, E (determined by the respective controls in each independent experiment) leading to different percentages of CD4<sup>+</sup> T cell subsets in J, O. Plots show the average of three biological replicates (10<sup>6</sup> splenocytes/sample) ±SD. ns = not significant (two-tailed unpaired Student's t-test).

Complexes I-IV of the ETC drive proton transport in the mitochondrial intermembrane space, generating membrane potential (Mitchell and Moyle, 1965). Given the respective roles of NDUFS4 and TTC19 in the assembly of complex I and complex III, I asked whether depletion of either of these two proteins could result in a decrease in mitochondrial membrane potential. In addition, as loss of mitochondrial membrane potential can trigger mitochondrial degradation (Narendra et al., 2008), I asked whether mitochondrial abundance was affected in NDUFS4- and TTC19-deficient T cells. MitoTracker Deep Red and TMRE were used to respectively measure mitochondrial mass and membrane potential in unstimulated (day 0 splenocytes) and *in vitro* activated *Ndufs4*<sup>-/-</sup> and *Ttc19*<sup>-/-</sup> CTLs (day 3, 5 and 7 post-stimulation). Loss of NDUFS4 (**Figure 4.3 A-D**) or TTC19 (**Figure 4.3 E-H**) caused little to no alteration in MitoTracker Deep Red or TMRE signal, suggesting that mitochondrial mass and membrane potential are maintained in *Ndufs4*<sup>-/-</sup> and *Ttc19*<sup>-/-</sup> CTLs.

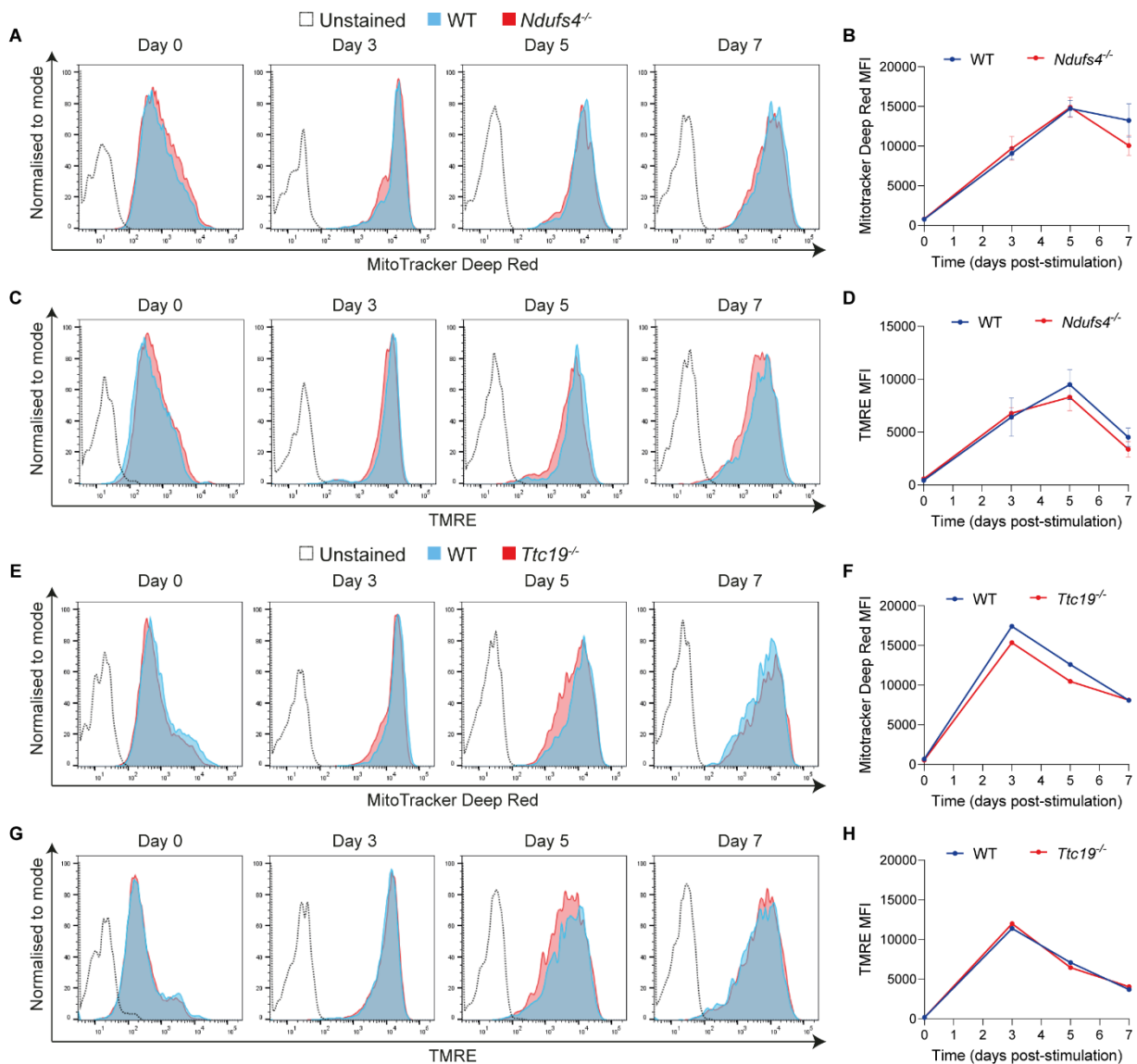


**Figure 4.3. Loss of NDUFS4 or TTC19 does not affect mitochondrial mass and membrane potential.**

(A-D) Time course of mitochondria labelled with (A, B) MitoTracker Deep Red and (C, D) TMRE in WT and *Ndufs4*<sup>-/-</sup> naïve CD8<sup>+</sup> T cells (day 0) as they mature into CTLs after stimulation (day 3-7). Plots in (B, D) quantitate MitoTracker and TMRE MFI in (A, C) respectively and display average  $\pm$ SD of three biological replicates. (E-H) Time course of mitochondria labelled with (E, F) MitoTracker Deep Red and (G, H) TMRE in WT and *Ttc19*<sup>-/-</sup> naïve CD8<sup>+</sup> T cells (day 0) as they mature into CTLs after stimulation (day 3-7). Plots in (F, H) Plots in (B, D) quantitate MitoTracker and TMRE MFI in (E, G) respectively and show average  $\pm$ SD of two biological replicates (day 0: 10<sup>6</sup> splenocytes/sample; days 3-7: 10<sup>5</sup> CTLs/sample).

Next, NDUFS4- and TTC19-deficient CTLs (5 days after activation) were assayed for their ability to recognise and kill target cells. LAMP1 degranulation and target cell killing were similar in WT and KO samples (**Figure 4.4 A-F**), suggesting that loss of either NDUFS4 or TTC19 did not affect cytotoxicity.

Overall, these results suggested that defects in complex I or complex III assembly did not affect mitochondrial nor CTL function as indicated by mitochondrial mass, membrane potential, degranulation and CTL killing capacity. Nevertheless, it remained possible that the loss of NDUFS4 and TTC19 did not affect ETC assembly in CTLs. In order to determine the severity of the OXPHOS deficiency in CTLs in these models, I assayed mitochondrial respiration using a Seahorse assay (**Figure 4.4G, H**). Measuring OCR in day 5 *Ndufs4*<sup>-/-</sup> and *Ttc19*<sup>-/-</sup> CTLs revealed that basal OXPHOS was only moderately diminished compared to WT CTLs. Moreover, while maximal OCR was decreased in *Ndufs4*<sup>-/-</sup> CTLs, indicating loss of spare respiratory capacity (**Figure 4.4G**), maximal OCR was unchanged in CTLs lacking TTC19 (**Figure 4.4H**). Furthermore, glycolysis was unperturbed in both *Ndufs4*<sup>-/-</sup> and *Ttc19*<sup>-/-</sup> CTLs as indicated by ECAR values (**Figure 4.4 I, J**). Given the increased reliance of CTLs on glycolysis (Menk et al., 2018), the differences in OCR between WT, *Ndufs4*<sup>-/-</sup> and *Ttc19*<sup>-/-</sup> may be less apparent in CTLs than in other tissues or cell types.

As neither the *Ttc19*<sup>-/-</sup> nor the *Ndufs4*<sup>-/-</sup> mouse models provided complete inhibition of basal mitochondrial respiration, I employed the same pharmacological treatments used in the Seahorse assay (FCCP, oligomycin, rotenone and antimycin A) to test the role of OXPHOS in CTL killing. This allowed for independent assessment of the contribution of mitochondrial membrane polarisation (FCCP), complex V (oligomycin), complex III (antimycin A) and complex I (rotenone) to cytotoxicity (Cunarro and Weiner, 1975; Heytler and Prichard, 1962; Lardy et al., 1958; Lindahl and Oberg, 1961; Potter and Reif, 1952). To mirror the conditions tested in the Seahorse assay, the effect of the combined rotenone and antimycin A treatment was also assessed. None of these pharmacological treatments inhibited cytotoxicity in day 5 WT CTLs (**Figure 4.4K**), suggesting that efficient OXPHOS was not required to sustain CTL killing. Of note, the high concentration of glucose in RPMI 1640 (10 mM) might have masked the contribution of OXPHOS to CTL killing by enabling an increased reliance on glycolysis. Supplementing the killing assay media with lower concentrations of glucose could clarify whether OXPHOS is required for CTL cytotoxicity in a physiological setting.

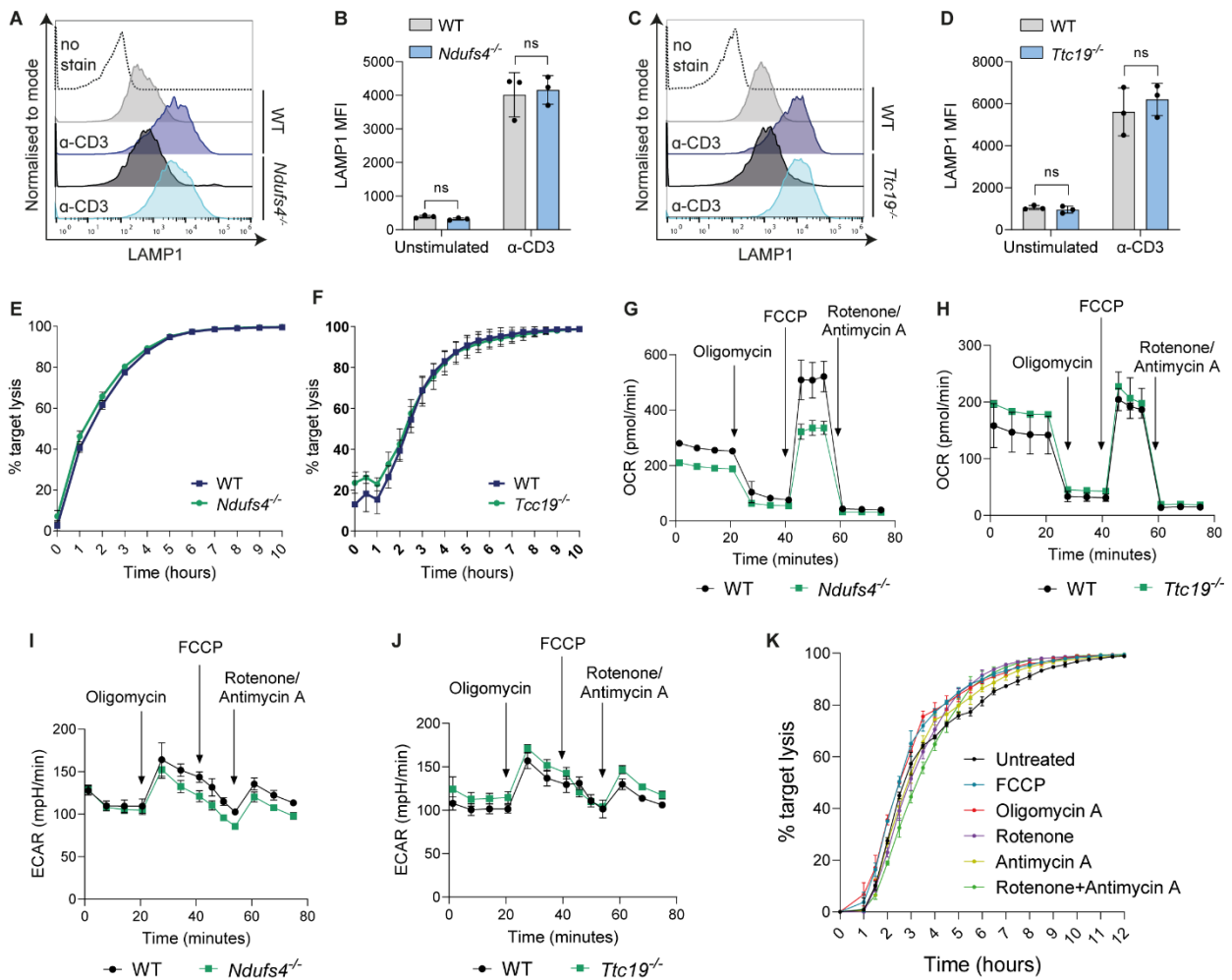


**Figure 4.4. Efficient OXPHOS is not required for CTL killing.**

(A) Histograms representing surface LAMP1 fluorescence intensity in WT and *Ndufs4*<sup>-/-</sup> CTLs before and after TCR stimulation ( $2 \times 10^5$  targets and  $2 \times 10^5$  CTLs per sample). (B) Quantitation of LAMP1 MFI in WT and *Ndufs4*<sup>-/-</sup> CTLs. (C) Histograms representing surface LAMP1 fluorescence intensity in WT and *Ttc19*<sup>-/-</sup> CTLs before and after TCR stimulation ( $2 \times 10^5$  targets and  $2 \times 10^5$  CTLs per sample). (D) Quantitation of LAMP1 MFI in WT and *Ttc19*<sup>-/-</sup> CTLs. ns=not significant (unpaired two-tailed Student's t-test). (E, F) Long-term (10h) killing assays showing percentage of target cell lysis over time (CTL:target ratio, 10:1) with (E) WT and *Ndufs4*<sup>-/-</sup> and (F) WT and *Ttc19*<sup>-/-</sup> CTLs ( $4 \times 10^3$  targets and  $4 \times 10^4$  CTLs per sample). (G, H) Mitochondrial respiratory capacity indicated by oxygen consumption rate (OCR) in (G) WT and *Ndufs4*<sup>-/-</sup> and (H) WT and *Ttc19*<sup>-/-</sup> CTLs ( $3 \times 10^5$  CTLs per sample) treated with 1  $\mu$ M oligomycin A, 1  $\mu$ M FCCP, 0.5  $\mu$ M rotenone and 0.5  $\mu$ M antimycin A. (I, J) Glycolytic flux measured by extracellular acidification rate (ECAR) in (I) WT and *Ndufs4*<sup>-/-</sup> and (J) WT and *Ttc19*<sup>-/-</sup> CTLs ( $3 \times 10^5$  CTLs per sample) treated as in (G, H). (K) Long-term (10h) killing assays showing percentage of target cell lysis over time (CTL:target ratio, 1:1) with WT CTLs treated with inhibitors of the electron transport chain ( $4 \times 10^4$  targets and  $4 \times 10^4$  CTLs per sample). Error bars in (B, D and E-J) display the average  $\pm$ SD of at least two biological replicates, while error bars in (K) represent average  $\pm$ SD of technical replicates within one experiment, representative of two biological replicates.

#### 4.4 Mitochondrial calcium flux: MCU CRISPR knockout CTLs

Calcium flux plays an important role in CTL signalling (Schwarz et al., 2013), and mitochondria localisation at the IS has been suggested to sustain calcium flux in CD4<sup>+</sup> T cells (Quintana et al., 2006). The mitochondrial calcium uniporter (MCU) mediates calcium influx into mitochondria (Baughman et al., 2011; De Stefani et al., 2011), while the Na<sup>+</sup>/Ca<sup>2+</sup> exchanger protein NCLX has been reported to act as the channel mediating calcium export (Palty et al., 2010).

To test whether mitochondrial calcium flux could sustain CTL cytotoxicity, I aimed to modulate the expression of MCU and NCLX by performing CRISPR/Cas9-mediated gene deletion via nucleofection. Immunoblotting revealed the presence of several bands for NCLX (expected molecular weight = 55 kDa, 70 kDa), none of which was affected by CRISPR KO (**Figure 4.5A**). By contrast, immunoblotting for MCU showed a band at the expected molecular weight and reduced MCU protein expression four days after CRISPR KO (**Figure 4.5B**). Complete loss of MCU could not be achieved, either because of the stability of pre-formed MCU protein or because complete MCU knockout was not compatible with viability.

Next, I assessed whether MCU deficiency would affect intracellular calcium flux in CTLs. I used the ratiometric calcium probe INDO-1 to measure intracellular calcium concentration in unstimulated, TCR-triggered, and ionomycin-treated CTLs. Calcium flux in non-nucleofected samples and in CTLs nucleofected with either no CRISPR reagents (nucleofection control) or non-targeting guide RNA (non-targeting control) was also monitored. The starting concentration of intracellular calcium was equivalent in all samples, and it showed a similar increase in control and *Mcu* CRISPR KO CTLs after both TCR crosslinking and ionomycin treatment (**Figure 4.5C**). This result indicated that lack of MCU did not affect intracellular calcium concentration in CTLs, although it remained possible that the residual MCU expression in CRISPR KO samples was sufficient for mitochondrial calcium flux to proceed unperturbed.

Cytotoxicity was measured in control and *Mcu* CRISPR KO samples, and no defects were observed (**Figure 4.5D**). Interestingly, nucleofected controls showed a minor yet reproducible increase in killing compared to non-nucleofected CTLs. The *Mcu* CRISPR KO CTLs killed as efficiently as the non-nucleofected CTLs. Taken together, these results suggested that a decrease in MCU expression was not sufficient to substantially impair CTL cytotoxicity.

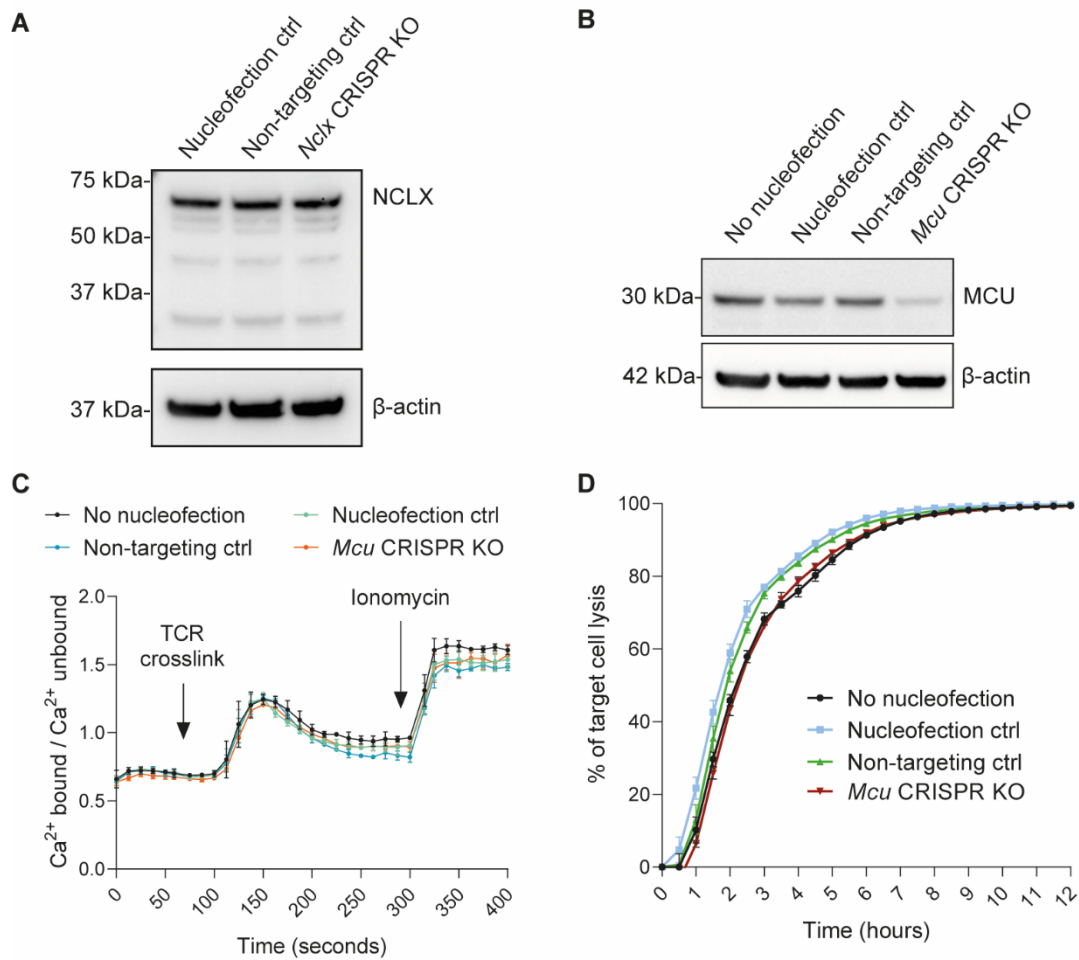


**Figure 4.5. Optimal MCU expression is not required for CTL calcium flux nor killing.**

(A, B) Immunoblot showing (A) NCLX and (B) MCU protein expression in WT CTL controls (nucleofection and non-targeting controls) and in CTLs nucleofected with guide crRNA for (A) *Nclx* and (B) *Mcu* (3.33  $\mu$ g lysate/sample). (C) INDO-1 calcium assay indicating changes in intracellular calcium concentration in control and *Mcu* CRISPR KO CTLs before ( $t=0-60s$ ) and after TCR crosslinking ( $t=60s$ ) or ionomycin addition ( $t=300s$ ) ( $10^6$  CTLs/sample). (D) Long-term (10h) killing assay displaying percentage of target cell lysis over time (CTL:target ratio, 10:1) with control and *Mcu* CRISPR KO CTLs ( $4 \times 10^3$  targets and  $4 \times 10^4$  CTLs per sample). Error bars indicate average  $\pm$ SD of technical replicates in one representative experiment. Data representative of (A, C) 2 or (B, D) three independent biological replicates.

#### 4.5 Analysis of mitochondrial protein synthesis in WT and *Usp30*<sup>-/-</sup> CTLs

Mitochondria possess their own transcriptional and translational machinery, which allows for the synthesis of 13 proteins, 22 tRNAs and 2 rRNAs, while the rest of the mitochondrial genome is encoded in the nucleus (D'Souza and Minczuk, 2018). The efficiency of mitochondrial translation can be selectively analysed by inhibiting cytosolic ribosomes using cycloheximide (Obrig et al., 1971; Schneider-Poetsch et al., 2010), which leaves mitochondrial protein synthesis unaffected (Clark-Walker and Linnane, 1966).

I tested whether mitochondrial translation could be measured by flow cytometry by assessing HPG incorporation in day 5 WT and *Usp30*<sup>-/-</sup> CTLs that were either untreated or incubated with CHX. As previously shown (**Figure 3.16B, C**), untreated WT CTLs could incorporate HPG more efficiently than untreated *Usp30*<sup>-/-</sup> CTLs, indicating inhibition of cytosolic protein synthesis upon USP30 depletion (**Figure 4.6A, B**). By contrast, HPG fluorescence was barely above the unstained control in both WT and *Usp30*<sup>-/-</sup> CTLs treated with CHX. No difference in HPG MFI between CHX-treated WT and *Usp30*<sup>-/-</sup> CTLs could be detected by flow cytometry.

A recently developed method employed HPG to preferentially label and visualise mitochondrial translation using microscopy (Zorkau et al., 2021a; Zorkau et al., 2021b). Following this method, I dialysed the FBS supplemented in the methionine-free CTL culture media to remove any additional source of methionine and to improve visualisation of mitochondrial translation. In addition, after incubation with HPG I labelled the mitochondrial matrix with PDH to confirm that CHX treatment led to the selective localisation of HPG within mitochondria. Immunofluorescence analysis in WT CTLs showed efficient HPG incorporation within 1h of incubation (**Figure 4.6 C-E**). The HPG-AF488 signal colocalised with PDH and confirmed that mitochondrial translation was preferentially labelled. By contrast, HPG signal in *Usp30*<sup>-/-</sup> CTLs was almost completely absent, indicating that mitochondrial translation was inhibited upon USP30 depletion.

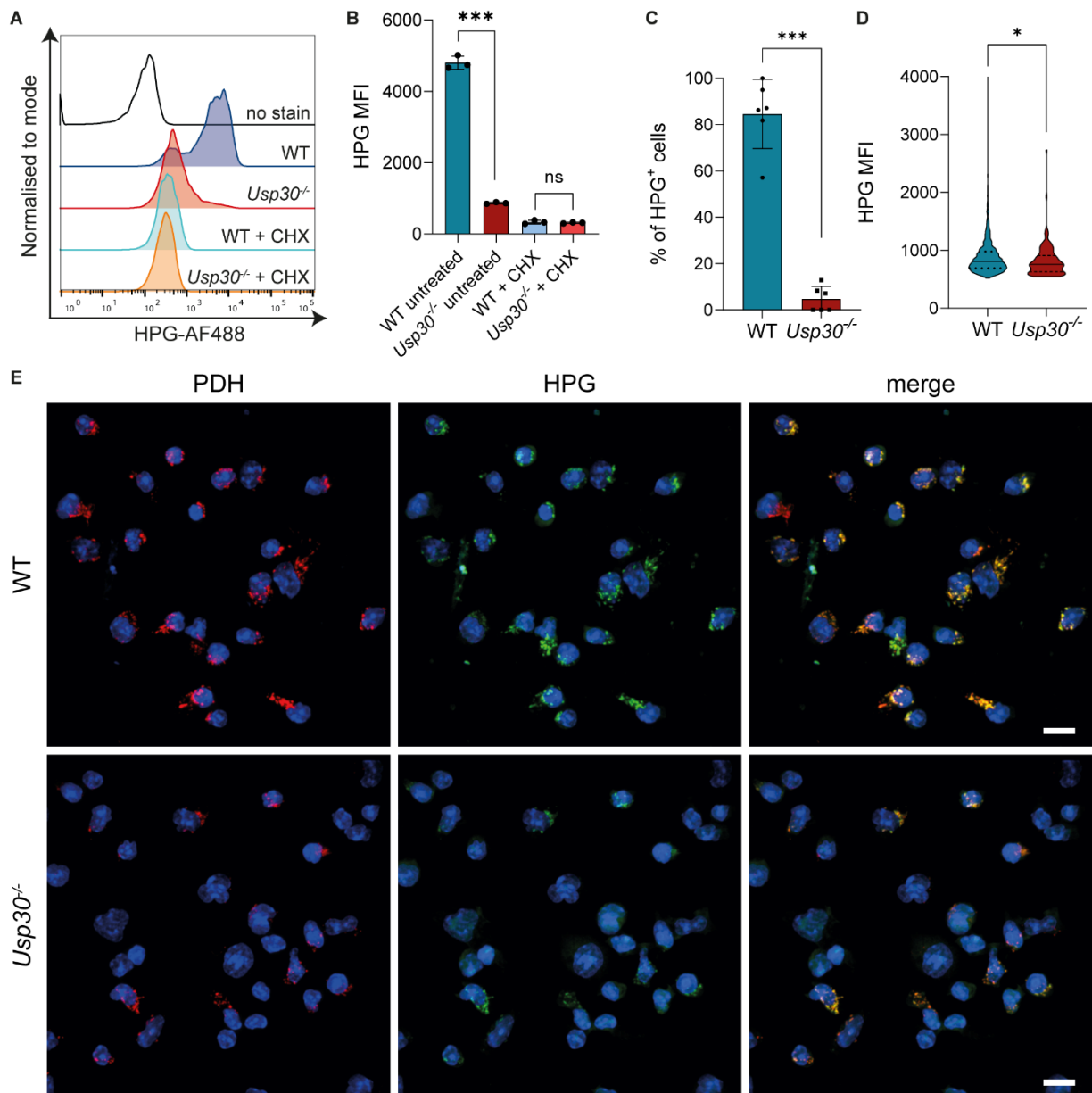


**Figure 4.6. Mitochondrial translation is inhibited in *Usp30*<sup>-/-</sup> CTLs.**

(A) HPG-AF488 incorporation by flow cytometry in day 5 WT and *Usp30*<sup>-/-</sup> CTLs either left untreated or treated with 100μg/ml CHX to inhibit cytosolic translation (2x10<sup>5</sup> CTLs/sample). (B) Flow cytometry analysis of HPG MFI in WT and *Usp30*<sup>-/-</sup> CTLs treated as in (A). (C) Percentage of CHX-treated CTLs (100μg/ml) incorporating HPG in day 5 WT and *Usp30*<sup>-/-</sup> CTLs as visualized by microscopy, shown by panels in (E). (D) HPG MFI in day 5 WT and *Usp30*<sup>-/-</sup> CTLs treated with 100μg/ml CHX (microscopy), shown by panels in (E). (E) Representative immunofluorescence of mitochondrial matrix (PDH) and HPG-AF488 incorporation in day 5 WT and *Usp30*<sup>-/-</sup> CTLs treated with 100μg/ml CHX (3x10<sup>4</sup> CTLs/sample). Scale bars = 10 μm. Error bars in (B, C) indicate average ±SD of technical replicates within one representative experiment. Solid and dotted lines in (D) show median and quartiles, respectively. \*\*\*=p<0.001, \*=p<0.05, ns=not significant (two-tailed unpaired Student's t-test). Data representative of at least three independent biological replicates.

#### 4.6 Genetic inhibition of mitochondrial translation: *mt-tRNA<sup>Ala</sup>* mice

Given the striking loss of mitochondrial protein synthesis in *Usp30<sup>-/-</sup>* CTLs, I asked whether inhibition of mitochondrial translation could affect CTL function. I started this investigation by using *mt-tRNA<sup>Ala</sup>* mice, a heteroplasmic model in which the mitochondrial tRNA gene for alanine is mutated, impairing mitochondrial protein synthesis (Kauppila et al., 2016). I quantified T cell populations in the spleen by assessing the percentage of CD4<sup>+</sup> and CD8<sup>+</sup> T cells, regulatory CD4<sup>+</sup> T cells, and naïve, central memory and effector memory T cells in both the CD4<sup>+</sup> and CD8<sup>+</sup> populations. No difference in numbers was observed in any of these populations, suggesting that T cells residing in the spleen are similar in WT and *mt-tRNA<sup>Ala</sup>* mice (**Figure 4.7**).

The 13 polypeptides synthesised by mitochondrial translation are incorporated into the ETC complexes (D'Souza and Minczuk, 2018), whose activity generates the mitochondrial membrane potential (Mitchell and Moyle, 1965). Therefore, I tested whether reduced mitochondrial protein synthesis in *mt-tRNA<sup>Ala</sup>* T cells would affect mitochondrial mass or mitochondrial membrane potential. WT and *mt-tRNA<sup>Ala</sup>* CD8<sup>+</sup> T cells were stained with Mitotracker Deep Red and TMRE before (day 0) and after *in vitro* activation (day 3, 5 and 7 post-stimulation). Both mitochondrial mass and membrane potential increased upon activation, showing a peak on day 3 (**Figure 4.8**). No substantial loss of mitochondrial mass nor membrane potential was detected in naïve CD8<sup>+</sup> *mt-tRNA<sup>Ala</sup>* T cells or mature *mt-tRNA<sup>Ala</sup>* CTLs when compared to their WT counterparts.

To investigate whether a defect in mitochondrial protein synthesis could affect CTL cytotoxicity, I assayed both degranulation and killing capacity in WT and *mt-tRNA<sup>Ala</sup>* CTLs 5 days after activation. No difference in degranulation was observed after TCR stimulation in *mt-tRNA<sup>Ala</sup>* CTLs (**Figure 4.9 A, B**). Next, I co-incubated WT and *mt-tRNA<sup>Ala</sup>* CTLs with target cells and measured target lysis at different CTL:target ratios (**Figure 4.9C**) or over time (**Figure 4.9D**). A moderate decrease in short-term killing was observed in *mt-tRNA<sup>Ala</sup>* CTLs when testing different CTL:target ratios (**Figure 4.9C**). However, this effect appeared negligible when cytotoxicity was monitored over time (**Figure 4.9D**).

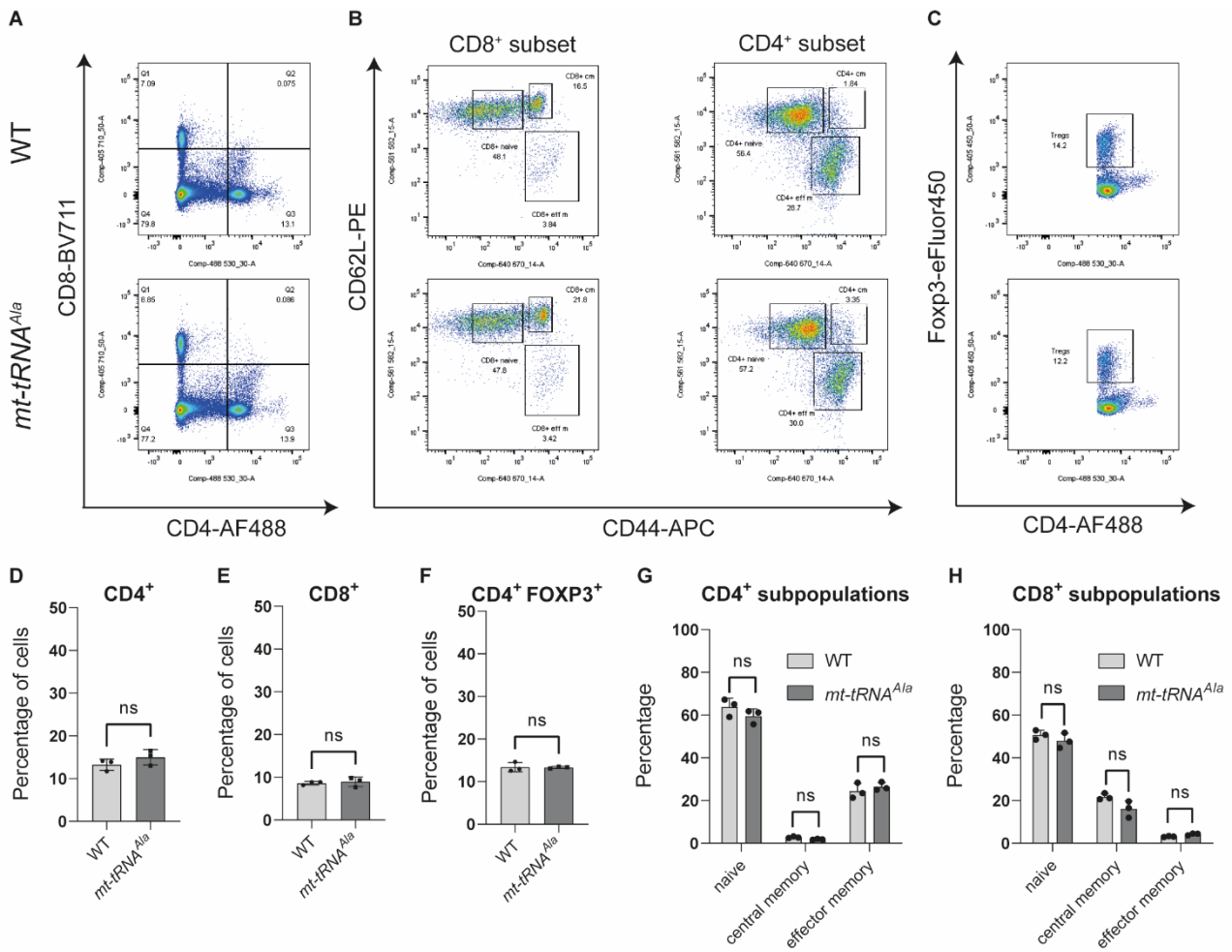


**Figure 4.7. Analysis of WT and *mt-tRNA<sup>Ala</sup>* splenocytes.**

(A) CD4<sup>+</sup>/CD8<sup>+</sup> ratio in WT and *mt-tRNA<sup>Ala</sup>* splenocytes. (B) CD4<sup>+</sup> and CD8<sup>+</sup> naïve (CD62L<sup>high</sup>, CD44<sup>low</sup>), central memory (CD62L<sup>high</sup>, CD44<sup>high</sup>) and effector memory (CD62L<sup>low</sup>, CD44<sup>high</sup>) T cell populations in WT and *mt-tRNA<sup>Ala</sup>* splenocytes. (C) Regulatory T cells (CD4<sup>+</sup>, FOXP3<sup>+</sup>) in WT and *mt-tRNA<sup>Ala</sup>* splenocytes. (D-H) Quantitation of (D) CD4<sup>+</sup>, (E) CD8<sup>+</sup>, (F) regulatory T cells, (G) total CD4<sup>+</sup> and (H) CD8<sup>+</sup> populations (naïve, central memory, effector memory) in WT and *mt-tRNA<sup>Ala</sup>* splenocytes. Plots show the average of three biological replicates (10<sup>6</sup> splenocytes/sample) ±SD. ns = not significant (two-tailed unpaired Student's t-test).

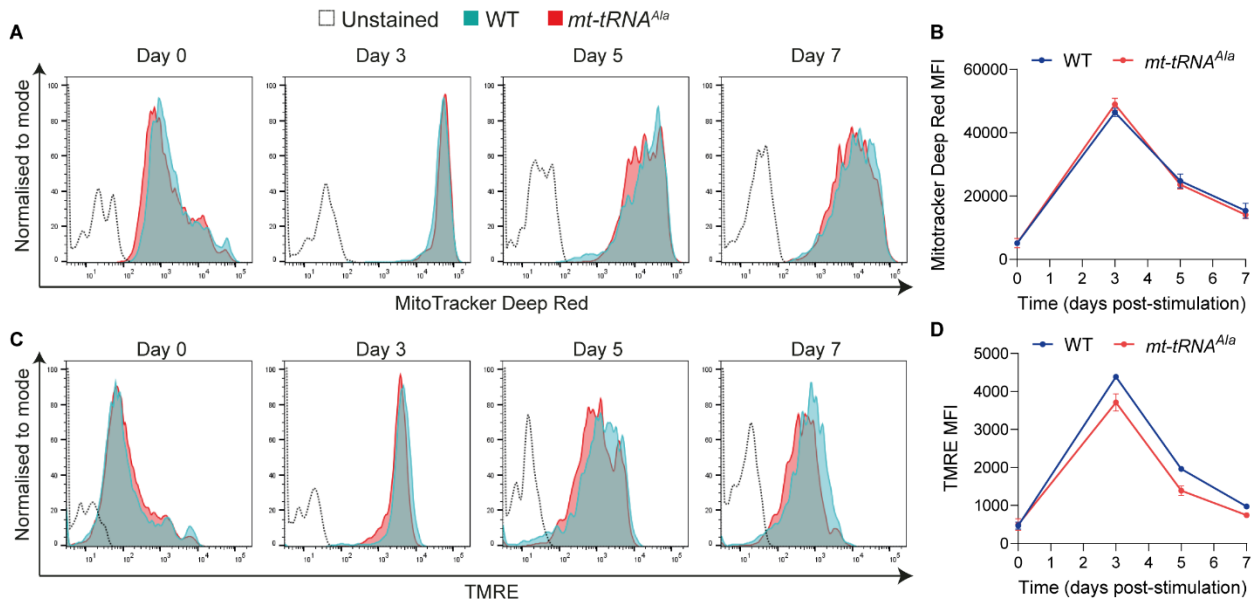


**Figure 4.8. *mt-tRNA<sup>Ala</sup>* mutation does not affect mitochondrial mass nor mitochondrial membrane potential.**

(A-D) Time course of mitochondria labelled with (A, B) MitoTracker Deep Red and (C, D) TMRE in WT and *mt-tRNA<sup>Ala</sup>* naïve CD8<sup>+</sup> T cells (day 0) and mature CTLs (day 3-7). Mitotracker Deep Red and TMRE MFI are plotted over time in (B, D). Error bars represent average  $\pm$ SD of two biological replicates (day 0:  $10^6$  splenocytes/sample; days 3-7:  $10^5$  CTLs/sample).

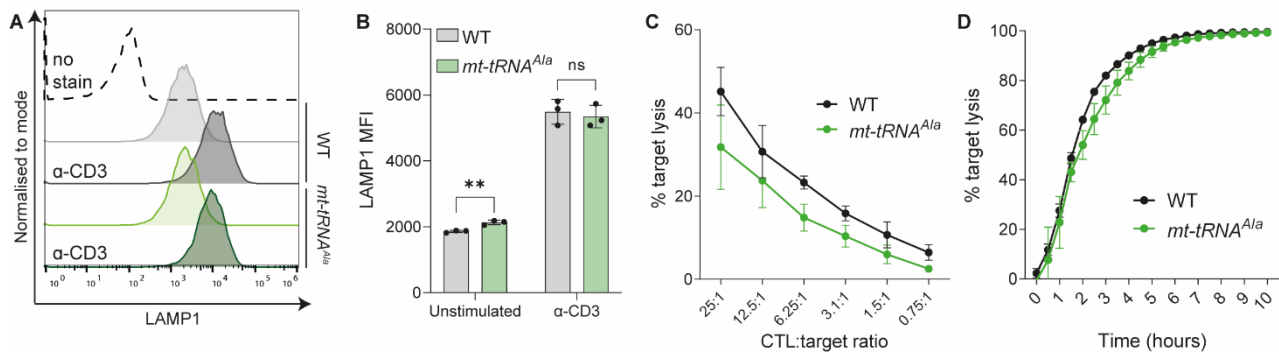


**Figure 4.9. Analysis of degranulation and cytotoxicity in *mt-tRNA<sup>Ala</sup>* CTLs.**

(A) Histogram of surface LAMP1 fluorescence intensity in WT and *mt-tRNA<sup>Ala</sup>* CTLs before and after TCR stimulation ( $2 \times 10^5$  targets and  $2 \times 10^5$  CTLs per sample). (B) Quantitation of LAMP1 MFI as shown in (A). (C) Short term (2.5h) killing assay with WT and *mt-tRNA<sup>Ala</sup>* CTLs, varying CTL:target ratio.  $10^4$  targets/sample. CTLs numbers varying according to ratio:  $2.5 \times 10^5$  (25:1),  $1.25 \times 10^5$  (12.5:1),  $6.25 \times 10^4$  (6.25:1),  $3.1 \times 10^4$  (3.1:1),  $1.5 \times 10^4$  (1.5:1) and  $7.5 \times 10^3$  (0.75:1) CTLs/sample. (D) Long-term killing assays (CTL:target, 10:1) displaying percentage of target cell lysis over time with WT and *mt-tRNA<sup>Ala</sup>* CTLs ( $4 \times 10^3$  targets and  $4 \times 10^4$  CTLs per sample). Error bars display the average  $\pm$ SD of (B) technical replicates, or (C, D) biological replicates. \*\*= $p < 0.01$ , ns=not significant (two-tailed unpaired Student's t-test). All data representative of at least two biological replicates.

Next, I assessed cytosolic protein synthesis in day 5 WT and *mt-tRNA<sup>Ala</sup>* CTLs measuring HPG incorporation by flow cytometry. HPG incorporation was decreased in both unstimulated and TCR-triggered *mt-tRNA<sup>Ala</sup>* CTLs (**Figure 4.10A, B**). To test whether this could affect the expression of cytolytic proteins, I used immunoblotting to examine granzyme B abundance in day 5 *mt-tRNA<sup>Ala</sup>* CTLs, and I found it to be reduced compared to WT (**Figure 4.10C**). TOM20 expression was examined as a control and showed no difference between WT and *mt-tRNA<sup>Ala</sup>* CTLs samples. Despite this, the extent of the downregulation of HPG incorporation and granzyme B expression was small compared to the results previously obtained in *Usp30<sup>-/-</sup>* CTLs (**Figure 3.15A**), and it exhibited variability between different *mt-tRNA<sup>Ala</sup>* biological replicates.

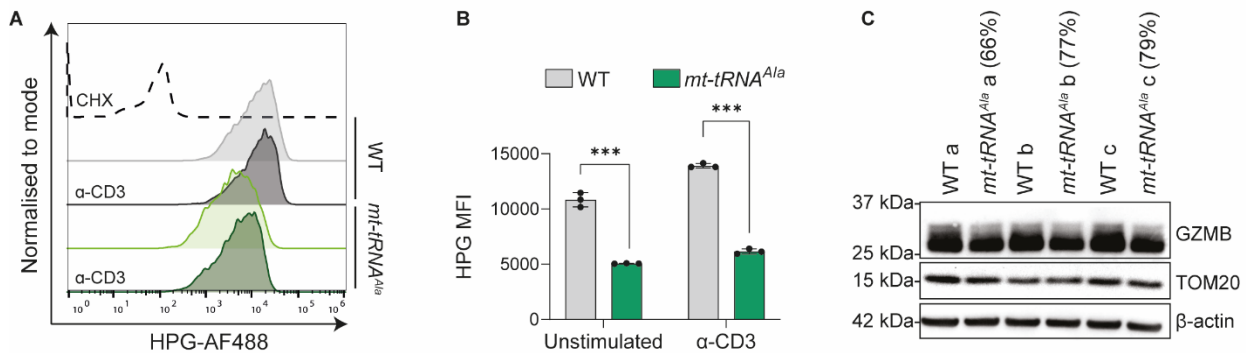


**Figure 4.10. *mt-tRNA<sup>Ala</sup>* mutation decreases cytosolic translation and granzyme B expression.**

(A) HPG-AF488 incorporation in day 5 WT and *mt-tRNA<sup>Ala</sup>* CTLs, stimulated with  $\alpha$ -CD3 (TCR crosslinking) where indicated, compared with cycloheximide-treated CTLs in which cytosolic translation is inhibited ( $2 \times 10^5$  CTLs/sample). (B) Quantitation of HPG MFI in day 5 WT and *mt-tRNA<sup>Ala</sup>* CTLs. Error bars indicate average  $\pm$ SD of three biological replicates. \*\*\*= $p < 0.001$  (two-tailed unpaired Student's t-test). (C) Immunoblot for granzyme B (GZMB) and TOM20 expression in day 5 WT and *mt-tRNA<sup>Ala</sup>* samples. Three biological replicates shown, labelled as (a-c) (3.33  $\mu$ g lysate/sample).

The *mt-tRNA<sup>Ala</sup>* mutational burden tends to be lower in rapidly dividing cells and peripheral blood cells (Kauppila et al., 2016). The variability in cytotoxicity, translation and granzyme B synthesis prompted further analysis of *mt-tRNA<sup>Ala</sup>* heteroplasmy. The percentage of *mt-tRNA<sup>Ala</sup>* mutation in mice was routinely assessed using skin biopsies. I asked whether the mutational burden in splenocytes was comparable to the one observed in skin cells, and whether it was retained upon CTL activation. To this end, we measured the percentage of *mt-Nd6* heteroplasmy. *Mt-Nd6* is a mitochondrial gene coding for a complex I subunit which displays a non-pathogenic mutation linked to *mt-tRNA<sup>Ala</sup>*. Therefore, *mt-Nd6* mutation levels can be used as an indicator of *mt-tRNA<sup>Ala</sup>* mutational burden.

I extracted polyadenylated RNA from WT and *mt-tRNA<sup>Ala</sup>* splenocytes and from activated CTLs 5 days after *in vitro* stimulation, and levels of *mt-Nd6* mutation were compared to the genotyping results obtained by skin biopsy. While a small percentage of mitochondria in WT splenocytes appeared to have the *mt-Nd6* mutation, heteroplasmy values were considerably higher in *mt-tRNA<sup>Ala</sup>* splenocytes (**Figure 4.11A**). In addition, this analysis showed that the skin biopsy could provide a reliable indication of the levels of heteroplasmy in the spleen.

Interestingly, the percentage of mitochondria bearing the *mt-Nd6* mutation remained constant in WT CTLs after stimulation, while it decreased in all mutant samples upon T cell activation. While the highest percentage of heteroplasmy in *mt-tRNA<sup>Ala</sup>* splenocytes was 74%, the highest level of heteroplasmy in activated *mt-tRNA<sup>Ala</sup>* CTLs was 66.7%. The reduction in heteroplasmy was consistently observed across all samples and found to be statistically significant (**Figure 4.11B**). While there is no established threshold for the pathogenicity of mitochondrial heteroplasmy, defects in mitochondrial translation in *mt-tRNA<sup>Ala</sup>* mutants have been reported to be most noticeable when the mutation burden is at least 67% (Kauppila et al., 2016). Therefore, the decrease in *mt-tRNA<sup>Ala</sup>* heteroplasmy upon T cell activation could potentially suggest that high heteroplasmy levels for tRNA<sup>Ala</sup> were not well tolerated in mature CTLs and were selected against during CTL activation.

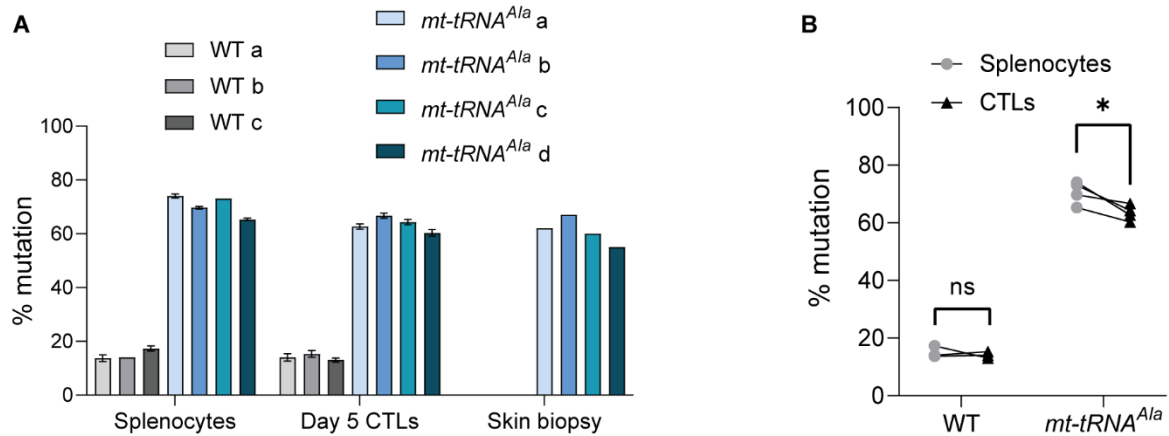


**Figure 4.11. Mutational burden decreases upon activation in *mt-tRNA<sup>Ala</sup>* CTLs.**

(A) Genotyping of WT and *mt-tRNA<sup>Ala</sup>* splenocytes and CTLs compared to skin biopsy of *mt-tRNA<sup>Ala</sup>* mice. Error bars display the average  $\pm$ SD of 3 (WT) and 4 (*mt-tRNA<sup>Ala</sup>*) biological replicates, identified as (a-d) (starting material: 100 ng cDNA/sample from splenocytes and day 5 CTLs). (B) Percentage of mitochondria bearing the *mt-Nd6* mutation in T cells derived from *mt-tRNA<sup>Ala</sup>* mice, showing mutational load in same sample before (splenocyte) and after (CTL) *in vitro* stimulation as in (A). \*= $p < 0.05$ , ns=not significant (two-tailed paired Student's t-test). ND6/*mt-tRNA<sup>Ala</sup>* genotyping was performed and analysed by Stephen Burr.

To determine whether the percentage of *mt-tRNA<sup>Ala</sup>* heteroplasmy in activated CTLs was sufficient to cause a defect in mitochondrial protein synthesis, I incubated WT and *mt-tRNA<sup>Ala</sup>* CTLs with HPG and CHX and I assayed mitochondrial translation by immunofluorescence. HPG was efficiently incorporated in both WT and *mt-tRNA<sup>Ala</sup>* mitochondria (**Figure 4.12A**). To further test whether HPG incorporation was affected by the *mt-tRNA<sup>Ala</sup>* mutation, I quantitated HPG MFI by immunofluorescence in all the genotyped WT and *mt-tRNA<sup>Ala</sup>* CTL samples. HPG MFI was similar in WT and *mt-tRNA<sup>Ala</sup>* CTLs, and variations in MFI did not correspond to the measured mutational burden (**Figure 4.12B**). Overall, these results indicated that the *mt-tRNA<sup>Ala</sup>* mutation in CTLs was not sufficient to induce a detectable and reproducible decrease in mitochondrial protein synthesis.

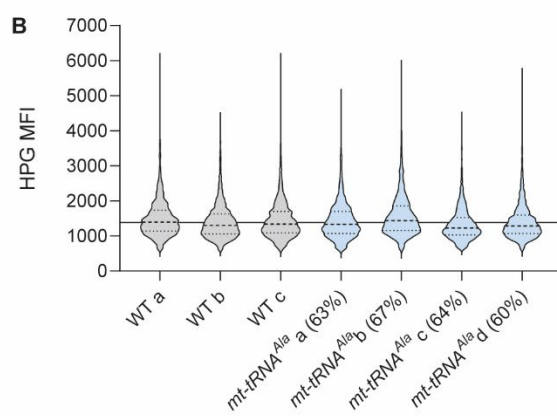
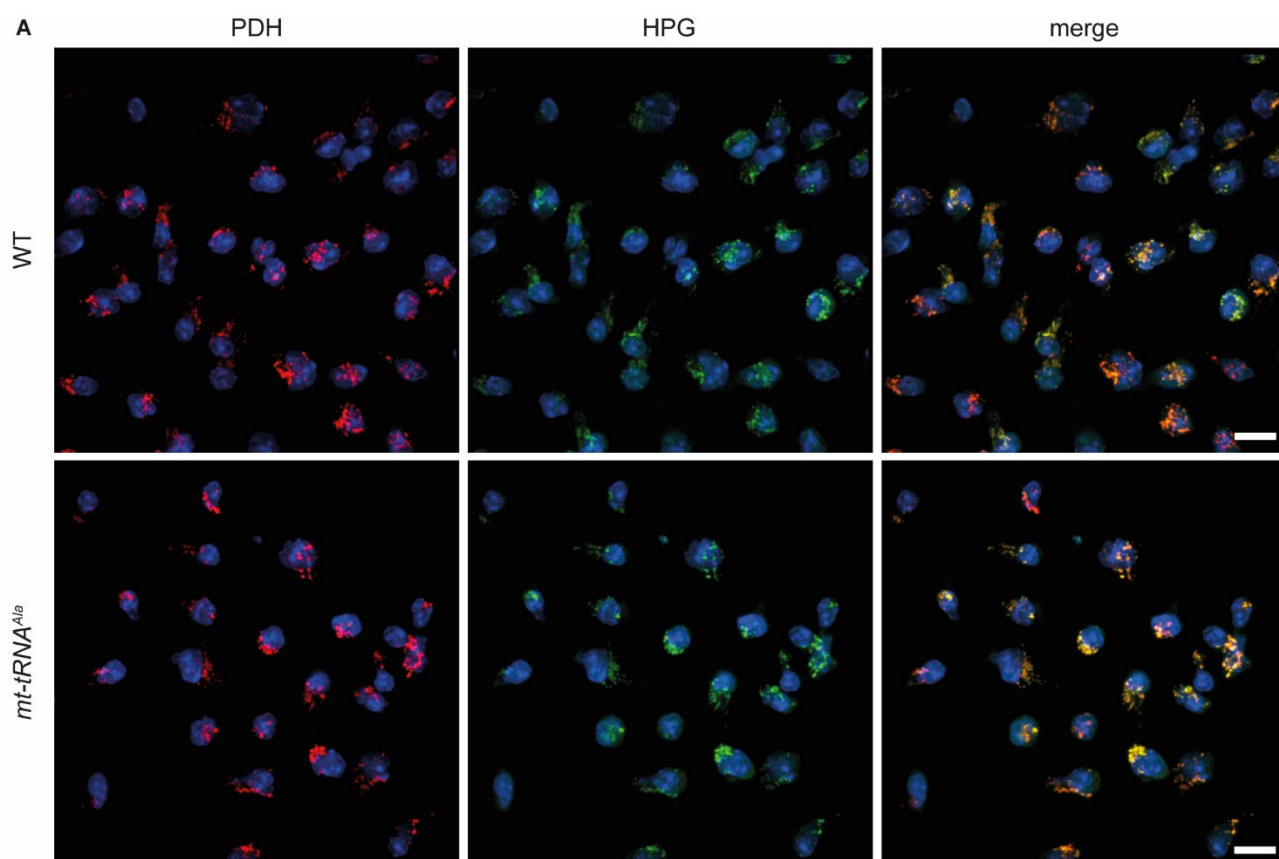


**Figure 4.12. *mt-tRNA<sup>Ala</sup>* CTLs show efficient mitochondrial protein synthesis.**

(A) Immunofluorescence of mitochondrial matrix (PDH) and HPG-AF488 incorporation in day 5 WT and *mt-tRNA<sup>Ala</sup>* CTLs treated with 100 $\mu$ g/ml CHX ( $3 \times 10^4$  CTLs/sample). Scale bars = 10  $\mu$ m. (B) Quantitation HPG MFI in in day 5 WT and *mt-tRNA<sup>Ala</sup>* CTLs where HPG was incorporated. Horizontal line denotes average HPG MFI in WT samples. Data representative of 3 (WT) and 4 (*mt-tRNA<sup>Ala</sup>*) biological replicates, indicated as (a-d). Mutation percentages were rounded to the closest integer.

#### 4.7 Genetic inhibition of mitochondrial translation: mito-ribosome CRISPR knockouts

The variability in the percentage of *mt-tRNA<sup>Ala</sup>* heteroplasmy made the results obtained in *mt-tRNA<sup>Ala</sup>* CTLs difficult to interpret. Despite this, the moderate decrease in cytosolic protein synthesis, granzyme B expression and cytotoxicity observed in some of the *mt-tRNA<sup>Ala</sup>* samples prompted a further investigation of the role of mitochondrial translation in CTLs. Therefore, I employed the CRISPR/Cas9 system to test whether inhibiting the expression of assembly (MRM2, MRM3, GTPBP10) or elongation factors (GFM1), or subunits of the mitochondrial ribosome (MRPS16, MRPS22, MRPS35, MRPL12, MRPL28, MRPL37, MRPL48, MRPL49) could affect mitochondrial protein synthesis.

Among the assembly factors tested, only GTPBP10 appeared to be recognised by immunoblot (expected molecular weight=43 kDa) (**Figure 4.13A**), while antibodies against MRM2 and MRM3 failed to recognise bands with the expected molecular weight (28 kDa and 51 kDa, respectively) (**Figure 4.13B, C**). I performed CRISPR/Cas9-mediated knockout for these three assembly factors to test whether any of them would be a valid target to pursue to modulate mitochondrial protein synthesis. None of the knockout samples displayed any change in the band pattern observed by immunoblot when compared to control samples (**Figure 4.13A-C**). CTL cytotoxicity was also not affected (**Figure 4.13D**).

Next, I tested the elongation factor GFM1, deletion of which was recently shown to reduce mitochondrial translation in CD4<sup>+</sup> T cells (Almeida et al., 2021). While GFM1 protein expression could be reliably detected by immunoblot, GFM1 abundance was unchanged three days after CRISPR-mediated knockout (**Figure 4.14A**). Furthermore, *Gfm1* CRISPR KO CTLs did not exhibit any defect in cytotoxicity (**Figure 4.14B**). Notably, cytotoxicity appeared moderately increased in all nucleofected samples when compared to non-nucleofected CTLs. To test whether the attempted gene deletion affected mitochondrial translation, control and *Gfm1* CRISPR KO CTLs were incubated with HPG in the presence of cycloheximide and analysed by immunofluorescence. HPG accumulated in the mitochondria of all samples, confirming that the *Gfm1* gene knockout was not efficient (**Figure 4.14C**).

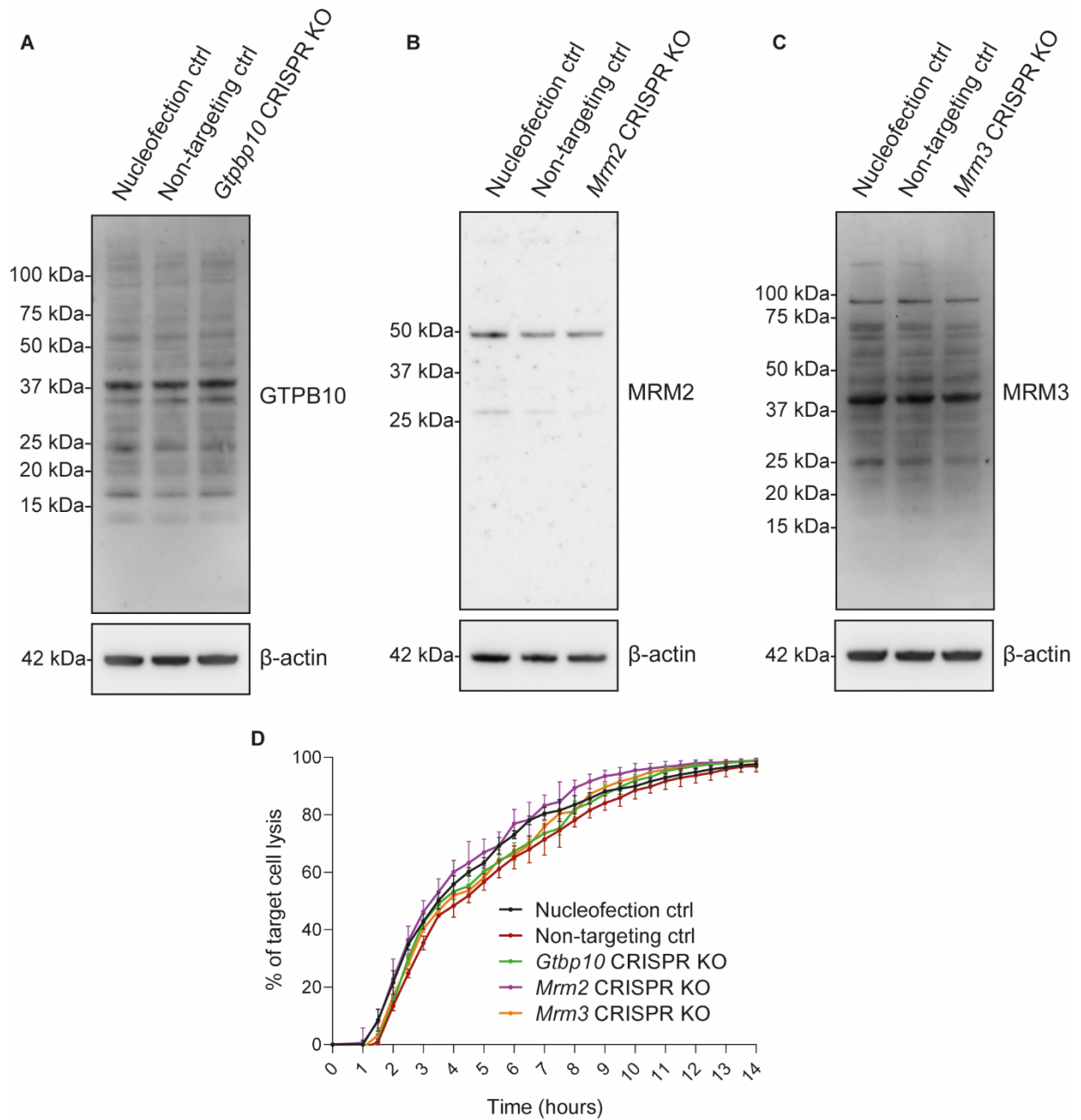


**Figure 4.13. Testing the role of mitochondrial ribosome assembly factors in CTL cytotoxicity.**

(A-C) Immunoblots showing (A) GTPBP10, (B) MRM2 and (C) MRM3 protein expression in WT CTL controls (nucleofection and non-targeting controls) and in CTLs nucleofected with guide crRNA for (A) *Gtpbp10*, (B) *Mrm2* and (C) *Mrm3* (3.33  $\mu$ g lysate/sample) (D) Long-term (10h) killing assay displaying percentage of target cell lysis over time (CTL:target ratio, 1:1) with control and *Gtpbp10*, *Mrm2* and *Mrm3* CRISPR KO CTLs ( $4 \times 10^4$  targets and  $4 \times 10^4$  CTLs per sample). Error bars indicate the average  $\pm$ SD of three technical replicates within one representative experiment. Data representative of three independent biological replicates.

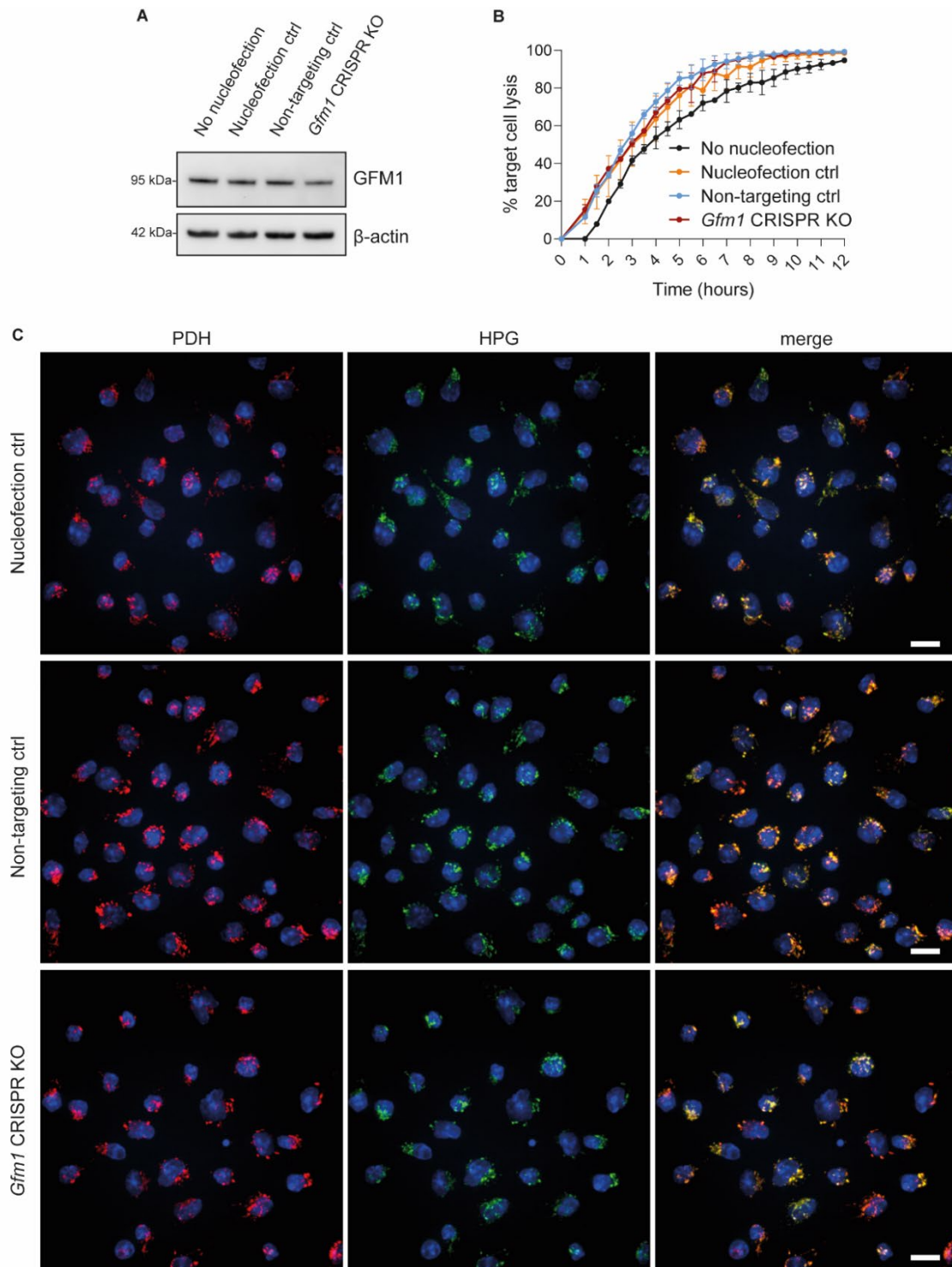


**Figure 4.14. *Gfm1* CRISPR KO fails to reduce GFM1 protein expression and mitochondrial translation.**

(A) Immunoblot showing GFM1 protein expression in WT CTL controls (no nucleofection, nucleofection and non-targeting controls) and in CTLs nucleofected with guide crRNA for *Gfm1* (3.33  $\mu\text{g}$  lysate/sample). (B) Long-term (10h) killing assay displaying percentage of target cell lysis over time (CTL:target ratio, 10:1) with control and *Gfm1* CRISPR KO CTLs ( $4 \times 10^4$  targets and  $4 \times 10^4$  CTLs per sample). Error bars indicate the average  $\pm$ SD of technical replicates within one representative experiment. (C) HPG-AF488 incorporation in day 7 control and CRISPR KO samples treated with 100 $\mu\text{g}/\text{ml}$  CHX to inhibit cytosolic protein synthesis ( $3 \times 10^4$  CTLs/sample). Scale bars = 10  $\mu\text{m}$ . Data representative of two biological replicates.

I next aimed to target the mitochondrial ribosome directly. To this end, I performed CRISPR/Cas9-mediated KO to inhibit the expression of subunits of the mitochondrial ribosome. Among the seven targets that were tested (MRPS16, MRPS22, MRPS35, MRPL12, MRPL28, MRPL37, MRPL48, MRPL49), the three proteins whose expression was consistently decreased four days after the knockout were MRPS16, MRPS22 and MRPL37 (**Figure 4.15**).

Control and CRISPR KO CTLs were incubated with CHX and HPG and analysed by immunofluorescence to test whether deletion of individual components of the mitochondrial ribosome would inhibit mitochondrial protein synthesis (**Figure 4.16A**). The methionine analogue was integrated in all control samples, while only 30-60% of CTLs could incorporate HPG in *Mrps16*, *Mrps22* and *Mrpl37* CRISPR KO CTLs (**Figure 4.16B**). The average HPG MFI was also reduced in a subset of the CRISPR KO samples, most notably in *Mrps16* CRISPR KO CTLs (**Figure 4.16C**). These results indicated that the genetic deletion of *Mrps16*, *Mrps22* and *Mrpl37* was sufficient to disrupt mitochondrial ribosome assembly and resulted in a partial loss of mitochondrial protein synthesis.

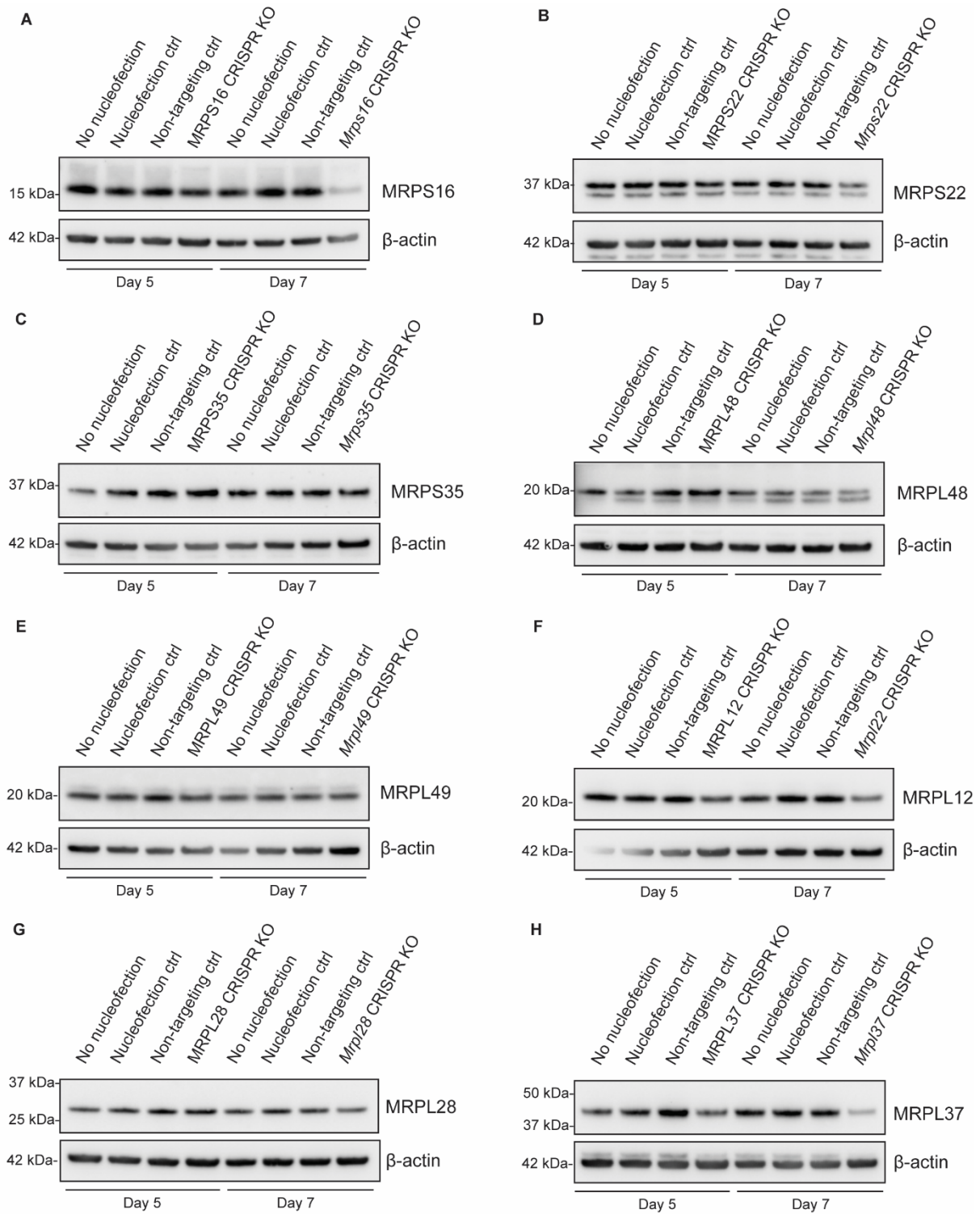


**Figure 4.15. Protein expression of small and large mitochondrial ribosome subunits after CRISPR KO.**

(A-H) Immunoblots showing protein expression in WT CTL controls (no nucleofection, nucleofection and non-targeting controls) and in CTLs nucleofected with guide crRNA for (A) *Mrps16*, (B) *Mrps22*, (C) *Mrps35*, (D) *Mrpl48*, (E) *Mrpl49*, (F) *Mrpl12*, (G) *Mrpl28* and (H) *Mrpl37*. Protein expression (3.33  $\mu$ g lysate/sample) was analysed on day 5 and day 7, respectively 2 and 4 days post-nucleofection with CRISPR reagents. Data representative of at least three independent biological replicates.

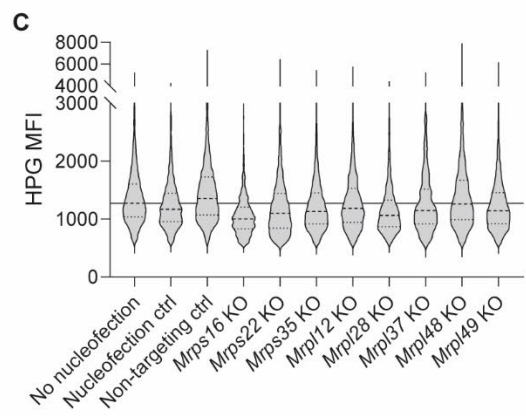
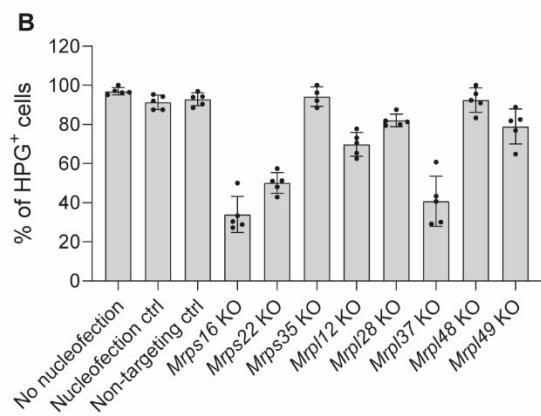
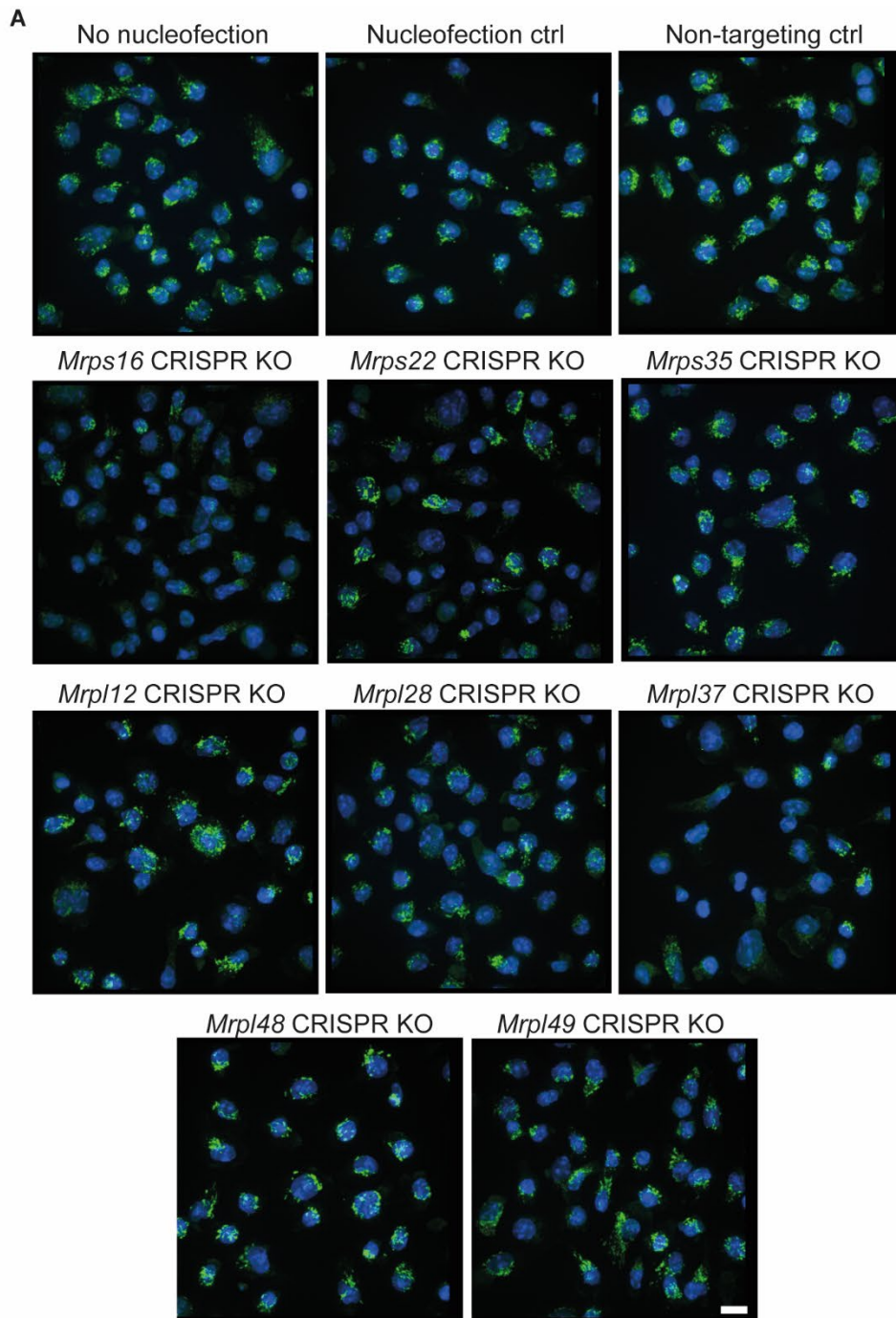


**Figure 4.16. Loss of MRPS16, MRPL22 and MRPL37 decreases mitochondrial protein synthesis.**

(A) HPG-AF488 incorporation in day 7 control and CRISPR KO samples treated with 100µg/ml CHX to inhibit cytosolic protein synthesis ( $3 \times 10^4$  CTLs/sample). Scale bar = 10 µm. (B, C) Quantitation of (B) percentage of CTLs incorporating HPG, and (C) HPG MFI in CTLs where HPG was incorporated. Error bars show the average  $\pm$ SD of technical replicates within one representative experiment. Horizontal line in (C) delineates HPG MFI in non-nucleofected CTLs. Data representative of at least two independent biological replicates.

The CRISPR KO samples were bulk populations composed of both WT CTLs and CTLs in which the expression of subunits of the mitochondrial ribosome had successfully been impaired. Therefore, I attempted to separate the WT and KO populations in the samples in which protein expression was most reliably decreased after nucleofection: *Mrps16* and *Mrpl37* CRISPR KO CTLs. I used flow cytometry to analyse control and knockout CTLs after intracellular staining with the same antibodies used by Western blot. These antibodies showed unspecific staining (**Figure 4.17A, B**), which was not consistent with the decrease in protein expression observed by immunoblot (**Figure 4.15**) nor with the reduced HPG incorporation observed in knockout CTLs by immunofluorescence (**Figure 4.16**).

As 13 subunits of ETC complexes are synthesised by mitochondrial translational (D'Souza and Minczuk, 2018), and the proton gradient generated by the ETC sustains the mitochondrial membrane potential (Mitchell and Moyle, 1965), I reasoned that membrane potential might be altered in CTLs with deficient mitochondrial protein synthesis. I stained control and CRISPR KO samples with TMRE and measured mitochondrial membrane potential by flow cytometry. Surprisingly, TMRE fluorescence was only moderately decreased in *Mrps16* and *Mrpl37* CRISPR KO CTLs (**Figure 4.17B**). Furthermore, no separate population displaying a lower mitochondrial membrane potential could be observed in either *Mrps16* or *Mrpl37* CRISPR KO CTLs, indicating that despite the reduction in mitochondrial protein synthesis, mitochondrial membrane potential could still be retained. Altogether, neither of these methods could successfully separate WT and KO CTLs within the *Mrps16* and *Mrpl37* CRISPR KO CTLs populations.

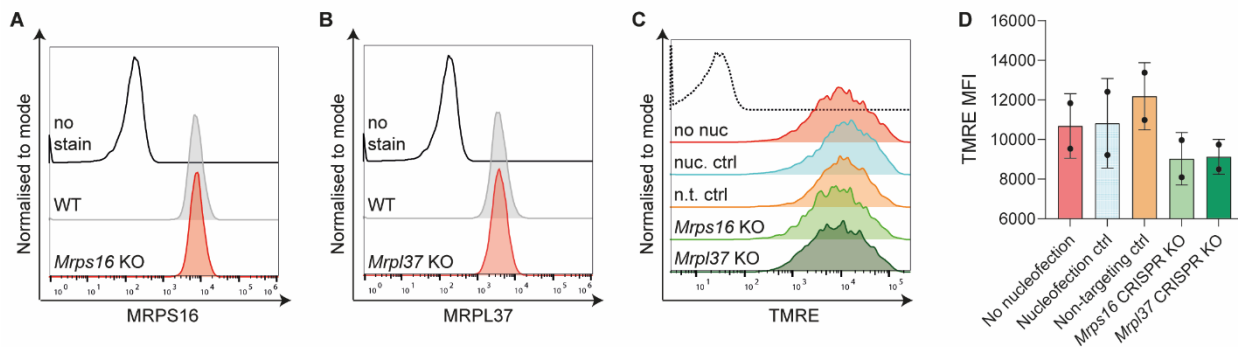


**Figure 4.17. Flow cytometry analysis of *Mrps16* and *Mrpl37* CRISPR KO CTLs.**

(A, B) Intracellular flow cytometry staining for (A) MRPS16 and (B) MRPL37 in WT and CRISPR KO CTLs ( $2 \times 10^5$  CTLs/sample). (C) Mitochondrial membrane potential as indicated by TMRE in day 7 non-nucleofected (no nuc), nucleofection control (nuc. ctrl), non-targeting control (n.t. ctrl), *Mrpl16* and *Mrpl37* CRISPR KO ( $10^5$  CTLs/sample). (D) TMRE MFI quantitation. Error bars represent average  $\pm$ SD of technical replicates. Data representative of one biological replicate.

Nevertheless, *Mrps16* and *Mrpl37* CRISPR KOs generated the most consistent decrease in mitochondrial protein synthesis and they were selected for further analysis of CTL function. First, I assessed granzyme B abundance in control, *Mrps16* and *Mrpl37* CRISPR KO CTLs (**Figure 4.18**). Interestingly, all control samples that had been nucleofected, either without CRISPR reagents (nucleofection control) or in the presence of Cas9, tracrRNA and non-targeting guide crRNA (non-targeting control) showed upregulation of granzyme B expression (**Figure 4.18A, B**). The abundance of granzyme B was downregulated in *Mrps16* and *Mrpl37* CRISPR KOs compared to the nucleofected controls. Nonetheless, this result was not always reproducible, possibly due to variations in knockout efficiency and the presence of a mixed population of WT and KO CTLs within the same CRISPR KO sample. Monitoring *de novo* synthesis of granzyme B by immunoblot revealed no difference between TCR-triggered control and MRPS16- or MRPL37-depleted CTLs (**Figure 4.18C, D**).

TNF $\alpha$  and IFN $\gamma$  production upon TCR stimulation was also not affected in CRISPR KO samples (**Figure 4.19A-C**). Surprisingly, CTL nucleofection and introduction of non-targeting CRISPR reagents was sufficient to alter cytokine synthesis, confounding the analysis of the effect of mitochondrial translation inhibition in the CRISPR KO samples. CTL killing did not appear to be affected by *Mrps16* or *Mrpl37* CRISPR KO (**Figure 4.19D**). All nucleofected samples reproducibly showed a modest increase in killing compared to non-nucleofected control CTLs, suggesting the upregulation of granzyme B observed upon nucleofection (**Figure 4.18A, B**) could be functionally significant in the context of cytotoxicity.

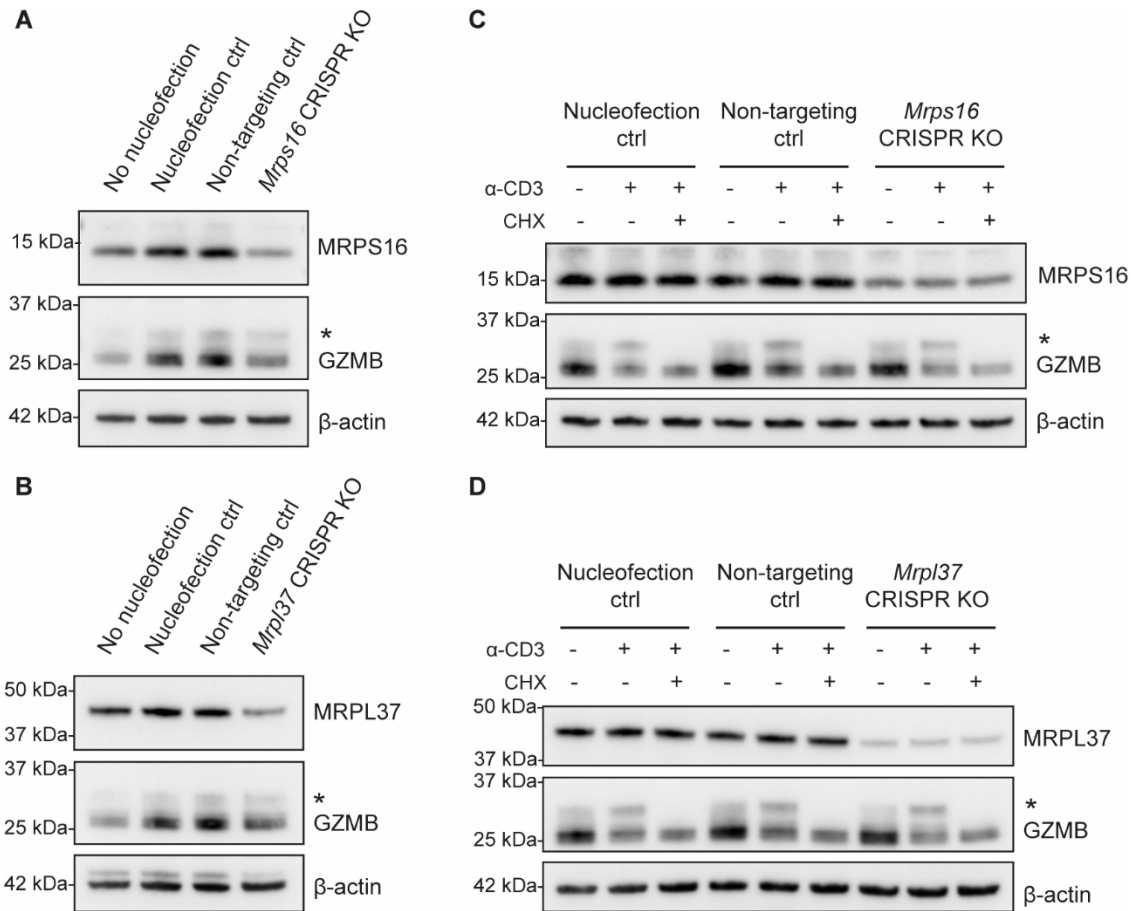


**Figure 4.18. Granzyme B expression in *Mrps16* and *Mrpl37* CRISPR KO samples.**

(A, B) Immunoblots for granzyme B (GZMB) in day 7 (A) *Mrps16* and (B) *Mrpl37* CRISPR KO and control CTLs. (C, D) Immunoblots showing granzyme B expression and synthesis in day 7 control and CRISPR KO CTLs, with TCR stimulation ( $\alpha$ -CD3) or cytosolic protein synthesis inhibition (100 $\mu$ g/ml CHX) where indicated. Newly synthesised GZMB labelled by (\*). Data representative of at least two independent biological replicates (3.33  $\mu$ g lysate/sample).

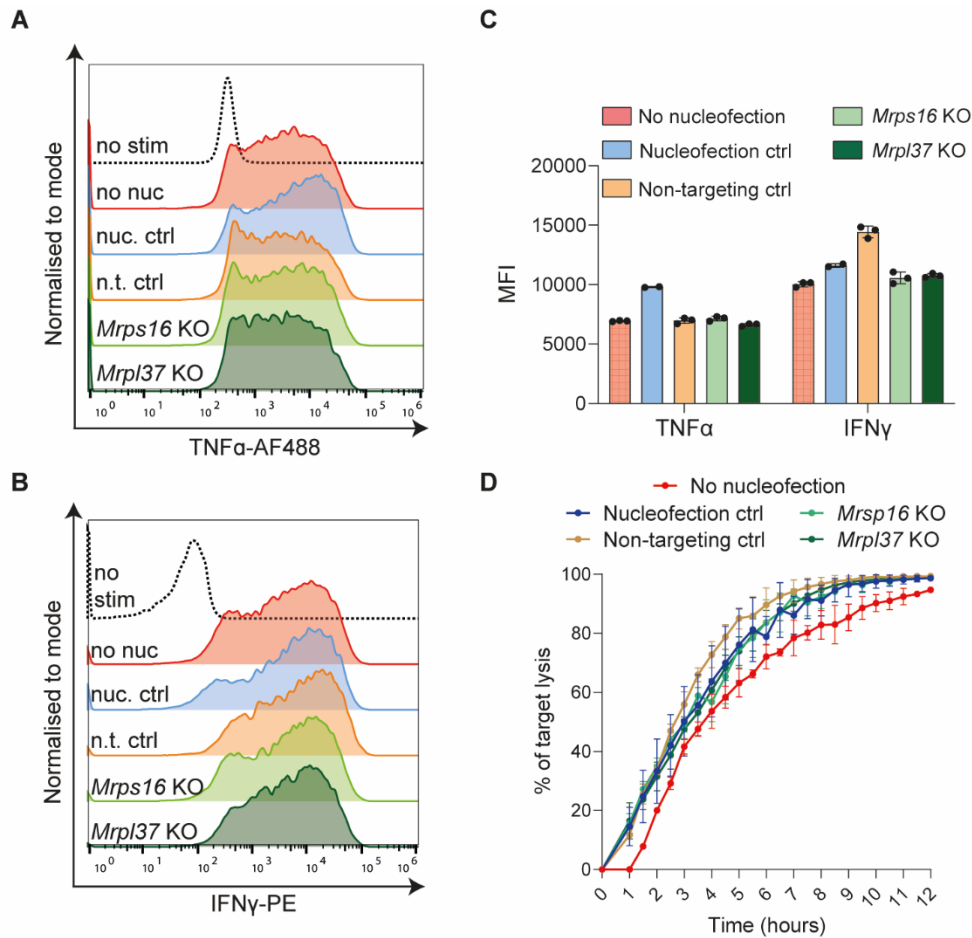


**Figure 4.19. Cytokine synthesis and cytotoxicity in *Mrps16* and *Mrpl37* CRISPR KO samples.**

(A, B) Intracellular staining for (A) TNF $\alpha$  and (B) IFN $\gamma$  in day 7 nucleofection control (nuc. ctrl), non-targeting control (n.t. ctrl), *Mrps16* and *Mrpl37* CRISPR KO ( $2 \times 10^5$  CTLs/sample). stimulated with  $\alpha$ -CD3 for 4.5h. no stim=unstimulated CTLs (control). (C) Quantitation of TNF $\alpha$  and IFN $\gamma$  MFI. (D) Long-term (12h) killing assay (CTL:target ratio, 1:1) displaying percentage target lysis with control and CRISPR KO CTLs ( $4 \times 10^4$  targets and  $4 \times 10^4$  CTLs per sample). Error bars indicate mean values  $\pm$ SD of technical replicates within one representative experiment. Data representative of at least three independent biological replicates.

The data obtained from *Usp30*<sup>-/-</sup> CTLs indicated that the killing and translation defects could be observed on day 5 post-stimulation. The first days after activation are the most translationally active time for CD8<sup>+</sup> T cells, with a peak in protein synthesis occurring on day 5 (Araki et al., 2017). By contrast, T cells used in CRISPR experiments were first stimulated (day 0-2) and CRISPR knockout was performed on day 3, after CD8<sup>+</sup> T cell isolation. Protein level was then assessed on day 5-7 to allow for degradation of previously formed proteins and functional experiments were performed on day 7, when protein downregulation could be observed (**Figure 4.15**). Given the confounding effect caused by the presence of a mixed population within the CRISPR KO samples, I asked whether testing CTL function on day 5 would more easily highlight a defect in translationally active CTLs. To this end I performed the CRISPR KO before *in vitro* stimulation (day 0) to allow for protein degradation to occur earlier and for CTL functionality to be tested on day 5 post-stimulation.

I isolated WT splenocytes and used them to perform CRISPR-mediated gene deletion of *Mrps16* and *Mrpl37* either before (**Figure 4.19A-C**) or after CD8<sup>+</sup> T cell isolation (**Figure 4.19D-F**). *Mcu* knockout was performed as a positive control given its reproducible efficiency (**Figure 4.5B**). Control and CRISPR KO samples were then stimulated as previously described (**Figure 3.2A; Materials and Methods**) and protein expression of MRPS16, MRPL37 and MCU was tested by immunoblot on day 5, 7 and 9 post-activation and post-nucleofection.

No difference in MRPS16, MRPL37 or MCU abundance could be detected in the CRISPR KO samples at any of the time points tested (**Figure 4.20**). This result suggests that either gene deletion was not efficient in freshly isolated CD8<sup>+</sup> T cells, or that efficiently knocked out T cells were not viable upon *in vitro* stimulation. The latter hypothesis would be consistent with experimental evidence showing that inhibition of different mitochondrial functions in immature T cells can prevent their proliferation and differentiation (Chang et al., 2013; Sena et al., 2013; Simula et al., 2018; Tan et al., 2017a; Yi et al., 2006).

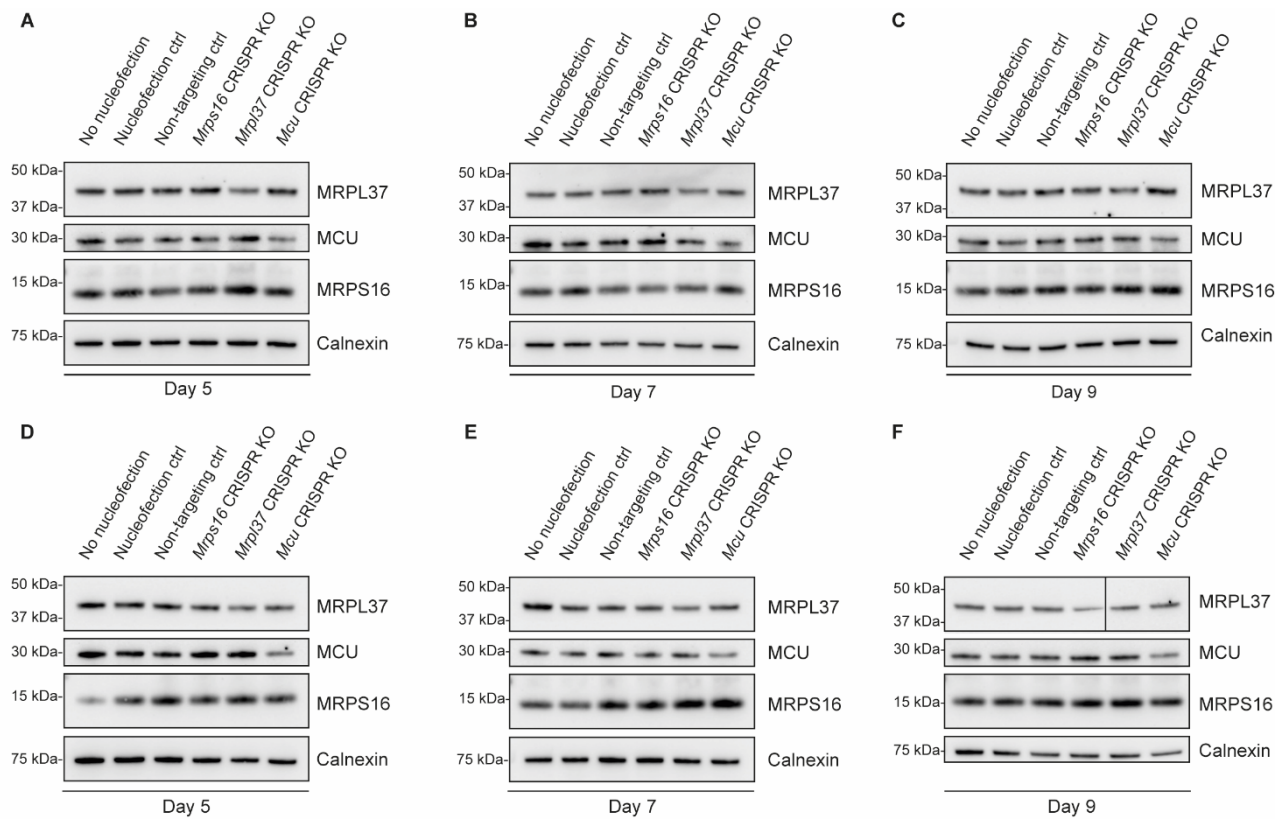


**Figure 4.20. CRISPR KO in naïve T cells results in poor KO efficiency.**

(A-F) Immunoblots showing MRPS16, MRPL37 and MCU protein expression in controls after CRISPR KO performed in naïve (A-C) unpurified or (D-F) CD8<sup>+</sup>-purified T cells nucleofected with guide crRNA for *Mrps16*, *Mrps37* or *Mcu* and control samples (no nucleofection, nucleofection and non-targeting control). Protein expression (3.33 µg lysate/sample) was assessed (A, D) 5 days, (B, E) 7 days and (C, F) 9 days post-nucleofection and *in vitro* activation. Data representative of two independent biological replicates.

#### 4.8 Pharmacological inhibition of mitochondrial translation: CAM and DOX

The results obtained with *mt-tRNA<sup>Ala</sup>* CTLs and with the *Mrps16* and *Mrpl37* CRISPR KOs highlighted the challenges of studying the downstream effects of mitochondrial protein synthesis in a mixed population. In addition, the nucleofection procedure appeared to alter the expression of cytosolic proteins and affect CTL killing. Therefore, I aimed to use two well-established pharmacological treatments to fully deplete mitochondrial translation: chloramphenicol (CAM) and doxycycline (DOX), which impair tRNA binding to the mitochondrial ribosome (Geigenmuller and Nierhaus, 1986; Pestka, 1969). Both treatments allowed for the study of mitochondrial protein synthesis while minimising the variability due to heteroplasmy, mixed knockout populations and nucleofection.

First, I verified that CAM and DOX treatment could affect mitochondrial protein synthesis. Day 5 WT and *Usp30<sup>-/-</sup>* CTLs were incubated with HPG and the media was supplemented with either cycloheximide only to inhibit cytosolic protein synthesis, or with cycloheximide combined with either chloramphenicol or doxycycline to impair both cytosolic and mitochondrial translation (**Figure 4.21**). HPG readily accumulated in the mitochondria of WT CTLs treated with CHX. By contrast, WT CTLs that were additionally treated with either chloramphenicol or doxycycline showed reduced HPG incorporation. As previously observed (**Figure 4.6**), little HPG incorporation was detectable in *Usp30<sup>-/-</sup>* CTLs, highlighting a marked decrease in mitochondrial protein synthesis. To verify whether chloramphenicol or doxycycline treatment would have an additive effect, *Usp30<sup>-/-</sup>* CTLs were incubated with HPG either in the presence of cycloheximide only, or with cycloheximide mixed with either chloramphenicol or doxycycline. Treatment with doxycycline or chloramphenicol abolished the residual mitochondrial protein synthesis observed in a minority of mitochondria in *Usp30<sup>-/-</sup>* CTLs. Overall, these results validated the use of chloramphenicol and doxycycline as inhibitors of mitochondrial translation in CTLs.

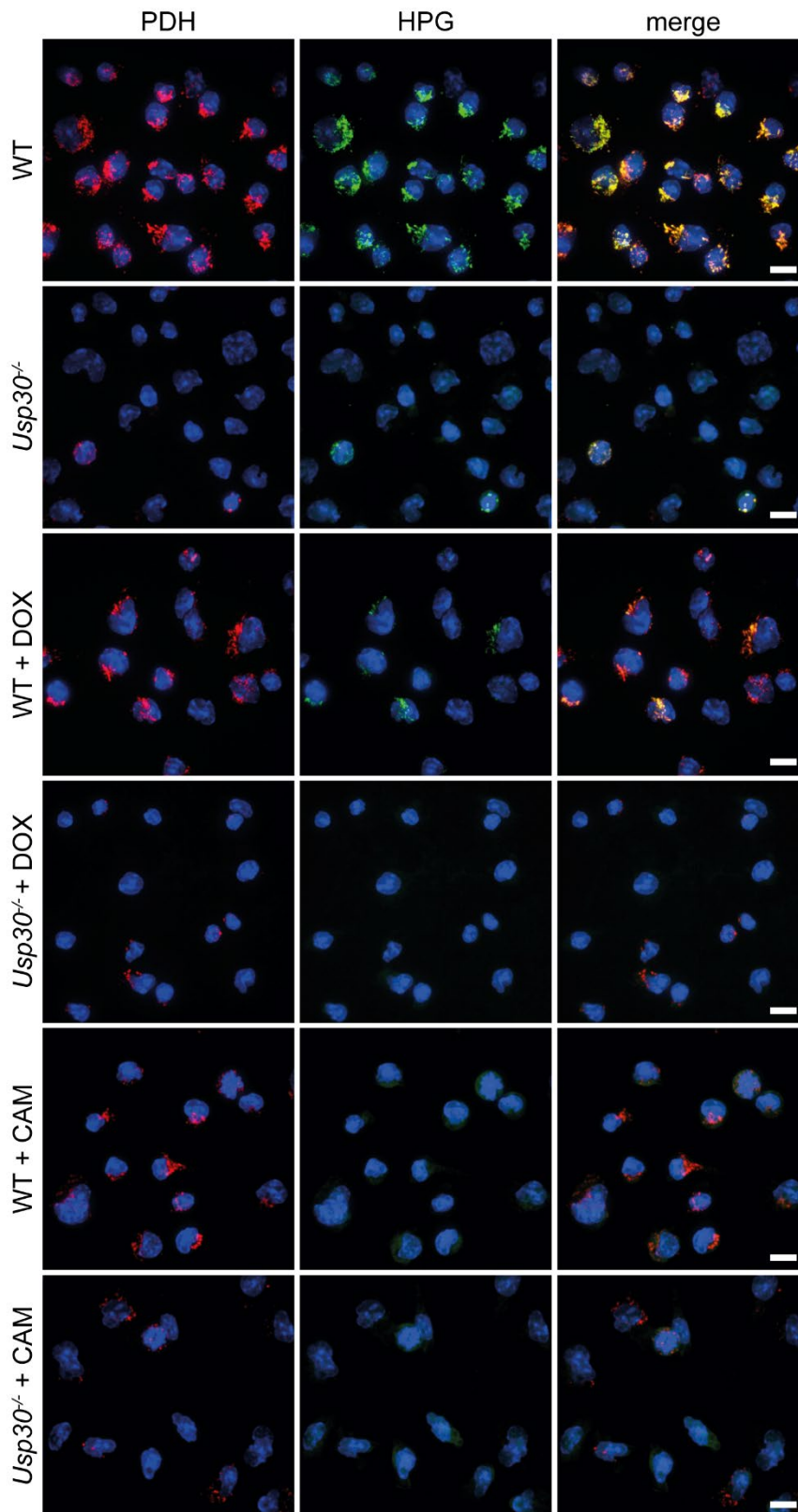


**Figure 4.21. Chloramphenicol and doxycycline inhibit mitochondrial protein synthesis.**

HPG-AF488 in day 5 WT and *Usp30*<sup>-/-</sup> CTLs treated with 100µg/ml CHX to inhibit cytosolic protein synthesis. 3x10<sup>4</sup> CTLs per sample were incubated with 500 µg/ml chloramphenicol (CAM) or 10 µg/ml doxycycline (DOX) where indicated. Mitochondrial matrix is labelled by PDH. Scale bars = 10 µm. Data representative of at least three independent biological replicates.

Next, I treated WT CTLs with increasing concentrations of chloramphenicol (50-500  $\mu\text{g/ml}$ ) or doxycycline (1-10  $\mu\text{g/ml}$ ) to test the effect of mitochondrial translation deficiency on CTL killing. Chloramphenicol treatment reduced CTL cytotoxicity in a dose-dependent manner, with the highest concentration (500  $\mu\text{g/ml}$ ) resulting in a marked inhibition of killing after 4h (**Figure 4.22A**). Doxycycline treatment impaired cytotoxicity at 10  $\mu\text{g/ml}$ , showing full inhibition after 4h of incubation (**Figure 4.22B**).

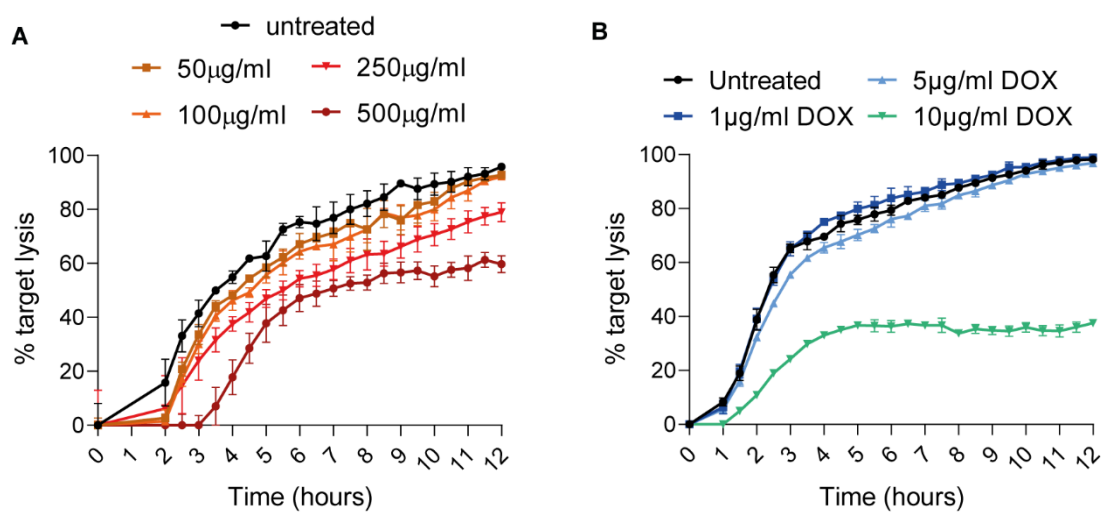


**Figure 4.22. Mitochondrial translation inhibition reduces CTL killing.**

(A, B) Long-term (12h) killing assays (CTL:target ratio, 1:1) displaying percentage target lysis with day 5 WT CTLs ( $4 \times 10^4$  targets and  $4 \times 10^4$  CTLs per sample). Cells were treated with (A) 50-500  $\mu\text{g/ml}$  chloramphenicol (CAM) or (B) 1-10  $\mu\text{g/ml}$  doxycycline (DOX). Error bars show mean values  $\pm$ SD of technical replicates. Data representative of at least three independent biological replicates.

To test whether complete inhibition of mitochondrial translation would affect cytosolic protein synthesis, I measured HPG incorporation by flow cytometry in chloramphenicol- and doxycycline-treated CTLs. Both pharmacological treatments reduced cytosolic HPG incorporation, while displaying different kinetics (**Figure 4.23**). In unstimulated CTLs, the effect of chloramphenicol appeared more pronounced than DOX after 1h of incubation. Interestingly, stimulation with  $\alpha$ -CD3 increased HPG incorporation in all treated samples, indicating that TCR activation can promote protein synthesis when the pharmacological treatment and  $\alpha$ -CD3 are introduced simultaneously. Despite this, CAM- and DOX-treated CTLs did not incorporate HPG as efficiently as untreated CTLs even in the presence of TCR stimulation.

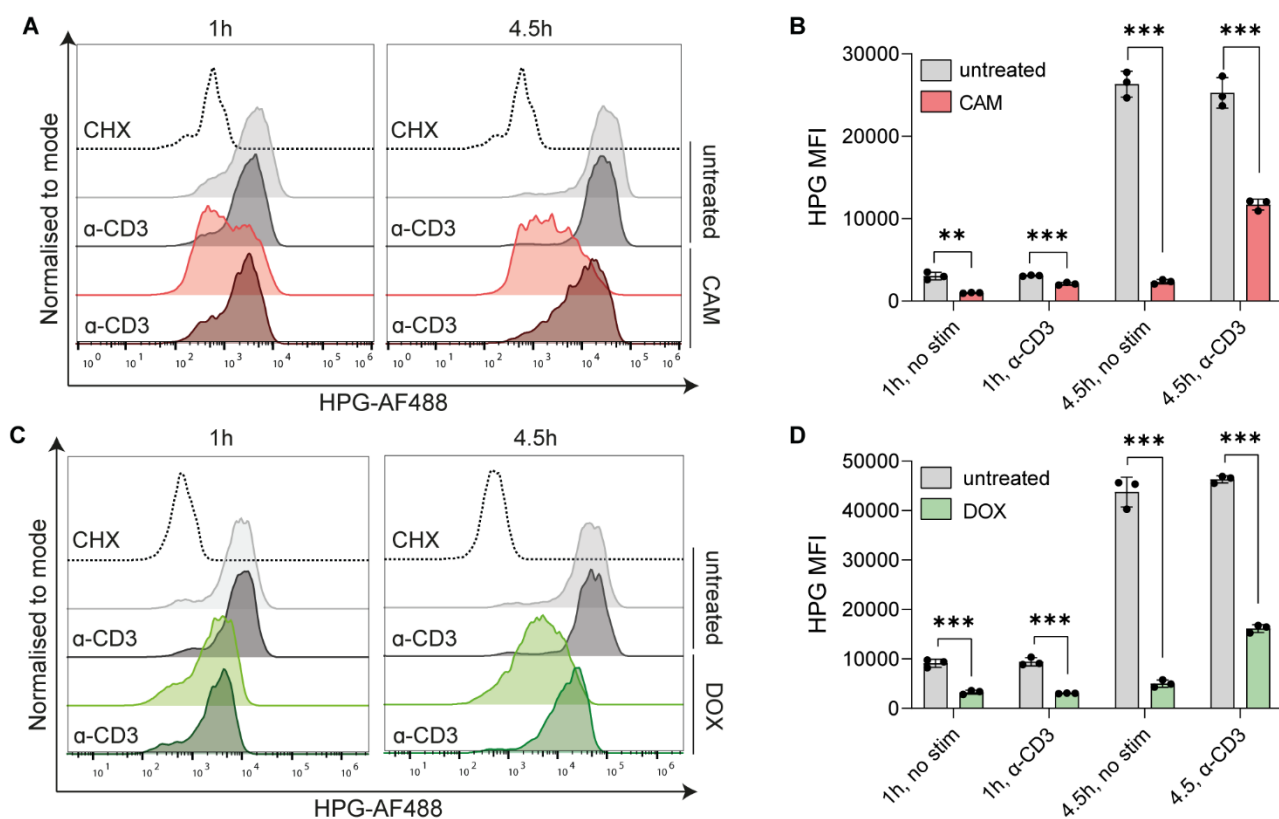


**Figure 4.23. Inhibition of mitochondrial translation impairs cytosolic protein synthesis.**

(A-D) HPG incorporation in untreated and (A, B) CAM-treated (500  $\mu\text{g/ml}$ ) or (C, D) DOX-treated (10  $\mu\text{g/ml}$ ) CTLs, with TCR stimulation ( $\alpha\text{-CD3}$ ) where indicated. 100 $\mu\text{g/ml}$  CHX was used in control samples to inhibit cytosolic protein synthesis. Plots in (B, D) show HPG MFI in (B) CAM-treated (500  $\mu\text{g/ml}$ ) or (D) DOX-treated (10  $\mu\text{g/ml}$ ) CTLs. All error bars indicate average  $\pm$ SD of technical replicates ( $2 \times 10^5$  CTLs/sample). \*\*\*= $p < 0.001$ , \*\*= $p < 0.01$  (two-tailed unpaired Student's t-test). Data representative of at least three independent biological replicates.

To determine whether the inhibition of HPG incorporation in CAM- and DOX-treated CTLs was a *bona fide* indicator of decreased cytosolic protein synthesis I examined the expression of granzyme B and perforin. Day 5 WT CTLs were stimulated with  $\alpha\text{-CD3}$  for 4.5h, during which they were either incubated in standard CTL culture media, or in media supplemented with either 500  $\mu\text{g/ml}$  chloramphenicol or 10  $\mu\text{g/ml}$  doxycycline. Cycloheximide treatment was added separately to control samples to distinguish newly synthesised proteins. Protein expression of granzyme B and perforin in unstimulated CTLs was not reproducibly altered by either CAM or DOX, suggesting that short incubations could not affect the expression of abundant proteins synthesised before the start of the

treatment (**Figure 4.24**). Nevertheless, newly synthesised granzyme B and perforin were reduced in both chloramphenicol- and doxycycline-treated CTLs upon TCR triggering. TOM20 expression was not altered in any of the DOX-treated samples, suggesting that cytolytic protein depletion occurred as a result of mitochondrial translation inhibition and without the concurrent loss of mitochondrial abundance observed in *Usp30*<sup>-/-</sup> CTLs. These results indicated that impairing mitochondrial translation reduced *de novo* protein synthesis of key mediators of the CTL killing response.

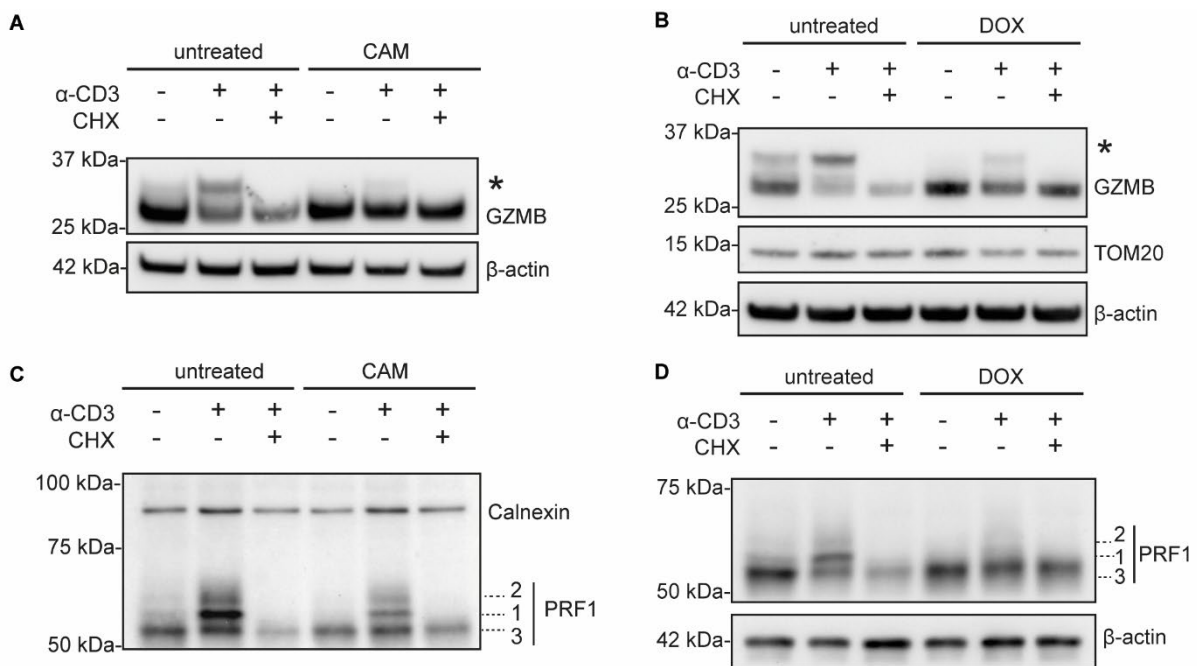


**Figure 4.24. Loss of mitochondrial translation impairs synthesis of granzyme B and perforin.**

(A, B) Immunoblots showing granzyme B (GzmB) expression and synthesis in day 5 CTLs treated with (A) 500  $\mu$ g/ml CAM or (B) 10  $\mu$ g/ml DOX. Newly synthesised GzmB labelled by (\*). (C, D) Immunoblots showing perforin (PRF1) expression and synthesis in day 5 CTLs treated with (C) 500  $\mu$ g/ml CAM or (D) 10  $\mu$ g/ml DOX. Immature (1), intermediate (2) and mature (3) forms of perforin are labelled. CTLs were stimulated with  $\alpha$ -CD3 (TCR stimulation) or treated with 100 $\mu$ g/ml CHX where indicated. All data representative of three independent biological replicates (3.33  $\mu$ g lysate/sample).

Immunoblot analysis of granzyme B and perforin in WT CTLs revealed a decrease in the mature form of these proteins upon  $\alpha$ -CD3 stimulation (**Figure 4.24 A-D**). This decrease was particularly noticeable in CTLs treated with CHX, in which *de novo* synthesis was precluded. As perforin and granzyme B are secreted during CTL killing, it is likely that the decrease in the mature forms of these proteins was due to secretion triggered by TCR stimulation. Interestingly, mature forms of granzyme B and perforin remained stably expressed in stimulated CAM- and DOX-treated CTLs (**Figure 4.24 A-D**).

To test whether treatment with chloramphenicol and doxycycline could affect the secretion of cytolytic proteins, I measured LAMP1 expression on CTL plasma membrane upon CAM and DOX treatment. LAMP1 abundance on unstimulated CTLs surface was similar in untreated and CAM- or DOX-treated CTLs (**Figure 4.25 A-D**). Upon stimulation, LAMP1 surface expression increased in both untreated and treated CTLs, indicating that chloramphenicol and doxycycline do not terminate the signalling cascade that leads to degranulation. Nonetheless, LAMP1 MFI was reduced in TCR-stimulated CAM- and DOX-treated samples when compared to untreated CTLs. This result suggests that while all CAM- and DOX-treated CTLs were degranulating, the extent to which degranulation occurred was diminished in all treated CTLs. Thus, the failure to detect a decrease in the mature forms of granzyme B and perforin by immunoblot was likely due to impaired secretion of lytic granule content upon CAM and DOX treatment, which further decreased CTL cytolytic potential.

As degranulation is dependent on calcium fluxes induced by TCR stimulation (Lancki et al., 1987; Lyubchenko et al., 2001; Takayama and Sitkovsky, 1987), I asked whether pharmacological inhibition of mitochondrial translation could alter intracellular calcium flux. I used the ratiometric calcium indicator INDO-1 to record intracellular calcium concentration in day 5 unstimulated, TCR-triggered and ionomycin-treated CTLs treated with CAM or DOX. Basal intracellular calcium concentration in unstimulated CTLs was similar in all samples, with a modest decrease in DOX-treated CTLs (**Figure 4.25E**). TCR crosslinking induced a surge in intracellular calcium flux in all samples, with CAM- and DOX-treated CTLs reaching a lower peak compared to untreated CTLs. Notably, the rise in intracellular calcium concentration was sustained for a shorter time in both treated samples compared to untreated CTLs. Analysis of maximal calcium flux in CTLs using the ionophore ionomycin (Lyll et al., 1980) augmented intracellular calcium concentration in all CTL samples. However, while untreated and CAM-treated CTLs reached the same maximal peak, the increase in intracellular calcium concentration was diminished in DOX-treated CTLs. These results indicated that CAM and DOX-treated CTLs could not sustain the rise in intracellular calcium concentration

upon TCR triggering, potentially providing a mechanism for the reduced degranulation observed in treated CTLs.

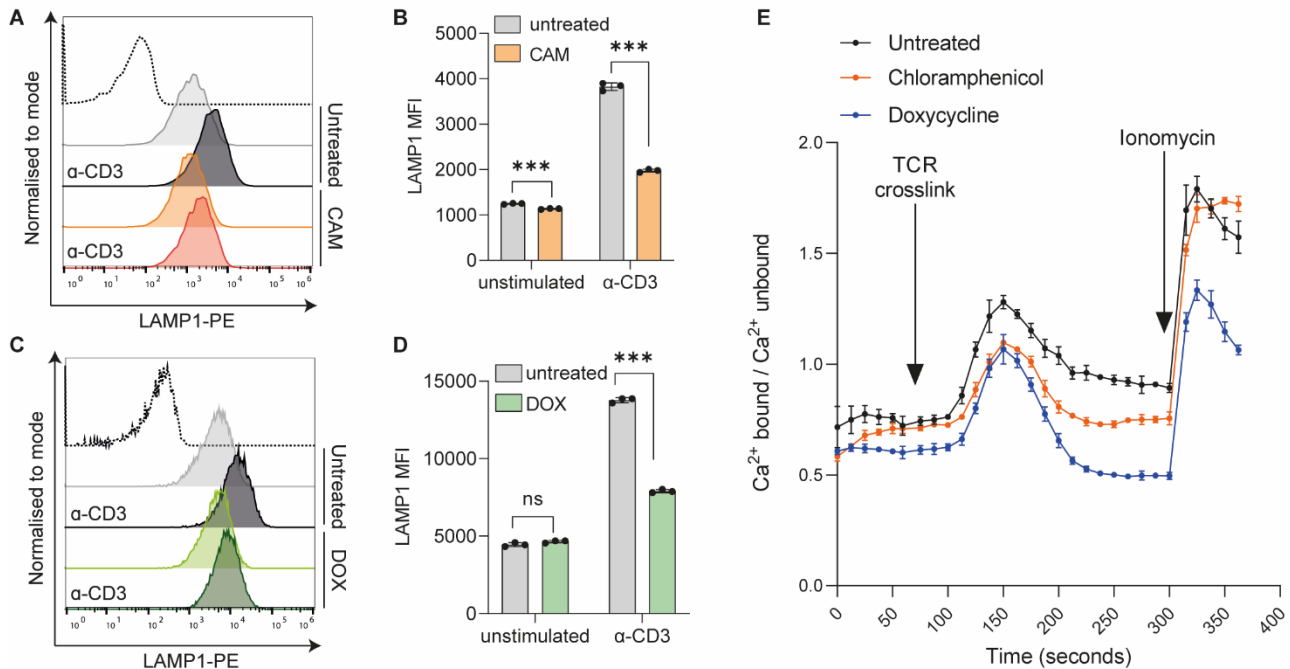


**Figure 4.25. CAM and DOX reduce degranulation and intracellular calcium flux upon TCR triggering.**

(A) Histograms representing surface LAMP1 fluorescence intensity in day 5 WT CTLs treated with 500  $\mu$ g/ml chloramphenicol (CAM) before and after TCR stimulation ( $2 \times 10^5$  CTLs/sample). (B) LAMP1 MFI in unstimulated and stimulated CAM-treated CTLs (500  $\mu$ g/ml). (C) Histograms representing surface LAMP1 fluorescence intensity in day 5 WT CTLs treated with 10  $\mu$ g/ml doxycycline (DOX) before and after TCR stimulation ( $2 \times 10^5$  CTLs/sample). (D) LAMP1 MFI in unstimulated and stimulated DOX-treated CTLs (10  $\mu$ g/ml). (E) INDO-1 calcium assay showing changes in intracellular calcium concentration in  $10^6$  CTLs before ( $t=0-60$ s) and after TCR crosslinking ( $t=60$ s) or ionomycin addition ( $t=300$ s). CTLs were treated with 500  $\mu$ g/ml chloramphenicol or 10  $\mu$ g/ml doxycycline. All error bars indicate average  $\pm$ SD of technical replicates in one representative experiment. \*\*\*= $p < 0.001$ , ns=not significant (two-tailed unpaired Student's t-test). Data representative of three independent biological replicates.

#### 4.9 Mass spectrometry of doxycycline-treated CTLs

To further characterise the effects of acute inhibition of mitochondrial protein synthesis, we examined the proteome of day 5 CTLs treated with doxycycline for 4.5h. CTLs were either left unstimulated or stimulated with  $\alpha$ -CD3 for the whole duration of the DOX treatment.

A total of 605 proteins were significantly downregulated in unstimulated DOX-treated CTLs ( $FDR < 10\%$ ) (**Figure 4.26A**). 23% were mitochondrial proteins, involved in mitochondrial translation (CHCHD1, HARS2, IARS2, MRPS18A, MRPS28, MRPL18, MRPL44, MRPL51, MRPL57,

MRPL58), mitochondrial RNA metabolism (PNPT1, SLIRP, SUPV3L1) and oxidative phosphorylation (ATP5F1A, ATP5F1B, ATP5PB, ATP5PO, ATP5PD, APT5MF, MTATP6, NDUFS6, NDUFB6, NDUFV2, NDUFS2, NDUFA9, NUBPL, COQ3, COQ8B, COQ9, SDHB). Mitochondrial metabolic processes were also affected by doxycycline treatment, as indicated by the downregulation of enzymes regulating the TCA cycle (PDHA1, PDHB, DLAT, DLD, SUCLA2, SDHB, SUCLG2, IDH3A) and redox homeostasis (TXN2, PRDX3, GSR). The abundance of some peroxisomal proteins (ABCD3, CAT) was also reduced, potentially suggesting that inhibition of mitochondrial translation could affect peroxisomes.

Interestingly, DOX induced the downregulation of several proteins involved in cytokine signalling cascades. These included the cytokine IL-3, the receptors CCR7, IL12RB1 and CD27, the metalloproteinase ADAM17 and the TNF $\alpha$  signalling mediators FADD and RIPK1. The kinase JAK1 and the IKK regulatory subunit IKBKG were also downregulated. IKBKG is involved in the degradation of I $\kappa$ B, an inhibitor of the NF $\kappa$ B transcription factor, which is involved in T cell signalling (Cantrell, 2015). Furthermore, DOX treatment reduced the expression of proteins involved in cytosolic translation, such as the eukaryotic translation initiation factors EIF2B3, EIF4B and EIF1AX, the tRNA ligases GARS1 and HARS1, and the serine/threonine kinase mTOR, a master regulator of cytosolic translation, metabolism and T cell proliferation (Saxton and Sabatini, 2017). Taken together, these results indicate that DOX treatment could affect cytokine signalling as well as mediators of cytosolic translation.

4 proteins were significantly upregulated (FDR<10%) by doxycycline treatment in unstimulated CTLs. Two of them were proteins associated with DNA-damage response and apoptosis (RAD17, MTCH1), suggesting a loss of homeostasis upon acute DOX treatment. In addition, doxycycline upregulated the expression of ARID5A, a DNA- and RNA-binding protein which stabilises the mRNA of IL-6, IL-16, STAT3 and T-BET (Nyati et al., 2020). DOX-treated CTLs also upregulated the expression of CMTM6, a transmembrane protein involved in the inhibition of T cell function by promoting the stabilisation of the PD-1 ligand PD-L1 on the plasma membrane (Mezzadra et al., 2017).

Next, I analysed how doxycycline treatment affects the proteome of day 5 TCR-triggered CTLs. 34 proteins were significantly downregulated (FDR<10%) when stimulated with  $\alpha$ -CD3 in the presence of doxycycline (**Figure 4.26B**). 29% were mitochondrial proteins, playing a role in mitochondrial DNA damage response (POLDIP2), mitochondrial protein synthesis by tRNA activity (YARS2), lipid metabolism (TAMM41), phosphate import into the mitochondria (SLC25A3), glycerol

metabolism (GPD2), oxidative phosphorylation (COQ9, MTDN3), modulation of mitochondrial reactive oxygen species (TXN2, ROMO1) and apoptosis (MCL1).

Several receptors on the T cell plasma membrane were specifically downregulated by DOX treatment in TCR-activated CTLs. These were TCB2, LY6E, SLAMF1, SLAMF7, CD27, LILRB4 and TNFRSF4. In addition, the transcription factors NR4A3, KLF13, EGR2 and the transcription-related protein NAB2, the NF $\kappa$ B inhibitor NFKBID and the cytokine IFN $\gamma$  were also downregulated by DOX in TCR-triggered CTLs. Altogether, these results suggested that DOX treatment likely altered CTL signalling upon TCR stimulation.

4 proteins were significantly upregulated in DOX-treated, TCR-stimulated CTLs. These proteins were involved in galactose metabolism (GALM), vitamin B6 metabolism (PLPBP), trafficking and cell division (EXOC5). Notably, PRKAR1A, a regulatory subunit of protein kinase A, which inhibits early events in the TCR signalling cascade such as phosphorylation of LCK and FYN (Vang et al., 2001), was also upregulated by DOX treatment in TCR-triggered CTLs.

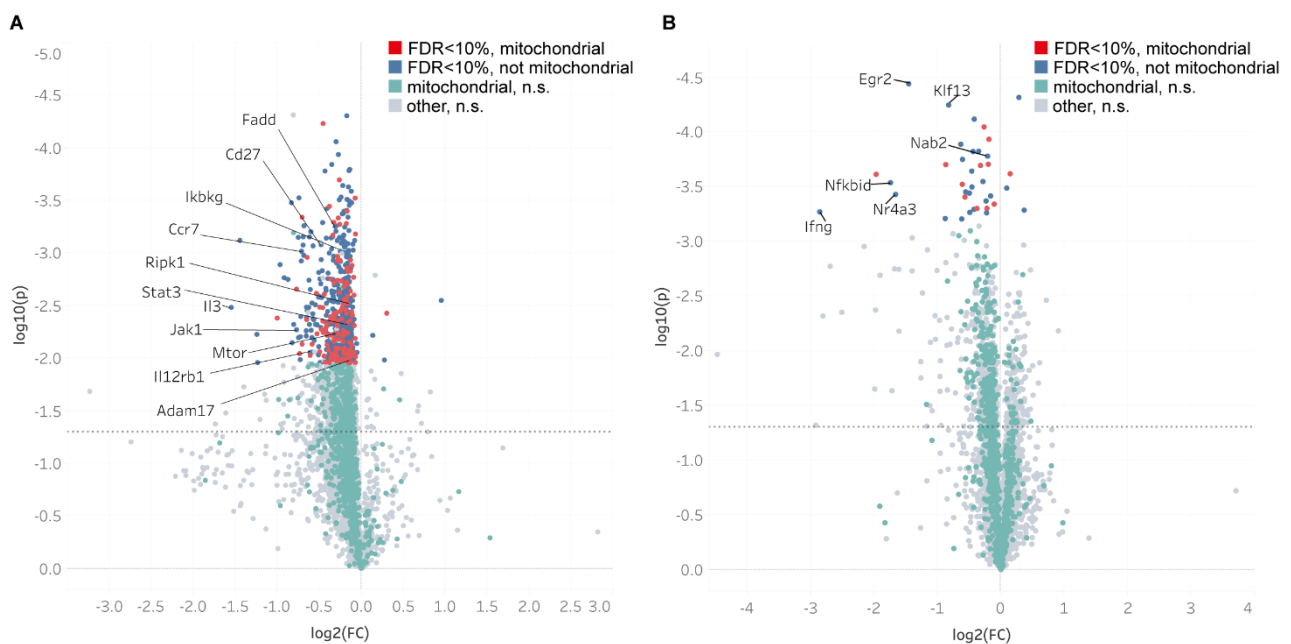


**Figure 4.26. Mass spectrometry analysis of unstimulated and TCR-triggered DOX-treated CTLs.**

(A, B) Volcano plots of upregulated (right quadrant) and downregulated (left quadrant) proteins in (A) unstimulated and (B) TCR-triggered day 5 CTLs treated with 10  $\mu$ g/ml doxycycline compared to untreated CTLs (1.5  $\mu$ g protein/sample). Horizontal bars correspond to the uncorrected  $p=0.05$  threshold. Coloured dots show hits within the 5% and 10% false discovery rate (FDR) range and GOCC-defined mitochondrial proteins. Downregulated proteins are labelled by gene names in (B). Data representative of 4 independent biological replicates. Julia M. Marchingo oversaw sample processing and conducted the initial peptide analysis and protein copy number quantification.

#### 4.10 Additive effect of doxycycline and chloramphenicol on USP30-depleted CTLs

Doxycycline and chloramphenicol treatment further inhibited mitochondrial protein synthesis in the remaining functional mitochondria in *Usp30*<sup>-/-</sup> CTLs (**Figure 4.21**). This result prompted the analysis of CTL effector functions in USP30-deficient samples upon CAM and DOX treatment. Specifically, I asked whether further depletion of mitochondrial translation in *Usp30*<sup>-/-</sup> CTLs would result in an additive effect on killing capacity, cytosolic protein synthesis, and cytokine production.

First, I tested whether CAM and DOX treatment could have an additive effect on *Usp30*<sup>-/-</sup> cytotoxicity. I co-incubated day 5 WT and *Usp30*<sup>-/-</sup> CTLs with target cells in standard CTL culture media, or in media supplemented with either 10 µg/ml doxycycline or 500 µg/ml chloramphenicol (**Figure 4.27**). Untreated WT CTLs killed quickly for the first 4h, after which the rate of cytotoxicity slowed down. Complete target cells lysis was achieved after 12h of incubation with untreated WT CTLs. USP30 depletion, CAM and DOX treatment all impaired CTL killing after 4h of incubation, as previously observed (**Figure 4.22**). However, DOX and CAM treatment further reduced the percentage of target cell lysis at 4h for both WT and *Usp30*<sup>-/-</sup> CTLs when compared to their untreated counterparts. DOX treatment on WT and *Usp30*<sup>-/-</sup> CTLs resulted in a similar killing phenotype as in the untreated *Usp30*<sup>-/-</sup> sample. By contrast, while CAM-treated WT CTLs exhibited similar cytotoxicity as untreated *Usp30*<sup>-/-</sup> CTLs, CAM treatment together with USP30 depletion resulted in a further reduction of CTL killing.

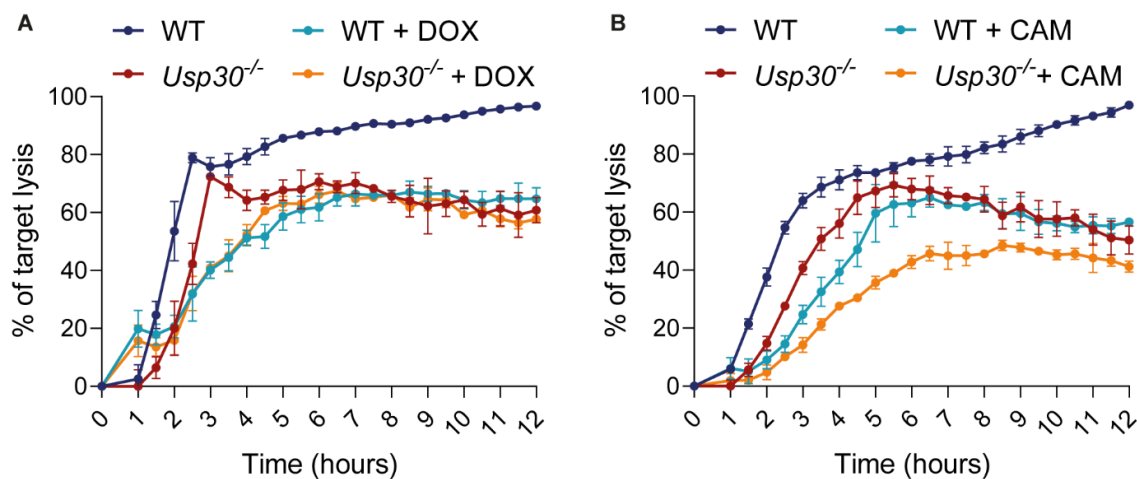


**Figure 4.27. Cytotoxicity of *Usp30*<sup>-/-</sup> treated with CAM and DOX CTLs.**

(A, B) Long-term (12h) killing assays (CTL:target ratio, 1:1) displaying percentage target lysis with day 5 WT and *Usp30*<sup>-/-</sup> CTLs treated with (A) 10 µg/ml doxycycline (DOX) or (B) 500 µg/ml chloramphenicol (CAM). Error bars indicate average  $\pm$ SD of technical replicates within one representative experiment ( $4 \times 10^4$  targets and  $4 \times 10^4$  CTLs/sample). Data representative of at least three independent biological replicates.

Next, I treated day 5 WT and *Usp30*<sup>-/-</sup> CTLs with either 10 µg/ml doxycycline or 500 µg/ml chloramphenicol while incubating them with HPG to measure cytosolic protein synthesis by flow cytometry. As previously described (**Figure 4.23**), inhibition of mitochondrial translation in WT CTLs diminished HPG incorporation, although not to the extent observed in USP30-depleted CTLs (**Figure 4.28A, B**). Treating *Usp30*<sup>-/-</sup> CTLs with either chloramphenicol or doxycycline did not substantially affect HPG incorporation. TCR stimulation partially rescued the effects of doxycycline and chloramphenicol treatment on WT CTLs, while no reproducible effect on HPG incorporation could be observed in DOX- and CAM-treated *Usp30*<sup>-/-</sup> CTLs after TCR triggering. These results indicated that neither CAM or DOX could further hinder cytosolic protein synthesis in *Usp30*<sup>-/-</sup> CTLs as detected by HPG incorporation.

The mass spectrometry analysis of DOX-treated CTLs highlighted the downregulation of several cytokine-related proteins (**Figure 4.26**). Therefore, I asked whether treating *Usp30*<sup>-/-</sup> CTLs with CAM or DOX would further decrease cytokine synthesis upon TCR stimulation. Day 5 WT and *Usp30*<sup>-/-</sup> CTLs were stimulated on α-CD3 for 4.5h either in standard CTL media, or in media supplemented with either 10 µg/ml doxycycline or 500 µg/ml chloramphenicol. TNFα and IFNγ expression was analysed intracellularly by flow cytometry. As previously observed (**Figure 3.19**), cytokine production was downregulated in USP30-depleted CTLs compared to WT (**Figure 4.28 C-F**). Chloramphenicol and doxycycline markedly blunted cytokine synthesis in WT CTLs, in agreement with the mass spectrometry data. Interestingly, DOX and CAM treatment in *Usp30*<sup>-/-</sup> CTLs induced a further reduction in TNFα and IFNγ synthesis, matching cytokine expression in CAM- and DOX-treated WT CTLs. These results suggested that acute pharmacological inhibition of the remaining mitochondrial translation in *Usp30*<sup>-/-</sup> CTLs can have a significant additive effect on cytokine synthesis.

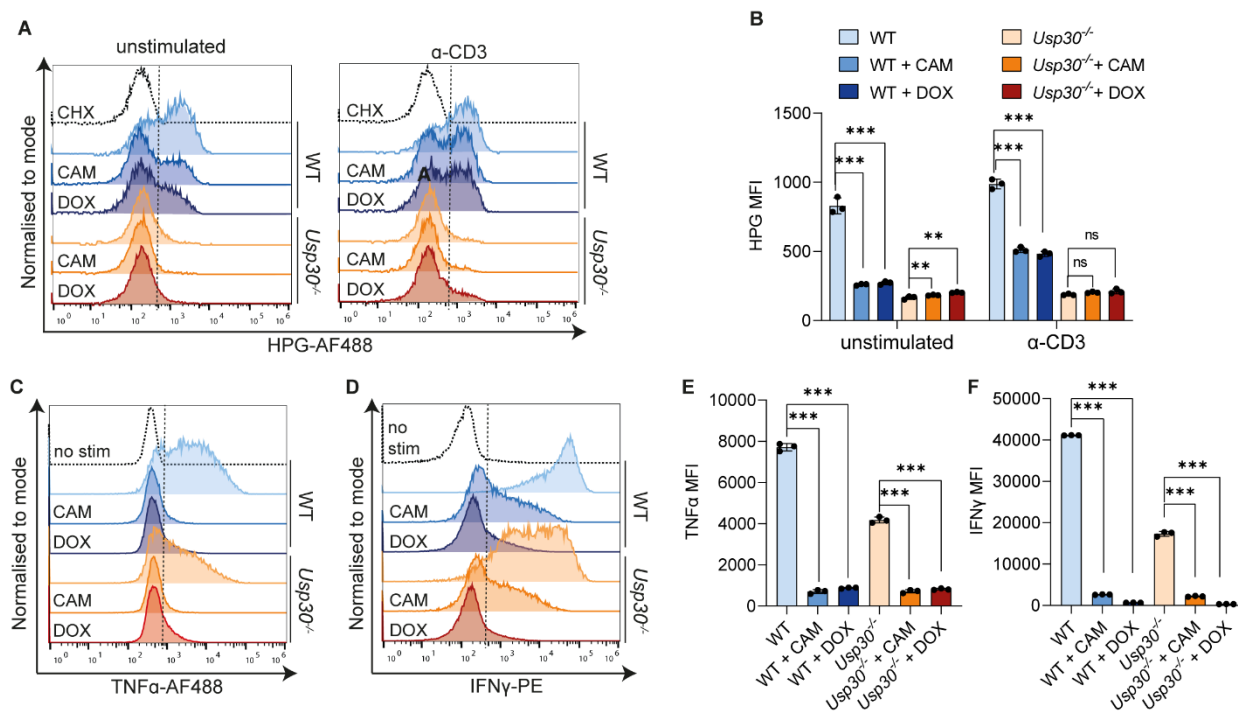


**Figure 4.28. CAM and DOX decrease cytokine synthesis in *Usp30*<sup>-/-</sup> CTLs.**

(A) HPG incorporation into day 5 WT and *Usp30*<sup>-/-</sup> CTLs treated for 1h with 500  $\mu$ g/ml CAM or 10  $\mu$ g/ml DOX to inhibit mitochondrial translation. CTLs were either unstimulated (left) or stimulated with  $\alpha$ -CD3 (right). Control samples were treated with 100 $\mu$ g/ml CHX to inhibit cytosolic translation. (B) Quantitation of HPG MFI shown in (A). (C, D) Intracellular cytokine staining for (C) TNF $\alpha$  and (D) IFN $\gamma$  in day 5  $\alpha$ -CD3-stimulated WT and *Usp30*<sup>-/-</sup> CTLs treated with 10  $\mu$ g/ml DOX or 500  $\mu$ g/ml CAM as indicated. Control sample shows cytokine expression in unstimulated day 5 WT CTLs. (E, F) Quantitation of (E) TNF $\alpha$  and (F) IFN $\gamma$  MFI. All error bars display average  $\pm$ SD of technical replicates within one representative experiment ( $2 \times 10^5$  CTLs/sample). \*\*\*= $p < 0.001$ , \*\*= $p < 0.01$ , ns=not significant (two-tailed unpaired Student's t-test). Data representative of three independent biological

#### 4.11 Comparison of DOX-treated and USP30-depleted CTL proteomes

The mass spectrometry datasets obtained during the course of this work allowed the comparison of CTL proteomes upon DOX treatment and USP30 depletion.

First, I compared protein expression in unstimulated CTLs. While no statistically significant (FDR<10%) protein was found to be upregulated in both *Usp30*<sup>-/-</sup> and DOX-treated unstimulated CTLs, 118 proteins were significantly downregulated (FDR<10%) by both USP30 depletion and DOX treatment (**Figure 4.29A**). Among the most overrepresented protein classes in these datasets I found proteins involved in mitochondrial translation (MRPS6, MRPS18A, MRPS18B, MRPS35,

MRPL16, MRPL20, MRPL38, MRPL51, MRPL53, MRPL58), mitochondrial transport (RHOT1), mitochondrial inner membrane organisation (CHCHD3, OXA1L) and mitochondrial transmembrane transport (SLC25A12, SLC25A5, SLC25A4, SLC25A30, MCAT).

Oxidative phosphorylation was downregulated in both datasets (NDUF6, NDUFV2, MTND3, SDHB, ATP5AF2, ATP5MF, ATP5PD), together with cholesterol transport and biosynthesis (HMGCS1, NPC2, CAT, LDLR, DHCR24, DHCR7, SQLE, SCP2, ACAT2, APOB), fatty acid oxidation (ACAT2, DEGS1, ACOT8, MCAT, ACSS2, ACADSB, ACOT2, SCP2), succinate metabolism (SDHB, SUCLG1, SUCLG2) and acetyl-CoA metabolism (ACOT2, ACOT8, ACOT9, HMGCS1, ACSA, ACADSB, ACSS2, SCP2, SUCLG1, SUCLG2). Overall, 64% of statistically significant proteins (FDR<10%) downregulated by both USP30 depletion and DOX treatment were classified by GO enrichment analysis as proteins related to cellular metabolism.

Furthermore, the CD3 $\epsilon$  subunit of the T cell receptor and the cytokine-regulating transcription factor ETS1 (Russell and Garrett-Sinha, 2010) showed reduced expression in both DOX-treated and *Usp30*<sup>-/-</sup> CTLs. ETS1 downregulation was more pronounced after doxycycline treatment, potentially providing a rationale for the enhanced reduction in cytokine synthesis observed in DOX-treated samples (**Figure 4.28 C-F**). While the expression of a few cytokines (TNF $\alpha$ , IL-10, XCL1, LT $\alpha$ ) and cytokine receptors (IL4R, IL2RB, CXCR4) was decreased in both USP30-depleted and DOX-treated unstimulated CTLs (**Figure 4.29B**), this effect was not statistically significant in both datasets.

Next, I compared the proteome of TCR-stimulated *Usp30*<sup>-/-</sup> and DOX-treated CTLs (**Figure 4.29C**). As in the unstimulated datasets, no protein was significantly upregulated (FDR<10%) by both DOX treatment and USP30 depletion. 12 proteins were significantly downregulated in both TCR-triggered datasets. Most of them were mitochondrial proteins (SLC25A3, GPD2, YARS2, TAMM41, POLDIP2, COQ9, MTND3, ROMO1, TXN2). LPCAT4, an ER-resident protein involved in phospholipid metabolism (Ye et al., 2005) was also downregulated upon TCR stimulation in both USP30-depleted and DOX-treated CTLs. Furthermore, the cytokine IFN $\gamma$  and plasma membrane receptor SLAMF7, which promotes the expression of exhaustion markers (O'Connell et al., 2021) were also reduced in TCR-triggered *Usp30*<sup>-/-</sup> and DOX-treated CTLs.

As in the unstimulated datasets, several cytokines and chemokines (IL-10, IL-3, LT $\alpha$ , LIF, CCL4, XCL1, TNFSF9, SPP1 and CSF2) together with the cytokine receptor IL4R appeared downregulated by both USP30 depletion and DOX treatment in TCR-triggered CTLs (**Figure 4.29D**). However, these changes in expression were not found to be statistically significant (FDR<10%) in both datasets.

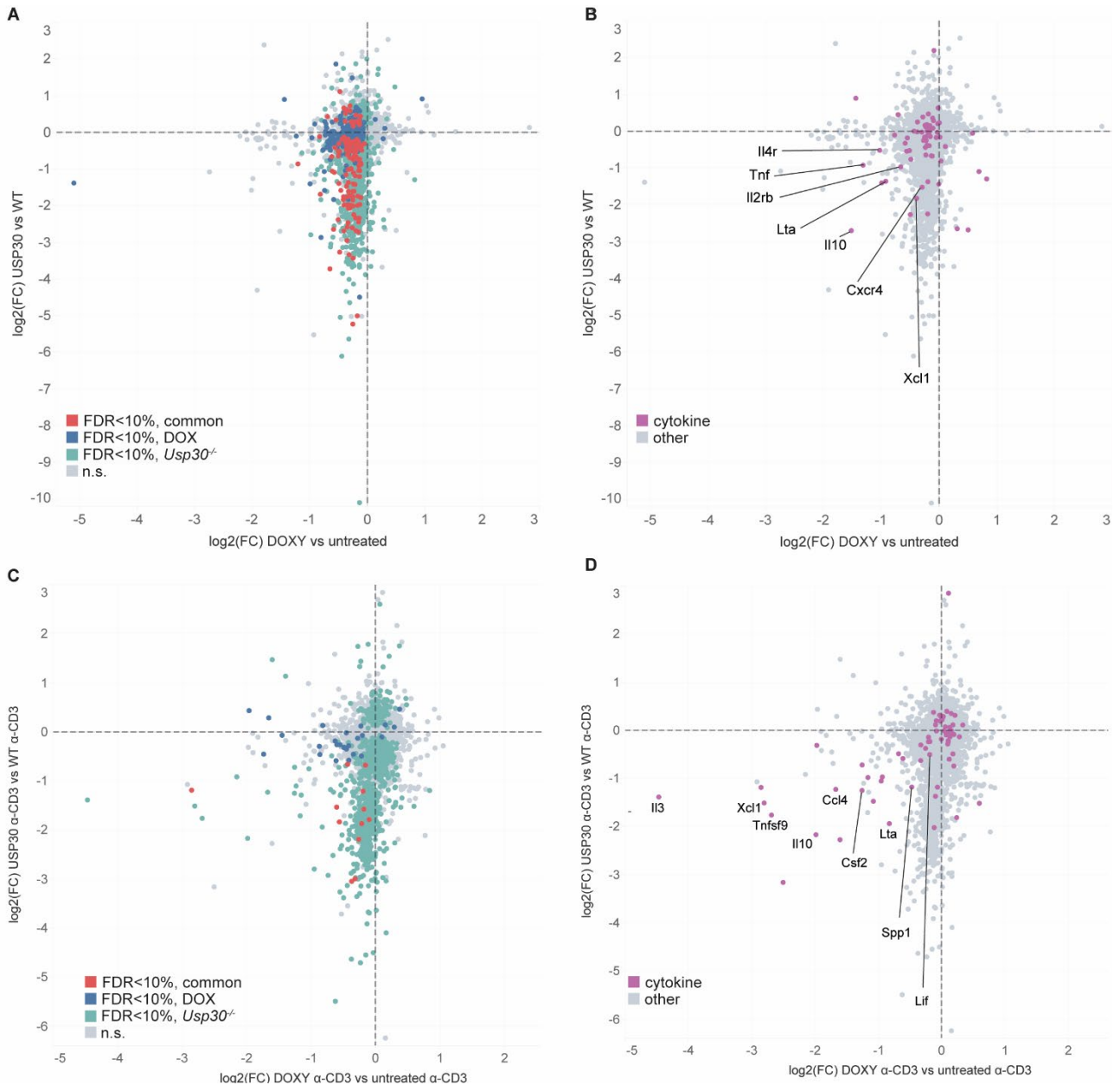


**Figure 4.29. Comparison of proteomic changes in DOX-treated and USP30-depleted CTLs.**

(A-D) Proteomes of day 5 CTLs from *Usps30*<sup>-/-</sup> CTLs compared with WT CTLs, and DOX-treated CTLs (10  $\mu\text{g}/\text{ml}$ ) in which mitochondrial protein synthesis was inhibited compared with untreated CTLs. Plots show mass spectrometry of (A, B) unstimulated and (C, D)  $\alpha$ -CD3-stimulated CTLs. Dashed lines correspond to  $\log_2(\text{FC})=0$ . Coloured dots in (A, C) indicate proteins within the 10% false discovery rate (FDR) in the *Usps30*<sup>-/-</sup> vs WT dataset (green) and in the DOX vs untreated dataset (blue). Red-labelled dots indicate proteins within the 10% FDR common to both datasets. Cytokines are highlighted in magenta in (B, D). n.s.=not significant. Data representative of 4 independent biological replicates (*Usps30*<sup>-/-</sup>: 2  $\mu\text{g}$  protein/sample; DOX: 1.5  $\mu\text{g}/\text{sample}$ ). Julia M. Marchingo oversaw the processing of mass spectrometry samples and conducted the initial peptide analysis and protein copy number quantification.

## 4.12 Summary

In this Chapter I aimed to modulate the expression of peroxisomal and mitochondrial proteins to assess whether the defects observed in *Usp30*<sup>-/-</sup> CTLs could be ascribed to the loss of a specific cellular function, rather than to a general loss of peroxisomes and mitochondria. During the course of this analysis I found a requirement for mitochondrial translation in CTL cytotoxicity. Inhibiting mitochondrial protein synthesis with chloramphenicol or doxycycline reduced killing and cytosolic translation and hindered the synthesis of perforin, granzyme B, TNF $\alpha$  and IFN $\gamma$  in stimulated CTLs. These results indicated that mitochondrial protein synthesis is required to sustain CTL killing.

Interestingly, calcium flux was differentially affected by chloramphenicol and doxycycline, potentially highlighting differences in the mode of action of these two pharmacological treatments. Furthermore, while USP30 depletion increased calcium flux in CTLs, DOX and CAM supplementation reduced intracellular calcium concentration. These results could be due to different effects caused by the removal of mitochondria (USP30 deletion) compared to the selective inhibition of mitochondrial translation (CAM, DOX), or they could indicate a difference between the downstream effect of chronic (*Usp30*<sup>-/-</sup>) versus acute (CAM, DOX) depletion of mitochondrial protein synthesis. Chloramphenicol and doxycycline treatment in *Usp30*<sup>-/-</sup> CTLs revealed a moderate additive effect on CTL killing and a substantial additive effect on cytokine synthesis. While this is likely to be caused by further inhibition of the remaining mitochondrial translation in *Usp30*<sup>-/-</sup> CTLs, additional effects of CAM and DOX cannot be excluded at this stage, especially after considering the downregulation of cytokine-related proteins observed by mass spectrometry in DOX-treated CTLs.

Finally, it is important to note that triggering peroxisomal defects (*Far1*<sup>-/-</sup> mouse) could have a downstream effect on mitochondria, and vice versa, pharmacological inhibition of mitochondrial function (DOX) could also affect peroxisomal protein expression. These results support previous observations in mouse models and human diseases (Baes and Van Veldhoven, 2012; Goldfischer et al., 1973) highlighting a complex interplay between peroxisomes and mitochondria.



## **CHAPTER 5**

### **Evaluation of mechanisms determining the inhibition of cytosolic protein synthesis and cytotoxicity in *Usp30*<sup>-/-</sup> CTL**



## 5.1 Background

Lack of USP30 resulted in loss in mitochondrial mass and function (**Figure 3.3-7**) but also in a decrease in cytosolic protein synthesis (**Figure 3.16B, C**). *De novo* protein synthesis was required for sustained CTL killing, and USP30 depletion prevented the replenishment of key cytolytic proteins, thus inhibiting cytotoxicity (**Figure 3.17**). Notably, impairing mitochondrial translation with chloramphenicol or doxycycline was sufficient to diminish cytosolic protein synthesis (**Figure 4.23**), resulting in reduced expression of cytolytic proteins upon TCR stimulation (**Figure 4.24**).

Given the importance of *de novo* protein synthesis in sustaining CTL killing, I aimed to examine how mitochondrial defects resulted in compromised cytosolic translation. Mitochondrial dysfunction can be communicated to the cytosol in several ways, including via lack of mitochondrial protein import, production of mitochondrial reactive oxygen species and activation of the integrated stress response, all of which can result in a decrease in cytosolic protein synthesis (Boos et al., 2020; Topf et al., 2019). It is currently unknown whether mitochondrial defects can trigger any of these responses in CTLs. To address this question, I tested whether potential pathways known to link mitochondrial homeostasis and cytosolic translation were altered in *Usp30*<sup>-/-</sup> CTLs.

## 5.2 Measurement of mitochondrial reactive oxygen species in *Usp30*<sup>-/-</sup> CTLs

Mitochondrial oxygen consumption results in the generation of mtROS, involved in naïve T cell activation (Fischer et al., 2018; Sena et al., 2013) as well as TCR signalling in mature CTLs (Devadas et al., 2002). However, mtROS generation in T cells can also be detrimental. Exhausted T cells, which exhibit both loss of cytolytic capacity and disrupted mitochondrial morphology, experience aberrant mtROS production, which further exacerbates cellular dysfunction (Scharping et al., 2021; Yu et al., 2020). Within the context of cytosolic translation, aberrant mtROS release can change the oxidation state of ribosomal proteins, inhibiting protein synthesis (Topf et al., 2018). Notably, mtROS have recently been indicated to hinder translation in CTLs by inducing tRNA fragmentation (Yue et al., 2021).

*Usp30*<sup>-/-</sup> CTLs showed loss of mitochondrial mass and disorganised cristae in the remaining mitochondrial structures, suggesting disruption of the ETC (**Figure 3.5**). This hypothesis was confirmed by measurement of mitochondrial membrane potential and OXPHOS, which were both decreased in *Usp30*<sup>-/-</sup> CTLs (**Figure 3.3A, B**; **Figure 3.6A**). As inhibition of ETC complexes can result in mtROS release (Murphy, 2009), I examined whether the remaining mitochondria in *Usp30*<sup>-/-</sup>

<sup>-/-</sup> CTLs were sites of mtROS production as a potential mechanism for the reduction in cytosolic protein synthesis observed in USP30-depleted CTLs.

I used the live cell superoxide indicator MitoSOX Red to quantify mtROS in day 5 WT and *Usp30*<sup>-/-</sup> CTLs. This probe is actively sequestered by mitochondria, and it exhibits fluorescence upon mtROS-mediated oxidation when excited at 510 nm. MitoSOX signal was barely detectable above the unstained control in WT CTLs, suggesting low levels of mtROS (**Figure 5.1**). Antimycin A was used to inhibit complex III of the ETC (Potter and Reif, 1952) and induce mtROS generation. The increase in MitoSOX fluorescence in antimycin A-treated WT CTLs confirmed that MitoSOX could respond to a surge in mtROS. By contrast, MitoSOX signal in *Usp30*<sup>-/-</sup> CTLs was lower than in WT, and antimycin A treatment led to a barely detectable upregulation of mtROS production.

While these results could suggest that the remaining mitochondria in *Usp30*<sup>-/-</sup> CTLs were not a source of aberrant mtROS release, it is important to note that MitoSOX fluorescence also depends on nucleic acid binding, as indicated by the manufacturer. mtDNA abundance was not measured in *Usp30*<sup>-/-</sup> CTLs. However, given the depletion of mitochondria caused by loss of USP30, the amount of mtDNA in *Usp30*<sup>-/-</sup> CTLs was likely to be lower than in WT. Therefore, scarcity of mtDNA might provide an alternative explanation for the low MitoSOX signal in untreated and antimycin A-treated *Usp30*<sup>-/-</sup> CTLs, as it could prevent MitoSOX binding and fluorescence independently from mtROS production.

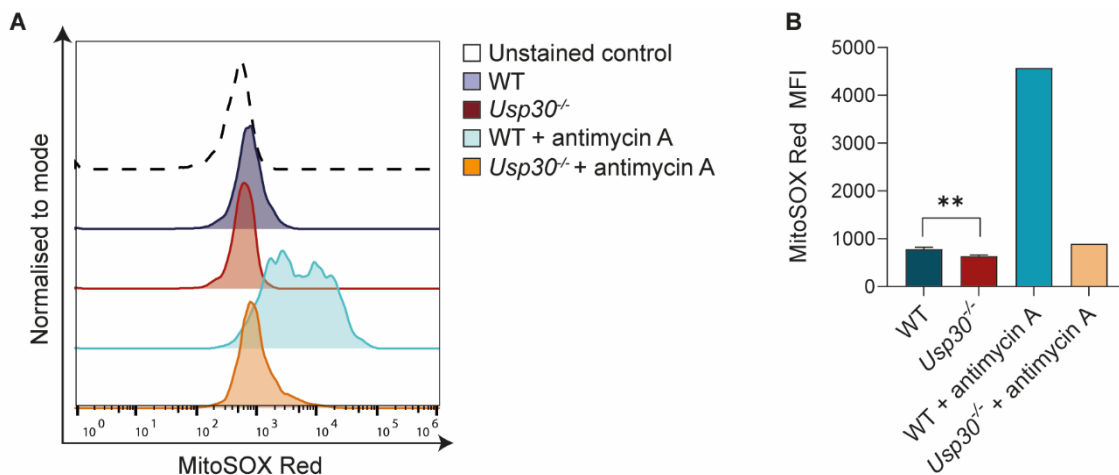


**Figure 5.1. *Usp30*<sup>-/-</sup> CTLs show low MitoSOX fluorescence and are insensitive to antimycin A treatment.**

(A) Flow cytometry analysis of MitoSOX Red in day 5 WT and *Usp30*<sup>-/-</sup> CTLs, treated with 10 $\mu$ M antimycin A where indicated. 5 $\times$ 10<sup>5</sup> CTLs were analysed per sample. (B) Quantitation of MitoSOX Red MFI in day 5 WT and *Usp30*<sup>-/-</sup> CTLs. Error bars show average  $\pm$ SD of technical replicates. \*\*= $p$ <0.01 (two-tailed unpaired Student's  $t$ -test). Data representative of two biological replicates.

### 5.3 Examination of mTOR signalling in USP30-depleted CTLs

mTOR is a serine/threonine protein kinase acting as a nexus coordinating nutrient availability, cell growth and catabolism (Saxton and Sabatini, 2017). mTOR can regulate cytosolic protein synthesis by a number of independent mechanisms that rely on the phosphorylation of the ribosomal S6 kinases (S6K1/2) and the eIF4E binding proteins (4EBP1/2) (Saxton and Sabatini, 2017). In addition to the ribosomal protein S6, S6K phosphorylates the eukaryotic initiation factors eIF4B and eIF3, promoting the assembly of the translation initiation complex (Holz et al., 2005). Moreover, S6K can phosphorylate PDCD4, a translational repressor that inhibits formation of the initiation complex by sequestering eIF4A (Loh et al., 2009). Phosphorylated PDCD4 is targeted for degradation, resulting in enhanced cytosolic protein synthesis (Dorrello et al., 2006). Furthermore, the mTOR target 4EBP can also act as a translational repressor by binding eIF4E and preventing its association with eIF4G (Haghighat et al., 1995). 4EBP phosphorylation allows for eIF4E release, which relieves translational repression (Pause et al., 1994).

TCR stimulation triggers mTOR signalling in both naïve CD8<sup>+</sup> T cells and CTLs. mTOR promotes proliferation in newly activated naïve CD8<sup>+</sup> T cells by inducing the expression of enzymes and transporters involved in glycolysis, fatty acid and sterol metabolism, as well as ribosomal and mitochondrial proteins (D'Souza et al., 2007; Howden et al., 2019). In activated CTLs, mTOR sustains granzyme B, perforin, TNF $\alpha$  and IFN $\gamma$  protein expression, while inhibition of mTOR upregulates CD62L (Hukelmann et al., 2016). Notably, granzyme B, perforin and cytokine synthesis were decreased in *Usp30*<sup>-/-</sup> CTLs (**Figure 3.15, 3.17-19**), while CD62L expression was increased (**Figure 3.2 F-I**). Given the well-described role for mTOR in cytosolic translation, I examined whether mTOR signalling was altered in USP30-depleted CTLs.

Mass cytometry analysis indicated that S6 phosphorylation was unperturbed in TCR-stimulated *Usp30*<sup>-/-</sup> CTLs (**Figure 3.12I, Figure 5.2A**). I further examined mTOR signalling by assessing the abundance and phosphorylation of S6 and 4EBP1 in unstimulated and TCR-triggered WT and *Usp30*<sup>-/-</sup> CTLs. Total and phosphorylated 4EBP1 were upregulated in unstimulated *Usp30*<sup>-/-</sup> CTLs (**Figure 5.2B**), while S6 expression and phosphorylation were unaffected (**Figure 5.2C**). Variability in total S6 abundance was not reproducible across biological replicates. TCR stimulation induced phosphorylation of S6 in both WT and *Usp30*<sup>-/-</sup> CTLs (**Figure 5.2C**), which was consistent with the mass cytometry results (**Figure 3.12I, Figure 5.2A**). By contrast, total and phosphorylated 4EBP1 were downregulated in TCR-triggered *Usp30*<sup>-/-</sup> CTLs (**Figure 5.2C**). Although 4EBP1 dephosphorylation is usually associated with inhibition of protein synthesis, the decrease in total 4EBP1 abundance suggested that lower levels of phospho-4EBP1 were due to a reduction in 4EBP1

expression rather than to specific alterations in 4EBP1 phosphorylation. 4EBP1 expression and phosphorylation were not reproducibly affected by TCR activation in WT CTLs.

The opposite trend in S6 and 4EBP1 phosphorylation was interesting, as phospho-S6 and phospho-4EBP1 both promote translation, and they are also both mTOR targets. I further investigated the nature of this phosphorylation event by treating CTLs with cycloheximide during TCR-mediated stimulation. While S6 was unperturbed in both WT and *Usp30*<sup>-/-</sup> CTLs stimulated in the presence of cycloheximide, the decrease in 4EBP1 expression and phosphorylation was not observed when cytosolic protein translation was inhibited (**Figure 5.2B**). These results indicated that the abundance of total and phosphorylated 4EBP1, but not S6, could be modulated by *de novo* protein synthesis in the context of TCR stimulation.

Lastly, I examined the expression of the translational repressor PDCD4, which is upregulated in CTLs upon mTOR inhibition (Howden et al., 2019). This protein was moderately upregulated in the mass spectrometry of unstimulated *Usp30*<sup>-/-</sup> CTLs. To validate this result, I measured protein abundance by immunoblot. PDCD4 expression was equivalent in day 5 WT and *Usp30*<sup>-/-</sup> CTLs (**Figure 5.2D**), indicating that the reduction in cytosolic protein synthesis observed in USP30-depleted CTLs was not caused by PDCD4 upregulation. Taken together, these results suggested that mTOR was unlikely to hinder cytosolic translation in *Usp30*<sup>-/-</sup> CTLs.

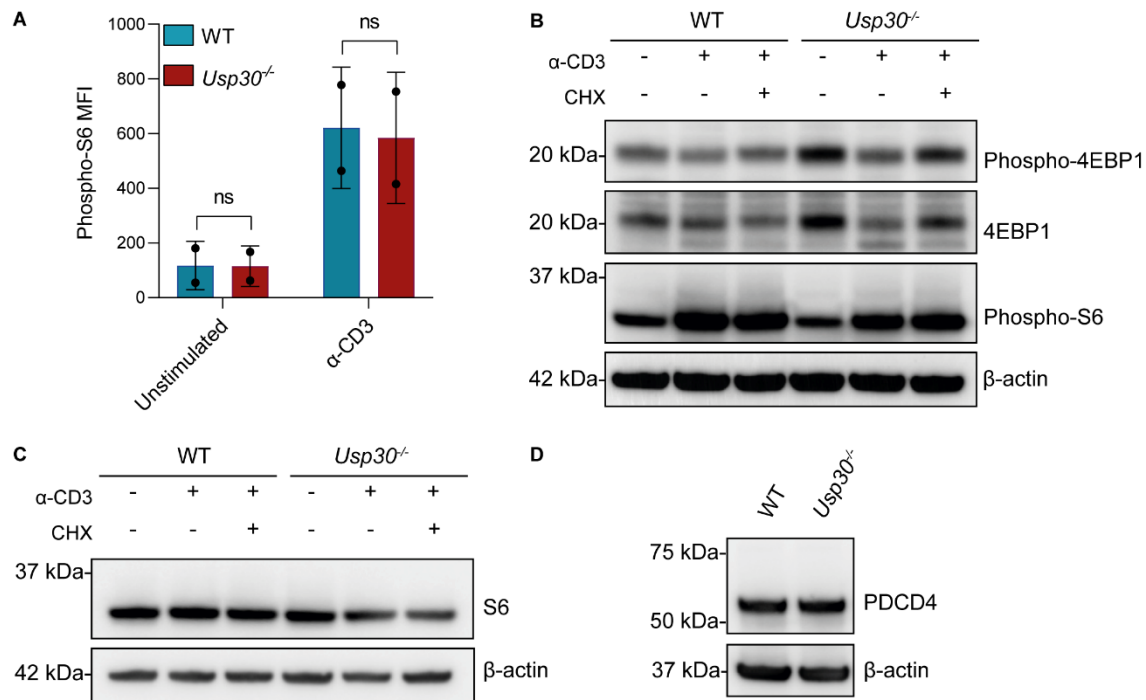


**Figure 5.2. mTOR signalling is unperturbed in WT and *Usp30*<sup>-/-</sup> CTLs.**

(A) Quantitation of phosphorylated S6 detected by mass cytometry in TCR-stimulated ( $\alpha$ -CD3) WT and *Usp30*<sup>-/-</sup> CTLs ( $1.6 \times 10^5$  cells/sample). Error bars indicate average  $\pm$ SD of two biological replicates. ns=not significant (two-tailed paired Student's t-test). (B-D) Immunoblots showing (B) total 4EBP1, phosphorylated 4EBP1, phosphorylated S6, (C) total S6 and (D) total PDCD4 expression in day 5 WT and *Usp30*<sup>-/-</sup> CTLs ( $3.33 \mu\text{g}$  lysate/sample). TCR stimulation ( $\alpha$ -CD3) and  $100 \mu\text{g/ml}$  CHX treatment were added where indicated. Data representative of at least two independent biological replicates.

#### 5.4 The ISR does not cause translation and cytotoxicity defects in *Usp30*<sup>-/-</sup> CTLs

Cellular insults including hypoxia, oxidative and ER stress, amino acid depletion, heme deprivation and viral infection can activate the ISR (Pakos-Zebrucka et al., 2016). The ISR is triggered by four kinases (GCN2, PERK, PRK, HRI) which phosphorylate the  $\alpha$  subunit of the initiation factor eIF2 (eIF2 $\alpha$ ). The GTP-bound form of the eIF2 complex mediates the association between the 40S ribosomal subunit and Met-tRNA<sub>F</sub>, supplying the initiator methionine required for protein synthesis (Safer et al., 1975). eIF2 is then released as a GDP-bound complex, and it is activated again by the GEF eIF2B, which catalyses the regeneration of GTP-bound eIF2 (Siekierka et al., 1982). eIF2 $\alpha$  phosphorylation by the ISR kinases impairs the GEF activity of eIF2B (Siekierka et al., 1982), resulting in inhibition of protein synthesis. Notably, a small subset of proteins displaying short open reading frames in their 5' UTR are preferentially translated upon ISR activation. These

include the ISR master transcription factor ATF4, which ameliorates the response to oxidative stress and upregulates amino acid transport (Harding et al., 2000; Harding et al., 2003).

Several studies have indicated that mitochondrial dysfunction, including inhibition of mitochondrial translation, can lead to downregulation of cytosolic protein synthesis (Boos et al., 2020; Topf et al., 2019). Specifically, the ISR has been suggested to act as a link between mitochondrial stress and cytosolic translation via the kinase HRI (Fessler et al., 2020; Guo et al., 2020) and the transcription factor ATF4 (Molenaars et al., 2020; Quiros et al., 2017). Therefore, I investigated whether the reduction of cytosolic translation in *Usp30*<sup>-/-</sup> CTLs was induced by activation of the ISR.

Mass spectrometry analysis of unstimulated day 5 *Usp30*<sup>-/-</sup> CTLs revealed that out of the 34 significantly upregulated proteins ( $\log_2(\text{FC}) > 1$ ,  $\text{FDR} < 10\%$ ), 11 were known to be associated with the ISR (CA2, AVIL, BCL2L11, CTH, NIBAN1, BBC3, SLC6A9, IFRD1, PLIN2, CEBPB, HMOX1), (**Figure 5.3A**). ATF4 was not detected by mass spectrometry. I used immunoblotting to analyse ATF4 expression in unstimulated day 5 WT and *Usp30*<sup>-/-</sup> CTLs. ATF4 was upregulated in CTLs lacking USP30 (**Figure 5.3B**). Interestingly, chloramphenicol treatment could also trigger an increase in ATF4 expression (**Figure 5.3C**). Taken together, these results suggested that loss of USP30 and mitochondrial translation inhibition could trigger the ISR.

Next, I assessed the expression of total and phosphorylated eIF2 $\alpha$  in day 5 unstimulated and TCR-triggered WT and *Usp30*<sup>-/-</sup> CTLs. Total eIF2 $\alpha$  was equivalent in WT and *Usp30*<sup>-/-</sup> CTLs, regardless of TCR stimulation (**Figure 5.3D**). Phosphorylation of eIF2 $\alpha$  appeared reduced in unstimulated *Usp30*<sup>-/-</sup> CTLs compared to their WT counterparts. TCR stimulation triggered eIF2 $\alpha$  dephosphorylation in the WT, while this effect was less pronounced in USP30-depleted CTLs. Cycloheximide treatment prevented eIF2 $\alpha$  dephosphorylation, indicating that this event depends on *de novo* cytosolic protein synthesis in the context of TCR signalling.

These results were surprising, as eIF2 $\alpha$  phosphorylation is associated with downregulation of cytosolic protein synthesis (Pakos-Zebrucka et al., 2016). However, cytosolic translation was more efficient in WT than in *Usp30*<sup>-/-</sup> CTLs (**Figure 3.16B, C**), suggesting that the higher levels of phospho-eIF2 $\alpha$  were not sufficient to result in translation inhibition. Furthermore, ATF4 upregulation depends on eIF2 $\alpha$  phosphorylation (Harding et al., 2000). However, phospho-eIF2 $\alpha$  was not upregulated in *Usp30*<sup>-/-</sup> CTLs (**Figure 5.3D**), while the expression of ATF4 was increased (**Figure 5.3B**), pointing to an eIF2 $\alpha$ -independent mechanism inducing ATF4 expression.

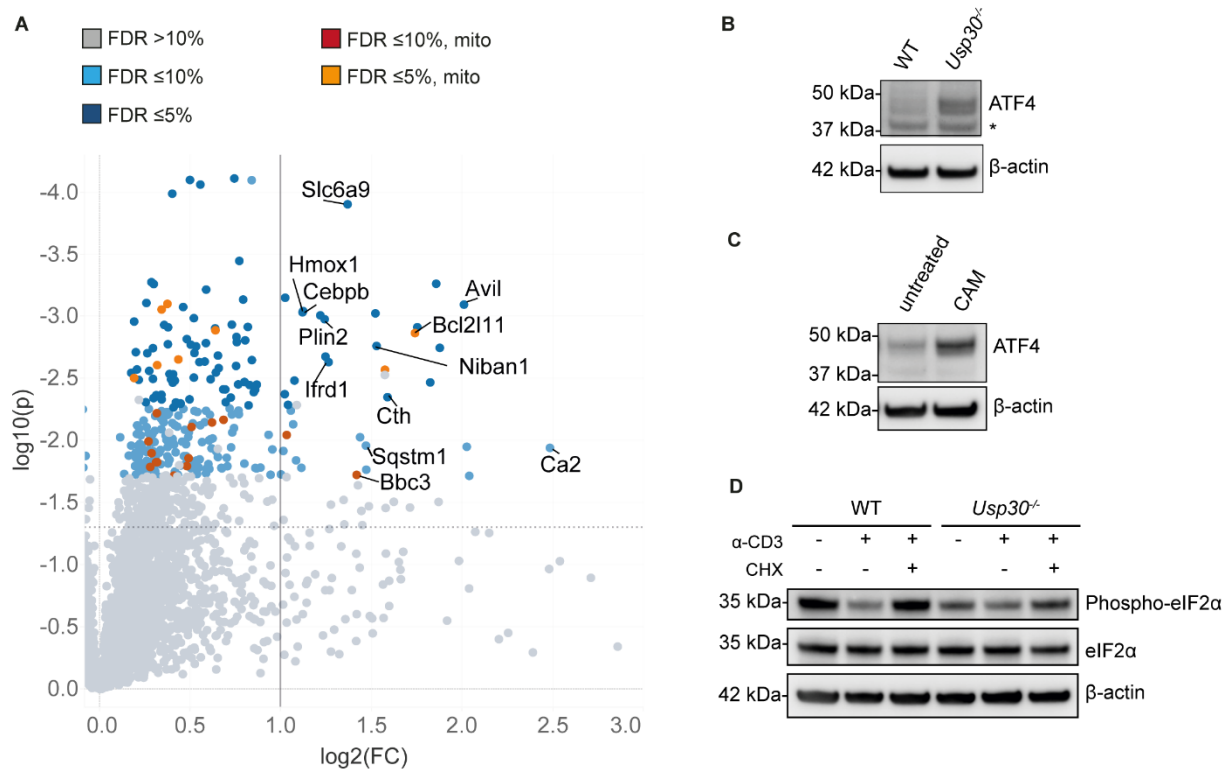


**Figure 5.3. The ISR is upregulated by loss of USP30 and inhibition of mitochondrial translation.**

(A) Volcano plot of upregulated proteins in day 5 *Usp30*<sup>-/-</sup> CTLs compared to WT (2 μg protein/sample). Vertical bar denotes  $\log_2(\text{FC}) > 1$ . Horizontal dotted line corresponds to the uncorrected  $p = 0.05$  threshold. Coloured dots show hits within the 5% and 10% false discovery rate (FDR) range and GOCC-defined mitochondrial proteins. ISR proteins are labelled by gene names. (B, C) Western blots showing ATF4 in day 5 unstimulated (B) WT and *Usp30*<sup>-/-</sup> CTLs, and (C) untreated and chloramphenicol (CAM)-treated CTLs (3.33 μg lysate/sample). Unspecific band in ATF4 immunoblot is labelled by (\*). (D) Total and phosphorylated eIF2α in day 5 WT and *Usp30*<sup>-/-</sup> CTLs, stimulated with α-CD3 and treated with 100 μg/ml CHX where indicated (3.33 μg lysate/sample). Data representative of (A) 4 and (B-D) three independent biological replicates. Julia M. Marchingo oversaw the processing of mass spectrometry samples and conducted the initial peptide analysis and protein copy number quantification.

As *Usp30*<sup>-/-</sup> CTLs showed upregulation of ATF4 and additional ISR markers, I tested whether suppressing the ISR would relieve the defect in cytosolic protein synthesis. I used the ISR inhibitor ISRIB (Sidrauski et al., 2013), which renders eIF2B insensitive to eIF2 $\alpha$  phosphorylation, thus promoting eIF2B GEF activity (Zyryanova et al., 2021).

First, I used ATF4 expression to test the efficiency of ISRIB. ATF4 abundance was analysed by immunoblot in ISRIB-treated day 5 WT and *Usp30*<sup>-/-</sup> CTLs. The effects of ISRIB were tested both in the presence and in the absence of TCR stimulation. As previously observed (**Figure 5.3B**), ATF4 expression was upregulated in unstimulated USP30-depleted CTLs (**Figure 5.4A**). ISRIB treatment downregulated ATF4 in both unstimulated WT and *Usp30*<sup>-/-</sup> CTLs, although ATF4 expression remained higher in the KO sample. These results indicated that ISRIB could inhibit the ISR in CTLs. Furthermore, these data suggested that the lower levels of eIF2 $\alpha$  phosphorylation in *Usp30*<sup>-/-</sup> CTLs (**Figure 5.3D**) were sufficient to trigger ATF4 upregulation. Intriguingly, TCR stimulation increased ATF4 expression, resulting in similar ATF4 abundance in TCR-activated WT and *Usp30*<sup>-/-</sup> CTLs. While ISRIB could decrease ATF4 in TCR-stimulated *Usp30*<sup>-/-</sup> CTLs, the enhanced ATF4 expression observed in stimulated WT CTLs was resistant to ISRIB. This result pointed to a TCR-dependent, eIF2 $\alpha$ /B-independent pathway for ATF4 upregulation that appeared to be active in WT but not USP30-depleted CTLs.

Next, I examined whether ISR inhibition would rescue cytosolic protein synthesis in USP30-depleted CTLs. Day 5 WT and *Usp30*<sup>-/-</sup> CTLs were incubated with HPG and ISRIB, and either left unstimulated or triggered by TCR activation. HPG incorporation was efficient in WT CTLs, and only modestly upregulated by TCR stimulation or ISRIB treatment (**Figure 5.4B, C**). As previously noted (**Figure 3.16B, C**), HPG incorporation was less efficient in *Usp30*<sup>-/-</sup> CTLs, and a bimodal distribution could be observed upon TCR triggering, highlighting a population of highly translating CTLs that mirrored WT HPG incorporation (**Figure 5.4B, C**). ISRIB treatment increased the percentage of CTLs in the efficiently translating population in both unstimulated and TCR-activated *Usp30*<sup>-/-</sup> CTLs. Nevertheless, neither TCR stimulation nor ISRIB treatment restored WT-like cytosolic protein synthesis in USP30-depleted CTLs. Prolonging the incubation with ISRIB and TCR stimulation (**Figure 5.4B, C**) improved HPG incorporation in all samples, although *Usp30*<sup>-/-</sup> CTLs still showed a deficiency when compared to their WT counterparts. These results indicated that ISR activation likely contributes to the decrease in cytosolic protein synthesis detected in USP30-depleted CTLs. However, the ISR did not appear to be the predominant mechanism inhibiting cytosolic translation, as ISRIB treatment could not fully restore cytosolic protein synthesis in *Usp30*<sup>-/-</sup> CTLs.

Given the partial increase in cytosolic protein synthesis observed upon ISRIB treatment in *Usp30*<sup>-/-</sup> CTLs, I assessed whether the expression of granzyme B and perforin would be similarly affected. CTLs were either left unstimulated to evaluate the abundance of cytolytic proteins at steady-state, or stimulated by TCR activation to determine *de novo* synthesis of cytolytic proteins (**Figure 5.4D, E**). Neither granzyme B nor perforin expression was substantially affected by the inhibition of the ISR. Granzyme B and perforin remained unperturbed in ISRIB-treated unstimulated WT CTLs, although a small upregulation could be observed in newly synthesised forms of both cytolytic proteins in TCR-stimulated WT samples treated with ISRIB. Unstimulated *Usp30*<sup>-/-</sup> CTLs appeared to show a moderate increase in granzyme B and perforin expression after ISRIB treatment, while *de novo* protein synthesis in *Usp30*<sup>-/-</sup> CTLs was only slightly upregulated for granzyme B upon both ISRIB treatment and TCR stimulation.

While inhibition of the ISR was found to partially rescue translation in *Usp30*<sup>-/-</sup> CTLs, granzyme B and perforin expression was not restored in ISRIB-treated *Usp30*<sup>-/-</sup> CTLs. Next, I tested whether ISRIB treatment would rescue cytotoxicity in USP30-depleted CTLs. CTLs and target cells were co-incubated in either standard CTL culture media, or in media supplemented with ISRIB (**Figure 5.4F**). Neither WT nor *Usp30*<sup>-/-</sup> killing was affected by ISRIB treatment, indicating that the ISR is not the primary cause for the loss of killing observed in USP30-depleted CTLs.

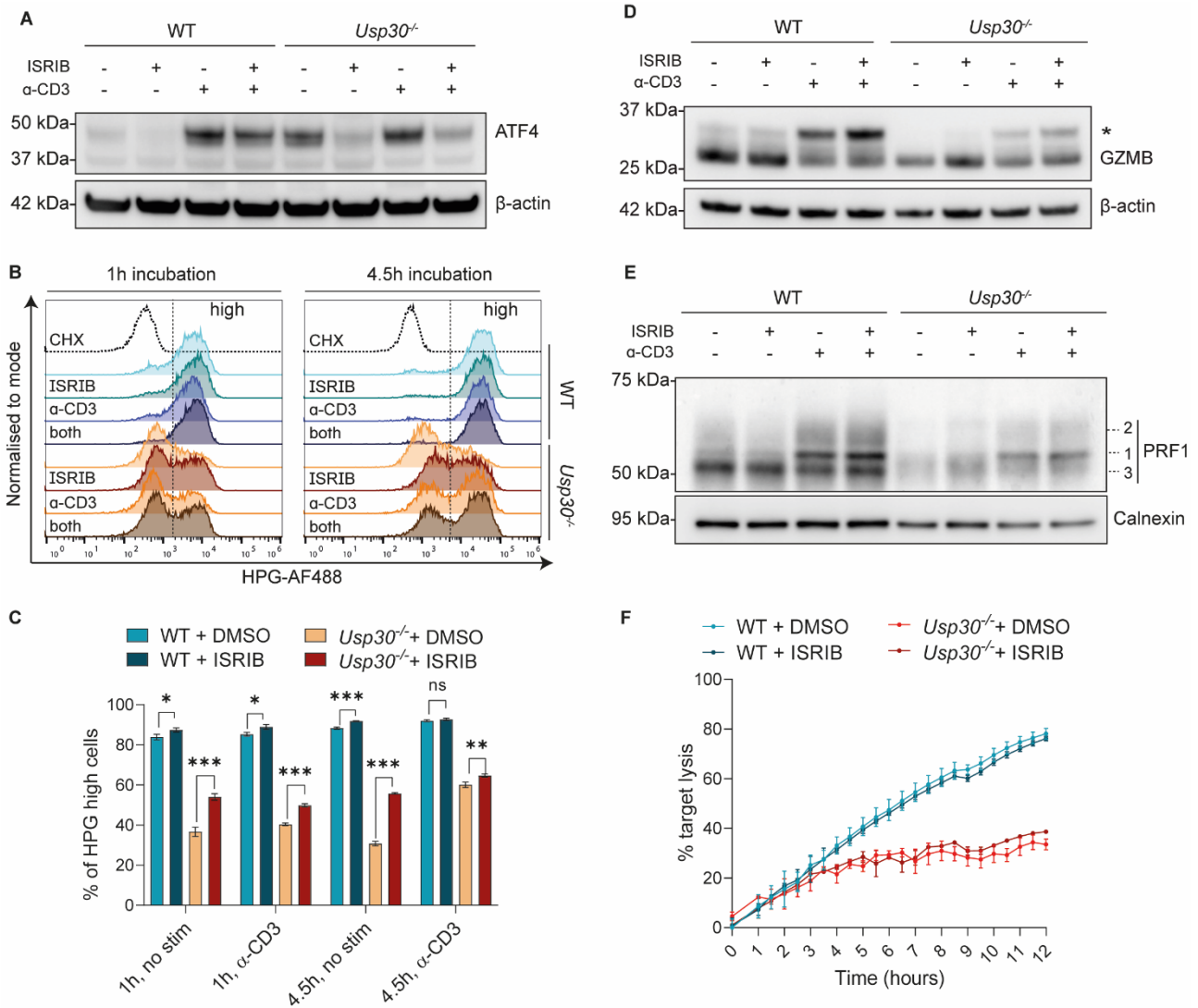


**Figure 5.4. ISR inhibition does not rescue translation and cytotoxicity in day 5 *Usp30*<sup>-/-</sup> CTLs.**

(A) Western blot showing ATF4 expression in day 5 WT and *Usp30*<sup>-/-</sup> CTLs (3.33 $\mu$ g lysate/sample) treated with 100nM ISRIB and stimulated by TCR triggering ( $\alpha$ -CD3). (B) HPG incorporation in in day 5 WT and *Usp30*<sup>-/-</sup> CTLs (2 $\times$ 10<sup>5</sup> cells/sample) treated with 100nM ISRIB, with  $\alpha$ -CD3 stimulation where indicated. 100 $\mu$ g/ml CHX was used in control samples to inhibit cytosolic protein synthesis. Dotted line delineates the position of the gate used to determine the percentage of CTLs showing high HPG incorporation. (C) Quantitation of populations expressing high HPG MFI as indicated in (B). no stim=unstimulated CTLs. (D) Immunoblot showing granzyme B (GZMB) expression and synthesis in day 5 WT and *Usp30*<sup>-/-</sup> CTLs (3.33  $\mu$ g lysate/sample) treated with 100nM ISRIB. Newly synthesised GZMB labelled by (\*). (E) Immunoblot showing perforin (PRF1) expression and synthesis in day 5 WT and *Usp30*<sup>-/-</sup> CTLs (1.5  $\mu$ g lysate/sample) treated with 100nM ISRIB. Immature (1), intermediate (2) and mature (3) forms of perforin are labelled. CTLs were stimulated with  $\alpha$ -CD3 (TCR stimulation) or treated with CHX where indicated. (F) Long-term (12h) killing assays (CTL:target ratio, 1:1) displaying percentage of target lysis with day 5 WT and *Usp30*<sup>-/-</sup> CTLs treated with 100nM ISRIB (4 $\times$ 10<sup>4</sup> targets and 4 $\times$ 10<sup>4</sup> CTLs per sample). Error bars show average  $\pm$ SD of technical replicates. \*\*\*= $p$ <0.001, \*\*= $p$ <0.01, \*= $p$ <0.05 (two-tailed unpaired Student's t-test). Data representative of at least three biological replicates.

## 5.5 Nucleofection alters CTL cytotoxicity and cytosolic protein synthesis

The results obtained with ISRIB showed that inhibiting the ISR by restoring eIF2B GEF activity could not restore protein synthesis and cytotoxicity in *Usp30*<sup>-/-</sup> CTLs. However, ATF4 upregulation in TCR-triggered CTLs indicated the presence of an eIF2 $\alpha$ -independent mechanism that could affect ATF4 expression. eIF2 $\alpha$ -independent activation of ATF4 has been previously reported (Mazor and Stipanuk, 2016; Munch and Harper, 2016). For instance, mTOR can induce ATF4 expression independently from eIF2 $\alpha$  phosphorylation to promote amino acid synthesis and transport (Ben-Sahra et al., 2016; Park et al., 2017). Mitochondrial dysfunction can also trigger ATF4 upregulation independently of canonical ISR kinases (Quiros et al., 2017). This results in a retrograde stress response in the cytosol which can be ablated by genetic deletion of ATF4 (Quiros et al., 2017).

To test whether mitochondrial dysfunction in CTLs could be mediated by ATF4, I used the CRISPR/Cas9 system to disrupt ATF4 expression in *Usp30*<sup>-/-</sup> CTLs. As described previously (Chapter 4), the CRISPR procedure was performed by nucleofection. Genetic deletion of *Atf4* was successful in both WT and *Usp30*<sup>-/-</sup> CTLs (**Figure 5.5A**). Notably, the nucleofection procedure upregulated ATF4 in WT CTLs, while nucleofection with non-targeting guide crRNA appeared to reduce ATF4 abundance in *Usp30*<sup>-/-</sup> CTLs. As previously observed (**Figure 4.18A, B**), nucleofection of WT CTLs increased granzyme B expression (**Figure 5.5B**). Intriguingly, nucleofection of USP30-depleted CTLs was also sufficient to upregulate granzyme B, and *Usp30*<sup>-/-</sup> *Atf4* CRISPR KO CTLs showed similar granzyme B expression as nucleofected WT CTLs. To test whether the upregulation of granzyme B was functionally relevant, I incubated control and CRISPR KO CTLs with target cells and measured target cell lysis. All WT samples exhibited similar cytotoxicity (**Figure 5.5C**). By contrast, nucleofection in the absence of any CRISPR KO reagent was sufficient to rescue cytotoxicity in USP30-depleted CTLs. CRISPR KO with non-targeting crRNA appeared to further enhance cytotoxicity in *Usp30*<sup>-/-</sup> CTLs.

Taken together, these results indicated that both nucleofection and introduction of CRISPR reagents altered ATF4 expression in CTLs, suggesting activation of the ISR. Furthermore, nucleofection upregulated the expression of the cytolytic protein granzyme B and rescued the killing defect observed in *Usp30*<sup>-/-</sup> CTLs. While these data did not conclusively point to an involvement for ATF4 in the inhibition of translation and cytotoxicity observed upon USP30 depletion, they showed that nucleofection significantly alters protein expression and cytolytic capacity in CTLs.

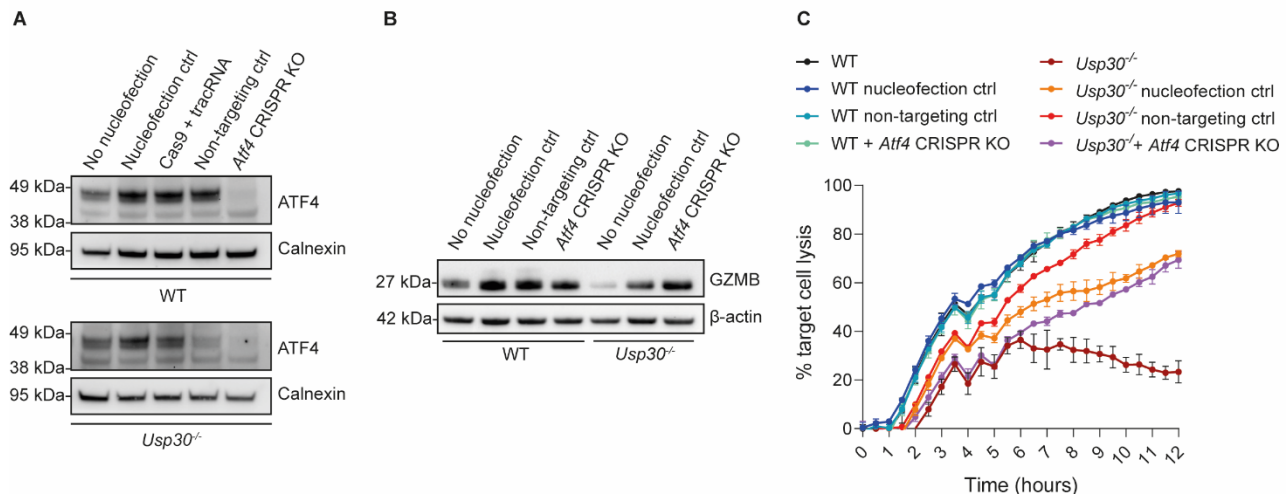


**Figure 5.5. Nucleofection is sufficient to rescue granzyme B expression and cytotoxicity in *Usp30*<sup>-/-</sup> CTLs.**

(A) Immunoblots for ATF4 expression in WT and *Usp30*<sup>-/-</sup> CTLs control and CRISPR KO samples (3.33 μg lysate/sample). (B) Immunoblot showing granzyme B (GzmB) expression in non-nucleofected and nucleofected WT and *Usp30*<sup>-/-</sup> CTLs (3.33 μg lysate/sample). (C) Long-term (12h) killing assays (CTL:target ratio, 1:1) displaying percentage of target lysis with WT and *Usp30*<sup>-/-</sup> control and CRISPR KO CTLs (4x10<sup>4</sup> targets and 4x10<sup>4</sup> CTLs per sample). Error bars indicate average ±SD of technical replicates. Data representative of two independent biological replicates.

The increase in granzyme B expression and cytotoxicity in nucleofected *Usp30*<sup>-/-</sup> CTLs was surprising, as it suggested that the nucleofection procedure in the absence of any other reagent was sufficient to rescue defects caused by mitochondrial depletion. However, it was unclear whether this rescue was caused by triggering of a stress pathway (e.g. the ISR, as shown by ATF4 upregulation) or by a direct effect of the nucleofection procedure on mitochondrial mass and function. To discriminate between these two possibilities, I conducted a preliminary experiment to measure mitochondrial mass and membrane potential in nucleofected CTLs.

MitoTracker Deep Red was used to quantify mitochondrial mass in WT and *Usp30*<sup>-/-</sup> CTLs (**Figure 5.6A-C**), while TMRE was used to detect mitochondrial membrane potential (**Figure 5.6D-F**). The percentage of USP30-deficient CTLs that were positive for either of these mitochondrial markers was increased upon nucleofection, indicating that a higher number of CTLs retained mitochondria, and that these mitochondria displayed a surge in membrane potential. While all WT CTLs exhibited MitoTracker Deep Red and TMRE signal both before and after nucleofection, the fluorescence intensity of these two mitochondrial markers appeared enhanced in some of the nucleofected CTLs. The ATF4 CRISPR KO yielded variable results that could not be confidently interpreted in the

context of this preliminary data. Nevertheless, these observations suggested that the nucleofection method might result in CTLs with elevated mitochondrial mass and membrane potential.

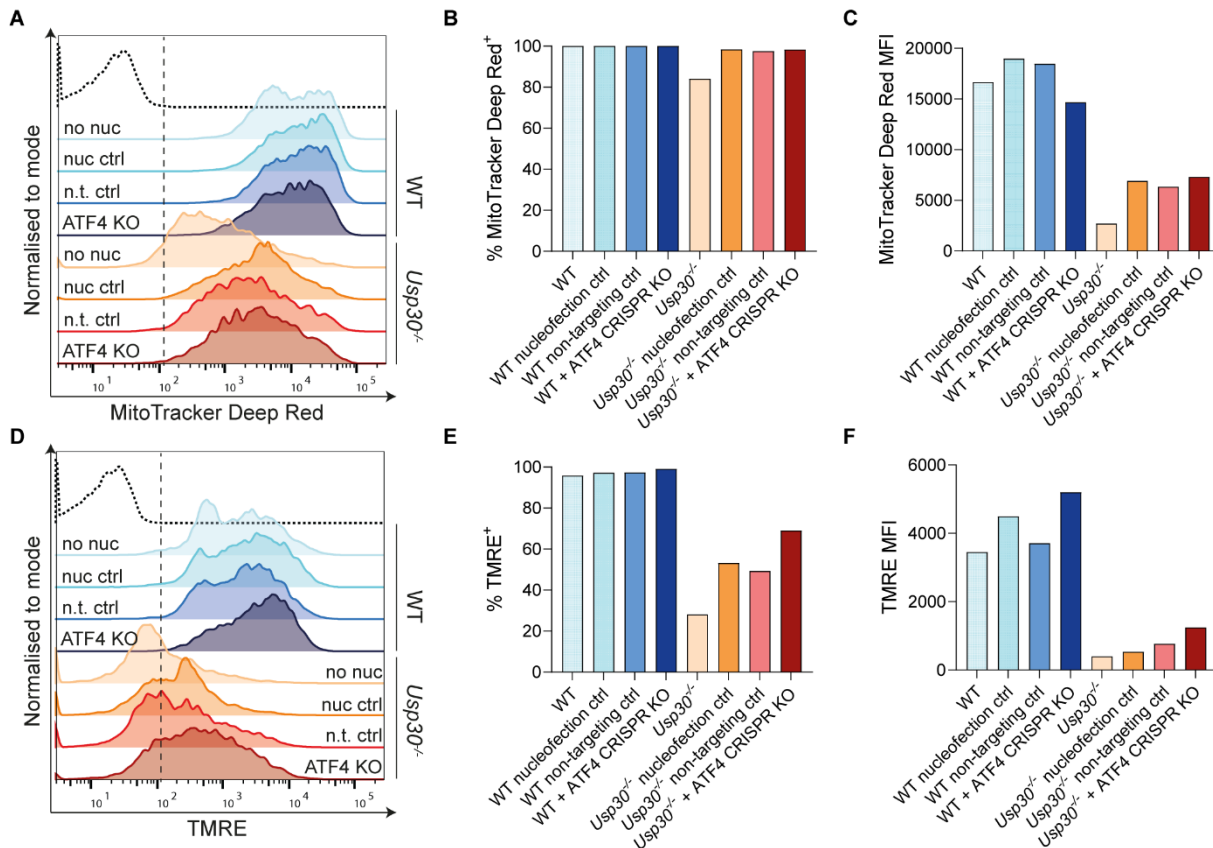


**Figure 5.6. Nucleofected CTLs show enhanced mitochondrial mass and membrane potential.**

(A) Flow cytometry analysis of Mitotracker Deep Red fluorescence in WT and *Usp30*<sup>-/-</sup> CTLs (10<sup>5</sup> CTLs per sample). (B, C) Quantitation of (B) percentage of CTLs displaying MitoTracker Deep Red signal, and (C) MitoTracker Deep Red MFI. (D) Flow cytometry analysis of TMRE fluorescence in WT and *Usp30*<sup>-/-</sup> CTLs (10<sup>5</sup> CTLs per sample). (E, F) Quantitation of (E) percentage of CTLs displaying TMRE signal, and (F) TMRE MFI. Samples were either not nucleofected (no nuc), nucleofected without CRISPR reagents (nuc ctrl), nucleofected with Cas9, tracrRNA and non-targeting guide crRNA (n.t. ctrl) or nucleofected with Cas9, tracrRNA and guide crRNA targeting *Atf4*. The unstained control is displayed as a dotted line curve. Dashed line indicates the threshold used to quantify positive signal in (C, E). Data representative of one biological replicate.

## 5.6 Metabolic enzyme expression is dysregulated in *Usp30*<sup>-/-</sup> CTLs

While several mechanisms have been suggested to link mitochondrial dysfunction to cytosolic protein synthesis, none of the pathways tested (increased ROS production, altered mTOR signalling, activation of the ISR) appeared to be the predominant cause for the loss of cytosolic translation observed in *Usp30*<sup>-/-</sup> CTLs. Of note, these mechanisms would inhibit all protein synthesis, while the downregulation of protein expression occurring upon loss of USP30 appeared to selectively affect a subset of proteins (**Figure 3.18**; **Figure 3.20**).

Protein abundance is known to be tightly regulated at the post-transcriptional level in cells of the immune system (Salerno et al., 2020; Turner and Diaz-Munoz, 2018). This confers selectivity to the regulation of protein expression upon TCR stimulation, allowing for rapid yet controlled synthesis of cytokines and cytolytic proteins. This regulation can be mediated by RNA-binding proteins (RBPs), which bind to either their own mRNA or to RNAs sharing a common motif. One of the most-well characterised motifs is an AU-rich element (ARE) found in the 3' UTR, which is common to several cytokines and thought to determine their mRNA stability (Shaw and Kamen, 1986). Given that loss of USP30 results in selective downregulation of protein synthesis, and specifically in reduced expression of cytokines, perforin and granzyme B, I asked whether post-transcriptional regulation by RBPs could modulate protein expression in *Usp30*<sup>-/-</sup> CTLs.

First, we tested whether the downregulated proteins in *Usp30*<sup>-/-</sup> CTLs shared a common AU-rich motif in their 3' UTR. The bioinformatics analysis was performed by Arianne Richard. We selected all proteins with a statistically significant decrease in expression (FDR<10%) that had not been described to localise nor transiently associate with mitochondria or peroxisomes. These proteins were unlikely to be direct targets of USP30, and could therefore reveal an alternative mechanism of post-transcriptional regulation. This list was first searched for the presence of 3' UTR ARE, which did not appear to be enriched in the mRNAs of downregulated proteins. Next, we asked whether changes in protein expression could be determined by a common motif other than ARE in their 5' or 3' UTR, or in the mRNA coding sequence. No common motif was found in any of the tested sequences. These results indicated that the selective downregulation of protein expression in USP30-deficient CTLs was not likely to be due to AU-rich motifs.

One of the most dramatic changes observed in *Usp30*<sup>-/-</sup> CTLs was loss of oxidative phosphorylation, together with enhanced reliance on glycolysis (**Figure 3.6**). Analysis of the mass spectrometry data highlighted a reduction in the expression of enzymes involved in cholesterol metabolism, TCA cycle, and surprisingly glycolysis (Chapter 3). Lack of USP30 also resulted in a decrease in peroxisomes

(**Figure 3.8**), which might suggest additional alterations in fatty acid oxidation. Taken together, these observations indicated that *Usp30*<sup>-/-</sup> CTLs experienced a profound metabolic rewiring.

Adaption to different nutrient sources can disengage specific enzymes from metabolism and allow them to moonlight as RNA-binding proteins (Chang et al., 2013). Several RBPs include enzymes involved in glycolysis, gluconeogenesis, the TCA cycle, fatty acid synthesis, and amino acids and nucleotide metabolism (Castello et al., 2015). RBPs can act as post-transcriptional regulators in CTLs, mediating the expression of key cytolytic proteins such as granzyme B, TNF $\alpha$  and IFN $\gamma$  (Chang et al., 2013; Salerno et al., 2020; Turner and Diaz-Munoz, 2018). The concerted action of multiple RBPs recognising different motifs could have hindered the detection of a common binding sequence in our analysis. Therefore, I examined whether the expression of multiple metabolic enzymes known to moonlight as RBPs was altered in our mass spectrometry dataset.

Proteomics data from both unstimulated and TCR-triggered day 5 *Usp30*<sup>-/-</sup> CTLs were searched for metabolic enzymes described as moonlighting RBPs (Beckmann et al., 2015; Castello et al., 2015; Ciesla, 2006; Garcin, 2019; Turner and Diaz-Munoz, 2018). NMT1 and ASS1 were upregulated in unstimulated *Usp30*<sup>-/-</sup> CTLs, while 29 RBP enzymes showed reduced expression (CAT, GDTP1, ENO1, IMPDH1, LDHA, FASN, PAFAH1B3, TPI1, ALDOA, DUT, PGK1, DHCR7, PKM, PGK2, ACO1, FDPS, DLD, HK2, IDH1, IDH2, MDH2, ATP5F1B, HSD17B10, ALDH18A1, FADS2, HADHB, ACAA2, CS, SUCLG1) (**Figure 5.7A**). Most of the downregulated RBPs were localised to either mitochondria or peroxisomes, indicating that their altered expression was likely due to increased mitophagy and pexophagy in *Usp30*<sup>-/-</sup> CTLs. Among them, ENO1, FADS2, PGK1 can either transiently localise to the mitochondria or interact with mitochondrial proteins (Didiasova et al., 2019; Park et al., 2015; Qattan et al., 2012), which might have resulted in their promiscuous ubiquitination in the absence of USP30. By contrast, other RBP enzymes that were found to be downregulated in *Usp30*<sup>-/-</sup> CTLs are not known to associate with mitochondria. These were either cytosolic (NMT1, IMPDH1, PAFAH1B3, ALDOA, PGK2 and TPI1) or ER-resident proteins (DHCR7).

To further characterise the expression of RBP metabolic enzymes in USP30-depleted CTLs, I searched for RBPs in the mass spectrometry dataset from TCR-activated CTLs. 32 RBP enzymes were downregulated in TCR-triggered *Usp30*<sup>-/-</sup> CTLs compared to their WT counterparts (**Figure 5.7B**). 84% of RBP enzymes showing decreased expression in TCR-triggered *Usp30*<sup>-/-</sup> were also downregulated in unstimulated conditions. While most of these proteins (24) were localised to either mitochondria or peroxisomes, 8 RBPs were either cytosolic or ER-resident proteins as detailed above (PAFAH1B3, ALDOA, PGK2, TPI1, DHCR7) or proteins that can transiently associate with

mitochondria, including the previously described ENO1 and PGK1, together with GAPDH (Tristan et al., 2011). No RBP enzyme was overexpressed in TCR-stimulated day 5 *Usp30*<sup>-/-</sup> CTLs.

Of note, inhibition of mitochondrial protein synthesis via DOX treatment could also alter the expression of metabolic enzymes moonlighting as RBPs. Analysis of unstimulated DOX-treated CTLs revealed that four metabolic RBPs were downregulated in both DOX-treated and USP30-depleted CTLs (ATP5F1B, DLD, DHCR7, CAT, IMPDH1) (**Figure 5.7C**). None of the RBP enzymes showing a statistically significant change in expression in *Usp30*<sup>-/-</sup> CTLs (FDR<10%) were significantly altered in the dataset from TCR-triggered, DOX-treated CTLs (**Figure 5.7D**).

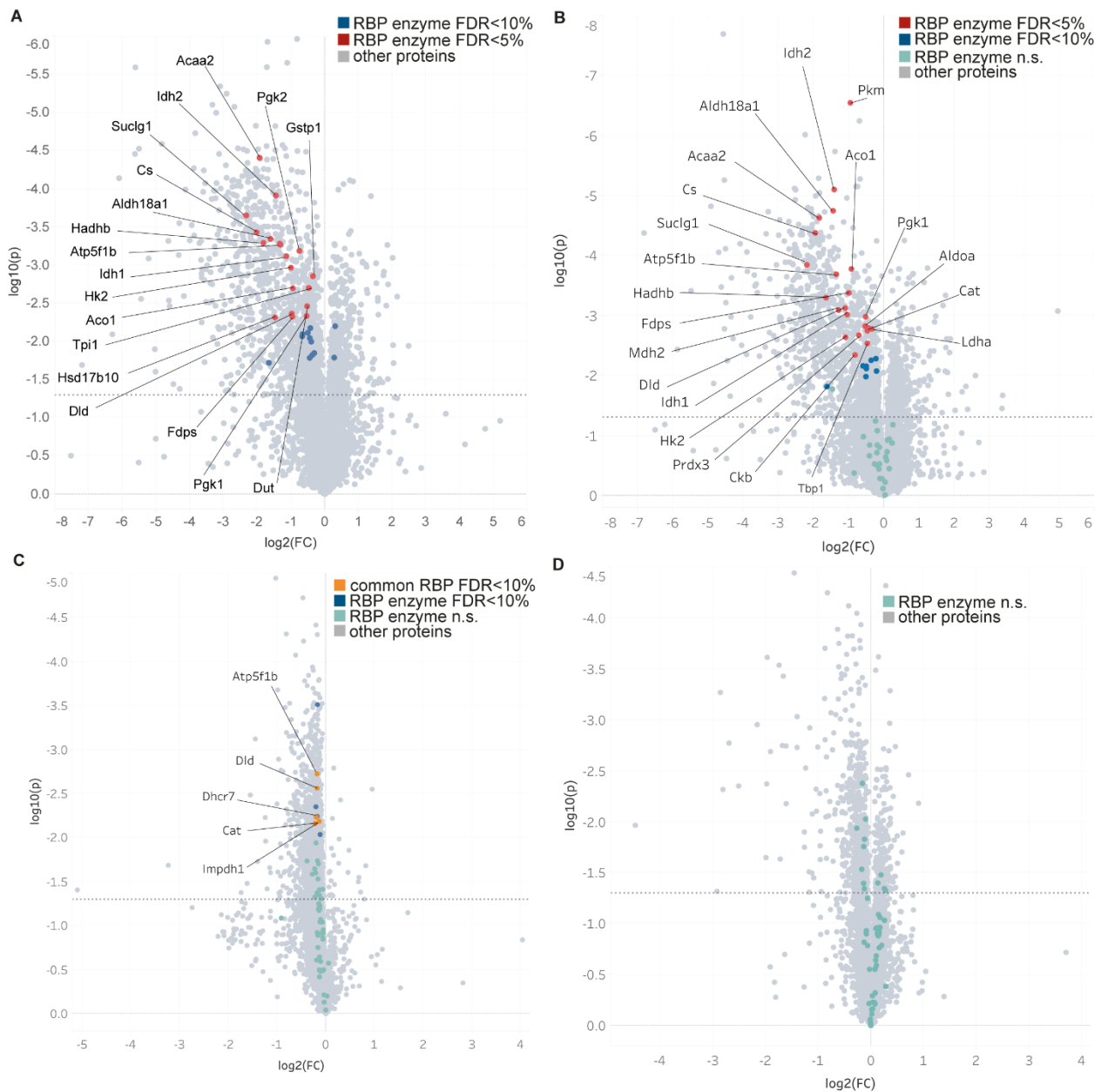


**Figure 5.7. Enzymes moonlighting as RBPs show altered expression in *Usp30*<sup>-/-</sup> and DOX-treated CTLs.**

(A, B) Volcano plots of upregulated (right quadrant) and downregulated (left quadrant) proteins in (A) unstimulated, and (B) TCR-triggered day 5 *Usp30*<sup>-/-</sup> CTLs compared to WT (2  $\mu$ g protein/sample). (C, D) Volcano plot of upregulated (right quadrant) and downregulated (left quadrant) proteins in (C) unstimulated, and (D) TCR-triggered DOX-treated CTLs (10  $\mu$ g/ml) compared to untreated (1.5  $\mu$ g protein/sample). Dotted horizontal line corresponds to the uncorrected  $p=0.05$  threshold. Coloured dots show hits within the 5% and 10% false discovery rate (FDR) range. RBP enzymes are labelled by gene name. n.s.=not significant. Data representative of 4 biological replicates. Julia M. Marchingo oversaw the processing of mass spectrometry samples and conducted the initial peptide analysis and protein copy number quantification.

## 5.7 Summary

The suboptimal cytosolic translation detected in *Usp30*<sup>-/-</sup> CTLs prompted an analysis of multiple pathways that could link mitochondrial dysfunction to the inhibition of cytosolic protein synthesis. While none of the tested mechanism could be conclusively determined to be the cause of the translational defect in *Usp30*<sup>-/-</sup> CTLs, a number of interesting observations were made during the course of this analysis.

First, I showed that ISR activation in *Usp30*<sup>-/-</sup> CTLs is not the primary cause of the deficiency in cytosolic protein synthesis. Inhibition of the ISR using ISRIB resulted in only partial restoration of cytosolic translation and had no substantial effect on cytotoxicity nor on the synthesis of granzyme B and perforin. This result was interesting, as a number of recent studies have highlighted the ISR as the key pathway mediating mitochondrial dysfunction (including defects in mitochondrial translation) and inhibition of cytosolic protein synthesis (Fessler et al., 2020; Guo et al., 2020; Molenaars et al., 2020; Quiros et al., 2017). Taken together, these observations point to the existence of additional mechanisms mediating the communication between mitochondrial homeostasis and protein synthesis in the cytosol.

One of these mechanisms could rely on post-transcriptional regulation of gene expression by RBPs. *Usp30*<sup>-/-</sup> CTLs show loss of enzymes involved in OXPHOS and the TCA cycle. Metabolic rewiring allows enzymes to moonlight as RNA-binding proteins (Chang et al., 2013). Interestingly, the expression of several metabolic RBPs was disrupted in both USP30-depleted and DOX-treated CTLs. RBPs could provide an additional level of regulation to the post-transcriptional control of protein synthesis, potentially suggesting a putative mechanism for the selective downregulation of protein expression observed in *Usp30*<sup>-/-</sup> CTLs.

Finally, I demonstrated that the nucleofection procedure used to introduce CRISPR reagents in CTLs induced changes in protein expression and mitochondrial phenotypes. Not only was ATF4 upregulated by nucleofection, indicating that this technique is likely to induce the integrated stress response, but an increase in granzyme B was also observed upon nucleofection. This effect was detectable in both WT and USP30-depleted CTLs, and likely contributed to the rescue of cytotoxicity observed in nucleofected *Usp30*<sup>-/-</sup> CTLs. Intriguingly, CTL nucleofection appeared to select for cells with enhanced mitochondrial mass and mitochondrial membrane potential. Given the evidence provided both in the existing literature and throughout the course of this work on how mitochondria can affect CTL function, this highlights an important limitation of the use of nucleofection for the manipulation of CTL gene expression.





## **CHAPTER 6**

### **Discussion**



## 6.1 Summary of Results

The overarching question addressed by this work was to define the role of mitochondria in CTL cytotoxicity. First, I asked how the loss of USP30 affected CTL killing. Secondly, I evaluated the contribution of different mitochondrial functions to cytotoxicity. Lastly, I investigated the connection between mitochondrial dysfunction and cytosolic protein synthesis in *Usp30*<sup>-/-</sup> CTLs.

In Chapter 3, I showed that loss of USP30 did not only result in a decrease in mitochondria and peroxisomes, as previously described (Bingol et al., 2014; Marcassa et al., 2018; Nakamura and Hirose, 2008; Riccio et al., 2019) but also in impairment of cytosolic protein synthesis. I demonstrated that *de novo* protein synthesis was essential to sustain prolonged CTL killing, and that either USP30 depletion or cytosolic protein synthesis inhibition precluded the replenishment of cytolytic proteins required for serial killing. Preventing mitophagy was sufficient to rescue the defects observed in *Usp30*<sup>-/-</sup> CTLs, confirming that mitochondria play a critical role in cytosolic translation and cytotoxicity.

In Chapter 4, I used both mouse models and the CRISPR/Cas9 technique to ask whether the reduction in cytosolic translation and killing could be ascribed to the deficiency of a specific peroxisomal or mitochondrial function. This work indicated that inhibiting mitochondrial protein synthesis was sufficient to decrease cytosolic translation, negatively affecting the *de novo* synthesis of granzyme B, perforin and cytokines upon TCR triggering. Overall, impairment of mitochondrial translation resulted in loss of sustained killing, similarly to *Usp30*<sup>-/-</sup> CTLs.

In Chapter 5, I examined potential mechanisms that could link mitochondrial homeostasis and cytosolic protein synthesis. Specifically, I tested the involvement of the ISR and showed that it was not the predominant pathway impairing cytosolic translation and killing in *Usp30*<sup>-/-</sup> CTLs. As the loss of USP30 appeared to selectively affect a subset of proteins, I analysed the expression of metabolic enzymes that can moonlight as RNA-binding proteins, thus modulating post-transcriptional expression in CTLs (Castello et al., 2015; Chang et al., 2013; Turner and Diaz-Munoz, 2018). RBP expression was altered in both *Usp30*<sup>-/-</sup> and DOX-treated CTLs, potentially providing a putative mechanism for the selective downregulation of cytosolic protein synthesis in CTLs exhibiting deficient mitochondrial function.

Overall, this work built on the initial findings from the 3i consortium (Abeler-Dörner et al., 2020) and revealed a novel role for both USP30 and mitochondrial translation in CTL cytotoxicity, thus uncovering a crucial mechanism promoting efficient adaptive immunity.

## 6.2 The *Usp30*<sup>-/-</sup> mouse as a model for studying mitochondria in CTL

One of the most important results of this work is the establishment of the *Usp30*<sup>-/-</sup> mouse as a model to study mitochondrial dysfunction in CTLs. Genetic deletion of *Usp30* did not impair the viability nor development of these mice. However, loss of USP30 affected both innate and adaptive immunity, as suggested by altered inflammation in DSS-induced colitis and decreased CD8<sup>+</sup> T cell cytotoxicity (Abeler-Dörner et al., 2020).

Perturbing mitochondrial function using either *in vivo* pharmacological treatments or constitutive mouse knockout models is known to cause defects in T cell development (Corrado et al., 2021; Desdin-Mico et al., 2020; Ramstead et al., 2020; Sena et al., 2013; Tan et al., 2017a), hindering the investigation of differentiated T cells. However, percentages of CD4<sup>+</sup> and CD8<sup>+</sup> T cells in murine spleens were not affected by the loss of USP30, nor were the relative ratios of naïve, memory, effector and regulatory T cells. These results suggested that USP30 is not essential during T cell development and differentiation. In addition, mitochondrial mass and membrane potential were equivalent in naïve WT and *Usp30*<sup>-/-</sup> T cells, with loss of mitochondria and peroxisomes occurring only 5-7 days after T cell activation. These results indicated that naïve CD8<sup>+</sup> T cells do not require USP30 to ensure maintenance of mitochondrial mass and function. Despite their reliance on OXPHOS, naïve T cells have little mitochondrial content (Chang et al., 2013; Levine et al., 2021; Sena et al., 2013; Tan et al., 2017a; Yi et al., 2006). Given their characteristic quiescent state (Pearce, 2010; Wolf et al., 2020), mitophagy rates are likely to be low in naïve T cells, thus relieving the need for USP30-dependent deubiquitination. Therefore, the *Usp30*<sup>-/-</sup> mouse model presents the opportunity to study the effects of mitochondrial depletion without skewing T cell differentiation.

By contrast, USP30 is required to maintain mitochondrial mass and function in activated T cells. TEM analysis showed a higher percentage of “ghost-like” mitochondria exhibiting either missing or highly disrupted inner cristae structure in *Usp30*<sup>-/-</sup> CTLs. These results were consistent with the role for USP30 described in other cell types (Bingol et al., 2014; Nakamura and Hirose, 2008). Not only does USP30 prevent mitophagy, but it also regulates protein import into the mitochondria by modulating the ubiquitination of the channel TOM20 (Phu et al., 2020). As over 90% of the mitochondrial proteome is synthesised in the cytosol and needs to be imported into the mitochondria (D'Souza and Minczuk, 2018), the appearance of “empty” mitochondria is consistent with impaired mitochondrial import upon loss of USP30.

It is interesting to note that the use of *Usp30*<sup>-/-</sup> CTLs might allow for investigation of PINK1/PARKIN-independent mitophagy. While disruption of mitochondrial membrane potential is

thought to allow for PINK1 stabilisation (Lin and Kang, 2008), no increase in PINK1 expression was detected in the mass spectrometry of *Usp30*<sup>-/-</sup> CTLs. PINK1 detection by immunoblot was also inconclusive. Flow cytometry analysis of WT and USP30-depleted CTLs showed equivalent mitochondrial mass and membrane potential on day 3 post-activation, followed by a sudden decrease in mitochondrial abundance and membrane potential in *Usp30*<sup>-/-</sup> CTLs by day 5 post-stimulation. As PINK1 expression was examined at the time point when the loss of mitochondria was more significant (day 5 post-stimulation), PINK1 accumulation might be more easily detectable at an earlier time point (day 3 or 4 post-stimulation) when mitophagy appears to be triggered.

Interestingly, PINK1 and PARKIN peptides were not found in either unstimulated nor activated CD4<sup>+</sup>, CD8<sup>+</sup> and NK cells according to the Immunological Proteome Resource database (<http://immpres.co.uk>), and PINK1 accumulation could not be detected by immunoblot in FCCP-treated CTLs. Both mouse (McWilliams et al., 2018) and *Drosophila* models (Lee et al., 2018) have shown that PINK1 and PARKIN deficiency do not preclude mitochondrial degradation, emphasising the existence of alternative pathways regulating mitophagy. Mitochondrial damage induces translocation of the inner mitochondrial membrane lipid cardiolipin to the OMM, where it can recruit the autophagosome via interaction with LC3 (Chu et al., 2013). In addition, several OMM proteins (BNIP3, NIX, FUNDC1, AMBRA1) can also act as autophagy receptors. As BNIP3 and NIX are required for removal of damaged mitochondria in NK cells (O'Sullivan et al., 2015), a similar pathway could promote mitophagy in USP30-depleted CTLs. Of note, p62 was upregulated in the mass spectrometry analysis of *Usp30*<sup>-/-</sup> CTLs, and p62-dependent mitophagy can occur without PINK1 and PARKIN (Yamada et al., 2019; Yamada et al., 2018). Taken together, these results may indicate that mitophagy is likely to proceed in a PINK1/PARKIN-independent fashion, and suggest that *Usp30*<sup>-/-</sup> CTLs might provide a novel model to study this process.

### **6.3 Mitochondria participate to calcium flux in TCR-stimulated CTLs**

Analysis of *Usp30*<sup>-/-</sup> CTLs showed that mitochondrial depletion results in enhanced calcium flux after both physiological (TCR crosslinking) and super-physiological (ionomycin) stimulation. These observations might at first seem at odds with the well-established role of mitochondria as calcium stores (Rizzuto et al., 2012). The fact that calcium flux was increased when mitochondria were depleted in *Usp30*<sup>-/-</sup> CTLs suggests that mitochondria are likely to uptake rather than release calcium upon TCR stimulation. This suggests that mitochondria act as calcium sinks in CTLs, limiting the propagation of calcium in the cytosol, as previously described in other cell types (Tinel et al., 1999).

Previous studies have shown that intracellular calcium concentration can affect CTL signalling by promoting calcineurin-mediated NFAT phosphorylation and translocation to the nucleus (Jain et al., 1993; Kincaid et al., 1987). While none of the TCR signalling nodes examined was perturbed in *Usp30*<sup>-/-</sup> CTLs, the increased calcium flux in TCR-stimulated CTLs might affect NFAT-dependent transcription. Therefore, analysis of the *Usp30*<sup>-/-</sup> transcriptome might provide insights into how mitochondria depletion modulates gene expression in CTLs. As only granzyme B and perforin mRNA expression was quantitated in USP30-depleted CTLs, it cannot be ruled out the expression of other genes might be affected at the transcriptional level.

#### 6.4 Mitochondrial fitness impacts cytosolic translation

*Usp30*<sup>-/-</sup> CTLs exhibited a clear inhibition of protein synthesis as measured by incorporation of the methionine analogue HPG. Translation efficiency is key in CD8<sup>+</sup> T cell activation, as it is required for ribosome biogenesis and proliferation (Tan et al., 2017b). Analysis of activated CTLs shows poor correlation between proteome and transcriptome, highlighting the importance of post-transcriptional regulation and efficient protein synthesis in the generation and maintenance of mature T cells (Hukelmann et al., 2016).

Interestingly, TCR stimulation had little to no effect on cytosolic protein synthesis in WT CTLs (**Figure 3.16B, C**). This result indicates that protein synthesis rates are maximised in day 5 WT CTLs even in the absence of TCR activation. It is unlikely that HPG could have been limiting at the 1h time point, as WT CTLs incubated with HPG for 4.5h showed increased incorporation compared to the 1h sample. However, HPG could have been limiting after 4.5h of incubation. Future studies involving either longer treatments or the use of different HPG titrations for the 4.5h incubation should clarify whether prolonged TCR stimulation can promote cytosolic protein synthesis in WT CTLs.

Cytosolic translation was not substantially affected by short-term (1h) TCR crosslinking in *Usp30*<sup>-/-</sup> CTLs. By contrast, prolonged TCR stimulation (4.5h) induced the appearance of two populations: one showing similar HPG incorporation efficiency to WT CTLs, and another one exhibiting lower HPG signal. While the increase in protein synthesis observed upon prolonged TCR stimulation was not sufficient to restore the abundance of cytosolic proteins, the sudden bimodal distribution of HPG signal in TCR-triggered *Usp30*<sup>-/-</sup> CTLs was interesting. Immunofluorescence analysis of TOM20 and PDH staining indicated that while TOM20 and PDH fluorescence intensity was diminished in all *Usp30*<sup>-/-</sup> samples, complete loss of these mitochondrial markers was only observed in ~50% of USP30-depleted CTLs (**Figure 3.4 D-G**). Intriguingly, this number is consistent with the percentage

of poorly translating CTLs showing low HPG fluorescence intensity upon prolonged TCR stimulation (**Figure 3.16B, C**). Therefore, it is possible to speculate that CTLs in which mitochondria were decreased, albeit not completely depleted, could upregulate translation efficiency upon prolonged stimulation, while CTLs suffering the most severe loss of mitochondria exhibited poor translation regardless of stimulation.

It remains undetermined how some *Usp30*<sup>-/-</sup> CTLs retain mitochondrial mass, while others lose it completely. This could result from a process of cell division involving uneven mitochondrial inheritance. Asymmetrical mitochondrial division has been previously observed in CTLs, and it is thought to affect differentiation into memory and effector T cell subsets (Adams et al., 2016). Notably, memory T cell differentiation also requires functional mitochondria and OXPHOS (Buck et al., 2016; van der Windt et al., 2012). While the analysis of T cells residing in WT and *Usp30*<sup>-/-</sup> spleens did not suggest any difference in the percentages of effector and memory T cells, it would be useful to follow WT and *Usp30*<sup>-/-</sup> CD8<sup>+</sup> T cell differentiation after *in vitro* stimulation to evaluate whether formation of a memory T cell pool is perturbed by lack of mitochondria.

### **6.5 A focus on mitochondrial translation as a requirement for CTL killing**

The use of pharmacological treatments to impair mitochondrial protein synthesis revealed that this function is essential to sustain CTL killing. Two recent studies have reported similar findings in both CD4<sup>+</sup> (Almeida et al., 2021) and CD8<sup>+</sup> T cells (O'Sullivan et al., 2021). In the first study, mitochondrial translation was disrupted either via linezolid treatment or via inhibition of the mitochondrial elongation factor GFM1. In both cases, cytokine production was impaired in CD4<sup>+</sup> T cells, decreasing autoimmunity in a mouse model of multiple sclerosis (Almeida et al., 2021). The second study investigated the response of CD8<sup>+</sup> effector T cells to febrile temperature. CTLs exposed to 39°C exhibited enhanced mitochondrial mass and function and provided improved anti-tumour protection in a mouse model of leukaemia. Inhibition of mitochondrial translation via CRISPR/Cas9 deletion of the mitochondrial ribosomal subunit MRPL39 prevented the increase in mitochondrial abundance, which correlated with a reduction in the anti-tumour response in CTLs exposed to febrile temperatures (O'Sullivan et al., 2021).

The present work provides further insights by identifying impaired cytosolic translation as the cause for the loss of effector function. CTLs lacking USP30 or treated with either CAM or DOX showed decreased cytosolic translation and precluded synthesis of cytokines and cytolytic proteins, preventing killing. Thus, mitochondrial translation is required to maintain effector function by

promoting *de novo* synthesis of proteins needed for sustained killing. Taken together with the recently published works, these results suggest that antibiotics targeting mitochondrial ribosomes should be used with caution (Moullan et al., 2015), as they are likely to trigger a signalling cascade impairing T cell activation, effector functions and cytosolic protein synthesis.

While CAM and DOX treatment partially phenocopied loss of USP30 in activated CTLs, some important differences were observed. For instance, calcium flux appeared enhanced upon mitochondria depletion, while loss of mitochondrial protein synthesis resulted in a reduction in intracellular calcium concentration. Specifically, CAM and DOX treatment prevented the sustained rise in intracellular calcium triggered by TCR activation. Secondly, incubation with DOX and CAM compromised both granzyme B and perforin secretion. As the TCR-triggered increase in calcium concentration is required for CTL secretion (Lancki et al., 1987; Takayama and Sitkovsky, 1987), it is likely that the shortened calcium flux in CAM- and DOX-treated CTLs might have impaired degranulation. Therefore, diminished secretion together with reduced synthesis of cytolytic proteins are both likely to have inhibited cytotoxicity in DOX- and CAM-treated CTLs.

Furthermore, mass spectrometry analysis of DOX-treated CTLs revealed a significant downregulation of cytokines, cytokine receptors and proteins mediating cytokine signalling in WT CTLs. While loss of USP30 reduced TNF $\alpha$  and IFN $\gamma$  synthesis upon TCR stimulation, CAM and DOX showed an additive effect by further decreasing TNF $\alpha$  and IFN $\gamma$  expression in *Usp30*<sup>-/-</sup> CTLs. This result was surprising, as the substantial decline in mitochondrial translation in USP30-depleted CTLs suggested that CAM and DOX treatment would only have a minor effect on the remaining functional mitochondria. These results could indicate that either CAM and DOX possess off-target effects that preferentially target cytokine signalling, or that complete versus partial depletion of mitochondrial translation have different effects on cytokine production.

Taken together, these results outline important differences between CAM and DOX treatment and loss of USP30. These discrepancies might stem from comparison of selective inhibition of mitochondrial protein synthesis (CAM, DOX) versus the complete loss of mitochondrial structures (*Usp30*<sup>-/-</sup>). Alternatively, these differences might be caused by the effects of acute (CAM, DOX) versus chronic (*Usp30*<sup>-/-</sup>) impairment of mitochondrial translation, as *Usp30*<sup>-/-</sup> CTLs may have adapted to the loss of mitochondrial protein synthesis. While day 5 CTLs were only treated for 4h with either chloramphenicol or doxycycline, other studies linking mitochondrial and cytosolic protein synthesis relied on treatments lasting 48h in cell culture models and two weeks in mice (Molenaars et al., 2020). Thus, it would be interesting to examine whether CTLs treated with DOX or CAM from day 3 to day 5 post-stimulation would be more similar to *Usp30*<sup>-/-</sup> CTLs.

## 6.6 The balance between mitochondrial homeostasis and cytosolic protein synthesis

The present work supported the existence of a link between mitochondrial and cytosolic protein synthesis, as previously postulated (Boos et al., 2020; Topf et al., 2019). The evidence presented in Chapter 5 argued against a predominant role for the ISR in the downregulation of cytosolic protein synthesis in *Usp30*<sup>-/-</sup> CTLs. However, the ISRIB experiments do not rule out an eIF2 $\alpha$ -independent pathway similar to the ISR could be active in CTLs. Of note, mitochondrial stress can elicit ATF4-dependent signalling independently from activation of the canonical eIF2 $\alpha$  kinases (Ben-Sahra et al., 2016; Quiros et al., 2017).

However, further investigation aimed at ISR inhibition in CTLs should be carefully monitored. It is worth noting that the ISR is not necessarily detrimental in T cells, as it regulates naïve CD4<sup>+</sup> T cell differentiation (Scheu et al., 2006) and it can potentiate TCR signalling in regulatory T cells. Furthermore, ISR signalling in CTLs can enhance effector function via binding of ISR-related transcription factors (including ATF4) to the promoter region of granzyme B and IL-2 (Chang et al., 2012). This indicates that that ISR ablation in CTLs is unlikely to result in full effector function.

Alternative pathways other than the ISR are also likely to link mitochondrial homeostasis and cytosolic translation. Aberrant mtROS production can oxidise cytosolic ribosomes and prevent protein synthesis (Topf et al., 2018) and cause tRNA fragmentation in CTLs (Yue et al., 2021). Analysis of WT and *Usp30*<sup>-/-</sup> CTLs showed low MitoSOX Red signal in both WT and USP30-depleted CTLs. However, the loss of mitochondria in *Usp30*<sup>-/-</sup> CTLs could also cause a reduction in MitoSOX signal independently from mtROS release. Further investigation could focus on measuring mtROS on day 3 and day 4 post-stimulation to investigate whether USP30 depletion causes aberrant mtROS release alongside the increase in mitochondrial degradation.

Inhibition of mitochondrial protein synthesis (Houtkooper et al., 2013) or protein misfolding within mitochondria (Zhao et al., 2002) can trigger the mtUPR. The mtUPR diminishes mitochondrial protein synthesis and upregulates the expression of mitochondrial matrix chaperonins to restore homeostasis (Munch and Harper, 2016). In addition, mtUPR activates the ISR, resulting in ATF4-dependent signalling (Quiros et al., 2017). Alternatively, lack of mitochondrial import can result in the accumulation of mitochondrial precursors in the cytosol, which promotes aggregate formation (Nowicka et al., 2021; Wrobel et al., 2015). This is referred to as the UPRam, which is thought to induce a retrograde signalling response characterised by upregulation of cytosolic chaperones, reduction of cytosolic protein synthesis and enhanced proteasomal degradation, thus resulting in the clearance of aggregates (Wrobel et al., 2015).

Given the multiple ways in which loss of mitochondrial homeostasis can trigger a retrograde response resulting in impaired cytosolic protein synthesis, it is possible that USP30 depletion and DOX or CAM treatment activated a different mitochondrial stress response in CTLs. The appearance of “empty” mitochondria in *Usp30*<sup>-/-</sup> CTLs is likely due to inhibited mitochondrial import as a consequence of TOM20 degradation (Phu et al., 2020). Therefore, mitochondrial precursors in USP30-depleted CTLs are likely to accumulate in the cytosol, thus triggering the UPRam. However, upregulation of cytosolic chaperones was not observed in *Usp30*<sup>-/-</sup> CTLs. Further analysis examining proteasome activity could provide more insight into whether the UPRam is activated upon loss of USP30. Moreover, the effect of blocking mitochondrial protein import could be tested pharmacologically (Quiros et al., 2017), to check whether lack of import is sufficient to decrease cytosolic protein synthesis and cytotoxicity.

By contrast, DOX treatment is thought to activate the mtUPR (Houtkooper et al., 2013). As the mtUPR triggers the ISR, it would be interesting to examine whether ISRIB treatment could be sufficient to restore cytosolic translation and cytotoxicity in DOX- and CAM-treated CTLs. Therefore, while both *Usp30* deletion and inhibition of mitochondrial translation appear to converge on reduced synthesis of cytolytic proteins and loss of cytotoxicity, it remains possible that this occurs via different pathways in mitochondria-depleted versus CAM- or DOX-treated CTLs.

### **6.7 The role of additional mitochondrial functions in *Usp30*<sup>-/-</sup> CTLs**

The reduction in cytosolic translation and cytotoxicity observed in *Usp30*<sup>-/-</sup> CTLs could be phenocopied by pharmacological interference with mitochondrial translation. However, given that loss of USP30 results in mitochondrial degradation, the involvement of other mitochondrial functions could not be thoroughly ruled out. For instance, while MCU depletion by CRISPR KO did not impair CTL killing, it is possible that the nucleofection procedure might have acted as a confounding factor. It would therefore be interesting to employ an alternative approach to study the effects of mitochondrial calcium flux disruption on CTL killing, for example via ruthenium red treatment (Moore, 1971) or using newly identified MCU inhibitors (De Mario et al., 2021).

Moreover, mass spectrometry analysis showed upregulation of exhaustion markers in *Usp30*<sup>-/-</sup> CTLs. Mitochondrial dysfunction and altered epigenetic modifications correlate with exhaustion phenotypes in CTLs (Desdin-Mico et al., 2020; Scharping et al., 2021; Yu et al., 2020), Epigenetics is influenced by cellular metabolism, as metabolites can alter chromatin accessibility and regulation (Franco et al., 2020). These metabolites include intermediates of the TCA cycle, which was disrupted upon loss of

USP30 due to the decrease in mitochondrial mass and function. Therefore, further investigation of *Usp30*<sup>-/-</sup> CTLs could involve metabolic and epigenetic profiling to investigate how mitochondrial depletion rewires metabolism and possibly epigenetic regulation of gene expression in effector CD8<sup>+</sup> T cells.

Lastly, the field of membrane contact sites has demonstrated that mitochondria can form physical associations with other organelles, including the ER, lysosomes, lipid droplets, peroxisomes (Valm et al., 2017) and even the nucleus (Desai et al., 2020). Mitochondria-ER contact sites have been suggested to promote memory T cell differentiation (Bantug et al., 2018). However, virtually nothing is known about contact sites in effector T cells, and it is not known whether they regulate the killing response. Given the remarkable decrease in mitochondrial abundance in *Usp30*<sup>-/-</sup> CTLs, many of these contact sites are likely to be reduced. This highlights *Usp30*<sup>-/-</sup> CTLs as a model to study organellar functions known to be regulated by physical association with mitochondria, to ask how they are affected by the absence of mitochondrial contact sites.

## **6.8 The crosstalk between mitochondria and peroxisomes**

Impaired peroxisome biogenesis in murine models can result in disrupted mitochondrial morphology (Baes and Van Veldhoven, 2012). Similarly, defective peroxisome biogenesis in humans (Zellweger's syndrome) has also been associated with defects in mitochondrial structure (Goldfischer et al., 1973). The crosstalk between mitochondria and peroxisomes is extensive and it involves several cellular pathways that can ultimately affect signalling and metabolism (Fransen et al., 2017). In addition to playing a role in ROS and lipid metabolism, mitochondria and peroxisomes share transcription factors regulating their biogenesis (PGC-1 $\alpha$ ) (Bagattin et al., 2010; Wu et al., 1999) and proteins mediating fission (FIS1, DRP1, MFF) (Gandre-Babbe and van der Blik, 2008; Koch et al., 2003; Koch et al., 2005). Of note, close physical association between mitochondria and peroxisomes has been suggested to facilitate exchange of metabolites between the two organelles (Fan et al., 2016).

In Chapter 4 I showed that *Far1* deletion in CTLs has effects extending beyond its known role as a regulator of fatty acid metabolism in peroxisomes (Cheng and Russell, 2004). FAR1 depletion resulted in a bimodal distribution of mitochondrial mass and in enhanced mitochondrial membrane potential. While the significance of these results in the context of mitochondrial and CTL function is currently unclear, this indicates that biogenesis defects are not the only peroxisomal dysfunction that can affect mitochondria. In addition, mass spectrometry analysis of doxycycline-treated CTLs

highlighted that incubation with DOX was sufficient to cause downregulation of peroxisomal proteins (ABCD3, CAT) suggesting that mitochondrial defects can also affect peroxisomal function.

These results support the existence of a crosstalk between mitochondria and peroxisomes. Furthermore, these data underscore the importance of evaluating peroxisomal function when investigating mitochondrial disruption, and vice versa. For this reason, it would be interesting to further study the effect of pharmacological inhibitors of mitochondrial protein synthesis (CAM, DOX) and mitochondria fission (mDIVI-1, M1) on peroxisomal proteins.

### **6.9 CTL nucleofection: altering T cell proteome, metabolism and beyond?**

During the course of this work I attempted to study individual mitochondrial and peroxisomal functions by using the CRISPR/Cas9 technique to delete genes involved in peroxisome biogenesis (*Pex16*), mitochondrial calcium flux (*Mcu*), mitochondrial translation (*Gtpbp10*, *Mrm2*, *Mrm3*, *Gfm1*, *Mrps16*, *Mrps22*, *Mrps35*, *Mrpl12*, *Mrpl28*, *Mrpl37*, *Mrpl48*, *Mrpl49*) and the integrated stress response (*Atf4*). The Cas9 protein, together with the scaffold tracrRNA and guide crRNA were introduced in CTLs via nucleofection, as previously described in primary human T cells (Schumann et al., 2015)

While most of these knockouts were unsuccessful, these experiments allowed the detection of a trend towards enhanced cytotoxicity in nucleofected CTLs (Chapters 4 & 5). Furthermore, I observed upregulation of granzyme B expression in both WT and *Usp30*<sup>-/-</sup> CTLs upon nucleofection (**Figure 4.18A, B; Figure 5.5B**). This evidence showed that the process of nucleofection itself, rather than the introduction of CRISPR reagents, is sufficient to rescue both the decrease in granzyme B and the loss of killing observed upon USP30 deficiency (**Figure 5.5C**). Preliminary analysis further indicated an increase in mitochondrial mass and membrane potential upon nucleofection (**Figure 5.6**). It would be tempting to speculate that the simultaneous surge in mitochondrial abundance, granzyme B expression and killing hints at a mitochondria-dependent rescue of cytotoxicity in *Usp30*<sup>-/-</sup> CTLs.

Overall, it appears that nucleofecting T cells alters key cellular functions that have a direct effect on cytotoxic potential. This could occur via a signalling pathway that responds to nucleofection and enhances cytosolic protein synthesis, which could affect mitochondrial mass, granzyme B expression and CTL killing. Alternatively, this method might be toxic to T cells, and it might result in only CTLs with high viability to survive the nucleofection procedure. In the case of *Usp30*<sup>-/-</sup>, these could be CTLs retaining functional mitochondria. It is also possible that T cells at distinct stages of activation might be differentially affected by nucleofection. If CTLs further along the process of differentiation

were more resistant to cellular stress, they would be more likely to survive, thus resulting in a post-nucleofection pool of CTLs with higher expression of cytolytic protein and enhanced killing capacity.

Taken together, these results indicate that nucleofection results in noteworthy changes in protein expression that can influence T cell effector function. Given the significant part that mitochondria play in metabolism (Chandel, 2015b), and the central role of metabolism in epigenetic control of gene expression (Franco et al., 2020), nucleofection-dependent alteration of mitochondria could have significant effects on CTL phenotypes. These results highlight the importance of comparing nucleofected CTLs to non-nucleofected samples to ensure that the phenotype of interest is not affected by the nucleofection method.

## 6.10 Outlook and concluding remarks

In recent years, mitochondria have emerged as an integral part of the complex signalling pathway regulating immune cell function. The work presented in this thesis identifies the deubiquitinase USP30 as a novel regulator of CTL cytotoxicity by counteracting degradation of mitochondria in activated CTLs. Mitochondrial depletion reduces cytosolic translation, and thus prevents *de novo* synthesis of cytolytic proteins needed to sustain the immune response. Furthermore, this work uncovered a critical role for mitochondrial protein synthesis in sustaining cytosolic translation and CTL killing.

These findings are of great relevance in the field of immunotherapy, as tuning T cell effector capacity can alter the outcome of immune responses to tumours and viral infections. As *Usp30* depletion and disruption of mitochondrial translation can both result in impaired cytosolic protein synthesis and killing, it would be interesting to test whether enhancing USP30 expression or increasing mitochondrial translation could promote CTL cytotoxicity. Conversely, in a context where an excessive immune response is damaging to surrounding tissues, USP30 expression or mitochondrial translation could be reduced to inhibit inflammation.

The importance of USP30 and mitochondrial protein synthesis is likely to extend beyond the field of immunology. USP30 is currently considered a target for the development of pharmacological treatments of Parkinson's disease, due to its involvement in PINK1/PARKIN-dependent mitophagy (Kluge et al., 2018; Rusilowicz-Jones et al., 2020; Yue et al., 2014). However, the clear link existing between mitochondrial homeostasis and cytosolic protein synthesis calls for caution, as pharmacological approaches aimed at downregulating USP30 expression might decrease cytosolic

protein synthesis, thus negatively affecting neuronal homeostasis and potentially resulting in immunodeficiency in treated patients.

Intriguingly, the disruption of mitochondrial compartments in neurons is known to negatively affect protein synthesis (Rangaraju et al., 2019; Spillane et al., 2013). While this effect has been attributed to ATP generation, several of these studies relied on mitochondrial depletion, which would also blunt mitochondrial translation. Notably, mitochondria are not necessary to sustain basal protein synthesis in neurons, but are needed to maximise translation to promote synaptic plasticity (Rangaraju et al., 2019) and axon branching (Spillane et al., 2013). It is therefore possible to draw an interesting parallel with the results of acute inhibition of mitochondrial translation in CTLs. While neither DOX nor CAM affected basal levels of granzyme B and perforin, *de novo* synthesis of cytolytic molecules was drastically reduced upon TCR stimulation. This suggests that the requirement for efficient mitochondrial translation to sustain high rates of cytosolic protein synthesis could extend beyond cells of the immune system and to other metabolically active tissue, such as cells of the nervous system.

In conclusion, the work outlined in this thesis contributes to the growing body of knowledge underscoring the importance of mitochondria in T cells. By highlighting a novel role for USP30 expression and mitochondrial translation, these findings could allow for further advancement in immunotherapy while informing basic aspects of cell biology involving the investigation of cytosolic protein synthesis, mitophagy, and organelle crosstalk.





## References

- Abdel-Hakeem, M.S., Manne, S., Beltra, J.C., Stelekati, E., Chen, Z., Nzingha, K., Ali, M.A., Johnson, J.L., Giles, J.R., Mathew, D., Greenplate, A.R., Vahedi, G., and Wherry, E.J. (2021). Epigenetic scarring of exhausted T cells hinders memory differentiation upon eliminating chronic antigenic stimulation. *Nat Immunol* 22, 1008-1019.
- Abeler-Dörner, L., Laing, A.G., Lorenc, A., Ushakov, D.S., Clare, S., Speak, A.O., Duque-Correa, M.A., White, J.K., Ramirez-Solis, R., Saran, N., Bull, K.R., Morón, B., Iwasaki, J., Barton, P.R., Caetano, S., Hng, K.I., Cambridge, E., Forman, S., Crockford, T.L., Griffiths, M., Kane, L., Harcourt, K., Brandt, C., Notley, G., Babalola, K.O., Warren, J., Mason, J.C., Meeniga, A., Karp, N.A., Melvin, D., Cawthorne, E., Weinrick, B., Rahim, A., Drissler, S., Meskas, J., Yue, A., Lux, M., Song-Zhao, G.X., Chan, A., Ballesteros Reviriego, C., Abeler, J., Wilson, H., Przemaska-Kosicka, A., Edmans, M., Strevens, N., Pasztopek, M., Meehan, T.F., Powrie, F., Brinkman, R., Dougan, G., Jacobs, W., Lloyd, C.M., Cornall, R.J., Maloy, K.J., Grecis, R.K., Griffiths, G.M., Adams, D.J., and Hayday, A.C. (2020). High-throughput phenotyping reveals expansive genetic and structural underpinnings of immune variation. *Nat Immunol* 21, 86-100.
- Adams, W.C., Chen, Y.H., Kratchmarov, R., Yen, B., Nish, S.A., Lin, W.W., Rothman, N.J., Luchsinger, L.L., Klein, U., Busslinger, M., Rathmell, J.C., Snoeck, H.W., and Reiner, S.L. (2016). Anabolism-Associated Mitochondrial Stasis Driving Lymphocyte Differentiation over Self-Renewal. *Cell Rep* 17, 3142-3152.
- Adebayo, M., Singh, S., Singh, A.P., and Dasgupta, S. (2021). Mitochondrial fusion and fission: The fine-tune balance for cellular homeostasis. *FASEB J* 35, e21620.
- Adrain, C., Murphy, B.M., and Martin, S.J. (2005). Molecular ordering of the caspase activation cascade initiated by the cytotoxic T lymphocyte/natural killer (CTL/NK) protease granzyme B. *The Journal of biological chemistry* 280, 4663-4673.
- Almeida, L., Dhillon-LaBrooy, A., Castro, C.N., Adossa, N., Carriche, G.M., Guderian, M., Lippens, S., Dennerlein, S., Hesse, C., Lambrecht, B.N., Berod, L., Schauser, L., Blazar, B.R., Kalesse, M., Muller, R., Moita, L.F., and Sparwasser, T. (2021). Ribosome-Targeting Antibiotics Impair T Cell Effector Function and Ameliorate Autoimmunity by Blocking Mitochondrial Protein Synthesis. *Immunity* 54, 68-83 e66.
- Anderson, N.S., and Haynes, C.M. (2020). Folding the Mitochondrial UPR into the Integrated Stress Response. *Trends Cell Biol* 30, 428-439.
- Anderson, P. (2008). Post-transcriptional control of cytokine production. *Nat Immunol* 9, 353-359.
- Araki, K., Morita, M., Bederman, A.G., Konieczny, B.T., Kissick, H.T., Sonenberg, N., and Ahmed, R. (2017). Translation is actively regulated during the differentiation of CD8 + effector T cells. *Nature immunology* 18, 1046-1057.
- Ardail, D., Gasnier, F., Lerme, F., Simonot, C., Louisot, P., and Gateau-Roesch, O. (1993). Involvement of mitochondrial contact sites in the subcellular compartmentalization of phospholipid biosynthetic enzymes. *J Biol Chem* 268, 25985-25992.
- Ashburner, M., Ball, C.A., Blake, J.A., Botstein, D., Butler, H., Cherry, J.M., Davis, A.P., Dolinski, K., Dwight, S.S., Eppig, J.T., Harris, M.A., Hill, D.P., Issel-Tarver, L., Kasarskis, A., Lewis, S., Matese, J.C., Richardson, J.E., Ringwald, M., Rubin, G.M., and Sherlock, G. (2000). Gene ontology: tool for the unification of biology. *The Gene Ontology Consortium. Nat Genet* 25, 25-29.
- Baes, M., and Van Veldhoven, P.P. (2012). Mouse models for peroxisome biogenesis defects and beta-oxidation enzyme deficiencies. *Bba-Mol Basis Dis* 1822, 1489-1500.
- Bagattin, A., Hugendubler, L., and Mueller, E. (2010). Transcriptional coactivator PGC-1alpha promotes peroxisomal remodeling and biogenesis. *Proc Natl Acad Sci U S A* 107, 20376-20381.
- Baixauli, F., Martin-Cofreces, N.B., Morlino, G., Carrasco, Y.R., Calabia-Linares, C., Veiga, E., Serrador, J.M., and Sanchez-Madrid, F. (2011). The mitochondrial fission factor dynamin-related protein 1 modulates T-cell receptor signalling at the immune synapse. *EMBO J* 30, 1238-1250.

- Bantug, G.R., Fischer, M., Grahlert, J., Balmer, M.L., Unterstab, G., Develioglu, L., Steiner, R., Zhang, L., Costa, A.S.H., Gubser, P.M., Burgener, A.V., Sauder, U., Loliger, J., Belle, R., Dimeloe, S., Lotscher, J., Jauch, A., Recher, M., Honger, G., Hall, M.N., Romero, P., Frezza, C., and Hess, C. (2018). Mitochondria-Endoplasmic Reticulum Contact Sites Function as Immunometabolic Hubs that Orchestrate the Rapid Recall Response of Memory CD8(+) T Cells. *Immunity* *48*, 542-555 e546.
- Barry, M., and Bleackley, R.C. (2002). Cytotoxic T lymphocytes: all roads lead to death. *Nature Reviews Immunology*.
- Basu, R., Whitlock, B.M., Husson, J., Le Floc'h, A., Jin, W., Oyler-Yaniv, A., Dotiwala, F., Giannone, G., Hivroz, C., Biais, N., Lieberman, J., Kam, L.C., and Huse, M. (2016). Cytotoxic T Cells Use Mechanical Force to Potentiate Target Cell Killing. *Cell* *165*, 100-110.
- Battersby, B.J., and Richter, U. (2013). Why translation counts for mitochondria-retrograde signalling links mitochondrial protein synthesis to mitochondrial biogenesis and cell proliferation. *Journal of Cell Science* *126*, 4331-4338.
- Baughman, J.M., Perocchi, F., Girgis, H.S., Plovanich, M., Belcher-Timme, C.A., Sancak, Y., Bao, X.R., Strittmatter, L., Goldberger, O., Bogorad, R.L., Kotliansky, V., and Mootha, V.K. (2011). Integrative genomics identifies MCU as an essential component of the mitochondrial calcium uniporter. *Nature* *476*, 341-345.
- Beckmann, B.M., Horos, R., Fischer, B., Castello, A., Eichelbaum, K., Alleaume, A.M., Schwarzl, T., Curk, T., Foehr, S., Huber, W., Krijgsveld, J., and Hentze, M.W. (2015). The RNA-binding proteomes from yeast to man harbour conserved enigmRBPs. *Nat Commun* *6*, 10127.
- Beilina, A., Van Der Brug, M., Ahmad, R., Kesavapany, S., Miller, D.W., Petsko, G.A., and Cookson, M.R. (2005). Mutations in PTEN-induced putative kinase 1 associated with recessive parkinsonism have differential effects on protein stability. *Proc Natl Acad Sci U S A* *102*, 5703-5708.
- Ben-Sahra, I., Hoxhaj, G., Ricoult, S.J.H., Asara, J.M., and Manning, B.D. (2016). mTORC1 induces purine synthesis through control of the mitochondrial tetrahydrofolate cycle. *Science* *351*, 728-733.
- Benador, I.Y., Veliova, M., Mahdaviani, K., Petcherski, A., Wikstrom, J.D., Assali, E.A., Acin-Perez, R., Shum, M., Oliveira, M.F., Cinti, S., Sztalryd, C., Barshop, W.D., Wohlschlegel, J.A., Corkey, B.E., Liesa, M., and Shirihai, O.S. (2018). Mitochondria Bound to Lipid Droplets Have Unique Bioenergetics, Composition, and Dynamics that Support Lipid Droplet Expansion. *Cell Metabolism* *27*, 869-+.
- Benjamini, Y., and Hochberg, Y. (1995). Controlling the False Discovery Rate: A Practical and Powerful Approach to Multiple Testing. *Journal of the Royal Statistical Society Series B (Methodological)* *57*, 289-300.
- Berke, G., Sullivan, K.A., and Amos, D.B. (1972). Tumor immunity in vitro: destruction of a mouse ascites tumor through a cycling pathway. *Science* *177*, 433-434.
- Bernhard, W., Haguenau, F., Gautier, A., and Oberling, C. (1952). Submicroscopical structure of cytoplasmic basophils in the liver, pancreas and salivary gland; study of ultrafine slices by electron microscope. *Z Zellforsch Mikrosk Anat* *37*, 281-300.
- Bietz, A., Zhu, H., Xue, M., and Xu, C. (2017). Cholesterol Metabolism in T Cells. *Front Immunol* *8*, 1664.
- Bingol, B., Tea, J.S., Phu, L., Reichelt, M., Bakalarski, C.E., Song, Q., Foreman, O., Kirkpatrick, D.S., and Sheng, M. (2014). The mitochondrial deubiquitinase USP30 opposes parkin-mediated mitophagy. *Nature* *510*, 370-375.
- Black, R.A., Rauch, C.T., Kozlosky, C.J., Peschon, J.J., Slack, J.L., Wolfson, M.F., Castner, B.J., Stocking, K.L., Reddy, P., Srinivasan, S., Nelson, N., Boiani, N., Schooley, K.A., Gerhart, M., Davis, R., Fitzner, J.N., Johnson, R.S., Paxton, R.J., March, C.J., and Cerretti, D.P. (1997). A metalloproteinase disintegrin that releases tumour-necrosis factor-alpha from cells. *Nature* *385*, 729-733.
- Blumenthal, R., Millard, P.J., Henkart, M.P., Reynolds, C.W., and Henkart, P.A. (1984). Liposomes as targets for granule cytolysin from cytotoxic large granular lymphocyte tumors. *Proceedings of the National Academy of Sciences* *81*, 5551-5555.
- Boos, F., Labbadia, J., and Herrmann, J.M. (2020). How the Mitoprotein-Induced Stress Response Safeguards the Cytosol: A Unified View. *Trends Cell Biol* *30*, 241-254.

- Booth, D.M., Enyedi, B., Geiszt, M., Varnai, P., and Hajnoczky, G. (2016). Redox Nanodomains Are Induced by and Control Calcium Signaling at the ER-Mitochondrial Interface. *Mol Cell* *63*, 240-248.
- Bottani, E., Cerutti, R., Harbour, M.E., Ravaglia, S., Dogan, S.A., Giordano, C., Fearnley, I.M., D'Amati, G., Viscomi, C., Fernandez-Vizarra, E., and Zeviani, M. (2017). TTC19 Plays a Husbandry Role on UQCRC1 Turnover in the Biogenesis of Mitochondrial Respiratory Complex III. *Mol Cell* *67*, 96-105 e104.
- Bowman, E.J., Siebers, A., and Altendorf, K. (1988). Bafilomycins: a class of inhibitors of membrane ATPases from microorganisms, animal cells, and plant cells. *Proc Natl Acad Sci U S A* *85*, 7972-7976.
- Braun, M.Y., Lowin, B., French, L., Acha-Orbea, H., and Tschopp, J. (1996). Cytotoxic T cells deficient in both functional fas ligand and perforin show residual cytolytic activity yet lose their capacity to induce lethal acute graft-versus-host disease. *J Exp Med* *183*, 657-661.
- Bravo, R., Vicencio, J.M., Parra, V., Troncoso, R., Munoz, J.P., Bui, M., Quiroga, C., Rodriguez, A.E., Verdejo, H.E., Ferreira, J., Iglewski, M., Chiong, M., Simmen, T., Zorzano, A., Hill, J.A., Rothermel, B.A., Szabadkai, G., and Lavandero, S. (2011). Increased ER-mitochondrial coupling promotes mitochondrial respiration and bioenergetics during early phases of ER stress. *J Cell Sci* *124*, 2143-2152.
- Breckenridge, D.G., Stojanovic, M., Marcellus, R.C., and Shore, G.C. (2003). Caspase cleavage product of BAP31 induces mitochondrial fission through endoplasmic reticulum calcium signals, enhancing cytochrome c release to the cytosol. *J Cell Biol* *160*, 1115-1127.
- Bruderer, R., Bernhardt, O.M., Gandhi, T., Miladinovic, S.M., Cheng, L.Y., Messner, S., Ehrenberger, T., Zanotelli, V., Butscheid, Y., Escher, C., Vitek, O., Rinner, O., and Reiter, L. (2015). Extending the limits of quantitative proteome profiling with data-independent acquisition and application to acetaminophen-treated three-dimensional liver microtissues. *Mol Cell Proteomics* *14*, 1400-1410.
- Buck, M.D., O'Sullivan, D., Klein Geltink, R.I., Curtis, J.D., Chang, C.H., Sanin, D.E., Qiu, J., Kretz, O., Braas, D., van der Windt, G.J., Chen, Q., Huang, S.C., O'Neill, C.M., Edelson, B.T., Pearce, E.J., Sesaki, H., Huber, T.B., Rambold, A.S., and Pearce, E.L. (2016). Mitochondrial Dynamics Controls T Cell Fate through Metabolic Programming. *Cell* *166*, 63-76.
- Buckman, J.F., Hernandez, H., Kress, G.J., Votyakova, T.V., Pal, S., and Reynolds, I.J. (2001). MitoTracker labeling in primary neuronal and astrocytic cultures: influence of mitochondrial membrane potential and oxidants. *J Neurosci Methods* *104*, 165-176.
- Burkhardt, J.K., Hester, S., Lapham, C.K., and Argon, Y. (1990). The lytic granules of natural killer cells are dual-function organelles combining secretory and pre-lysosomal compartments. *The Journal of cell biology* *111*, 2327-2340.
- Calvo, S.E., Clauser, K.R., and Mootha, V.K. (2016). MitoCarta2.0: an updated inventory of mammalian mitochondrial proteins. *Nucleic Acids Res* *44*, D1251-1257.
- Campello, S., Lacalle, R.A., Bettella, M., Mañes, S., Scorrano, L., and Viola, A. (2006). Orchestration of lymphocyte chemotaxis by mitochondrial dynamics. *The Journal of Experimental Medicine* *203*, 2879-2886.
- Cantor, J.R., Abu-Remaileh, M., Kanarek, N., Freinkman, E., Gao, X., Louissaint, A., Jr., Lewis, C.A., and Sabatini, D.M. (2017). Physiologic Medium Rewires Cellular Metabolism and Reveals Uric Acid as an Endogenous Inhibitor of UMP Synthase. *Cell* *169*, 258-272 e217.
- Cantrell, D. (2015). Signaling in lymphocyte activation. *Cold Spring Harb Perspect Biol* *7*.
- Caputo, A., Garner, R.S., Winkler, U., Hudig, D., and Bleackley, R.C. (1993). Activation of recombinant murine cytotoxic cell proteinase-1 requires deletion of an amino-terminal dipeptide. *The Journal of biological chemistry* *268*, 17672-17675.
- Carr, E.L., Kelman, A., Wu, G.S., Gopaul, R., Senkevitch, E., Aghvanyan, A., Turay, A.M., and Frauwirth, K.A. (2010). Glutamine uptake and metabolism are coordinately regulated by ERK/MAPK during T lymphocyte activation. *J Immunol* *185*, 1037-1044.
- Carswell, E.A., Old, L.J., Kassel, R.L., Green, S., Fiore, N., and Williamson, B. (1975). An endotoxin-induced serum factor that causes necrosis of tumors. *Proc Natl Acad Sci U S A* *72*, 3666-3670.

- Castello, A., Hentze, M.W., and Preiss, T. (2015). Metabolic Enzymes Enjoying New Partnerships as RNA-Binding Proteins. *Trends Endocrinol Metab* 26, 746-757.
- Castro, F., Cardoso, A.P., Goncalves, R.M., Serre, K., and Oliveira, M.J. (2018). Interferon-Gamma at the Crossroads of Tumor Immune Surveillance or Evasion. *Front Immunol* 9, 847.
- Castro, J.E., Listman, J.A., Jacobson, B.A., Wang, Y., Lopez, P.A., Ju, S., Finn, P.W., and Perkins, D.L. (1996). Fas modulation of apoptosis during negative selection of thymocytes. *Immunity* 5, 617-627.
- Chakraborty, J., von Stockum, S., Marchesan, E., Caicci, F., Ferrari, V., Rakovic, A., Klein, C., Antonini, A., Bubacco, L., and Ziviani, E. (2018). USP14 inhibition corrects an in vivo model of impaired mitophagy. *EMBO Mol Med* 10.
- Chakraborty, J., and Ziviani, E. (2020). Deubiquitinating Enzymes in Parkinson's Disease. *Front Physiol* 11, 535.
- Chan, N.C., Salazar, A.M., Pham, A.H., Sweredoski, M.J., Kolawa, N.J., Graham, R.L., Hess, S., and Chan, D.C. (2011). Broad activation of the ubiquitin-proteasome system by Parkin is critical for mitophagy. *Hum Mol Genet* 20, 1726-1737.
- Chandel, N.S. (2015a). Evolution of Mitochondria as Signaling Organelles. *Cell Metab* 22, 204-206.
- Chandel, N.S. (2015b). *Navigating metabolism* (Cold Spring Harbor, New York: Cold Spring Harbor Laboratory Press).
- Chang, C.H., Curtis, J.D., Maggi, L.B., Faubert, B., Villarino, A.V., O'Sullivan, D., Huang, S.C.C., Van Der Windt, G.J.W., Blagih, J., Qiu, J., Weber, J.D., Pearce, E.J., Jones, R.G., and Pearce, E.L. (2013). Posttranscriptional control of T cell effector function by aerobic glycolysis. *Cell* 153, 1239-1239.
- Chang, J.S., Ocvirk, S., Berger, E., Kisling, S., Binder, U., Skerra, A., Lee, A.S., and Haller, D. (2012). Endoplasmic reticulum stress response promotes cytotoxic phenotype of CD8 $\alpha\beta$ <sup>+</sup> intraepithelial lymphocytes in a mouse model for Crohn's disease-like ileitis. *J Immunol* 189, 1510-1520.
- Chen, C., Qin, H., Tang, J., Hu, Z., Tan, J., and Zeng, L. (2021). USP30 protects against oxygen-glucose deprivation/reperfusion induced mitochondrial fragmentation and ubiquitination and degradation of MFN2. *Aging (Albany NY)* 13, 6194-6204.
- Cheng, J.B., and Russell, D.W. (2004). Mammalian wax biosynthesis. I. Identification of two fatty acyl-Coenzyme A reductases with different substrate specificities and tissue distributions. *J Biol Chem* 279, 37789-37797.
- Chinnaiyan, A.M., O'Rourke, K., Tewari, M., and Dixit, V.M. (1995). FADD, a novel death domain-containing protein, interacts with the death domain of Fas and initiates apoptosis. *Cell* 81, 505-512.
- Christiansen, E.G. (1949). Orientation of the mitochondria during mitosis. *Nature* 163, 361.
- Chu, C.T., Ji, J., Dagda, R.K., Jiang, J.F., Tyurina, Y.Y., Kapralov, A.A., Tyurin, V.A., Yanamala, N., Shrivastava, I.H., Mohammadyani, D., Wang, K.Z.Q., Zhu, J., Klein-Seetharaman, J., Balasubramanian, K., Amoscato, A.A., Borisenko, G., Huang, Z., Gusdon, A.M., Cheikhi, A., Steer, E.K., Wang, R., Baty, C., Watkins, S., Bahar, I., Bayir, H., and Kagan, V.E. (2013). Cardiolipin externalization to the outer mitochondrial membrane acts as an elimination signal for mitophagy in neuronal cells. *Nat Cell Biol* 15, 1197-1205.
- Ciesla, J. (2006). Metabolic enzymes that bind RNA: yet another level of cellular regulatory network? *Acta Biochim Pol* 53, 11-32.
- Cioni, J.M., Lin, J.Q., Holtermann, A.V., Koppers, M., Jakobs, M.A.H., Azizi, A., Turner-Bridger, B., Shigeoka, T., Franze, K., Harris, W.A., and Holt, C.E. (2019). Late Endosomes Act as mRNA Translation Platforms and Sustain Mitochondria in Axons. *Cell* 176, 56-72 e15.
- Cipolat, S., de Brito, O.M., Dal Zilio, B., and Scorrano, L. (2004). OPA1 requires mitofusin 1 to promote mitochondrial fusion. *Proceedings of the National Academy of Sciences* 101, 15927-15932.
- Clark-Walker, G.D., and Linnane, A.W. (1966). In vivo differentiation of yeast cytoplasmic and mitochondrial protein synthesis with antibiotics. *Biochem Biophys Res Commun* 25, 8-13.

- Clark, R.H., Stinchcombe, J.C., Day, A., Blott, E., Booth, S., Bossi, G., Hamblin, T., Davies, E.G., and Griffiths, G.M. (2003). Adaptor protein 3-dependent microtubule-mediated movement of lytic granules to the immunological synapse. *Nat Immunol* *4*, 1111-1120.
- Cogliati, S., Enriquez, J.A., and Scorrano, L. (2016). Mitochondrial Cristae: Where Beauty Meets Functionality. *Trends Biochem Sci* *41*, 261-273.
- Collins, T.J., Berridge, M.J., Lipp, P., and Bootman, M.D. (2002). Mitochondria are morphologically and functionally heterogeneous within cells. *EMBO J* *21*, 1616-1627.
- Contento, R.L., Campello, S., Trovato, A.E., Magrini, E., Anselmi, F., and Viola, A. (2010). Adhesion shapes T cells for prompt and sustained T-cell receptor signalling. *EMBO J* *29*, 4035-4047.
- Cornelissen, T., Haddad, D., Wauters, F., Van Humbeeck, C., Mandemakers, W., Koentjoro, B., Sue, C., Gevaert, K., De Strooper, B., Verstreken, P., and Vandenberghe, W. (2014). The deubiquitinase USP15 antagonizes Parkin-mediated mitochondrial ubiquitination and mitophagy. *Human molecular genetics*.
- Corrado, M., Samardzic, D., Giacomello, M., Rana, N., Pearce, E.L., and Scorrano, L. (2021). Deletion of the mitochondria-shaping protein Opa1 during early thymocyte maturation impacts mature memory T cell metabolism. *Cell Death Differ*.
- Courtney, A.H., Lo, W.L., and Weiss, A. (2018). TCR Signaling: Mechanisms of Initiation and Propagation. *Trends Biochem Sci* *43*, 108-123.
- Couvillion, M.T., Soto, I.C., Shipkovenska, G., and Churchman, L.S. (2016). Synchronized mitochondrial and cytosolic translation programs. *Nature* *533*, 499-503.
- Craven, L., Alston, C.L., Taylor, R.W., and Turnbull, D.M. (2017). Recent Advances in Mitochondrial Disease. *Annu Rev Genomics Hum Genet* *18*, 257-275.
- Craven, P.A., and Basford, R.E. (1969). Brain hexokinase: immunohistochemical localization at the light microscopic level. *Biochemistry* *8*, 3520-3525.
- Csordas, G., Thomas, A.P., and Hajnoczky, G. (1999). Quasi-synaptic calcium signal transmission between endoplasmic reticulum and mitochondria. *Embo Journal* *18*, 96-108.
- Cunarro, J., and Weiner, M.W. (1975). Mechanism of action of agents which uncouple oxidative phosphorylation: direct correlation between proton-carrying and respiratory-releasing properties using rat liver mitochondria. *Biochim Biophys Acta* *387*, 234-240.
- Cunningham, C.N., Baughman, J.M., Phu, L., Tea, J.S., Yu, C., Coons, M., Kirkpatrick, D.S., Bingol, B., and Corn, J.E. (2015). USP30 and parkin homeostatically regulate atypical ubiquitin chains on mitochondria. *Nat Cell Biol* *17*, 160-169.
- D'Angelo, M.E., Bird, P.I., Peters, C., Reinheckel, T., Trapaniand, J.A., and Sutton, V.R. (2010). Cathepsin H is an additional convertase of pro-granzyme B. *Journal of Biological Chemistry*.
- D'Souza, A.D., Parikh, N., Kaeck, S.M., and Shadel, G.S. (2007). Convergence of multiple signaling pathways is required to coordinately up-regulate mtDNA and mitochondrial biogenesis during T cell activation. *Mitochondrion* *7*, 374-385.
- D'Souza, A.R., and Minczuk, M. (2018). Mitochondrial transcription and translation: overview. *Essays Biochem* *62*, 309-320.
- Dadsena, S., King, L.E., and Garcia-Saez, A.J. (2021). Apoptosis regulation at the mitochondria membrane level. *Biochim Biophys Acta Biomembr*, 183716.
- Dai, H., Smith, A., Meng, X.W., Schneider, P.A., Pang, Y.P., and Kaufmann, S.H. (2011). Transient binding of an activator BH3 domain to the Bak BH3-binding groove initiates Bak oligomerization. *J Cell Biol* *194*, 39-48.
- de Jong, R., Brouwer, M., Miedema, F., and van Lier, R.A. (1991). Human CD8+ T lymphocytes can be divided into CD45RA+ and CD45RO+ cells with different requirements for activation and differentiation. *J Immunol* *146*, 2088-2094.

- De Mario, A., Tosatto, A., Hill, J.M., Kriston-Vizi, J., Ketteler, R., Vecellio Reane, D., Cortopassi, G., Szabadkai, G., Rizzuto, R., and Mammucari, C. (2021). Identification and functional validation of FDA-approved positive and negative modulators of the mitochondrial calcium uniporter. *Cell Rep* 35, 109275.
- de Saint Basile, G., Menasche, G., and Fischer, A. (2010). Molecular mechanisms of biogenesis and exocytosis of cytotoxic granules. *Nat Rev Immunol* 10, 568-579.
- De Stefani, D., Raffaello, A., Teardo, E., Szabo, I., and Rizzuto, R. (2011). A forty-kilodalton protein of the inner membrane is the mitochondrial calcium uniporter. *Nature* 476, 336-340.
- Deol, K.K., Eyles, S.J., and Strieter, E.R. (2020). Quantitative Middle-Down MS Analysis of Parkin-Mediated Ubiquitin Chain Assembly. *J Am Soc Mass Spectrom* 31, 1132-1139.
- Desai, R., East, D.A., Hardy, L., Faccenda, D., Rigon, M., Crosby, J., Alvarez, M.S., Singh, A., Mainenti, M., Hussey, L.K., Bentham, R., Szabadkai, G., Zappulli, V., Dhoot, G.K., Romano, L.E., Xia, D., Coppens, I., Hamacher-Brady, A., Chapple, J.P., Abeti, R., Fleck, R.A., Vizcay-Barrena, G., Smith, K., and Campanella, M. (2020). Mitochondria form contact sites with the nucleus to couple prosurvival retrograde response. *Sci Adv* 6.
- Desdin-Mico, G., Soto-Herederó, G., Aranda, J.F., Oller, J., Carrasco, E., Gabande-Rodríguez, E., Blanco, E.M., Alfranca, A., Cusso, L., Desco, M., Ibanez, B., Gortazar, A.R., Fernandez-Marcos, P., Navarro, M.N., Hernaez, B., Alcamí, A., Baixauli, F., and Mittelbrunn, M. (2020). T cells with dysfunctional mitochondria induce multimorbidity and premature senescence. *Science* 368, 1371-1376.
- Devadas, S., Zaritskaya, L., Rhee, S.G., Oberley, L., and Williams, M.S. (2002). Discrete generation of superoxide and hydrogen peroxide by T cell receptor stimulation: selective regulation of mitogen-activated protein kinase activation and fas ligand expression. *J Exp Med* 195, 59-70.
- Diaz Arguello, O.A., and Haisma, H.J. (2021). Apoptosis-Inducing TNF Superfamily Ligands for Cancer Therapy. *Cancers (Basel)* 13.
- Didiasova, M., Schaefer, L., and Wygrecka, M. (2019). When Place Matters: Shuttling of Enolase-1 Across Cellular Compartments. *Front Cell Dev Biol* 7, 61.
- Dieckmann, N.M., Frazer, G.L., Asano, Y., Stinchcombe, J.C., and Griffiths, G.M. (2016). The cytotoxic T lymphocyte immune synapse at a glance. *J Cell Sci* 129, 2881-2886.
- Dolman, N.J., Gerasimenko, J.V., Gerasimenko, O.V., Voronina, S.G., Petersen, O.H., and Tepikin, A.V. (2005). Stable Golgi-mitochondria complexes and formation of Golgi Ca(2+) gradients in pancreatic acinar cells. *J Biol Chem* 280, 15794-15799.
- Dorrello, N.V., Peschiaroli, A., Guardavaccaro, D., Colburn, N.H., Sherman, N.E., and Pagano, M. (2006). S6K1- and betaTRCP-mediated degradation of PDCD4 promotes protein translation and cell growth. *Science* 314, 467-471.
- Douanne, T., and Griffiths, G.M. (2021). Cytoskeletal control of the secretory immune synapse. *Curr Opin Cell Biol* 71, 87-94.
- Dower, N.A., Stang, S.L., Bottorff, D.A., Ebinu, J.O., Dickie, P., Ostergaard, H.L., and Stone, J.C. (2000). RasGRP is essential for mouse thymocyte differentiation and TCR signaling. *Nat Immunol* 1, 317-321.
- Dupre, L., Houmadi, R., Tang, C., and Rey-Barroso, J. (2015). T Lymphocyte Migration: An Action Movie Starring the Actin and Associated Actors. *Front Immunol* 6, 586.
- Durcan, T.M., Kontogiannea, M., Thorarinsdottir, T., Fallon, L., Williams, A.J., Djarmati, A., Fantaneanu, T., Paulson, H.L., and Fon, E.A. (2011). The Machado-Joseph disease-associated mutant form of ataxin-3 regulates parkin ubiquitination and stability. *Hum Mol Genet* 20, 141-154.
- Durcan, T.M., Tang, M.Y., Perusse, J.R., Dashti, E.A., Aguilera, M.A., McLelland, G.L., Gros, P., Shaler, T.A., Faubert, D., Coulombe, B., and Fon, E.A. (2014). USP8 regulates mitophagy by removing K6-linked ubiquitin conjugates from parkin. *EMBO J* 33, 2473-2491.

- Ebinu, J.O., Stang, S.L., Teixeira, C., Bottorff, D.A., Hooton, J., Blumberg, P.M., Barry, M., Bleakley, R.C., Ostergaard, H.L., and Stone, J.C. (2000). RasGRP links T-cell receptor signaling to Ras. *Blood* 95, 3199-3203.
- Esensten, J.H., Helou, Y.A., Chopra, G., Weiss, A., and Bluestone, J.A. (2016). CD28 Costimulation: From Mechanism to Therapy. *Immunity* 44, 973-988.
- Fadok, V.A., Voelker, D.R., Campbell, P.A., Cohen, J.J., Bratton, D.L., and Henson, P.M. (1992). Exposure of phosphatidylserine on the surface of apoptotic lymphocytes triggers specific recognition and removal by macrophages. *J Immunol* 148, 2207-2216.
- Fan, J.J., Li, X.L., Issop, L., Culty, M., and Papadopoulos, V. (2016). ACBD2/ECI2-Mediated Peroxisome-Mitochondria Interactions in Leydig Cell Steroid Biosynthesis. *Mol Endocrinol* 30, 763-782.
- Feldmann, J., Callebaut, I., Raposo, G., Certain, S., Bacq, D., Dumont, C., Lambert, N., Ouachee-Chardin, M., Chedeville, G., Tamary, H., Minard-Colin, V., Vilmer, E., Blanche, S., Le Deist, F., Fischer, A., and de Saint Basile, G. (2003). Munc13-4 is essential for cytolytic granules fusion and is mutated in a form of familial hemophagocytic lymphohistiocytosis (FHL3). *Cell* 115, 461-473.
- Ferrick, D.A., Neilson, A., and Beeson, C. (2008). Advances in measuring cellular bioenergetics using extracellular flux. *Drug Discov Today* 13, 268-274.
- Fessler, E., Eckl, E.M., Schmitt, S., Mancilla, I.A., Meyer-Bender, M.F., Hanf, M., Philippou-Massier, J., Krebs, S., Zischka, H., and Jae, L.T. (2020). A pathway coordinated by DELE1 relays mitochondrial stress to the cytosol. *Nature* 579, 433-437.
- Fiek, C., Benz, R., Roos, N., and Brdiczka, D. (1982). Evidence for identity between the hexokinase-binding protein and the mitochondrial porin in the outer membrane of rat liver mitochondria. *Biochim Biophys Acta* 688, 429-440.
- Finco, T.S., Kadlecsek, T., Zhang, W., Samelson, L.E., and Weiss, A. (1998). LAT is required for TCR-mediated activation of PLCgamma1 and the Ras pathway. *Immunity* 9, 617-626.
- Fiorese, C.J., Schulz, A.M., Lin, Y.F., Rosin, N., Pellegrino, M.W., and Haynes, C.M. (2016). The Transcription Factor ATF5 Mediates a Mammalian Mitochondrial UPR. *Curr Biol* 26, 2037-2043.
- Fischer, M., Bantug, G.R., Dimeloe, S., Gubser, P.M., Burgener, A.-V., Grählert, J., Balmer, M.L., Develioglou, L., Steiner, R., Unterstab, G., Sauder, U., Hoenger, G., and Hess, C. (2018). Early effector maturation of naïve human CD8<sup>+</sup> T cells requires mitochondrial biogenesis. *European Journal of Immunology*.
- Franco, F., Jaccard, A., Romero, P., Yu, Y.R., and Ho, P.C. (2020). Metabolic and epigenetic regulation of T-cell exhaustion. *Nat Metab* 2, 1001-1012.
- Franke, T.F., Yang, S.I., Chan, T.O., Datta, K., Kazlauskas, A., Morrison, D.K., Kaplan, D.R., and Tschlis, P.N. (1995). The protein kinase encoded by the Akt proto-oncogene is a target of the PDGF-activated phosphatidylinositol 3-kinase. *Cell* 81, 727-736.
- Fransen, L., Van der Heyden, J., Ruyschaert, R., and Fiers, W. (1986). Recombinant tumor necrosis factor: its effect and its synergism with interferon-gamma on a variety of normal and transformed human cell lines. *Eur J Cancer Clin Oncol* 22, 419-426.
- Fransen, M., Lismont, C., and Walton, P. (2017). The Peroxisome-Mitochondria Connection: How and Why? *Int J Mol Sci* 18.
- Frauwirth, K.A., Riley, J.L., Harris, M.H., Parry, R.V., Rathmell, J.C., Plas, D.R., Elstrom, R.L., June, C.H., and Thompson, C.B. (2002). The CD28 signaling pathway regulates glucose metabolism. *Immunity* 16, 769-777.
- Freeman, G.J., Long, A.J., Iwai, Y., Bourque, K., Chernova, T., Nishimura, H., Fitz, L.J., Malenkovich, N., Okazaki, T., Byrne, M.C., Horton, H.F., Fouser, L., Carter, L., Ling, V., Bowman, M.R., Carreno, B.M., Collins, M., Wood, C.R., and Honjo, T. (2000). Engagement of the PD-1 immunoinhibitory receptor by a novel B7 family member leads to negative regulation of lymphocyte activation. *J Exp Med* 192, 1027-1034.

- Freiberg, B.A., Kupfer, H., Maslanik, W., Delli, J., Kappler, J., Zaller, D.M., and Kupfer, A. (2002). Staging and resetting T cell activation in SMACs. *Nature immunology* 3, 911-917.
- Frezza, C., Cipolat, S., Martins de Brito, O., Micaroni, M., Beznoussenko, G.V., Rudka, T., Bartoli, D., Polishuck, R.S., Danial, N.N., De Strooper, B., and Scorrano, L. (2006). OPA1 controls apoptotic cristae remodeling independently from mitochondrial fusion. *Cell* 126, 177-189.
- Friedman, J.R., Lackner, L.L., West, M., DiBenedetto, J.R., Nunnari, J., and Voeltz, G.K. (2011). ER tubules mark sites of mitochondrial division. *Science* 334, 358-362.
- Fu, H., Ward, E.J., and Marelli-Berg, F.M. (2016). Mechanisms of T cell organotropism. *Cell Mol Life Sci* 73, 3009-3033.
- Galkina, E., Tanousis, K., Preece, G., Tolaini, M., Kioussis, D., Florey, O., Haskard, D.O., Tedder, T.F., and Ager, A. (2003). L-selectin shedding does not regulate constitutive T cell trafficking but controls the migration pathways of antigen-activated T lymphocytes. *J Exp Med* 198, 1323-1335.
- Gallatin, W.M., Weissman, I.L., and Butcher, E.C. (1983). A cell-surface molecule involved in organ-specific homing of lymphocytes. *Nature* 304, 30-34.
- Gandre-Babbe, S., and van der Blik, A.M. (2008). The novel tail-anchored membrane protein Mff controls mitochondrial and peroxisomal fission in mammalian cells. *Mol Biol Cell* 19, 2402-2412.
- Garcin, E.D. (2019). GAPDH as a model non-canonical AU-rich RNA binding protein. *Semin Cell Dev Biol* 86, 162-173.
- Garewal, H.S., Ahmann, F.R., Schiffman, R.B., and Celniker, A. (1986). ATP assay: ability to distinguish cytostatic from cytotoxic anticancer drug effects. *J Natl Cancer Inst* 77, 1039-1045.
- Gasser, S.M., Daum, G., and Schatz, G. (1982). Import of proteins into mitochondria. Energy-dependent uptake of precursors by isolated mitochondria. *J Biol Chem* 257, 13034-13041.
- Gawden-Bone, C.M., Frazer, G.L., Richard, A.C., Ma, C.Y., Strege, K., and Griffiths, G.M. (2018). PIP5 Kinases Regulate Membrane Phosphoinositide and Actin Composition for Targeted Granule Secretion by Cytotoxic Lymphocytes. *Immunity* 49, 427-437 e424.
- Geigenmuller, U., and Nierhaus, K.H. (1986). Tetracycline can inhibit tRNA binding to the ribosomal P site as well as to the A site. *Eur J Biochem* 161, 723-726.
- Geiger, R., Rieckmann, J.C., Wolf, T., Basso, C., Feng, Y., Fuhrer, T., Kogadeeva, M., Picotti, P., Meissner, F., Mann, M., Zamboni, N., Sallusto, F., and Lanzavecchia, A. (2016). L-Arginine Modulates T Cell Metabolism and Enhances Survival and Anti-tumor Activity. *Cell* 167, 829-842 e813.
- Geisler, S., Holmström, K.M., Skujat, D., Fiesel, F.C., Rothfuss, O.C., Kahle, P.J., and Springer, W. (2010). PINK1/Parkin-mediated mitophagy is dependent on VDAC1 and p62/SQSTM1. *Nature cell biology* 12, 119-131.
- Gene Ontology, C. (2021). The Gene Ontology resource: enriching a GOLD mine. *Nucleic Acids Res* 49, D325-D334.
- Gersch, M., Gladkova, C., Schubert, A.F., Michel, M.A., Maslen, S., and Komander, D. (2017). Mechanism and regulation of the Lys6-selective deubiquitinase USP30. *Nature Structural and Molecular Biology*.
- Ghezzi, D., Arzuffi, P., Zordan, M., Da Re, C., Lamperti, C., Benna, C., D'Adamo, P., Diodato, D., Costa, R., Mariotti, C., Uziel, G., Smiderle, C., and Zeviani, M. (2011). Mutations in TTC19 cause mitochondrial complex III deficiency and neurological impairment in humans and flies. *Nat Genet* 43, 259-263.
- Goldfischer, S., Moore, C.L., Johnson, A.B., Spiro, A.J., Valsamis, M.P., Wisniewski, H.K., Ritch, R.H., Norton, W.T., Rapin, I., and Gartner, L.M. (1973). Peroxisomal and Mitochondrial Defects in Cerebro-Hepato-Renal Syndrome. *Science* 182, 62-64.
- Golstein, P., and Griffiths, G.M. (2018). An early history of T cell-mediated cytotoxicity. *Nat Rev Immunol* 18, 527-535.

- Gordaliza-Alaguero, I., Canto, C., and Zorzano, A. (2019). Metabolic implications of organelle-mitochondria communication. *Embo Reports* 20.
- Gots, R.E., and Bessman, S.P. (1974). The functional compartmentation of mitochondrial hexokinase. *Arch Biochem Biophys* 163, 7-14.
- Gray, S.M., Kaech, S.M., and Staron, M.M. (2014). The interface between transcriptional and epigenetic control of effector and memory CD8(+) T-cell differentiation. *Immunol Rev* 261, 157-168.
- Grayson, J.M., Laniewski, N.G., Lanier, J.G., and Ahmed, R. (2003). Mitochondrial potential and reactive oxygen intermediates in antigen-specific CD8+ T cells during viral infection. *J Immunol* 170, 4745-4751.
- Greene, A.W., Grenier, K., Aguilera, M.A., Muise, S., Farazifard, R., Haque, M.E., McBride, H.M., Park, D.S., and Fon, E.A. (2012). Mitochondrial processing peptidase regulates PINK1 processing, import and Parkin recruitment. *EMBO Rep* 13, 378-385.
- Griffiths, G.M., and Isaza, S. (1993). Granzymes A and B are targeted to the lytic granules of lymphocytes by the mannose-6-phosphate receptor. *Journal of Cell Biology*.
- Grou, C.P., Francisco, T., Rodrigues, T.A., Freitas, M.O., Pinto, M.P., Carvalho, A.F., Domingues, P., Wood, S.A., Rodriguez-Borges, J.E., Sa-Miranda, C., Fransen, M., and Azevedo, J.E. (2012). Identification of ubiquitin-specific protease 9X (USP9X) as a deubiquitinase acting on ubiquitin-peroxin 5 (PEX5) thioester conjugate. *J Biol Chem* 287, 12815-12827.
- Gubser, P.M., Bantug, G.R., Razik, L., Fischer, M., Dimeloe, S., Hoenger, G., Durovic, B., Jauch, A., and Hess, C. (2013). Rapid effector function of memory CD8+ T cells requires an immediate-early glycolytic switch. *Nat Immunol* 14, 1064-1072.
- Guo, X., Aviles, G., Liu, Y., Tian, R., Unger, B.A., Lin, Y.-H.T., Wiita, A.P., Xu, K., Correia, M.A., and Kampmann, M. (2020). Mitochondrial stress is relayed to the cytosol by an OMA1–DELE1–HRI pathway. *Nature*.
- Gustafsson, C.M., Falkenberg, M., and Larsson, N.G. (2016). Maintenance and Expression of Mammalian Mitochondrial DNA. *Annu Rev Biochem* 85, 133-160.
- Hackenbrock, C.R. (1966). Ultrastructural bases for metabolically linked mechanical activity in mitochondria. I. Reversible ultrastructural changes with change in metabolic steady state in isolated liver mitochondria. *J Cell Biol* 30, 269-297.
- Haddad, E.K., Wu, X., Hammer, J.A., 3rd, and Henkart, P.A. (2001). Defective granule exocytosis in Rab27a-deficient lymphocytes from Ashen mice. *J Cell Biol* 152, 835-842.
- Haghighat, A., Mader, S., Pause, A., and Sonenberg, N. (1995). Repression of cap-dependent translation by 4E-binding protein 1: competition with p220 for binding to eukaryotic initiation factor-4E. *EMBO J* 14, 5701-5709.
- Harding, F.A., and Allison, J.P. (1993). CD28-B7 interactions allow the induction of CD8+ cytotoxic T lymphocytes in the absence of exogenous help. *J Exp Med* 177, 1791-1796.
- Harding, F.A., McArthur, J.G., Gross, J.A., Raulet, D.H., and Allison, J.P. (1992). CD28-mediated signalling co-stimulates murine T cells and prevents induction of anergy in T-cell clones. *Nature* 356, 607-609.
- Harding, H.P., Novoa, I., Zhang, Y., Zeng, H., Wek, R., Schapira, M., and Ron, D. (2000). Regulated translation initiation controls stress-induced gene expression in mammalian cells. *Mol Cell* 6, 1099-1108.
- Harding, H.P., Zhang, Y., Zeng, H., Novoa, I., Lu, P.D., Calfon, M., Sadri, N., Yun, C., Popko, B., Paules, R., Stojdl, D.F., Bell, J.C., Hettmann, T., Leiden, J.M., and Ron, D. (2003). An integrated stress response regulates amino acid metabolism and resistance to oxidative stress. *Mol Cell* 11, 619-633.
- Hedekov, C.J. (1968). Early effects of phytohaemagglutinin on glucose metabolism of normal human lymphocytes. *Biochem J* 110, 373-380.

- Heytler, P.G., and Prichard, W.W. (1962). A new class of uncoupling agents--carbonyl cyanide phenylhydrazones. *Biochem Biophys Res Commun* 7, 272-275.
- Holt, O., Kanno, E., Bossi, G., Booth, S., Daniele, T., Santoro, A., Arico, M., Saegusa, C., Fukuda, M., and Griffiths, G.M. (2008). Slp1 and Slp2-a localize to the plasma membrane of CTL and contribute to secretion from the immunological synapse. *Traffic* 9, 446-457.
- Holz, M.K., Ballif, B.A., Gygi, S.P., and Blenis, J. (2005). mTOR and S6K1 mediate assembly of the translation preinitiation complex through dynamic protein interchange and ordered phosphorylation events. *Cell* 123, 569-580.
- Honsho, M., Tamura, S., Shimozawa, N., Suzuki, Y., Kondo, N., and Fujiki, Y. (1998). Mutation in PEX16 is causal in the peroxisome-deficient Zellweger syndrome of complementation group D. *Am J Hum Genet* 63, 1622-1630.
- Hoth, M., Button, D.C., and Lewis, R.S. (2000). Mitochondrial control of calcium-channel gating: a mechanism for sustained signaling and transcriptional activation in T lymphocytes. *Proc Natl Acad Sci U S A* 97, 10607-10612.
- Hoth, M., Fanger, C.M., and Lewis, R.S. (1997). Mitochondrial regulation of store-operated calcium signaling in T lymphocytes. *J Cell Biol* 137, 633-648.
- Houtkooper, R.H., Mouchiroud, L., Ryu, D., Moullan, N., Katsyuba, E., Knott, G., Williams, R.W., and Auwerx, J. (2013). Mitonuclear protein imbalance as a conserved longevity mechanism. *Nature* 497, 451-457.
- Howden, A.J.M., Hukelmann, J.L., Brenes, A., Spinelli, L., Sinclair, L.V., Lamond, A.I., and Cantrell, D.A. (2019). Quantitative analysis of T cell proteomes and environmental sensors during T cell differentiation. *Nat Immunol* 20, 1542-1554.
- Hukelmann, J.L., Anderson, K.E., Sinclair, L.V., Grzes, K.M., Murillo, A.B., Hawkins, P.T., Stephens, L.R., Lamond, A.I., and Cantrell, D.A. (2016). The cytotoxic T cell proteome and its shaping by the kinase mTOR. *Nat Immunol* 17, 104-112.
- Imboden, J.B., and Stobo, J.D. (1985). Transmembrane signalling by the T cell antigen receptor. Perturbation of the T3-antigen receptor complex generates inositol phosphates and releases calcium ions from intracellular stores. *The Journal of experimental medicine* 161, 446-456.
- Isaaz, S., Baetz, K., Olsen, K., Podack, E., and Griffiths, G.M. (1995). Serial killing by cytotoxic T lymphocytes: T cell receptor triggers degranulation, re-filling of the lytic granules and secretion of lytic proteins via a non-granule pathway. *European Journal of Immunology* 25, 1071-1079.
- Jacobs, S.R., Herman, C.E., Maciver, N.J., Wofford, J.A., Wieman, H.L., Hammen, J.J., and Rathmell, J.C. (2008). Glucose uptake is limiting in T cell activation and requires CD28-mediated Akt-dependent and independent pathways. *J Immunol* 180, 4476-4486.
- Jain, J., McCaffrey, P.G., Miner, Z., Kerppola, T.K., Lambert, J.N., Verdine, G.L., Curran, T., and Rao, A. (1993). The T-cell transcription factor NFATp is a substrate for calcineurin and interacts with Fos and Jun. *Nature* 365, 352-355.
- Jenkins, M.K., and Schwartz, R.H. (1987). Antigen presentation by chemically modified splenocytes induces antigen-specific T cell unresponsiveness in vitro and in vivo. *The Journal of Experimental Medicine*.
- Jenkins, M.R., Tsun, A., Stinchcombe, J.C., and Griffiths, G.M. (2009). The strength of T cell receptor signal controls the polarization of cytotoxic machinery to the immunological synapse. *Immunity* 31, 621-631.
- Jin, S.M., Lazarou, M., Wang, C., Kane, L.A., Narendra, D.P., and Youle, R.J. (2010). Mitochondrial membrane potential regulates PINK1 import and proteolytic destabilization by PARL. *Journal of Cell Biology*.
- Jinek, M., Chylinski, K., Fonfara, I., Hauer, M., Doudna, J.A., and Charpentier, E. (2012). A programmable dual-RNA-guided DNA endonuclease in adaptive bacterial immunity. *Science* 337, 816-821.
- Joffre, O.P., Segura, E., Savina, A., and Amigorena, S. (2012). Cross-presentation by dendritic cells. *Nat Rev Immunol* 12, 557-569.

- June, C.H., Ledbetter, J.A., Gillespie, M.M., Lindsten, T., and Thompson, C.B. (1987). T-cell proliferation involving the CD28 pathway is associated with cyclosporine-resistant interleukin 2 gene expression. *Molecular and cellular biology* 7, 4472-4481.
- Jung, T.M., Gallatin, W.M., Weissman, I.L., and Dailey, M.O. (1988). Down-regulation of homing receptors after T cell activation. *J Immunol* 141, 4110-4117.
- Kaech, S.M., Hemby, S., Kersh, E., and Ahmed, R. (2002). Molecular and functional profiling of memory CD8 T cell differentiation. *Cell* 111, 837-851.
- Kane, K.P., Sherman, L.A., and Mescher, M.F. (1989). Molecular interactions required for triggering alloantigen-specific cytolytic T lymphocytes. *Journal of immunology (Baltimore, Md : 1950)* 142, 4153-4160.
- Kataoka, T., Takaku, K., Magae, J., Shinohara, N., Takayama, H., Kondo, S., and Nagai, K. (1994). Acidification is essential for maintaining the structure and function of lytic granules of CTL. Effect of concanamycin A, an inhibitor of vacuolar type H(+)-ATPase, on CTL-mediated cytotoxicity. *Journal of immunology (Baltimore, Md : 1950)* 153, 3938-3947.
- Kaupilla, J.H.K., Baines, H.L., Bratic, A., Larsson, N.-G.R., Greaves, L.C., and Correspondence, J.B.S. (2016). A Phenotype-Driven Approach to Generate Mouse Models with Pathogenic mtDNA Mutations Causing Mitochondrial Disease. *Cell Reports* 16, 2980-2990.
- Keij, J.F., Bell-Prince, C., and Steinkamp, J.A. (2000). Staining of mitochondrial membranes with 10-nonyl acridine orange, MitoFluor Green, and MitoTracker Green is affected by mitochondrial membrane potential altering drugs. *Cytometry* 39, 203-210.
- Khan, N.A., Nikkanen, J., Yatsuga, S., Jackson, C., Wang, L., Pradhan, S., Kivela, R., Pessia, A., Velagapudi, V., and Suomalainen, A. (2017). mTORC1 Regulates Mitochondrial Integrated Stress Response and Mitochondrial Myopathy Progression. *Cell Metab* 26, 419-428 e415.
- Kidani, Y., Elsaesser, H., Hock, M.B., Vergnes, L., Williams, K.J., Argus, J.P., Marbois, B.N., Komisopoulou, E., Wilson, E.B., Osborne, T.F., Graeber, T.G., Reue, K., Brooks, D.G., and Bensinger, S.J. (2013). Sterol regulatory element-binding proteins are essential for the metabolic programming of effector T cells and adaptive immunity. *Nat Immunol* 14, 489-499.
- Kim, H., Rafiuddin-Shah, M., Tu, H.C., Jeffers, J.R., Zambetti, G.P., Hsieh, J.J., and Cheng, E.H. (2006a). Hierarchical regulation of mitochondrion-dependent apoptosis by BCL-2 subfamilies. *Nat Cell Biol* 8, 1348-1358.
- Kim, H.E., Grant, A.R., Simic, M.S., Kohnz, R.A., Nomura, D.K., Durieux, J., Riera, C.E., Sanchez, M., Kapernick, E., Wolff, S., and Dillin, A. (2016). Lipid Biosynthesis Coordinates a Mitochondrial-to-Cytosolic Stress Response. *Cell* 166, 1539-1552 e1516.
- Kim, P.K., Mullen, R.T., Schumann, U., and Lippincott-Schwartz, J. (2006b). The origin and maintenance of mammalian peroxisomes involves a de novo PEX16-dependent pathway from the ER. *J Cell Biol* 173, 521-532.
- Kincaid, R.L., Takayama, H., Billingsley, M.L., and Sitkovsky, M.V. (1987). Differential expression of calmodulin-binding proteins in B, T lymphocytes and thymocytes. *Nature* 330, 176-178.
- Kitada, T., Asakawa, S., Hattori, N., Matsumine, H., Yamamura, Y., Minoshima, S., Yokochi, M., Mizuno, Y., and Shimizu, N. (1998). Mutations in the parkin gene cause autosomal recessive juvenile parkinsonism. *Nature* 392, 605-608.
- Kleele, T., Rey, T., Winter, J., Zaganelli, S., Mahecic, D., Perreten Lambert, H., Ruberto, F.P., Nemir, M., Wai, T., Pedrazzini, T., and Manley, S. (2021). Distinct fission signatures predict mitochondrial degradation or biogenesis. *Nature*.
- Klein Geltink, R.I., O'Sullivan, D., Corrado, M., Bremser, A., Buck, M.D., Buescher, J.M., Firat, E., Zhu, X., Niedermann, G., Caputa, G., Kelly, B., Warthorst, U., Rensing-Ehl, A., Kyle, R.L., Vandersarren, L., Curtis, J.D., Patterson, A.E., Lawless, S., Grzes, K., Qiu, J., Sanin, D.E., Kretz, O., Huber, T.B., Janssens, S., Lambrecht, B.N., Rambold, A.S., Pearce, E.J., and Pearce, E.L. (2017). Mitochondrial Priming by CD28. *Cell* 171, 385-397 e311.
- Klein, L., Kyewski, B., Allen, P.M., and Hogquist, K.A. (2014). Positive and negative selection of the T cell repertoire: what thymocytes see (and don't see). *Nat Rev Immunol* 14, 377-391.

Klionsky, D.J., Abdel-Aziz, A.K., Abdelfatah, S., Abdellatif, M., Abdoli, A., Abel, S., Abeliovich, H., Abildgaard, M.H., Abudu, Y.P., Acevedo-Arozena, A., Adamopoulos, I.E., Adeli, K., Adolph, T.E., Adornetto, A., Aflaki, E., Agam, G., Agarwal, A., Aggarwal, B.B., Agnello, M., Agostinis, P., Agrewala, J.N., Agrotis, A., Aguilar, P.V., Ahmad, S.T., Ahmed, Z.M., Ahumada-Castro, U., Aits, S., Aizawa, S., Akkoc, Y., Akoumianaki, T., Akpinar, H.A., Al-Abd, A.M., Al-Akra, L., Al-Gharaibeh, A., Alaoui-Jamali, M.A., Alberti, S., Alcocer-Gomez, E., Alessandri, C., Ali, M., Alim Al-Bari, M.A., Aliwaini, S., Alizadeh, J., Almacellas, E., Almasan, A., Alonso, A., Alonso, G.D., Altan-Bonnet, N., Altieri, D.C., Alvarez, E.M.C., Alves, S., Alves da Costa, C., Alzaharna, M.M., Amadio, M., Amantini, C., Amaral, C., Ambrosio, S., Amer, A.O., Ammanathan, V., An, Z., Andersen, S.U., Andrabi, S.A., Andrade-Silva, M., Andres, A.M., Angelini, S., Ann, D., Anozie, U.C., Ansari, M.Y., Antas, P., Antebi, A., Anton, Z., Anwar, T., Apetoh, L., Apostolova, N., Araki, T., Araki, Y., Arasaki, K., Araujo, W.L., Araya, J., Arden, C., Arevalo, M.A., Arguelles, S., Arias, E., Arikath, J., Arimoto, H., Ariosa, A.R., Armstrong-James, D., Arnaune-Pelloquin, L., Aroca, A., Arroyo, D.S., Arsov, I., Artero, R., Asaro, D.M.L., Aschner, M., Ashrafzadeh, M., Ashur-Fabian, O., Atanasov, A.G., Au, A.K., Auberger, P., Auner, H.W., Aurelian, L., Autelli, R., Avagliano, L., Avalos, Y., Aveic, S., Aveleira, C.A., Avin-Wittenberg, T., Aydin, Y., Ayton, S., Ayyadevara, S., Azzopardi, M., Baba, M., Backer, J.M., Backues, S.K., Bae, D.H., Bae, O.N., Bae, S.H., Baehrecke, E.H., Baek, A., Baek, S.H., Baek, S.H., Bagetta, G., Bagniewska-Zadworna, A., Bai, H., Bai, J., Bai, X., Bai, Y., Bairagi, N., Baksi, S., Balbi, T., Baldari, C.T., Balduini, W., Ballabio, A., Ballester, M., Balazadeh, S., Balzan, R., Bandopadhyay, R., Banerjee, S., Banerjee, S., Banreti, A., Bao, Y., Baptista, M.S., Baracca, A., Barbati, C., Bargiela, A., Barila, D., Barlow, P.G., Barmada, S.J., Barreiro, E., Barreto, G.E., Bartek, J., Bartel, B., Bartolome, A., Barve, G.R., Basagoudanavar, S.H., Bassham, D.C., Bast, R.C., Jr., Basu, A., Batoko, H., Batten, I., Baulieu, E.E., Baumgarner, B.L., Bayry, J., Beale, R., Beau, I., Beaumatin, F., Bechara, L.R.G., Beck, G.R., Jr., Beers, M.F., Begun, J., Behrends, C., Behrens, G.M.N., Bei, R., Bejarano, E., Bel, S., Behl, C., Belaid, A., Belgareh-Touze, N., Bellarosa, C., Belleudi, F., Bello Perez, M., Bello-Morales, R., Beltran, J.S.O., Beltran, S., Benbrook, D.M., Bendorius, M., Benitez, B.A., Benito-Cuesta, I., Bensalem, J., Berchtold, M.W., Berezowska, S., Bergamaschi, D., Bergami, M., Bergmann, A., Berliocchi, L., Berlioz-Torrent, C., Bernard, A., Berthoux, L., Besirli, C.G., Besteiro, S., Betin, V.M., Beyaert, R., Bezbradica, J.S., Bhaskar, K., Bhatia-Kissova, I., Bhattacharya, R., Bhattacharya, S., Bhattacharyya, S., Bhuiyan, M.S., Bhutia, S.K., Bi, L., Bi, X., Biden, T.J., Bijian, K., Billes, V.A., Binart, N., Bincchetto, C., Birgisdottir, A.B., Bjorkoy, G., Blanco, G., Blas-Garcia, A., Blasiak, J., Blomgran, R., Blomgren, K., Blum, J.S., Boada-Romero, E., Boban, M., Boesze-Battaglia, K., Boeuf, P., Boland, B., Bomont, P., Bonaldo, P., Bonam, S.R., Bonfili, L., Bonifacino, J.S., Boone, B.A., Bootman, M.D., Bordi, M., Borner, C., Bornhauser, B.C., Borthakur, G., Bosch, J., Bose, S., Botana, L.M., Botas, J., Boulanger, C.M., Boulton, M.E., Bourdenx, M., Bourgeois, B., Bourke, N.M., Bousquet, G., Boya, P., Bozhkov, P.V., Bozi, L.H.M., Bozkurt, T.O., Brackney, D.E., Brandts, C.H., Braun, R.J., Braus, G.H., Bravo-Sagua, R., Bravo-San Pedro, J.M., Brest, P., Bringer, M.A., Briones-Herrera, A., Broaddus, V.C., Brodersen, P., Brodsky, J.L., Brody, S.L., Bronson, P.G., Bronstein, J.M., Brown, C.N., Brown, R.E., Brum, P.C., Brumell, J.H., Brunetti-Pierri, N., Bruno, D., Bryson-Richardson, R.J., Bucci, C., Buchrieser, C., Bueno, M., Buitrago-Molina, L.E., Buraschi, S., Buch, S., Buchan, J.R., Buckingham, E.M., Budak, H., Budini, M., Bultynck, G., Burada, F., Burgoyne, J.R., Buron, M.I., Bustos, V., Buttner, S., Butturini, E., Byrd, A., Cabas, I., Cabrera-Benitez, S., Cadwell, K., Cai, J., Cai, L., Cai, Q., Cairo, M., Calbet, J.A., Caldwell, G.A., Caldwell, K.A., Call, J.A., Calvani, R., Calvo, A.C., Calvo-Rubio Barrera, M., Camara, N.O., Camonis, J.H., Camougrand, N., Campanella, M., Campbell, E.M., Campbell-Valois, F.X., Campello, S., Campesi, I., Campos, J.C., Camuzard, O., Cancino, J., Candido de Almeida, D., Canesi, L., Caniggia, I., Canonico, B., Canti, C., Cao, B., Caraglia, M., Carames, B., Carchman, E.H., Cardenal-Munoz, E., Cardenas, C., Cardenas, L., Cardoso, S.M., Carew, J.S., Carle, G.F., Carleton, G., Carloni, S., Carmona-Gutierrez, D., Carneiro, L.A., Carnevali, O., Carosi, J.M., Carra, S., Carrier, A., Carrier, L., Carroll, B., Carter, A.B., Carvalho, A.N., Casanova, M., Casas, C., Casas, J., Cassioli, C., Castillo, E.F., Castillo, K., Castillo-Lluva, S., Castoldi, F., Castori, M., Castro, A.F., Castro-Caldas, M., Castro-Hernandez, J., Castro-Obregon, S., Catz, S.D., Cavadas, C., Cavaliere, F., Cavallini, G., Cavinato, M., Cayuela, M.L., Cebollada Rica, P., Cecarini, V., Cecconi, F., Cechowska-Pasko, M., Cenci, S., Ceperuelo-Mallafre, V., Cerqueira, J.J., Cerutti, J.M., Cervia, D., Cetintas, V.B., Cetrullo, S., Chae, H.J., Chagin, A.S., Chai, C.Y., Chakrabarti, G., Chakrabarti, O., Chakraborty, T., Chakraborty, T., Chami, M., Chamilos, G., Chan, D.W., Chan, E.Y.W., Chan, E.D., Chan, H.Y.E., Chan, H.H., Chan, H., Chan, M.T.V., Chan, Y.S., Chandra, P.K., Chang, C.P., Chang, C., Chang, H.C., Chang, K., Chao, J., Chapman, T., Charlet-Berguerand, N., Chatterjee, S., Chaube, S.K., Chaudhary, A., Chauhan, S., Chaum, E., Checler, F., Cheetham, M.E., Chen, C.S., Chen, G.C., Chen, J.F., Chen, L.L., Chen, L., Chen, L., Chen, M., Chen, M.K., Chen, N., Chen, Q., Chen, R.H., Chen, S., Chen, W., Chen, W., Chen, X.M., Chen, X.W., Chen, X., Chen, Y., Chen, Y.G., Chen, Y., Chen, Y., Chen, Y.J., Chen, Y.Q., Chen, Z.S., Chen, Z., Chen, Z.H., Chen, Z.J., Chen, Z., Cheng, H., Cheng, J., Cheng, S.Y., Cheng, W., Cheng, X., Cheng, X.T., Cheng, Y., Cheng, Z., Chen, Z., Cheong, H., Cheong, J.K., Chernyak, B.V., Cherry, S., Cheung, C.F.R., Cheung, C.H.A., Cheung, K.H., Chevet, E., Chi, R.J., Chiang, A.K.S., Chiaradonna, F., Chiarelli, R., Chiariello, M., Chica, N., Chiocca, S., Chiong, M., Chiou, S.H., Chiramel, A.I., Chiurciu, V., Cho, D.H., Choe, S.K., Choi, A.M.K., Choi, M.E., Choudhury, K.R., Chow, N.S., Chu, C.T., Chua, J.P., Chua, J.J.E., Chung, H., Chung, K.P., Chung, S., Chung, S.H., Chung, Y.L., Cianfanelli, V., Ciechomska, I.A., Cifuentes, M., Cinque, L., Cirak, S., Cirone, M., Clague, M.J., Clarke, R., Clementi, E., Coccia, E.M., Codogno, P., Cohen, E., Cohen, M.M., Colasanti, T., Colasuonno, F., Colbert, R.A., Colell, A., Colic, M., Coll, N.S., Collins, M.O., Colombo, M.I., Colon-Ramos, D.A., Combaret, L., Comincini, S., Cominetti, M.R., Consiglio, A., Conte, A., Conti, F., Contu, V.R., Cookson, M.R., Coombs, K.M., Coppens, I., Corasaniti, M.T., Corkery, D.P., Cordes, N., Cortese, K., Costa, M.D.C., Costantino, S., Costelli, P., Coto-

Montes, A., Crack, P.J., Crespo, J.L., Criollo, A., Crippa, V., Cristofani, R., Csizmadia, T., Cuadrado, A., Cui, B., Cui, J., Cui, Y., Cui, Y., Culetto, E., Cumino, A.C., Cybulsky, A.V., Czaja, M.J., Czuczwar, S.J., D'Adamo, S., D'Amelio, M., D'Arcangelo, D., D'Lugos, A.C., D'Orazi, G., da Silva, J.A., Dafsari, H.S., Dagda, R.K., Dagdas, Y., Daglia, M., Dai, X., Dai, Y., Dai, Y., Dal Col, J., Dalhaimer, P., Dalla Valle, L., Dallenga, T., Dalmasso, G., Damme, M., Dando, I., Dantuma, N.P., Darling, A.L., Das, H., Dasarathy, S., Dasari, S.K., Dash, S., Daumke, O., Dauphinee, A.N., Davies, J.S., Davila, V.A., Davis, R.J., Davis, T., Dayalan Naidu, S., De Amicis, F., De Bosscher, K., De Felice, F., De Franceschi, L., De Leonibus, C., de Mattos Barbosa, M.G., De Meyer, G.R.Y., De Milito, A., De Nunzio, C., De Palma, C., De Santi, M., De Virgilio, C., De Zio, D., Debnath, J., DeBosch, B.J., Decuypere, J.P., Deehan, M.A., Deflorian, G., DeGregori, J., Dehay, B., Del Rio, G., Delaney, J.R., Delbridge, L.M.D., Delorme-Axford, E., Delpino, M.V., Demarchi, F., Dembitz, V., Demers, N.D., Deng, H., Deng, Z., Dengjel, J., Dent, P., Denton, D., DePamphilis, M.L., Der, C.J., Deretic, V., Descoteaux, A., Devis, L., Devkota, S., Devuyt, O., Dewson, G., Dharmasivam, M., Dhiman, R., di Bernardo, D., Di Cristina, M., Di Domenico, F., Di Fazio, P., Di Fonzo, A., Di Guardo, G., Di Guglielmo, G.M., Di Leo, L., Di Malta, C., Di Nardo, A., Di Rienzo, M., Di Sano, F., Diallinas, G., Diao, J., Diaz-Araya, G., Diaz-Laviada, I., Dickinson, J.M., Diederich, M., Dieude, M., Dikic, I., Ding, S., Ding, W.X., Dini, L., Dinic, J., Dinic, M., Dinkova-Kostova, A.T., Dionne, M.S., Distler, J.H.W., Diwan, A., Dixon, I.M.C., Djavaheri-Mergny, M., Dobrinski, I., Dobrovinskaya, O., Dobrowolski, R., Dobson, R.C.J., Dokic, J., Dokmeci Emre, S., Donadelli, M., Dong, B., Dong, X., Dong, Z., Dorn, G.W., Dotsch, V., Dou, H., Dou, J., Dowaidar, M., Dridi, S., Drucker, L., Du, A., Du, C., Du, G., Du, H.N., Du, L.L., du Toit, A., Duan, S.B., Duan, X., Duarte, S.P., Dubrovskaya, A., Dunlop, E.A., Dupont, N., Duran, R.V., Dwarakanath, B.S., Dyshlovoy, S.A., Ebrahimi-Fakhari, D., Eckhart, L., Edelstein, C.L., Efferth, T., Eftekharpour, E., Eichinger, L., Eid, N., Eisenberg, T., Eissa, N.T., Eissa, S., Ejarque, M., El Andaloussi, A., El-Hage, N., El-Naggar, S., Eleuteri, A.M., El-Shafey, E.S., Elgendy, M., Eliopoulos, A.G., Elizalde, M.M., Elks, P.M., Elsasser, H.P., Elsherbiny, E.S., Emerling, B.M., Emre, N.C.T., Eng, C.H., Engedal, N., Engelbrecht, A.M., Engelsen, A.S.T., Enserink, J.M., Escalante, R., Esclatine, A., Escobar-Henriques, M., Eskelinen, E.L., Espert, L., Eusebio, M.O., Fabrias, G., Fabrizi, C., Facchiano, A., Facchiano, F., Fadeel, B., Fader, C., Faesen, A.C., Fairlie, W.D., Falco, A., Falkenburger, B.H., Fan, D., Fan, J., Fan, Y., Fang, E.F., Fang, Y., Fang, Y., Fanto, M., Farfel-Becker, T., Faure, M., Fazeli, G., Fedele, A.O., Feldman, A.M., Feng, D., Feng, J., Feng, L., Feng, Y., Feng, Y., Feng, W., Fenz Araujo, T., Ferguson, T.A., Fernandez, A.F., Fernandez-Checa, J.C., Fernandez-Veledo, S., Fernie, A.R., Ferrante, A.W., Jr., Ferraresi, A., Ferrari, M.F., Ferreira, J.C.B., Ferro-Novick, S., Figueras, A., Filadi, R., Filigheddu, N., Filippi-Chiela, E., Filomeni, G., Fimia, G.M., Fineschi, V., Finetti, F., Finkbeiner, S., Fisher, E.A., Fisher, P.B., Flamigni, F., Fliesler, S.J., Flo, T.H., Florance, I., Florey, O., Florio, T., Fodor, E., Follo, C., Fon, E.A., Forlino, A., Fornai, F., Fortini, P., Fracassi, A., Fraldi, A., Franco, B., Franco, R., Franconi, F., Frankel, L.B., Friedman, S.L., Frohlich, L.F., Fruhbeck, G., Fuentes, J.M., Fujiki, Y., Fujita, N., Fujiwara, Y., Fukuda, M., Fulda, S., Furic, L., Furuya, N., Fusco, C., Gack, M.U., Gaffke, L., Galadari, S., Galasso, A., Galindo, M.F., Gallolu Kankanamalage, S., Galluzzi, L., Galy, V., Gammoh, N., Gan, B., Ganley, I.G., Gao, F., Gao, H., Gao, M., Gao, P., Gao, S.J., Gao, W., Gao, X., Garcera, A., Garcia, M.N., Garcia, V.E., Garcia-Del Portillo, F., Garcia-Escudero, V., Garcia-Garcia, A., Garcia-Macia, M., Garcia-Moreno, D., Garcia-Ruiz, C., Garcia-Sanz, P., Garg, A.D., Gargini, R., Garofalo, T., Garry, R.F., Gassen, N.C., Gatica, D., Ge, L., Ge, W., Geiss-Friedlander, R., Gelfi, C., Genschik, P., Gentle, I.E., Gerbino, V., Gerhardt, C., Germain, K., Germain, K., Gewirtz, D.A., Ghasemipour Afshar, E., Ghavami, S., Ghigo, A., Ghosh, M., Giamas, G., Giampietri, C., Giatromanolaki, A., Gibson, G.E., Gibson, S.B., Ginot, V., Giniger, E., Giorgi, C., Girao, H., Girardin, S.E., Giridharan, M., Giuliano, S., Giulivi, C., Giuriato, S., Giustiniani, J., Gluschko, A., Goder, V., Goginashvili, A., Golab, J., Goldstone, D.C., Golebiewska, A., Gomes, L.R., Gomez, R., Gomez-Sanchez, R., Gomez-Puerto, M.C., Gomez-Sintes, R., Gong, Q., Goni, F.M., Gonzalez-Gallego, J., Gonzalez-Hernandez, T., Gonzalez-Polo, R.A., Gonzalez-Reyes, J.A., Gonzalez-Rodriguez, P., Goping, I.S., Gorbatyuk, M.S., Gorbunov, N.V., Gorgulu, K., Gorjod, R.M., Gorski, S.M., Goruppi, S., Gotor, C., Gottlieb, R.A., Gozes, I., Gozuacik, D., Graef, M., Graler, M.H., Granatiero, V., Grasso, D., Gray, J.P., Green, D.R., Greenhough, A., Gregory, S.L., Griffin, E.F., Grinstaff, M.W., Gros, F., Grose, C., Gross, A.S., Gruber, F., Grumati, P., Grune, T., Gu, X., Guan, J.L., Guardia, C.M., Guda, K., Guerra, F., Guerri, C., Guha, P., Guillen, C., Gujar, S., Gukovskaya, A., Gukovsky, I., Gunst, J., Gunther, A., Guntur, A.R., Guo, C., Guo, C., Guo, H., Guo, L.W., Guo, M., Gupta, P., Gupta, S.K., Gupta, S., Gupta, V.B., Gupta, V., Gustafsson, A.B., Gutterman, D.D., H, B.R., Haapasalo, A., Haber, J.E., Hac, A., Hadano, S., Hafren, A.J., Haidar, M., Hall, B.S., Hallden, G., Hamacher-Brady, A., Hamann, A., Hamasaki, M., Han, W., Hansen, M., Hanson, P.I., Hao, Z., Harada, M., Harhaji-Trajkovic, L., Hariharan, N., Haroon, N., Harris, J., Hasegawa, T., Hasima Nagoor, N., Haspel, J.A., Haucke, V., Hawkins, W.D., Hay, B.A., Haynes, C.M., Hayrabyan, S.B., Hays, T.S., He, C., He, Q., He, R.R., He, Y.W., He, Y.Y., Heikal, Y., Heberle, A.M., Hejtmancik, J.F., Helgason, G.V., Henkel, V., Herb, M., Hergovich, A., Herman-Antosiewicz, A., Hernandez, A., Hernandez, C., Hernandez-Diaz, S., Hernandez-Gea, V., Herpin, A., Herreros, J., Hervas, J.H., Hesselton, D., Hetz, C., Heussler, V.T., Higuchi, Y., Hilfiker, S., Hill, J.A., Hlavacek, W.S., Ho, E.A., Ho, I.H.T., Ho, P.W., Ho, S.L., Ho, W.Y., Hobbs, G.A., Hochstrasser, M., Hoet, P.H.M., Hofius, D., Hofman, P., Hohn, A., Holmberg, C.I., Hombrebueno, J.R., Yi-Ren Hong, C.H., Hooper, L.V., Hoppe, T., Horos, R., Hoshida, Y., Hsin, I.L., Hsu, H.Y., Hu, B., Hu, D., Hu, L.F., Hu, M.C., Hu, R., Hu, W., Hu, Y.C., Hu, Z.W., Hua, F., Hua, J., Hua, Y., Huan, C., Huang, C., Huang, C., Huang, C., Huang, H., Huang, K., Huang, M.L.H., Huang, R., Huang, S., Huang, T., Huang, X., Huang, Y.J., Huber, T.B., Hubert, V., Hubner, C.A., Hughes, S.M., Hughes, W.E., Humbert, M., Hummer, G., Hurley, J.H., Hussain, S., Hussain, S., Hussey, P.J., Hutabarat, M., Hwang, H.Y., Hwang, S., Ieni, A., Ikeda, F., Imagawa, Y., Imai, Y., Imbriano, C., Imoto, M., Inman, D.M., Inoki, K., Iovanna, J., Iozzo, R.V., Ippolito, G., Irazoqui, J.E., Iribarren,

P., Ishaq, M., Ishikawa, M., Ishimwe, N., Isidoro, C., Ismail, N., Issazadeh-Navikas, S., Itakura, E., Ito, D., Ivankovic, D., Ivanova, S., Iyer, A.K.V., Izquierdo, J.M., Izumi, M., Jaattela, M., Jabir, M.S., Jackson, W.T., Jacobo-Herrera, N., Jacomin, A.C., Jacquin, E., Jadiya, P., Jaeschke, H., Jagannath, C., Jakobi, A.J., Jakobsson, J., Janji, B., Jansen-Durr, P., Jansson, P.J., Jantsch, J., Januszewski, S., Jassey, A., Jean, S., Jeltsch-David, H., Jendelova, P., Jenny, A., Jensen, T.E., Jessen, N., Jewell, J.L., Ji, J., Jia, L., Jia, R., Jiang, L., Jiang, Q., Jiang, R., Jiang, T., Jiang, X., Jiang, Y., Jimenez-Sanchez, M., Jin, E.J., Jin, F., Jin, H., Jin, L., Jin, L., Jin, M., Jin, S., Jo, E.K., Joffre, C., Johansen, T., Johnson, G.V.W., Johnston, S.A., Jokitalo, E., Jolly, M.K., Joosten, L.A.B., Jordan, J., Joseph, B., Ju, D., Ju, J.S., Ju, J., Juarez, E., Judith, D., Juhasz, G., Jun, Y., Jung, C.H., Jung, S.C., Jung, Y.K., Jungbluth, H., Jungverdorben, J., Just, S., Kaarniranta, K., Kaasik, A., Kabuta, T., Kaganovich, D., Kahana, A., Kain, R., Kajimura, S., Kalamvoki, M., Kalia, M., Kalinowski, D.S., Kaludercic, N., Kalvari, I., Kaminska, J., Kaminsky, V.O., Kanamori, H., Kanasaki, K., Kang, C., Kang, R., Kang, S.S., Kaniyappan, S., Kanki, T., Kanneganti, T.D., Kanthasamy, A.G., Kanthasamy, A., Kantorow, M., Kapuy, O., Karamouzis, M.V., Karim, M.R., Karmakar, P., Katare, R.G., Kato, M., Kaufmann, S.H.E., Kauppinen, A., Kaushal, G.P., Kaushik, S., Kawasaki, K., Kazan, K., Ke, P.Y., Keating, D.J., Keber, U., Kehrl, J.H., Keller, K.E., Keller, C.W., Kemper, J.K., Kenific, C.M., Kepp, O., Kermorgant, S., Kern, A., Ketteler, R., Keulers, T.G., Khalfin, B., Khalil, H., Khambu, B., Khan, S.Y., Khandelwal, V.K.M., Khandia, R., Kho, W., Khobreakar, N.V., Khuansuwan, S., Khundadze, M., Killackey, S.A., Kim, D., Kim, D.R., Kim, D.H., Kim, D.E., Kim, E.Y., Kim, E.K., Kim, H.R., Kim, H.S., Hyung-Ryong, K., Kim, J.H., Kim, J.K., Kim, J.H., Kim, J., Kim, J.H., Kim, K.I., Kim, P.K., Kim, S.J., Kimball, S.R., Kimchi, A., Kimmelman, A.C., Kimura, T., King, M.A., Kinghorn, K.J., Kinsey, C.G., Kirkin, V., Kirshenbaum, L.A., Kiselev, S.L., Kishi, S., Kitamoto, K., Kitaoka, Y., Kitazato, K., Kitsis, R.N., Kittler, J.T., Kjaerulff, O., Klein, P.S., Klopstock, T., Klucken, J., Knaevelsrud, H., Knorr, R.L., Ko, B.C.B., Ko, F., Ko, J.L., Kobayashi, H., Kobayashi, S., Koch, I., Koch, J.C., Koenig, U., Kogel, D., Koh, Y.H., Koike, M., Kohlwein, S.D., Kocaturk, N.M., Komatsu, M., Konig, J., Kono, T., Kopp, B.T., Korcsmaros, T., Korkmaz, G., Korolchuk, V.I., Korsnes, M.S., Koskela, A., Kota, J., Kotake, Y., Kotler, M.L., Kou, Y., Koukourakis, M.I., Koustas, E., Kovacs, A.L., Kovacs, T., Koya, D., Kozako, T., Kraft, C., Krainc, D., Kramer, H., Krasnodembskaya, A.D., Kretz-Remy, C., Kroemer, G., Ktistakis, N.T., Kuchitsu, K., Kuenen, S., Kuerschner, L., Kukar, T., Kumar, A., Kumar, A., Kumar, D., Kumar, D., Kumar, S., Kume, S., Kumsta, C., Kundu, C.N., Kundu, M., Kunnumakkara, A.B., Kurgan, L., Kutateladze, T.G., Kutlu, O., Kwak, S., Kwon, H.J., Kwon, T.K., Kwon, Y.T., Kyrmizi, I., La Spada, A., Labonte, P., Ladoire, S., Laface, I., Lafont, F., Lagace, D.C., Lahiri, V., Lai, Z., Laird, A.S., Lakkaraju, A., Lamark, T., Lan, S.H., Landajuela, A., Lane, D.J.R., Lane, J.D., Lang, C.H., Lange, C., Langel, U., Langer, R., Lapaquette, P., Laporte, J., LaRusso, N.F., Lastres-Becker, I., Lau, W.C.Y., Laurie, G.W., Lavandero, S., Law, B.Y.K., Law, H.K., Layfield, R., Le, W., Le Stunff, H., Leary, A.Y., Lebrun, J.J., Leck, L.Y.W., Leduc-Gaudet, J.P., Lee, C., Lee, C.P., Lee, D.H., Lee, E.B., Lee, E.F., Lee, G.M., Lee, H.J., Lee, H.K., Lee, J.M., Lee, J.S., Lee, J.A., Lee, J.Y., Lee, J.H., Lee, M., Lee, M.G., Lee, M.J., Lee, M.S., Lee, S.Y., Lee, S.J., Lee, S.Y., Lee, S.B., Lee, W.H., Lee, Y.R., Lee, Y.H., Lee, Y., Lefebvre, C., Legouis, R., Lei, Y.L., Lei, Y., Leikin, S., Leitinger, G., Lemus, L., Leng, S., Lenoir, O., Lenz, G., Lenz, H.J., Lenzi, P., Leon, Y., Leopoldino, A.M., Leszczczyk, C., Leskela, S., Letellier, E., Leung, C.T., Leung, P.S., Leventhal, J.S., Levine, B., Lewis, P.A., Ley, K., Li, B., Li, D.Q., Li, J., Li, J., Li, J., Li, K., Li, L., Li, M., Li, M., Li, M., Li, M., Li, M., Li, P.L., Li, M.Q., Li, Q., Li, S., Li, T., Li, W., Li, W., Li, X., Li, Y.P., Li, Y., Li, Z., Li, Z., Li, Z., Lian, J., Liang, C., Liang, Q., Liang, W., Liang, Y., Liang, Y., Liao, G., Liao, L., Liao, M., Liao, Y.F., Librizzi, M., Lie, P.P.Y., Lilly, M.A., Lim, H.J., Lima, T.R.R., Limana, F., Lin, C., Lin, C.W., Lin, D.S., Lin, F.C., Lin, J.D., Lin, K.M., Lin, K.H., Lin, L.T., Lin, P.H., Lin, Q., Lin, S., Lin, S.J., Lin, W., Lin, X., Lin, Y.X., Lin, Y.S., Linden, R., Lindner, P., Ling, S.C., Lingor, P., Linnemann, A.K., Liou, Y.C., Lipinski, M.M., Lipovsek, S., Lira, V.A., Lisiak, N., Liton, P.B., Liu, C., Liu, C.H., Liu, C.F., Liu, C.H., Liu, F., Liu, H., Liu, H.S., Liu, H.F., Liu, H., Liu, J., Liu, J., Liu, J., Liu, L., Liu, L., Liu, M., Liu, Q., Liu, W., Liu, W., Liu, X.H., Liu, X., Liu, X., Liu, X., Liu, X., Liu, Y., Liu, Y., Liu, Y., Liu, Y., Liu, Y., Livingston, J.A., Lizard, G., Lizcano, J.M., Ljubojevic-Holzer, S., ME, L.L., Llobet-Navas, D., Llorente, A., Lo, C.H., Lobato-Marquez, D., Long, Q., Long, Y.C., Loos, B., Loos, J.A., Lopez, M.G., Lopez-Domenech, G., Lopez-Guerrero, J.A., Lopez-Jimenez, A.T., Lopez-Perez, O., Lopez-Valero, I., Lorenowicz, M.J., Lorente, M., Lorincz, P., Lossi, L., Lotersztajn, S., Lovat, P.E., Lovell, J.F., Lovy, A., Low, P., Lu, G., Lu, H., Lu, J.H., Lu, J.J., Lu, M., Lu, S., Luciani, A., Lucocq, J.M., Ludovico, P., Luftig, M.A., Luhr, M., Luis-Ravelo, D., Lum, J.J., Luna-Dulcey, L., Lund, A.H., Lund, V.K., Lunemann, J.D., Luningschror, P., Luo, H., Luo, R., Luo, S., Luo, Z., Luparello, C., Luscher, B., Luu, L., Lyakhovich, A., Lyamzaev, K.G., Lystad, A.H., Lytvynchuk, L., Ma, A.C., Ma, C., Ma, M., Ma, N.F., Ma, Q.H., Ma, X., Ma, Y., Ma, Z., MacDougald, O.A., Macian, F., MacIntosh, G.C., MacKeigan, J.P., Macleod, K.F., Maday, S., Madeo, F., Madesh, M., Madl, T., Madrigal-Matute, J., Maeda, A., Maejima, Y., Magarinos, M., Mahavadi, P., Maiani, E., Maiese, K., Maiti, P., Maiuri, M.C., Majello, B., Major, M.B., Makareeva, E., Malik, F., Mallilankaraman, K., Malorni, W., Maloyan, A., Mammadova, N., Man, G.C.W., Manai, F., Mancias, J.D., Mandelkow, E.M., Mandell, M.A., Manfredi, A.A., Manjili, M.H., Manjithaya, R., Manque, P., Manshian, B.B., Manzano, R., Manzoni, C., Mao, K., Marchese, C., Marchetti, S., Marconi, A.M., Marcucci, F., Mardente, S., Mareninova, O.A., Margeta, M., Mari, M., Marinelli, S., Marinelli, O., Marino, G., Mariotto, S., Marshall, R.S., Marten, M.R., Martens, S., Martin, A.P.J., Martin, K.R., Martin, S., Martin, S., Martin-Segura, A., Martin-Acebes, M.A., Martin-Burriel, I., Martin-Rincon, M., Martin-Sanz, P., Martina, J.A., Martinet, W., Martinez, A., Martinez, A., Martinez, J., Martinez Velazquez, M., Martinez-Lopez, N., Martinez-Vicente, M., Martins, D.O., Martins, J.O., Martins, W.K., Martins-Marques, T., Marzetti, E., Masaldan, S., Masclaux-Daubresse, C., Mashek, D.G., Massa, V., Massieu, L., Masson, G.R., Masuelli, L., Masyuk, A.I., Masyuk, T.V., Matarrese, P., Matheu, A., Matoba, S., Matsuzaki, S., Mattar, P., Matte, A., Mattoscio, D., Mauriz, J.L., Mauthe, M.,

Mauvezin, C., Maverakis, E., Maycotte, P., Mayer, J., Mazzoccoli, G., Mazzoni, C., Mazzulli, J.R., McCarty, N., McDonald, C., McGill, M.R., McKenna, S.L., McLaughlin, B., McLoughlin, F., McNiven, M.A., McWilliams, T.G., Mechta-Grigoriou, F., Medeiros, T.C., Medina, D.L., Megeney, L.A., Megyeri, K., Mehrpour, M., Mehta, J.L., Meijer, A.J., Meijer, A.H., Mejlvang, J., Melendez, A., Melk, A., Memisoglu, G., Mendes, A.F., Meng, D., Meng, F., Meng, T., Menna-Barreto, R., Menon, M.B., Mercer, C., Mercier, A.E., Mergny, J.L., Merighi, A., Merkle, S.D., Merla, G., Meske, V., Mestre, A.C., Metur, S.P., Meyer, C., Meyer, H., Mi, W., Miallet-Perez, J., Miao, J., Micala, L., Miki, Y., Milan, E., Milczarek, M., Miller, D.L., Miller, S.I., Miller, S., Millward, S.W., Milosevic, I., Minina, E.A., Mirzaei, H., Mirzaei, H.R., Mirzaei, M., Mishra, A., Mishra, N., Mishra, P.K., Misirkic Marjanovic, M., Misasi, R., Misra, A., Misso, G., Mitchell, C., Mitou, G., Miura, T., Miyamoto, S., Miyazaki, M., Miyazaki, M., Miyazaki, T., Miyazawa, K., Mizushima, N., Mogensen, T.H., Mograbi, B., Mohammadinejad, R., Mohamud, Y., Mohanty, A., Mohapatra, S., Mohlmann, T., Mohammed, A., Moles, A., Moley, K.H., Molinari, M., Mollace, V., Moller, A.B., Mollereau, B., Mollinedo, F., Montagna, C., Monteiro, M.J., Montella, A., Montes, L.R., Montico, B., Mony, V.K., Monzio Compagnoni, G., Moore, M.N., Moosavi, M.A., Mora, A.L., Mora, M., Morales-Alamo, D., Moratalla, R., Moreira, P.I., Morelli, E., Moreno, S., Moreno-Blas, D., Moresi, V., Morga, B., Morgan, A.H., Morin, F., Morishita, H., Moritz, O.L., Moriyama, M., Moriyasu, Y., Morleo, M., Morselli, E., Moruno-Manchon, J.F., Moscat, J., Mostowy, S., Motori, E., Moura, A.F., Moustaid-Moussa, N., Mrakovcic, M., Mucino-Hernandez, G., Mukherjee, A., Mukhopadhyay, S., Mulcahy Levy, J.M., Mulero, V., Muller, S., Munch, C., Munjal, A., Munoz-Canoves, P., Munoz-Galdeano, T., Munz, C., Murakawa, T., Muratori, C., Murphy, B.M., Murphy, J.P., Murthy, A., Myohanen, T.T., Mysorekar, I.U., Mytych, J., Nabavi, S.M., Nabissi, M., Nagy, P., Nah, J., Nahimana, A., Nakagawa, I., Nakamura, K., Nakatogawa, H., Nandi, S.S., Nanjundan, M., Nanni, M., Napolitano, G., Nardacci, R., Narita, M., Nassif, M., Nathan, I., Natsumeda, M., Naude, R.J., Naumann, C., Naveiras, O., Navid, F., Nawrocki, S.T., Nazarko, T.Y., Nazio, F., Negoita, F., Neill, T., Neisch, A.L., Neri, L.M., Netea, M.G., Neubert, P., Neufeld, T.P., Neumann, D., Neutzner, A., Newton, P.T., Ney, P.A., Nezis, I.P., Ng, C.C.W., Ng, T.B., Nguyen, H.T.T., Nguyen, L.T., Ni, H.M., Ni Cheallaigh, C., Ni, Z., Nicolao, M.C., Nicoli, F., Nieto-Diaz, M., Nilsson, P., Ning, S., Niranjana, R., Nishimune, H., Niso-Santano, M., Nixon, R.A., Nobili, A., Nobrega, C., Noda, T., Nogueira-Recalde, U., Nolan, T.M., Nombela, I., Novak, I., Novoa, B., Nozawa, T., Nukina, N., Nussbaum-Krammer, C., Nylandsted, J., O'Donovan, T.R., O'Leary, S.M., O'Rourke, E.J., O'Sullivan, M.P., O'Sullivan, T.E., Oddo, S., Oehme, I., Ogawa, M., Ogier-Denis, E., Ogmundsdottir, M.H., Ogretmen, B., Oh, G.T., Oh, S.H., Oh, Y.J., Ohama, T., Ohashi, Y., Ohmuraya, M., Oikonomou, V., Ojha, R., Okamoto, K., Okazawa, H., Oku, M., Oliven, S., Oliveira, J.M.A., Ollmann, M., Olzmann, J.A., Omari, S., Omary, M.B., Onal, G., Ondrej, M., Ong, S.B., Ong, S.G., Onnis, A., Orellana, J.A., Orellana-Munoz, S., Ortega-Villaizan, M.D.M., Ortiz-Gonzalez, X.R., Ortona, E., Osiewacz, H.D., Osman, A.K., Osta, R., Otegui, M.S., Otsu, K., Ott, C., Ottobriani, L., Ou, J.J., Outeiro, T.F., Oynebraten, I., Ozturk, M., Pages, G., Pahari, S., Pajares, M., Pajvani, U.B., Pal, R., Paladino, S., Pallet, N., Palmieri, M., Palmisano, G., Palumbo, C., Pampaloni, F., Pan, L., Pan, Q., Pan, W., Pan, X., Panasyuk, G., Pandey, R., Pandey, U.B., Pandya, V., Paneni, F., Pang, S.Y., Panzarini, E., Papademetrio, D.L., Papaleo, E., Papinski, D., Papp, D., Park, E.C., Park, H.T., Park, J.M., Park, J.I., Park, J.T., Park, J., Park, S.C., Park, S.Y., Parola, A.H., Parys, J.B., Pasquier, A., Pasquier, B., Passos, J.F., Pastore, N., Patel, H.H., Patschan, D., Patingre, S., Pedraza-Alva, G., Pedraza-Chaverri, J., Pedrozo, Z., Pei, G., Pei, J., Peled-Zehavi, H., Pellegrini, J.M., Pelletier, J., Penalva, M.A., Peng, D., Peng, Y., Penna, F., Pennuto, M., Pentimalli, F., Pereira, C.M., Pereira, G.J.S., Pereira, L.C., Pereira de Almeida, L., Perera, N.D., Perez-Lara, A., Perez-Oliva, A.B., Perez-Perez, M.E., Periyasamy, P., Perl, A., Perrotta, C., Perrotta, I., Pestell, R.G., Petersen, M., Petrache, I., Petrovski, G., Pffirmann, T., Pfister, A.S., Philips, J.A., Pi, H., Picca, A., Pickrell, A.M., Picot, S., Pierantoni, G.M., Pierdominici, M., Pierre, P., Pierrefite-Carle, V., Pierzynowska, K., Pietrocola, F., Pietruczuk, M., Pignata, C., Pimentel-Muinos, F.X., Pinar, M., Pinheiro, R.O., Pinkas-Kramarski, R., Pinton, P., Piracs, K., Piya, S., Pizzo, P., Plantinga, T.S., Platta, H.W., Plaza-Zabala, A., Plomann, M., Plotnikov, E.Y., Plun-Favreau, H., Pluta, R., Pocock, R., Poggeler, S., Pohl, C., Poirot, M., Poletti, A., Ponpuak, M., Popelka, H., Popova, B., Porta, H., Porte Alcon, S., Portilla-Fernandez, E., Post, M., Potts, M.B., Poulton, J., Powers, T., Prahlad, V., Prajsnar, T.K., Pratico, D., Prencipe, R., Priault, M., Proikas-Cezanne, T., Promponas, V.J., Proud, C.G., Puertollano, R., Puglielli, L., Pulinilkunnil, T., Puri, D., Puri, R., Puyal, J., Qi, X., Qi, Y., Qian, W., Qiang, L., Qiu, Y., Quadrilatero, J., Quarleri, J., Raben, N., Rabinowich, H., Ragona, D., Ragusa, M.J., Rahimi, N., Rahmati, M., Raia, V., Raimundo, N., Rajasekaran, N.S., Ramachandra Rao, S., Rami, A., Ramirez-Pardo, I., Ramsden, D.B., Randow, F., Rangarajan, P.N., Ranieri, D., Rao, H., Rao, L., Rao, R., Rathore, S., Ratnayaka, J.A., Ratovitski, E.A., Ravanan, P., Ravegnini, G., Ray, S.K., Razani, B., Rebecca, V., Reggiori, F., Regnier-Vigouroux, A., Reichert, A.S., Reigada, D., Reiling, J.H., Rein, T., Reipert, S., Rekha, R.S., Ren, H., Ren, J., Ren, W., Renault, T., Renga, G., Reue, K., Rewitz, K., Ribeiro de Andrade Ramos, B., Riazuddin, S.A., Ribeiro-Rodrigues, T.M., Ricci, J.E., Ricci, R., Riccio, V., Richardson, D.R., Rikihisa, Y., Risbud, M.V., Risueno, R.M., Ritis, K., Rizza, S., Rizzuto, R., Roberts, H.C., Roberts, L.D., Robinson, K.J., Roccheri, M.C., Rocchi, S., Rodney, G.G., Rodrigues, T., Rodrigues Silva, V.R., Rodriguez, A., Rodriguez-Barrueco, R., Rodriguez-Henche, N., Rodriguez-Rocha, H., Roelofs, J., Rogers, R.S., Rogov, V.V., Rojo, A.I., Rolka, K., Romanello, V., Romani, L., Romano, A., Romano, P.S., Romeo-Guitart, D., Romero, L.C., Romero, M., Roney, J.C., Rongo, C., Roperto, S., Rosenfeldt, M.T., Rosenstiel, P., Rosenwald, A.G., Roth, K.A., Roth, L., Roth, S., Rouschop, K.M.A., Roussel, B.D., Roux, S., Rovere-Querini, P., Roy, A., Rozieres, A., Ruano, D., Rubinsztein, D.C., Rubtsova, M.P., Ruckdeschel, K., Ruckenstuhl, C., Rudolf, E., Rudolf, R., Ruggieri, A., Ruparelia, A.A., Rusmini, P., Russell, R.R., Russo, G.L., Russo, M., Russo, R., Ryabaya, O.O., Ryan, K.M., Ryu, K.Y., Sabater-Arcis, M., Sachdev, U., Sacher, M., Sachse, C., Sadhu, A., Sadoshima, J., Safren, N., Saftig, P., Sagona, A.P., Sahay, G., Sahebkar, A., Sahin, M., Sahin, O.,

Sahni, S., Saito, N., Saito, S., Saito, T., Sakai, R., Sakai, Y., Sakamaki, J.I., Saksela, K., Salazar, G., Salazar-Degracia, A., Salekdeh, G.H., Saluja, A.K., Sampaio-Marques, B., Sanchez, M.C., Sanchez-Alcazar, J.A., Sanchez-Vera, V., Sancho-Shimizu, V., Sanderson, J.T., Sandri, M., Santaguida, S., Santambrogio, L., Santana, M.M., Santoni, G., Sanz, A., Sanz, P., Saran, S., Sardiello, M., Sargeant, T.J., Sarin, A., Sarkar, C., Sarkar, S., Sarrias, M.R., Sarkar, S., Sarmah, D.T., Sarparanta, J., Sathyanarayan, A., Sathyanarayanan, R., Scaglione, K.M., Scatozza, F., Schaefer, L., Schafer, Z.T., Schaible, U.E., Schapira, A.H.V., Scharl, M., Schatzl, H.M., Schein, C.H., Scheper, W., Scheuring, D., Schiaffino, M.V., Schiappacassi, M., Schindl, R., Schlattner, U., Schmidt, O., Schmitt, R., Schmidt, S.D., Schmitz, I., Schmukler, E., Schneider, A., Schneider, B.E., Schober, R., Schoijet, A.C., Schott, M.B., Schramm, M., Schroder, B., Schuh, K., Schuller, C., Schulze, R.J., Schurmanns, L., Schwamborn, J.C., Schwarten, M., Scialo, F., Sciarretta, S., Scott, M.J., Scotto, K.W., Scovassi, A.I., Scrima, A., Scrivo, A., Sebastian, D., Sebti, S., Sedej, S., Segatori, L., Segev, N., Seglen, P.O., Seiliez, I., Seki, E., Selleck, S.B., Sellke, F.W., Selsby, J.T., Sendtner, M., Senturk, S., Seranova, E., Sergi, C., Serra-Moreno, R., Sesaki, H., Settembre, C., Setty, S.R.G., Sgarbi, G., Sha, O., Shacka, J.J., Shah, J.A., Shang, D., Shao, C., Shao, F., Sharbati, S., Sharkey, L.M., Sharma, D., Sharma, G., Sharma, K., Sharma, P., Sharma, S., Shen, H.M., Shen, H., Shen, J., Shen, M., Shen, W., Shen, Z., Sheng, R., Sheng, Z., Sheng, Z.H., Shi, J., Shi, X., Shi, Y.H., Shiba-Fukushima, K., Shieh, J.J., Shimada, Y., Shimizu, S., Shimozaawa, M., Shintani, T., Shoemaker, C.J., Shojai, S., Shoji, I., Shrivage, B.V., Shridhar, V., Shu, C.W., Shu, H.B., Shui, K., Shukla, A.K., Shutt, T.E., Sica, V., Siddiqui, A., Sierra, A., Sierra-Torre, V., Signorelli, S., Sil, P., Silva, B.J.A., Silva, J.D., Silva-Pavez, E., Silvente-Poirot, S., Simmonds, R.E., Simon, A.K., Simon, H.U., Simons, M., Singh, A., Singh, L.P., Singh, R., Singh, S.V., Singh, S.K., Singh, S.B., Singh, S., Singh, S.P., Sinha, D., Sinha, R.A., Sinha, S., Sirko, A., Sirohi, K., Sivridis, E.L., Skendros, P., Skirycz, A., Slaninova, I., Smaili, S.S., Smertenko, A., Smith, M.D., Soenen, S.J., Sohn, E.J., Sok, S.P.M., Solaini, G., Soldati, T., Soleimanpour, S.A., Soler, R.M., Solovchenko, A., Somarelli, J.A., Sonawane, A., Song, F., Song, H.K., Song, J.X., Song, K., Song, Z., Soria, L.R., Sorice, M., Soukas, A.A., Soukup, S.F., Sousa, D., Sousa, N., Spagnuolo, P.A., Spector, S.A., Srinivas Bharath, M.M., St Clair, D., Stagni, V., Staiano, L., Stalneck, C.A., Stankov, M.V., Stathopoulos, P.B., Stefan, K., Stefan, S.M., Stefanis, L., Steffan, J.S., Steinkasserer, A., Stenmark, H., Sternecker, J., Stevens, C., Stoka, V., Storch, S., Stork, B., Strappazon, F., Strohecker, A.M., Stupack, D.G., Su, H., Su, L.Y., Su, L., Suarez-Fontes, A.M., Subauste, C.S., Subbian, S., Subirada, P.V., Sudhandiran, G., Sue, C.M., Sui, X., Summers, C., Sun, G., Sun, J., Sun, K., Sun, M.X., Sun, Q., Sun, Y., Sun, Z., Sunahara, K.K.S., Sundberg, E., Susztak, K., Sutovsky, P., Suzuki, H., Sweeney, G., Symons, J.D., Sze, S.C.W., Szewczyk, N.J., Tabecka-Lonczynska, A., Tabolacci, C., Tacke, F., Taegtmeier, H., Tafani, M., Tagaya, M., Tai, H., Tait, S.W.G., Takahashi, Y., Takats, S., Talwar, P., Tam, C., Tam, S.Y., Tampellini, D., Tamura, A., Tan, C.T., Tan, E.K., Tan, Y.Q., Tanaka, M., Tanaka, M., Tang, D., Tang, J., Tang, T.S., Tanida, I., Tao, Z., Taouis, M., Tatenhorst, L., Tavernarakis, N., Taylor, A., Taylor, G.A., Taylor, J.M., Tcheta, E., Tee, A.R., Tegeder, I., Teis, D., Teixeira, N., Teixeira-Clerc, F., Tekirdag, K.A., Tencomnao, T., Tenreiro, S., Tepikin, A.V., Testillano, P.S., Tettamanti, G., Tharaux, P.L., Thedieck, K., Thekkinghat, A.A., Thellung, S., Thinwa, J.W., Thirumalaikumar, V.P., Thomas, S.M., Thomes, P.G., Thorburn, A., Thukral, L., Thum, T., Thumm, M., Tian, L., Tichy, A., Till, A., Timmerman, V., Titorenko, V.I., Todi, S.V., Todorova, K., Toivonen, J.M., Tomaipitina, L., Tomar, D., Tomas-Zapico, C., Tomic, S., Tong, B.C., Tong, C., Tong, X., Tooze, S.A., Torgersen, M.L., Torii, S., Torres-Lopez, L., Torriglia, A., Towers, C.G., Towns, R., Toyokuni, S., Trajkovic, V., Tramontano, D., Tran, Q.G., Travassos, L.H., Trelford, C.B., Tremel, S., Trougakov, I.P., Tso, B.P., Tschan, M.P., Tse, H.F., Tse, T.F., Tsugawa, H., Tsvetkov, A.S., Tumbarello, D.A., Tumtas, Y., Tunon, M.J., Turcotte, S., Turk, B., Turk, V., Turner, B.J., Tuxworth, R.I., Tyler, J.K., Tyutereva, E.V., Uchiyama, Y., Ugun-Klusek, A., Uhlig, H.H., Ulemek-Kozioł, M., Ulasov, I.V., Umekawa, M., Ungermann, C., Unno, R., Urbe, S., Uribe-Carretero, E., Ustun, S., Uversky, V.N., Vaccari, T., Vaccaro, M.I., Vahsen, B.F., Vakifahmetoglu-Norberg, H., Valdor, R., Valente, M.J., Valko, A., Vallee, R.B., Valverde, A.M., Van den Berghe, G., van der Veen, S., Van Kaer, L., van Loosdregt, J., van Wijk, S.J.L., Vandenbergh, W., Vanhorebeek, I., Vannier-Santos, M.A., Vannini, N., Vanrell, M.C., Vantaggiato, C., Varano, G., Varela-Nieto, I., Varga, M., Vasconcelos, M.H., Vats, S., Vavvas, D.G., Vega-Naredo, I., Vega-Rubin-de-Celis, S., Velasco, G., Velazquez, A.P., Vellai, T., Vellenga, E., Velotti, F., Verdier, M., Verginis, P., Vergne, I., Verkade, P., Verma, M., Verstreken, P., Vervliet, T., Vervoorts, J., Vessoni, A.T., Victor, V.M., Vidal, M., Vidoni, C., Vieira, O.V., Vierstra, R.D., Viganò, S., Vihinen, H., Vijayan, V., Vila, M., Vilar, M., Villalba, J.M., Villalobo, A., Villarejo-Zori, B., Villarroya, F., Villarroya, J., Vincent, O., Vindis, C., Viret, C., Viscomi, M.T., Visnjic, D., Vitale, I., Vocado, D.J., Voitsekhojskaja, O.V., Volonte, C., Volta, M., Vomero, M., Von Haefen, C., Vooijs, M.A., Voos, W., Vucicevic, L., Wade-Martins, R., Waguri, S., Waite, K.A., Wakatsuki, S., Walker, D.W., Walker, M.J., Walker, S.A., Walter, J., Wandosell, F.G., Wang, B., Wang, C.Y., Wang, C., Wang, C., Wang, C., Wang, C.Y., Wang, D., Wang, F., Wang, F., Wang, F., Wang, G., Wang, H., Wang, H., Wang, H., Wang, H.G., Wang, J., Wang, J., Wang, J., Wang, J., Wang, K., Wang, L., Wang, L., Wang, M.H., Wang, M., Wang, N., Wang, P., Wang, P., Wang, P., Wang, P., Wang, Q.J., Wang, Q., Wang, Q.K., Wang, Q.A., Wang, W.T., Wang, W., Wang, X., Wang, X., Wang, Y., Wang, Y., Wang, Y., Wang, Y.Y., Wang, Y., Wang, Y., Wang, Y., Wang, Y., Wang, Z., Wang, Z., Wang, Z., Warnes, G., Warnsmann, V., Watada, H., Watanabe, E., Watchon, M., Wawrzynska, A., Weaver, T.E., Wegrzyn, G., Wehman, A.M., Wei, H., Wei, L., Wei, T., Wei, Y., Weiergraber, O.H., Wehl, C.C., Weindl, G., Weiskirchen, R., Wells, A., Wen, R.H., Wen, X., Werner, A., Weykopf, B., Wheatley, S.P., Whitton, J.L., Whitworth, A.J., Wiktorska, K., Wildenberg, M.E., Wileman, T., Wilkinson, S., Willbold, D., Williams, B., Williams, R.S.B., Williams, R.L., Williamson, P.R., Wilson, R.A., Winner, B., Winsor, N.J., Witkin, S.S., Wodrich, H., Woehlbier, U., Wollert, T., Wong, E., Wong, J.H., Wong, R.W., Wong, V.K.W., Wong, W.W., Wu, A.G., Wu, C., Wu, J., Wu, J., Wu, K.K., Wu, M., Wu, S.Y., Wu, S., Wu, S.Y., Wu, S., Wu, W.K.K., Wu, X.,

Wu, X., Wu, Y.W., Wu, Y., Xavier, R.J., Xia, H., Xia, L., Xia, Z., Xiang, G., Xiang, J., Xiang, M., Xiang, W., Xiao, B., Xiao, G., Xiao, H., Xiao, H.T., Xiao, J., Xiao, L., Xiao, S., Xiao, Y., Xie, B., Xie, C.M., Xie, M., Xie, Y., Xie, Z., Xie, Z., Xilouri, M., Xu, C., Xu, E., Xu, H., Xu, J., Xu, J., Xu, L., Xu, W.W., Xu, X., Xue, Y., Yakhine-Diop, S.M.S., Yamaguchi, M., Yamaguchi, O., Yamamoto, A., Yamashina, S., Yan, S., Yan, S.J., Yan, Z., Yanagi, Y., Yang, C., Yang, D.S., Yang, H., Yang, H.T., Yang, H., Yang, J.M., Yang, J., Yang, J., Yang, L., Yang, L., Yang, M., Yang, P.M., Yang, Q., Yang, S., Yang, S., Yang, S.F., Yang, W., Yang, W.Y., Yang, X., Yang, X., Yang, Y., Yang, Y., Yao, H., Yao, S., Yao, X., Yao, Y.G., Yao, Y.M., Yasui, T., Yazdankhah, M., Yen, P.M., Yi, C., Yin, X.M., Yin, Y., Yin, Z., Yin, Z., Ying, M., Ying, Z., Yip, C.K., Yiu, S.P.T., Yoo, Y.H., Yoshida, K., Yoshii, S.R., Yoshimori, T., Yousefi, B., Yu, B., Yu, H., Yu, J., Yu, J., Yu, L., Yu, M.L., Yu, S.W., Yu, V.C., Yu, W.H., Yu, Z., Yu, Z., Yuan, J., Yuan, L.Q., Yuan, S., Yuan, S.F., Yuan, Y., Yuan, Z., Yue, J., Yue, Z., Yun, J., Yung, R.L., Zacks, D.N., Zaffagnini, G., Zambelli, V.O., Zanella, I., Zang, Q.S., Zanivan, S., Zappavigna, S., Zaragoza, P., Zarbalis, K.S., Zarebkohan, A., Zarrouk, A., Zeitlin, S.O., Zeng, J., Zeng, J.D., Zerovnik, E., Zhan, L., Zhang, B., Zhang, D.D., Zhang, H., Zhang, H.L., Zhang, J., Zhang, J., Zhang, J.P., Zhang, K.Y.B., Zhang, L.W., Zhang, L., Zhang, L., Zhang, L., Zhang, L., Zhang, M., Zhang, P., Zhang, S., Zhang, W., Zhang, X., Zhang, X.W., Zhang, X., Zhang, X., Zhang, X., Zhang, X., Zhang, X.D., Zhang, Y., Zhang, Y., Zhang, Y., Zhang, Y.D., Zhang, Y., Zhang, Y.Y., Zhang, Y., Zhang, Z., Zhang, Z., Zhang, Z., Zhang, Z., Zhao, H., Zhao, L., Zhao, S., Zhao, T., Zhao, X.F., Zhao, Y., Zhao, Y., Zhao, Y., Zhao, Y., Zheng, G., Zheng, K., Zheng, L., Zheng, S., Zheng, X.L., Zheng, Y., Zheng, Z.G., Zhivotovsky, B., Zhong, Q., Zhou, A., Zhou, B., Zhou, C., Zhou, G., Zhou, H., Zhou, H., Zhou, H., Zhou, J., Zhou, J., Zhou, J., Zhou, J., Zhou, K., Zhou, R., Zhou, X.J., Zhou, Y., Zhou, Y., Zhou, Y., Zhou, Z.Y., Zhou, Z., Zhu, B., Zhu, C., Zhu, G.Q., Zhu, H., Zhu, H., Zhu, H., Zhu, W.G., Zhu, Y., Zhu, Y., Zhuang, H., Zhuang, X., Zientara-Rytter, K., Zimmermann, C.M., Ziviani, E., Zoladek, T., Zong, W.X., Zorov, D.B., Zorzano, A., Zou, W., Zou, Z., Zou, Z., Zuryn, S., Zwerschke, W., Brand-Saberi, B., Dong, X.C., Kenchappa, C.S., Li, Z., Lin, Y., Oshima, S., Rong, Y., Sluimer, J.C., Stallings, C.L., and Tong, C.K. (2021). Guidelines for the use and interpretation of assays for monitoring autophagy (4th edition)(1). *Autophagy* 17, 1-382.

Kluge, A.F., Lagu, B.R., Maiti, P., Jaleel, M., Webb, M., Malhotra, J., Mallat, A., Srinivas, P.A., and Thompson, J.E. (2018). Novel highly selective inhibitors of ubiquitin specific protease 30 (USP30) accelerate mitophagy. *Bioorganic & Medicinal Chemistry Letters* 28, 2655-2659.

Koch, A., Thiemann, M., Grabenbauer, M., Yoon, Y., McNiven, M.A., and Schrader, M. (2003). Dynamin-like protein 1 is involved in peroxisomal fission. *J Biol Chem* 278, 8597-8605.

Koch, A., Yoon, Y., Bonekamp, N.A., McNiven, M.A., and Schrader, M. (2005). A role for Fis1 in both mitochondrial and peroxisomal fission in mammalian cells. *Mol Biol Cell* 16, 5077-5086.

Kondapalli, C., Kazlauskaitė, A., Zhang, N., Woodroof, H.I., Campbell, D.G., Gourlay, R., Burchell, L., Walden, H., Macartney, T.J., Deak, M., Knebel, A., Alessi, D.R., and Muqit, M.M. (2012). PINK1 is activated by mitochondrial membrane potential depolarization and stimulates Parkin E3 ligase activity by phosphorylating Serine 65. *Open Biol* 2, 120080.

Konjar, Š., Sutton, V.R., Hoves, S., Repnik, U., Yagita, H., Reinheckel, T., Peters, C., Turk, V., Turk, B., Trapani, J.A., and Kopitar-Jerala, N. (2010). Human and mouse perforin are processed in part through cleavage by the lysosomal cysteine proteinase cathepsin L. *Immunology* 131, 257-267.

Korobova, F., Ramabhadran, V., and Higgs, H.N. (2013). An actin-dependent step in mitochondrial fission mediated by the ER-associated formin INF2. *Science* 339, 464-467.

Koshiba, T., Detmer, S.A., Kaiser, J.T., Chen, H., McCaffery, J.M., and Chan, D.C. (2004). Structural basis of mitochondrial tethering by mitofusin complexes. *Science* 305, 858-862.

Koyano, F., Okatsu, K., Kosako, H., Tamura, Y., Go, E., Kimura, M., Kimura, Y., Tsuchiya, H., Yoshihara, H., Hirokawa, T., Endo, T., Fon, E.A., Trempe, J.F., Saeki, Y., Tanaka, K., and Matsuda, N. (2014). Ubiquitin is phosphorylated by PINK1 to activate parkin. *Nature* 510, 162-166.

Krawczyk, P.A., Laub, M., and Kozik, P. (2020). To Kill But Not Be Killed: Controlling the Activity of Mammalian Pore-Forming Proteins. *Front Immunol* 11, 601405.

Kropp, E.S., and Wilson, J.E. (1970). Hexokinase binding sites on mitochondrial membranes. *Biochem Biophys Res Commun* 38, 74-79.

- Kruse, S.E., Watt, W.C., Marcinek, D.J., Kapur, R.P., Schenkman, K.A., and Palmiter, R.D. (2008). Mice with mitochondrial complex I deficiency develop a fatal encephalomyopathy. *Cell Metab* 7, 312-320.
- Kumar, A., Chamoto, K., Chowdhury, P.S., and Honjo, T. (2020). Tumors attenuating the mitochondrial activity in T cells escape from PD-1 blockade therapy. *Elife* 9.
- Kupfer, A., and Dennert, G. (1984). Reorientation of the microtubule-organizing center and the Golgi apparatus in cloned cytotoxic lymphocytes triggered by binding to lysable target cells. *Journal of immunology (Baltimore, Md : 1950)* 133, 2762-2766.
- Kurts, C., Heath, W.R., Kosaka, H., Miller, J.F., and Carbone, F.R. (1998). The peripheral deletion of autoreactive CD8+ T cells induced by cross-presentation of self-antigens involves signaling through CD95 (Fas, Apo-1). *J Exp Med* 188, 415-420.
- Lamb, J.R., Skidmore, B.J., Green, N., Chiller, J.M., and Feldmann, M. (1983). Induction of tolerance in influenza virus-immune T lymphocyte clones with synthetic peptides of influenza hemagglutinin. *J Exp Med* 157, 1434-1447.
- Lancki, D.W., Weiss, A., and Fitch, F.W. (1987). Requirements for triggering of lysis by cytolytic T lymphocyte clones. *J Immunol* 138, 3646-3653.
- Lardy, H.A., Johnson, D., and Mc, M.W. (1958). Antibiotics as tools for metabolic studies. I. A survey of toxic antibiotics in respiratory, phosphorylative and glycolytic systems. *Arch Biochem Biophys* 78, 587-597.
- Lasky, L.A., Singer, M.S., Yednock, T.A., Dowbenko, D., Fennie, C., Rodriguez, H., Nguyen, T., Stachel, S., and Rosen, S.D. (1989). Cloning of a lymphocyte homing receptor reveals a lectin domain. *Cell* 56, 1045-1055.
- Leach, D.R., Krummel, M.F., and Allison, J.P. (1996). Enhancement of antitumor immunity by CTLA-4 blockade. *Science* 271, 1734-1736.
- Lee, J.J., Sanchez-Martinez, A., Martinez Zarate, A., Beninca, C., Mayor, U., Clague, M.J., and Whitworth, A.J. (2018). Basal mitophagy is widespread in Drosophila but minimally affected by loss of Pink1 or parkin. *J Cell Biol* 217, 1613-1622.
- Leone, R.D., Zhao, L., Englert, J.M., Sun, I.M., Oh, M.H., Sun, I.H., Arwood, M.L., Bettencourt, I.A., Patel, C.H., Wen, J., Tam, A., Blosser, R.L., Prchalova, E., Alt, J., Rais, R., Slusher, B.S., and Powell, J.D. (2019). Glutamine blockade induces divergent metabolic programs to overcome tumor immune evasion. *Science* 366, 1013-1021.
- Levine, L.S., Hiam-Galvez, K.J., Marquez, D.M., Tenvooren, I., Madden, M.Z., Contreras, D.C., Dahunsi, D.O., Irish, J.M., Oluwole, O.O., Rathmell, J.C., and Spitzer, M.H. (2021). Single-cell analysis by mass cytometry reveals metabolic states of early-activated CD8(+) T cells during the primary immune response. *Immunity* 54, 829-844 e825.
- Li, P., Nijhawan, D., Budihardjo, I., Srinivasula, S.M., Ahmad, M., Alnemri, E.S., and Wang, X. (1997). Cytochrome c and dATP-dependent formation of Apaf-1/caspase-9 complex initiates an apoptotic protease cascade. *Cell* 91, 479-489.
- Liang, J.R., Martinez, A., Lane, J.D., Mayor, U., Clague, M.J., and Urbe, S. (2015). USP30 deubiquitylates mitochondrial Parkin substrates and restricts apoptotic cell death. *EMBO reports*.
- Lin, W., and Kang, U.J. (2008). Characterization of PINK1 processing, stability, and subcellular localization. *J Neurochem* 106, 464-474.
- Lindahl, P.E., and Oberg, K.E. (1961). The effect of rotenone on respiration and its point of attack. *Exp Cell Res* 23, 228-237.
- Linden, M., Gellerfors, P., and Nelson, B.D. (1982). Pore protein and the hexokinase-binding protein from the outer membrane of rat liver mitochondria are identical. *FEBS Lett* 141, 189-192.
- Lindstein, T., June, C.H., Ledbetter, J.A., Stella, G., and Thompson, C.B. (1989). Regulation of lymphokine messenger RNA stability by a surface-mediated T cell activation pathway. *Science* 244, 339-343.

- Liu, X., Kim, C.N., Yang, J., Jemmerson, R., and Wang, X. (1996). Induction of apoptotic program in cell-free extracts: requirement for dATP and cytochrome c. *Cell* 86, 147-157.
- Liu, X., Wang, Y., Lu, H., Li, J., Yan, X., Xiao, M., Hao, J., Alekseev, A., Khong, H., Chen, T., Huang, R., Wu, J., Zhao, Q., Wu, Q., Xu, S., Wang, X., Jin, W., Yu, S., Wei, L., Wang, A., Zhong, B., Ni, L., Nurieva, R., Ye, L., Tian, Q., Bian, X.W., and Dong, C. (2019). Genome-wide analysis identifies NR4A1 as a key mediator of T cell dysfunction. *Nature* 567, 525-529.
- Loh, P.G., Yang, H.S., Walsh, M.A., Wang, Q., Wang, X., Cheng, Z., Liu, D., and Song, H. (2009). Structural basis for translational inhibition by the tumour suppressor Pcd4. *EMBO J* 28, 274-285.
- Luckheeram, R.V., Zhou, R., Verma, A.D., and Xia, B. (2012). CD4(+)T cells: differentiation and functions. *Clin Dev Immunol* 2012, 925135.
- Lunt, S.Y., and Vander Heiden, M.G. (2011). Aerobic glycolysis: meeting the metabolic requirements of cell proliferation. *Annu Rev Cell Dev Biol* 27, 441-464.
- Luo, H., Krigman, J., Zhang, R., Yang, M., and Sun, N. (2021). Pharmacological Inhibition of USP30 activates Tissue-specific Mitophagy. *Acta Physiol (Oxf)*, e13666.
- Lyall, R.M., Dubois, J.H., and Crumpton, M.J. (1980). Ionomycin stimulates T-lymphocytes to grow. *Biochem Soc Trans* 8, 720-721.
- Lyubchenko, T.A., Wurth, G.A., and Zweifach, A. (2001). Role of calcium influx in cytotoxic T lymphocyte lytic granule exocytosis during target cell killing. *Immunity* 15, 847-859.
- Ma, C.Y., Marioni, J.C., Griffiths, G.M., and Richard, A.C. (2020). Stimulation strength controls the rate of initiation but not the molecular organisation of TCR-induced signalling. *Elife* 9.
- Ma, E.H., Verway, M.J., Johnson, R.M., Roy, D.G., Steadman, M., Hayes, S., Williams, K.S., Sheldon, R.D., Samborska, B., Kosinski, P.A., Kim, H., Griss, T., Faubert, B., Condotta, S.A., Krawczyk, C.M., DeBerardinis, R.J., Stewart, K.M., Richer, M.J., Chubukov, V., Roddy, T.P., and Jones, R.G. (2019). Metabolic Profiling Using Stable Isotope Tracing Reveals Distinct Patterns of Glucose Utilization by Physiologically Activated CD8+ T Cells. *Immunity* 51, 856-870.e855.
- Machesky, L.M., and Insall, R.H. (1998). Scar1 and the related Wiskott–Aldrich syndrome protein, WASP, regulate the actin cytoskeleton through the Arp2/3 complex. *Current Biology* 8, 1347-1356.
- Mackay, L.K., Rahimpour, A., Ma, J.Z., Collins, N., Stock, A.T., Hafon, M.L., Vega-Ramos, J., Lauzurica, P., Mueller, S.N., Stefanovic, T., Tschärke, D.C., Heath, W.R., Inouye, M., Carbone, F.R., and Gebhardt, T. (2013). The developmental pathway for CD103(+)CD8+ tissue-resident memory T cells of skin. *Nat Immunol* 14, 1294-1301.
- Madden, M.Z., and Rathmell, J.C. (2021). The Complex Integration of T-cell Metabolism and Immunotherapy. *Cancer Discov*.
- Marcassa, E., Kallinos, A., Jardine, J., Rusilowicz-Jones, E.V., Martinez, A., Kuehl, S., Islinger, M., Clague, M.J., and Urbé, S. (2018). Dual role of USP30 in controlling basal pexophagy and mitophagy. *EMBO Rep* 19.
- Marchingo, J.M., Sinclair, L.V., Howden, A.J., and Cantrell, D.A. (2020). Quantitative analysis of how Myc controls T cell proteomes and metabolic pathways during T cell activation. *Elife* 9.
- Mariani, S.M., Matiba, B., Armandola, E.A., and Krammer, P.H. (1997). Interleukin 1 beta-converting enzyme related proteases/caspases are involved in TRAIL-induced apoptosis of myeloma and leukemia cells. *J Cell Biol* 137, 221-229.
- Martin-Cofreces, N.B., Baixauli, F., and Sanchez-Madrid, F. (2014). Immune synapse: conductor of orchestrated organelle movement. *Trends Cell Biol* 24, 61-72.
- Martinez-Lorenzo, M.J., Alava, M.A., Gamen, S., Kim, K.J., Chuntharapai, A., Pineiro, A., Naval, J., and Anel, A. (1998). Involvement of APO2 ligand/TRAIL in activation-induced death of Jurkat and human peripheral blood T cells. *Eur J Immunol* 28, 2714-2725.

- Masson, D., Zamai, M., and Tschopp, J. (1986). Identification of granzyme A isolated from cytotoxic T-lymphocyte-granules as one of the proteases encoded by CTL-specific genes. *FEBS letters* 208, 84-88.
- Matsuda, N., Sato, S., Shiba, K., Okatsu, K., Saisho, K., Gautier, C.A., Sou, Y.S., Saiki, S., Kawajiri, S., Sato, F., Kimura, M., Komatsu, M., Hattori, N., and Tanaka, K. (2010). PINK1 stabilized by mitochondrial depolarization recruits Parkin to damaged mitochondria and activates latent Parkin for mitophagy. *J Cell Biol* 189, 211-221.
- Mazor, K.M., and Stipanuk, M.H. (2016). GCN2- and eIF2 $\alpha$ -phosphorylation-independent, but ATF4-dependent, induction of CARE-containing genes in methionine-deficient cells. *Amino Acids* 48, 2831-2842.
- McAdam, A.J., Schweitzer, A.N., and Sharpe, A.H. (1998). The role of B7 co-stimulation in activation and differentiation of CD4+ and CD8+ T cells. *Immunol Rev* 165, 231-247.
- McWilliams, T.G., Prescott, A.R., Montava-Garriga, L., Ball, G., Singh, F., Barini, E., Muqit, M.M.K., Brooks, S.P., and Ganley, I.G. (2018). Basal Mitophagy Occurs Independently of PINK1 in Mouse Tissues of High Metabolic Demand. *Cell Metab* 27, 439-449.e435.
- Mehta, M.M., Weinberg, S.E., and Chandel, N.S. (2017). Mitochondrial control of immunity: beyond ATP. *Nat Rev Immunol* 17, 608-620.
- Mehta, M.M., Weinberg, S.E., Steinert, E.M., Chhiba, K., Martinez, C.A., Gao, P., Perlman, H.R., Bryce, P., Hay, N., and Chandel, N.S. (2018). Hexokinase 2 is dispensable for T cell-dependent immunity. *Cancer Metab* 6, 10.
- Menasche, G., Pastural, E., Feldmann, J., Certain, S., Ersoy, F., Dupuis, S., Wulffraat, N., Bianchi, D., Fischer, A., Le Deist, F., and de Saint Basile, G. (2000). Mutations in RAB27A cause Griscelli syndrome associated with haemophagocytic syndrome. *Nat Genet* 25, 173-176.
- Menk, A.V., Scharping, N.E., Moreci, R.S., Zeng, X., Guy, C., Salvatore, S., Bae, H., Xie, J., Young, H.A., Wendell, S.G., and Delgoffe, G.M. (2018). Early TCR Signaling Induces Rapid Aerobic Glycolysis Enabling Distinct Acute T Cell Effector Functions. *Cell Rep* 22, 1509-1521.
- Meuer, S.C., Hussey, R.E., Cantrell, D.A., Hodgdon, J.C., Schlossman, S.F., Smith, K.A., and Reinherz, E.L. (1984). Triggering of the T3-Ti antigen-receptor complex results in clonal T-cell proliferation through an interleukin 2-dependent autocrine pathway. *Proc Natl Acad Sci U S A* 81, 1509-1513.
- Mezzadra, R., Sun, C., Jae, L.T., Gomez-Eerland, R., de Vries, E., Wu, W., Logtenberg, M.E.W., Slagter, M., Rozeman, E.A., Hofland, I., Brooks, A., Horlings, H.M., Wessels, L.F.A., Blank, C.U., Xiao, Y., Heck, A.J.R., Borst, J., Brummelkamp, T.R., and Schumacher, T.N.M. (2017). Identification of CMTM6 and CMTM4 as PD-L1 protein regulators. *Nature* 549, 106-110.
- Miller, S., and Muqit, M.M.K. (2019). Therapeutic approaches to enhance PINK1/Parkin mediated mitophagy for the treatment of Parkinson's disease. *Neurosci Lett* 705, 7-13.
- Mitchell, P., and Moyle, J. (1965). Evidence discriminating between the chemical and the chemiosmotic mechanisms of electron transport phosphorylation. *Nature* 208, 1205-1206.
- Molenaars, M., Janssens, G.E., Williams, E.G., Jongejan, A., Lan, J., Rabot, S., Joly, F., Moerland, P.D., Schomakers, B.V., Lezzerini, M., Liu, Y.J., McCormick, M.A., Kennedy, B.K., van Weeghel, M., van Kampen, A.H.C., Aebersold, R., MacInnes, A.W., and Houtkooper, R.H. (2020). A Conserved Mito-Cytosolic Translational Balance Links Two Longevity Pathways. *Cell Metabolism* 31, 549-563.e547.
- Monks, C.R., Freiberg, B.A., Kupfer, H., Sciaky, N., and Kupfer, A. (1998). Three-dimensional segregation of supramolecular activation clusters in T cells. *Nature* 395, 82-86.
- Moore, A.S., Coscia, S.M., Simpson, C.L., Ortega, F.E., Wait, E.C., Heddleston, J.M., Nirschl, J.J., Obara, C.J., Guedes-Dias, P., Boecker, C.A., Chew, T.L., Theriot, J.A., Lippincott-Schwartz, J., and Holzbaur, E.L.F. (2021). Actin cables and comet tails organize mitochondrial networks in mitosis. *Nature* 591, 659-664.
- Moore, C.L. (1971). Specific inhibition of mitochondrial Ca<sup>++</sup> transport by ruthenium red. *Biochem Biophys Res Commun* 42, 298-305.

- Moss, M.L., Jin, S.L., Milla, M.E., Bickett, D.M., Burkhart, W., Carter, H.L., Chen, W.J., Clay, W.C., Didsbury, J.R., Hassler, D., Hoffman, C.R., Kost, T.A., Lambert, M.H., Leesnitzer, M.A., McCauley, P., McGeehan, G., Mitchell, J., Moyer, M., Pahel, G., Rocque, W., Overton, L.K., Schoenen, F., Seaton, T., Su, J.L., Becherer, J.D., and et al. (1997). Cloning of a disintegrin metalloproteinase that processes precursor tumour-necrosis factor- $\alpha$ . *Nature* *385*, 733-736.
- Moullan, N., Mouchiroud, L., Wang, X., Ryu, D., Williams, E.G., Mottis, A., Jovaisaite, V., Frochoux, M.V., Quiros, P.M., Deplancke, B., Houtkooper, R.H., and Auwerx, J. (2015). Tetracyclines Disturb Mitochondrial Function across Eukaryotic Models: A Call for Caution in Biomedical Research. *Cell Rep* *10*, 1681-1691.
- Munch, C., and Harper, J.W. (2016). Mitochondrial unfolded protein response controls matrix pre-RNA processing and translation. *Nature* *534*, 710-713.
- Muntel, J., Kirkpatrick, J., Bruderer, R., Huang, T., Vitek, O., Ori, A., and Reiter, L. (2019). Comparison of Protein Quantification in a Complex Background by DIA and TMT Workflows with Fixed Instrument Time. *J Proteome Res* *18*, 1340-1351.
- Murphy, K., and Weaver, C. (2017). *Janeway's Immunobiology*, 9th Edition. *Janeway's Immunobiology*, 9th Edition, 1-904.
- Murphy, M.P. (2009). How mitochondria produce reactive oxygen species. *Biochem J* *417*, 1-13.
- Murray, R.Z., Kay, J.G., Sangermani, D.G., and Stow, J.L. (2005). A role for the phagosome in cytokine secretion. *Science* *310*, 1492-1495.
- Nagashima, S., Tabara, L.C., Tilokani, L., Paupe, V., Anand, H., Pogson, J.H., Zunino, R., McBride, H.M., and Prudent, J. (2020). Golgi-derived PI(4)P-containing vesicles drive late steps of mitochondrial division. *Science* *367*, 1366-1371.
- Nagy, E., and Rigby, W.F. (1995). Glyceraldehyde-3-phosphate dehydrogenase selectively binds AU-rich RNA in the NAD(+)-binding region (Rossmann fold). *J Biol Chem* *270*, 2755-2763.
- Nakamura, N., and Hirose, S. (2008). Regulation of mitochondrial morphology by USP30, a deubiquitinating enzyme present in the mitochondrial outer membrane. *Mol Biol Cell* *19*, 1903-1911.
- Narendra, D., Tanaka, A., Suen, D.-F., and Youle, R.J. (2008). Parkin is recruited selectively to impaired mitochondria and promotes their autophagy. *The Journal of Cell Biology* *183*, 795-803.
- Narendra, D.P., Jin, S.M., Tanaka, A., Suen, D.F., Gautier, C.A., Shen, J., Cookson, M.R., and Youle, R.J. (2010). PINK1 is selectively stabilized on impaired mitochondria to activate Parkin. *PLoS Biol* *8*, e1000298.
- Nargund, A.M., Pellegrino, M.W., Fiorese, C.J., Baker, B.M., and Haynes, C.M. (2012). Mitochondrial import efficiency of ATFS-1 regulates mitochondrial UPR activation. *Science* *337*, 587-590.
- Nowicka, U., Chroscicki, P., Stroobants, K., Sladowska, M., Turek, M., Uszczynska-Ratajczak, B., Kundra, R., Goral, T., Perni, M., Dobson, C.M., Vendruscolo, M., and Chacinska, A. (2021). Cytosolic aggregation of mitochondrial proteins disrupts cellular homeostasis by stimulating the aggregation of other proteins. *Elife* *10*.
- Nyati, K.K., Zaman, M.M., Sharma, P., and Kishimoto, T. (2020). Arid5a, an RNA-Binding Protein in Immune Regulation: RNA Stability, Inflammation, and Autoimmunity. *Trends Immunol* *41*, 255-268.
- O'Connell, P., Hyslop, S., Blake, M.K., Godbehere, S., Amalfitano, A., and Aldhamen, Y.A. (2021). SLAMF7 Signaling Reprograms T Cells toward Exhaustion in the Tumor Microenvironment. *J Immunol* *206*, 193-205.
- O'Neill, L.A., Kishton, R.J., and Rathmell, J. (2016). A guide to immunometabolism for immunologists. *Nat Rev Immunol* *16*, 553-565.
- O'Sullivan, D., Stanczak, M.A., Villa, M., Uhl, F.M., Corrado, M., Klein Geltink, R.I., Sanin, D.E., Apostolova, P., Rana, N., Edwards-Hicks, J., Grzes, K.M., Kabat, A.M., Kyle, R.L., Fabri, M., Curtis, J.D., Buck, M.D., Patterson, A.E., Regina, A., Field, C.S., Baixauli, F., Puleston, D.J., Pearce, E.J., Zeiser, R., and Pearce, E.L. (2021). Fever supports CD8(+) effector T cell responses by promoting mitochondrial translation. *Proc Natl Acad Sci U S A* *118*.

- O'Sullivan, T.E., Johnson, L.R., Kang, H.H., and Sun, J.C. (2015). BNIP3- and BNIP3L-Mediated Mitophagy Promotes the Generation of Natural Killer Cell Memory. *Immunity* *43*, 331-342.
- Obrig, T.G., Culp, W.J., McKeehan, W.L., and Hardesty, B. (1971). The mechanism by which cycloheximide and related glutarimide antibiotics inhibit peptide synthesis on reticulocyte ribosomes. *J Biol Chem* *246*, 174-181.
- Ordureau, A., Paulo, J.A., Zhang, J., An, H., Swatek, K.N., Cannon, J.R., Wan, Q., Komander, D., and Harper, J.W. (2020). Global Landscape and Dynamics of Parkin and USP30-Dependent Ubiquitylomes in iNeurons during Mitophagic Signaling. *Mol Cell* *77*, 1124-1142 e1110.
- Ostergaard, H.L., Kane, K.P., Mescher, M.F., and Clark, W.R. (1987). Cytotoxic T lymphocyte mediated lysis without release of serine esterase. *Nature* *330*, 71-72.
- Owen-Schaub, L.B., Yonehara, S., Crump, W.L., 3rd, and Grimm, E.A. (1992). DNA fragmentation and cell death is selectively triggered in activated human lymphocytes by Fas antigen engagement. *Cell Immunol* *140*, 197-205.
- Pakos-Zebrucka, K., Koryga, I., Mnich, K., Ljujic, M., Samali, A., and Gorman, A.M. (2016). The integrated stress response. *EMBO Rep* *17*, 1374-1395.
- Palade, G.E. (1952). The fine structure of mitochondria. *Anat Rec* *114*, 427-451.
- Palty, R., Silverman, W.F., Hershfinkel, M., Caporale, T., Sensi, S.L., Parnis, J., Nolte, C., Fishman, D., Shoshan-Barmatz, V., Herrmann, S., Khananshvili, D., and Sekler, I. (2010). NCLX is an essential component of mitochondrial Na<sup>+</sup>/Ca<sup>2+</sup> exchange. *Proc Natl Acad Sci U S A* *107*, 436-441.
- Park, H.G., Park, W.J., Kothapalli, K.S., and Brenna, J.T. (2015). The fatty acid desaturase 2 (FADS2) gene product catalyzes Delta4 desaturation to yield n-3 docosahexaenoic acid and n-6 docosapentaenoic acid in human cells. *FASEB J* *29*, 3911-3919.
- Park, Y., Reyna-Neyra, A., Philippe, L., and Thoreen, C.C. (2017). mTORC1 Balances Cellular Amino Acid Supply with Demand for Protein Synthesis through Post-transcriptional Control of ATF4. *Cell Reports* *19*, 1083-1090.
- Paul, W.E., and Seder, R.A. (1994). Lymphocyte responses and cytokines. *Cell* *76*, 241-251.
- Pause, A., Belsham, G.J., Gingras, A.C., Donze, O., Lin, T.A., Lawrence, J.C., Jr., and Sonenberg, N. (1994). Insulin-dependent stimulation of protein synthesis by phosphorylation of a regulator of 5'-cap function. *Nature* *371*, 762-767.
- Pearce, E.L. (2010). Metabolism in T cell activation and differentiation.
- Pearce, E.L., Mullen, A.C., Martins, G.A., Krawczyk, C.M., Hutchins, A.S., Zediak, V.P., Banica, M., DiCioccio, C.B., Gross, D.A., Mao, C.A., Shen, H., Cereb, N., Yang, S.Y., Lindsten, T., Rossant, J., Hunter, C.A., and Reiner, S.L. (2003). Control of effector CD8<sup>+</sup> T cell function by the transcription factor Eomesodermin. *Science* *302*, 1041-1043.
- Pearce, E.L., Poffenberger, M.C., Chang, C.H., and Jones, R.G. (2013). Fueling immunity: insights into metabolism and lymphocyte function. *Science* *342*, 1242-1245.
- Pendergrass, W., Wolf, N., and Poot, M. (2004). Efficacy of MitoTracker Green and CMXRosamine to measure changes in mitochondrial membrane potentials in living cells and tissues. *Cytometry A* *61*, 162-169.
- Perez-Riverol, Y., Csordas, A., Bai, J., Bernal-Llinares, M., Hewapathirana, S., Kundu, D.J., Inuganti, A., Griss, J., Mayer, G., Eisenacher, M., Perez, E., Uszkoreit, J., Pfeuffer, J., Sachsenberg, T., Yilmaz, S., Tiwary, S., Cox, J., Audain, E., Walzer, M., Jarnuczak, A.F., Ternent, T., Brazma, A., and Vizcaino, J.A. (2019). The PRIDE database and related tools and resources in 2019: improving support for quantification data. *Nucleic Acids Res* *47*, D442-D450.
- Pestka, S. (1969). Studies on the formation of transfer ribonucleic acid-ribosome complexes. X. Phenylalanyl-oligonucleotide binding to ribosomes and the mechanism of chloramphenicol action. *Biochem Biophys Res Commun* *36*, 589-595.

- Peters, P.J., Borst, J., Oorschot, V., Fukuda, M., Krahenbuhl, O., Tschopp, J., Slot, J.W., and Geuze, H.J. (1991). Cytotoxic T lymphocyte granules are secretory lysosomes, containing both perforin and granzymes. *J Exp Med* *173*, 1099-1109.
- Petruzzella, V., Vergari, R., Puzziferri, I., Boffoli, D., Lamantea, E., Zeviani, M., and Papa, S. (2001). A nonsense mutation in the NDUFS4 gene encoding the 18 kDa (AQDQ) subunit of complex I abolishes assembly and activity of the complex in a patient with Leigh-like syndrome. *Hum Mol Genet* *10*, 529-535.
- Pham, C.T., and Ley, T.J. (1999). Dipeptidyl peptidase I is required for the processing and activation of granzymes A and B in vivo. *Proc Natl Acad Sci U S A*.
- Philip, M., Fairchild, L., Sun, L., Horste, E.L., Camara, S., Shakiba, M., Scott, A.C., Viale, A., Lauer, P., Merghoub, T., Hellmann, M.D., Wolchok, J.D., Leslie, C.S., and Schietinger, A. (2017). Chromatin states define tumour-specific T cell dysfunction and reprogramming. *Nature* *545*, 452-456.
- Phu, L., Rose, C.M., Tea, J.S., Wall, C.E., Verschueren, E., Cheung, T.K., Kirkpatrick, D.S., and Bingol, B. (2020). Dynamic Regulation of Mitochondrial Import by the Ubiquitin System. *Mol Cell* *77*, 1107-1123 e1110.
- Pickrell, A.M., and Youle, R.J. (2015). The roles of PINK1, parkin, and mitochondrial fidelity in Parkinson's disease. *Neuron* *85*, 257-273.
- Pitti, R.M., Marsters, S.A., Ruppert, S., Donahue, C.J., Moore, A., and Ashkenazi, A. (1996). Induction of apoptosis by Apo-2 ligand, a new member of the tumor necrosis factor cytokine family. *J Biol Chem* *271*, 12687-12690.
- Podack, E.R., and Konigsberg, P.J. (1984). Cytolytic T cell granules. Isolation, structural, biochemical, and functional characterization. *The Journal of experimental medicine* *160*, 695-710.
- Poewe, W., Seppi, K., Tanner, C.M., Halliday, G.M., Brundin, P., Volkman, J., Schrag, A.E., and Lang, A.E. (2017). Parkinson disease. *Nat Rev Dis Primers* *3*, 17013.
- Ponta, H., Sherman, L., and Herrlich, P.A. (2003). CD44: from adhesion molecules to signalling regulators. *Nat Rev Mol Cell Biol* *4*, 33-45.
- Pores-Fernando, A.T., Bauer, R.A., Wurth, G.A., and Zweifach, A. (2005). Exocytic responses of single leukaemic human cytotoxic T lymphocytes stimulated by agents that bypass the T cell receptor. *J Physiol* *567*, 891-903.
- Potter, V.R., and Reif, A.E. (1952). Inhibition of an electron transport component by antimycin A. *J Biol Chem* *194*, 287-297.
- Prinz, W.A., Toulmay, A., and Balla, T. (2020). The functional universe of membrane contact sites. *Nat Rev Mol Cell Biol* *21*, 7-24.
- Puleston, D.J., Buck, M.D., Klein Geltink, R.I., Kyle, R.L., Caputa, G., O'Sullivan, D., Cameron, A.M., Castoldi, A., Musa, Y., Kabat, A.M., Zhang, Y., Flachsmann, L.J., Field, C.S., Patterson, A.E., Scherer, S., Alfei, F., Baixauli, F., Austin, S.K., Kelly, B., Matsushita, M., Curtis, J.D., Grzes, K.M., Villa, M., Corrado, M., Sanin, D.E., Qiu, J., Pällman, N., Paz, K., Maccari, M.E., Blazar, B.R., Mittler, G., Buescher, J.M., Zehn, D., Rospert, S., Pearce, E.J., Balabanov, S., and Pearce, E.L. (2019). Polyamines and eIF5A Hypusination Modulate Mitochondrial Respiration and Macrophage Activation. *Cell Metab* *30*, 352-363.e358.
- Qattan, A.T., Radulovic, M., Crawford, M., and Godovac-Zimmermann, J. (2012). Spatial distribution of cellular function: the partitioning of proteins between mitochondria and the nucleus in MCF7 breast cancer cells. *J Proteome Res* *11*, 6080-6101.
- Quan, L.T., Tewari, M., O'Rourke, K., Dixit, V., Snipas, S.J., Poirier, G.G., Ray, C., Pickup, D.J., and Salvesen, G.S. (1996). Proteolytic activation of the cell death protease Yama/CPP32 by granzyme B. *Proceedings of the National Academy of Sciences of the United States of America* *93*, 1972-1976.
- Quintana, A., Schwarz, E.C., Schwindling, C., Lipp, P., Kaestner, L., and Hoth, M. (2006). Sustained activity of calcium release-activated calcium channels requires translocation of mitochondria to the plasma membrane. *Journal of Biological Chemistry*.

- Quintana, A., Schwindling, C., Wenning, A.S., Becherer, U., Rettig, J., Schwarz, E.C., and Hoth, M. (2007). T cell activation requires mitochondrial translocation to the immunological synapse. *Proceedings of the National Academy of Sciences* *104*, 14418-14423.
- Quiros, P.M., Prado, M.A., Zamboni, N., D'Amico, D., Williams, R.W., Finley, D., Gygi, S.P., and Auwerx, J. (2017). Multi-omics analysis identifies ATF4 as a key regulator of the mitochondrial stress response in mammals. *J Cell Biol* *216*, 2027-2045.
- Ramstead, A.G., Wallace, J.A., Lee, S.-H., Bauer, K.M., Tang, W.W., Ekiz, H.A., Lane, T.E., Cluntun, A.A., Bettini, M.L., Round, J.L., Rutter, J., and O'Connell, R.M. (2020). Mitochondrial Pyruvate Carrier 1 Promotes Peripheral T Cell Homeostasis through Metabolic Regulation of Thymic Development. *Cell Reports* *30*, 2889-2899.e2886.
- Randzavola, L.O., Strege, K., Juzans, M., Asano, Y., Stinchcombe, J.C., Gawden-Bone, C.M., Seaman, M.N., Kuijpers, T.W., and Griffiths, G.M. (2019). Loss of ARPC1B impairs cytotoxic T lymphocyte maintenance and cytolytic activity. *J Clin Invest* *129*, 5600-5614.
- Rangaraju, V., Lauterbach, M., and Schuman, E.M. (2019). Spatially Stable Mitochondrial Compartments Fuel Local Translation during Plasticity. *Cell* *176*, 73-84 e15.
- Reinfeld, B.I., Madden, M.Z., Wolf, M.M., Chytil, A., Bader, J.E., Patterson, A.R., Sugiura, A., Cohen, A.S., Ali, A., Do, B.T., Muir, A., Lewis, C.A., Hongo, R.A., Young, K.L., Brown, R.E., Todd, V.M., Huffstater, T., Abraham, A., O'Neil, R.T., Wilson, M.H., Xin, F., Tantawy, M.N., Merryman, W.D., Johnson, R.W., Williams, C.S., Mason, E.F., Mason, F.M., Beckermann, K.E., Vander Heiden, M.G., Manning, H.C., Rathmell, J.C., and Rathmell, W.K. (2021). Cell-programmed nutrient partitioning in the tumour microenvironment. *Nature*.
- Reth, M. (1989). Antigen receptor tail clue. *Nature* *338*, 383-384.
- Riccio, V., Demers, N., Hua, R., Vissa, M., Cheng, D.T., Strilchuk, A.W., Wang, Y., McQuibban, G.A., and Kim, P.K. (2019). Deubiquitinating enzyme USP30 maintains basal peroxisome abundance by regulating pexophagy. *The Journal of cell biology* *218*, 798-807.
- Ritter, A.T., Angus, K.L., and Griffiths, G.M. (2013). The role of the cytoskeleton at the immunological synapse. *Immunological Reviews*.
- Ritter, A.T., Asano, Y., Stinchcombe, J.C., Dieckmann, N.M., Chen, B.C., Gawden-Bone, C., van Engelenburg, S., Legant, W., Gao, L., Davidson, M.W., Betzig, E., Lippincott-Schwartz, J., and Griffiths, G.M. (2015). Actin depletion initiates events leading to granule secretion at the immunological synapse. *Immunity* *42*, 864-876.
- Ritter, A.T., Kapnick, S.M., Murugesan, S., Schwartzberg, P.L., Griffiths, G.M., and Lippincott-Schwartz, J. (2017). Cortical actin recovery at the immunological synapse leads to termination of lytic granule secretion in cytotoxic T lymphocytes. *Proceedings of the National Academy of Sciences*.
- Rizzuto, R., Brini, M., Murgia, M., and Pozzan, T. (1993). Microdomains with high Ca<sup>2+</sup> close to IP<sub>3</sub>-sensitive channels that are sensed by neighboring mitochondria. *Science* *262*, 744-747.
- Rizzuto, R., De Stefani, D., Raffaello, A., and Mammucari, C. (2012). Mitochondria as sensors and regulators of calcium signalling. *Nat Rev Mol Cell Biol* *13*, 566-578.
- Rosendahl, M.S., Ko, S.C., Long, D.L., Brewer, M.T., Rosenzweig, B., Hedl, E., Anderson, L., Pyle, S.M., Moreland, J., Meyers, M.A., Kohno, T., Lyons, D., and Lichenstein, H.S. (1997). Identification and characterization of a pro-tumor necrosis factor- $\alpha$ -processing enzyme from the ADAM family of zinc metalloproteases. *J Biol Chem* *272*, 24588-24593.
- Rosignol, R., Faustin, B., Rocher, C., Malgat, M., Mazat, J.P., and Letellier, T. (2003). Mitochondrial threshold effects. *Biochem J* *370*, 751-762.
- Rott, R., Szargel, R., Haskin, J., Bandopadhyay, R., Lees, A.J., Shani, V., and Engelender, S. (2011).  $\alpha$ -Synuclein fate is determined by USP9X-regulated monoubiquitination. *Proc Natl Acad Sci U S A* *108*, 18666-18671.
- Rous, B.A., Reaves, B.J., Ihrke, G., Briggs, J.A., Gray, S.R., Stephens, D.J., Banting, G., and Luzio, J.P. (2002). Role of adaptor complex AP-3 in targeting wild-type and mutated CD63 to lysosomes. *Mol Biol Cell* *13*, 1071-1082.

- Rudd-Schmidt, J.A., Hodel, A.W., Noori, T., Lopez, J.A., Cho, H.J., Verschoor, S., Ciccone, A., Trapani, J.A., Hoogenboom, B.W., and Voskoboinik, I. (2019). Lipid order and charge protect killer T cells from accidental death. *Nat Commun* *10*, 5396.
- Rusilowicz-Jones, E.V., Jardine, J., Kallinos, A., Pinto-Fernandez, A., Guenther, F., Giurrandino, M., Barone, F.G., McCarron, K., Burke, C.J., Murad, A., Martinez, A., Marcassa, E., Gersch, M., Buckmelter, A.J., Kayser-Bricker, K.J., Lamoliatte, F., Gajbhiye, A., Davis, S., Scott, H.C., Murphy, E., England, K., Mortiboys, H., Komander, D., Trost, M., Kessler, B.M., Ioannidis, S., Ahlijanian, M.K., Urbe, S., and Clague, M.J. (2020). USP30 sets a trigger threshold for PINK1-PARKIN amplification of mitochondrial ubiquitylation. *Life Sci Alliance* *3*.
- Rusinol, A.E., Cui, Z., Chen, M.H., and Vance, J.E. (1994). A unique mitochondria-associated membrane fraction from rat liver has a high capacity for lipid synthesis and contains pre-Golgi secretory proteins including nascent lipoproteins. *J Biol Chem* *269*, 27494-27502.
- Russell, L., and Garrett-Sinha, L.A. (2010). Transcription factor Ets-1 in cytokine and chemokine gene regulation. *Cytokine* *51*, 217-226.
- Safer, B., Adams, S.L., Anderson, W.F., and Merrick, W.C. (1975). Binding of MET-TRNA<sup>f</sup> and GTP to homogeneous initiation factor MP. *J Biol Chem* *250*, 9076-9082.
- Salerno, F., Paolini, N.A., Stark, R., von Lindern, M., and Wolkers, M.C. (2017). Distinct PKC-mediated posttranscriptional events set cytokine production kinetics in CD8(+) T cells. *Proc Natl Acad Sci U S A* *114*, 9677-9682.
- Salerno, F., Turner, M., and Wolkers, M.C. (2020). Dynamic Post-Transcriptional Events Governing CD8+ T Cell Homeostasis and Effector Function (Elsevier Ltd), pp. 240-254.
- Sallusto, F., Geginat, J., and Lanzavecchia, A. (2004). Central memory and effector memory T cell subsets: function, generation, and maintenance. *Annu Rev Immunol* *22*, 745-763.
- Sallusto, F., Lenig, D., Forster, R., Lipp, M., and Lanzavecchia, A. (1999). Two subsets of memory T lymphocytes with distinct homing potentials and effector functions. *Nature* *401*, 708-712.
- Sanchez, J., Jackson, I., Flaherty, K.R., Muliaditan, T., and Schurich, A. (2020). Divergent Impact of Glucose Availability on Human Virus-Specific and Generically Activated CD8 T Cells. *Metabolites* *10*.
- Sanderson, C.J. (1976). The mechanism of T cell mediated cytotoxicity II. Morphological studies of cell death by time-lapse microcinematography, pp. 241-255.
- Santel, A., Frank, S., Gaume, B., Herrler, M., Youle, R.J., and Fuller, M.T. (2003). Mitofusin-1 protein is a generally expressed mediator of mitochondrial fusion in mammalian cells. *J Cell Sci* *116*, 2763-2774.
- Santel, A., and Fuller, M.T. (2001). Control of mitochondrial morphology by a human mitofusin. *Journal of cell science* *114*, 867-874.
- Sato, Y., Okatsu, K., Saeki, Y., Yamano, K., Matsuda, N., Kaiho, A., Yamagata, A., Goto-Ito, S., Ishikawa, M., Hashimoto, Y., Tanaka, K., and Fukui, S. (2017). Structural basis for specific cleavage of Lys6-linked polyubiquitin chains by USP30. *Nat Struct Mol Biol* *24*, 911-919.
- Saxton, R.A., and Sabatini, D.M. (2017). mTOR Signaling in Growth, Metabolism, and Disease. *Cell* *169*, 361-371.
- Scharping, N.E., Menk, A.V., Moreci, R.S., Whetstone, R.D., Dadey, R.E., Watkins, S.C., Ferris, R.L., and Delgoffe, G.M. (2016). The Tumor Microenvironment Represses T Cell Mitochondrial Biogenesis to Drive Intratumoral T Cell Metabolic Insufficiency and Dysfunction. *Immunity* *45*, 701-703.
- Scharping, N.E., Rivadeneira, D.B., Menk, A.V., Vignali, P.D.A., Ford, B.R., Rittenhouse, N.L., Peralta, R., Wang, Y., Wang, Y., DePeaux, K., Poholek, A.C., and Delgoffe, G.M. (2021). Mitochondrial stress induced by continuous stimulation under hypoxia rapidly drives T cell exhaustion. *Nat Immunol* *22*, 205-215.
- Schenkel, J.M., and Masopust, D. (2014). Tissue-resident memory T cells. *Immunity* *41*, 886-897.

- Scheu, S., Stetson, D.B., Reinhardt, R.L., Leber, J.H., Mohrs, M., and Locksley, R.M. (2006). Activation of the integrated stress response during T helper cell differentiation. *Nat Immunol* 7, 644-651.
- Schleyer, M., Schmidt, B., and Neupert, W. (1982). Requirement of a membrane potential for the posttranslational transfer of proteins into mitochondria. *Eur J Biochem* 125, 109-116.
- Schmidt, O., Pfanner, N., and Meisinger, C. (2010). Mitochondrial protein import: from proteomics to functional mechanisms. *Nat Rev Mol Cell Biol* 11, 655-667.
- Schneider-Poetsch, T., Ju, J., Eyler, D.E., Dang, Y., Bhat, S., Merrick, W.C., Green, R., Shen, B., and Liu, J.O. (2010). Inhibition of eukaryotic translation elongation by cycloheximide and lactimidomycin. *Nat Chem Biol* 6, 209-217.
- Schulz, O., Hammerschmidt, S.I., Moschovakis, G.L., and Forster, R. (2016). Chemokines and Chemokine Receptors in Lymphoid Tissue Dynamics. *Annu Rev Immunol* 34, 203-242.
- Schumann, K., Lin, S., Boyer, E., Simeonov, D.R., Subramaniam, M., Gate, R.E., Haliburton, G.E., Ye, C.J., Bluestone, J.A., Doudna, J.A., and Marson, A. (2015). Generation of knock-in primary human T cells using Cas9 ribonucleoproteins. *Proc Natl Acad Sci U S A* 112, 10437-10442.
- Schwarz, E.C., Qu, B., and Hoth, M. (2013). Calcium, cancer and killing: the role of calcium in killing cancer cells by cytotoxic T lymphocytes and natural killer cells. *Biochim Biophys Acta* 1833, 1603-1611.
- Schwindling, C., Quintana, A., Krause, E., and Hoth, M. (2010). Mitochondria positioning controls local calcium influx in T cells. *J Immunol* 184, 184-190.
- Scollay, R.G., Butcher, E.C., and Weissman, I.L. (1980). Thymus cell migration. Quantitative aspects of cellular traffic from the thymus to the periphery in mice. *Eur J Immunol* 10, 210-218.
- Scorrano, L., De Matteis, M.A., Emr, S., Giordano, F., Hajnoczky, G., Kornmann, B., Lackner, L.L., Levine, T.P., Pellegrini, L., Reinisch, K., Rizzuto, R., Simmen, T., Stenmark, H., Ungermann, C., and Schuldiner, M. (2019). Coming together to define membrane contact sites. *Nat Commun* 10, 1287.
- Sen, D.R., Kaminski, J., Barnitz, R.A., Kurachi, M., Gerdemann, U., Yates, K.B., Tsao, H.W., Godec, J., LaFleur, M.W., Brown, F.D., Tonnerre, P., Chung, R.T., Tully, D.C., Allen, T.M., Frahm, N., Lauer, G.M., Wherry, E.J., Yosef, N., and Haining, W.N. (2016). The epigenetic landscape of T cell exhaustion. *Science* 354, 1165-1169.
- Sena, L.A., Li, S., Jairaman, A., Prakriya, M., Ezponda, T., Hildeman, D.A., Wang, C.R., Schumacker, P.T., Licht, J.D., Perlman, H., Bryce, P.J., and Chandel, N.S. (2013). Mitochondria Are Required for Antigen-Specific T Cell Activation through Reactive Oxygen Species Signaling. *Immunity* 38, 225-236.
- Shaw, G., and Kamen, R. (1986). A conserved AU sequence from the 3' untranslated region of GM-CSF mRNA mediates selective mRNA degradation. *Cell* 46, 659-667.
- Shaw, J.P., Utz, P.J., Durand, D.B., Toole, J.J., Emmel, E.A., and Crabtree, G.R. (1988). Identification of a putative regulator of early T cell activation genes. *Science* 241, 202-205.
- Shiba-Fukushima, K., Imai, Y., Yoshida, S., Ishihama, Y., Kanao, T., Sato, S., and Hattori, N. (2012). PINK1-mediated phosphorylation of the Parkin ubiquitin-like domain primes mitochondrial translocation of Parkin and regulates mitophagy. *Scientific Reports*.
- Shiver, J.W., and Henkart, P.A. (1991). A noncytotoxic mast cell tumor line exhibits potent IgE-dependent cytotoxicity after transfection with the cytolysin/perforin gene. *Cell*.
- Sidrauski, C., Acosta-Alvear, D., Khoutorsky, A., Vedantham, P., Hearn, B.R., Li, H., Gamache, K., Gallagher, C.M., Ang, K.K., Wilson, C., Okreglak, V., Ashkenazi, A., Hann, B., Nader, K., Arkin, M.R., Renslo, A.R., Sonenberg, N., and Walter, P. (2013). Pharmacological brake-release of mRNA translation enhances cognitive memory. *Elife* 2, e00498.
- Siegelman, M.H., van de Rijn, M., and Weissman, I.L. (1989). Mouse lymph node homing receptor cDNA clone encodes a glycoprotein revealing tandem interaction domains. *Science* 243, 1165-1172.

- Siekierka, J., Mauser, L., and Ochoa, S. (1982). Mechanism of polypeptide chain initiation in eukaryotes and its control by phosphorylation of the alpha subunit of initiation factor 2. *Proc Natl Acad Sci U S A* *79*, 2537-2540.
- Silvestri, L., Caputo, V., Bellacchio, E., Atorino, L., Dallapiccola, B., Valente, E.M., and Casari, G. (2005). Mitochondrial import and enzymatic activity of PINK1 mutants associated to recessive parkinsonism. *Hum Mol Genet* *14*, 3477-3492.
- Sims, T.N., Soos, T.J., Xenias, H.S., Dubin-Thaler, B., Hofman, J.M., Waite, J.C., Cameron, T.O., Thomas, V.K., Varma, R., Wiggins, C.H., Sheetz, M.P., Littman, D.R., and Dustin, M.L. (2007). Opposing Effects of PKC $\theta$  and WASp on Symmetry Breaking and Relocation of the Immunological Synapse. *Cell* *129*, 773-785.
- Simula, L., Pacella, I., Colamatteo, A., Procaccini, C., Cancila, V., Bordi, M., Tregnago, C., Corrado, M., Pigazzi, M., Barnaba, V., Tripodo, C., Matarese, G., Piconese, S., and Campello, S. (2018). Drp1 Controls Effective T Cell Immune-Surveillance by Regulating T Cell Migration, Proliferation, and cMyc-Dependent Metabolic Reprogramming. *Cell Rep* *25*, 3059-3073 e3010.
- Singh, R., and Green, M.R. (1993). Sequence-specific binding of transfer RNA by glyceraldehyde-3-phosphate dehydrogenase. *Science* *259*, 365-368.
- Smirnova, E., Griparic, L., Shurland, D.L., and van der Bliek, A.M. (2001). Dynamin-related protein Drp1 is required for mitochondrial division in mammalian cells. *Mol Biol Cell* *12*, 2245-2256.
- Spillane, M., Ketschek, A., Merianda, T.T., Twiss, J.L., and Gallo, G. (2013). Mitochondria coordinate sites of axon branching through localized intra-axonal protein synthesis. *Cell Rep* *5*, 1564-1575.
- Spirin, A.S. (1969). The second Sir Hans Krebs Lecture. Informosomes. *Eur J Biochem* *10*, 20-35.
- Sprent, J. (1976). Fate of H2-activated T lymphocytes in syngeneic hosts. I. Fate in lymphoid tissues and intestines traced with 3H-thymidine, 125I-deoxyuridine and 51chromium. *Cell Immunol* *21*, 278-302.
- Stinchcombe, J.C., Barral, D.C., Mules, E.H., Booth, S., Hume, A.N., Machesky, L.M., Seabra, M.C., and Griffiths, G.M. (2001a). Rab27a is required for regulated secretion in cytotoxic T lymphocytes. *J Cell Biol* *152*, 825-834.
- Stinchcombe, J.C., Bossi, G., Booth, S., and Griffiths, G.M. (2001b). The immunological synapse of CTL contains a secretory domain and membrane bridges. *Immunity*.
- Stinchcombe, J.C., Majorovits, E., Bossi, G., Fuller, S., and Griffiths, G.M. (2006). Centrosome polarization delivers secretory granules to the immunological synapse. *Nature* *443*, 462-465.
- Stinchcombe, J.C., Page, L.J., and Griffiths, G.M. (2000). Secretory lysosome biogenesis in cytotoxic T lymphocytes from normal and Chediak Higashi syndrome patients. *Traffic* *1*, 435-444.
- Stinchcombe, J.C., Randzavola, L.O., Angus, K.L., Mantell, J.M., Verkade, P., and Griffiths, G.M. (2015). Mother Centriole Distal Appendages Mediate Centrosome Docking at the Immunological Synapse and Reveal Mechanistic Parallels with Ciliogenesis. *Curr Biol* *25*, 3239-3244.
- Stone, S.J., and Vance, J.E. (2000). Phosphatidylserine synthase-1 and -2 are localized to mitochondria-associated membranes. *J Biol Chem* *275*, 34534-34540.
- Suda, T., and Nagata, S. (1994). Purification and characterization of the Fas-ligand that induces apoptosis. *J Exp Med* *179*, 873-879.
- Sukumar, M., Liu, J., Ji, Y., Subramanian, M., Crompton, J.G., Yu, Z., Roychoudhuri, R., Palmer, D.C., Muranski, P., Karoly, E.D., Mohny, R.P., Klebanoff, C.A., Lal, A., Finkel, T., Restifo, N.P., and Gattinoni, L. (2013). Inhibiting glycolytic metabolism enhances CD8<sup>+</sup> T cell memory and antitumor function. *J Clin Invest* *123*, 4479-4488.
- Sun, N., Malide, D., Liu, J., Rovira, I.I., Combs, C.A., and Finkel, T. (2017a). A fluorescence-based imaging method to measure in vitro and in vivo mitophagy using mt-Keima. *Nature Protocols* *12*, 1576-1587.
- Sun, N., Malide, D., Liu, J., Rovira, I.I., Combs, C.A., and Finkel, T. (2017b). A fluorescence-based imaging method to measure in vitro and in vivo mitophagy using mt-Keima. *Nat Protoc* *12*, 1576-1587.

- Sun, N., Yun, J., Liu, J., Malide, D., Liu, C., Rovira, I.I., Holmström, K.M., Fergusson, M.M., Yoo, Y.H., Combs, C.A., and Finkel, T. (2015). Measuring In Vivo Mitophagy. *Molecular cell* *60*, 685-696.
- Szabadkai, G., Bianchi, K., Varnai, P., De Stefani, D., Wieckowski, M.R., Cavagna, D., Nagy, A.I., Balla, T., and Rizzuto, R. (2006). Chaperone-mediated coupling of endoplasmic reticulum and mitochondrial Ca<sup>2+</sup> channels. *J Cell Biol* *175*, 901-911.
- Szalai, G., Krishnamurthy, R., and Hajnoczky, G. (1999). Apoptosis driven by IP(3)-linked mitochondrial calcium signals. *EMBO J* *18*, 6349-6361.
- Takayama, H., and Sitkovsky, M.V. (1987). Antigen receptor-regulated exocytosis in cytotoxic T lymphocytes. *J Exp Med* *166*, 725-743.
- Tamzalit, F., Tran, D., Jin, W., Boyko, V., Bazzi, H., Kepecs, A., Kam, L.C., Anderson, K.V., and Huse, M. (2020). Centrioles control the capacity, but not the specificity, of cytotoxic T cell killing. *Proc Natl Acad Sci U S A* *117*, 4310-4319.
- Tan, H., Yang, K., Li, Y., Shaw, T.I., Wang, Y., Blanco, D.B., Wang, X., Cho, J.H., Wang, H., Rankin, S., Guy, C., Peng, J., and Chi, H. (2017a). Integrative Proteomics and Phosphoproteomics Profiling Reveals Dynamic Signaling Networks and Bioenergetics Pathways Underlying T Cell Activation. *Immunity* *46*, 488-503.
- Tan, T.C.J., Knight, J., Sbarato, T., Dudek, K., Willis, A.E., and Zamoyska, R. (2017b). Suboptimal T-cell receptor signaling compromises protein translation, ribosome biogenesis, and proliferation of mouse CD8 T cells.
- Thobois, S. (2015). USP30: a new promising target for Parkinson's disease? *Mov Disord* *30*, 340.
- Tinel, H., Cancela, J.M., Mogami, H., Gerasimenko, J.V., Gerasimenko, O.V., Tepikin, A.V., and Petersen, O.H. (1999). Active mitochondria surrounding the pancreatic acinar granule region prevent spreading of inositol trisphosphate-evoked local cytosolic Ca(2+) signals. *EMBO J* *18*, 4999-5008.
- Topf, U., Suppanz, I., Samluk, L., Wrobel, L., Böser, A., Sakowska, P., Knapp, B., Pietrzyk, M.K., Chacinska, A., and Warscheid, B. (2018). Quantitative proteomics identifies redox switches for global translation modulation by mitochondrially produced reactive oxygen species. *Nature Communications* *9*.
- Topf, U., Uszczyńska-Ratajczak, B., and Chacinska, A. (2019). Mitochondrial stress-dependent regulation of cellular protein synthesis.
- Topf, U., Wrobel, L., and Chacinska, A. (2016). Chatty Mitochondria: Keeping Balance in Cellular Protein Homeostasis. *Trends Cell Biol* *26*, 577-586.
- Townsend, A.R., Rothbard, J., Gotch, F.M., Bahadur, G., Wraith, D., and McMichael, A.J. (1986). The epitopes of influenza nucleoprotein recognized by cytotoxic T lymphocytes can be defined with short synthetic peptides. *Cell* *44*, 959-968.
- Trauth, B.C., Klas, C., Peters, A.M., Matzku, S., Moller, P., Falk, W., Debatin, K.M., and Krammer, P.H. (1989). Monoclonal antibody-mediated tumor regression by induction of apoptosis. *Science* *245*, 301-305.
- Trenn, G., Takayama, H., and Sitkovsky, M.V. (1987). Exocytosis of cytolytic granules may not be required for target cell lysis by cytotoxic T-lymphocytes. *Nature* *330*, 72-74.
- Treves, S., Di Virgilio, F., Cerundolo, V., Zanovello, P., Collavo, D., and Pozzan, T. (1987). Calcium and inositolphosphates in the activation of T cell-mediated cytotoxicity. *The Journal of experimental medicine* *166*, 33-42.
- Tristan, C., Shahani, N., Sedlak, T.W., and Sawa, A. (2011). The diverse functions of GAPDH: views from different subcellular compartments. *Cell Signal* *23*, 317-323.
- Tsun, A., Qureshi, I., Stinchcombe, J.C., Jenkins, M.R., De La Roche, M., Kleczkowska, J., Zamoyska, R., and Griffiths, G.M. (2011). Centrosome docking at the immunological synapse is controlled by Lck signaling. *Journal of Cell Biology*.

- Turner, M., and Diaz-Munoz, M.D. (2018). RNA-binding proteins control gene expression and cell fate in the immune system. *Nat Immunol* *19*, 120-129.
- Twig, G., Elorza, A., Molina, A.J., Mohamed, H., Wikstrom, J.D., Walzer, G., Stiles, L., Haigh, S.E., Katz, S., Las, G., Alroy, J., Wu, M., Py, B.F., Yuan, J., Deeney, J.T., Corkey, B.E., and Shirihai, O.S. (2008). Fission and selective fusion govern mitochondrial segregation and elimination by autophagy. *EMBO J* *27*, 433-446.
- Ueda, Y., Levine, B.L., Huang, M.L., Freeman, G.J., Nadler, L.M., June, C.H., and Ward, S.G. (1995). Both CD28 ligands CD80 (B7-1) and CD86 (B7-2) activate phosphatidylinositol 3-kinase, and wortmannin reveals heterogeneity in the regulation of T cell IL-2 secretion. *Int Immunol* *7*, 957-966.
- Uellner, R., Zvelebil, M.J., Hopkins, J., Jones, J., MacDougall, L.K., Morgan, B.P., Podack, E., Waterfield, M.D., and Griffiths, G.M. (1997). Perforin is activated by a proteolytic cleavage during biosynthesis which reveals a phospholipid-binding C2 domain. *The EMBO journal* *16*, 7287-7296.
- Unoki, M., and Nakamura, Y. (2001). Growth-suppressive effects of BPOZ and EGR2, two genes involved in the PTEN signaling pathway. *Oncogene* *20*, 4457-4465.
- Urbe, S., Liu, H., Hayes, S.D., Heride, C., Rigden, D.J., and Clague, M.J. (2012). Systematic survey of deubiquitinase localization identifies USP21 as a regulator of centrosome- and microtubule-associated functions. *Mol Biol Cell* *23*, 1095-1103.
- Vainio, T., Koskimies, O., Perlmann, P., Perlmann, H., and Klein, G. (1964). In Vitro Cytotoxic Effect of Lymphoid Cells from Mice Immunized with Allogeneic Tissue. *Nature* *204*, 453-455.
- Valente, E.M., Abou-Sleiman, P.M., Caputo, V., Muqit, M.M., Harvey, K., Gispert, S., Ali, Z., Del Turco, D., Bentivoglio, A.R., Healy, D.G., Albanese, A., Nussbaum, R., Gonzalez-Maldonado, R., Deller, T., Salvi, S., Cortelli, P., Gilks, W.P., Latchman, D.S., Harvey, R.J., Dallapiccola, B., Auburger, G., and Wood, N.W. (2004). Hereditary early-onset Parkinson's disease caused by mutations in PINK1. *Science* *304*, 1158-1160.
- Valm, A.M., Cohen, S., Legant, W.R., Melunis, J., Hershberg, U., Wait, E., Cohen, A.R., Davidson, M.W., Betzig, E., and Lippincott-Schwartz, J. (2017). Applying systems-level spectral imaging and analysis to reveal the organelle interactome. *Nature* *546*, 162-167.
- Van Acker, H.H., Ma, S., Scolaro, T., Kaeck, S.M., and Mazzone, M. (2021). How metabolism bridles cytotoxic CD8(+) T cells through epigenetic modifications. *Trends Immunol.*
- van der Windt, G.J., Everts, B., Chang, C.H., Curtis, J.D., Freitas, T.C., Amiel, E., Pearce, E.J., and Pearce, E.L. (2012). Mitochondrial respiratory capacity is a critical regulator of CD8+ T cell memory development. *Immunity* *36*, 68-78.
- van der Windt, G.J., O'Sullivan, D., Everts, B., Huang, S.C., Buck, M.D., Curtis, J.D., Chang, C.H., Smith, A.M., Ai, T., Faubert, B., Jones, R.G., Pearce, E.J., and Pearce, E.L. (2013). CD8 memory T cells have a bioenergetic advantage that underlies their rapid recall ability. *Proc Natl Acad Sci U S A* *110*, 14336-14341.
- Vance, J.E. (1990). Phospholipid synthesis in a membrane fraction associated with mitochondria. *J Biol Chem* *265*, 7248-7256.
- Vande Voorde, J., Ackermann, T., Pfetzer, N., Sumpton, D., Mackay, G., Kalna, G., Nixon, C., Blyth, K., Gottlieb, E., and Tardito, S. (2019). Improving the metabolic fidelity of cancer models with a physiological cell culture medium. *Sci Adv* *5*, eaau7314.
- Vandenabeele, P., Declercq, W., Vanhaesebroeck, B., Grooten, J., and Fiers, W. (1995). Both TNF receptors are required for TNF-mediated induction of apoptosis in PC60 cells. *J Immunol* *154*, 2904-2913.
- Vang, T., Torgersen, K.M., Sundvold, V., Saxena, M., Levy, F.O., Skalhegg, B.S., Hansson, V., Mustelin, T., and Tasken, K. (2001). Activation of the COOH-terminal Src kinase (Csk) by cAMP-dependent protein kinase inhibits signaling through the T cell receptor. *J Exp Med* *193*, 497-507.
- Villa, E., Marchetti, S., and Ricci, J.E. (2018). No Parkin Zone: Mitophagy without Parkin. *Trends Cell Biol* *28*, 882-895.

- Vives-Bauza, C., Zhou, C., Huang, Y., Cui, M., de Vries, R.L., Kim, J., May, J., Tocilescu, M.A., Liu, W., Ko, H.S., Magrane, J., Moore, D.J., Dawson, V.L., Grailhe, R., Dawson, T.M., Li, C., Tieu, K., and Przedborski, S. (2010). PINK1-dependent recruitment of Parkin to mitochondria in mitophagy. *Proc Natl Acad Sci U S A* *107*, 378-383.
- Wanders, R.J., Waterham, H.R., and Ferdinandusse, S. (2015). Metabolic Interplay between Peroxisomes and Other Subcellular Organelles Including Mitochondria and the Endoplasmic Reticulum. *Front Cell Dev Biol* *3*, 83.
- Wang, Y., Serricchio, M., Jauregui, M., Shanbhag, R., Stoltz, T., Di Paolo, C.T., Kim, P.K., and McQuibban, G.A. (2015). Deubiquitinating enzymes regulate PARK2-mediated mitophagy. *Autophagy* *11*, 595-606.
- Warburg, O. (1956). On the origin of cancer cells. *Science* *123*, 309-314.
- Wei, Y., Chiang, W.C., Sumpter, R., Jr., Mishra, P., and Levine, B. (2017). Prohibitin 2 Is an Inner Mitochondrial Membrane Mitophagy Receptor. *Cell* *168*, 224-238 e210.
- Wherry, E.J., and Kurachi, M. (2015). Molecular and cellular insights into T cell exhaustion. *Nat Rev Immunol* *15*, 486-499.
- Wick, A.N., Drury, D.R., Nakada, H.I., and Wolfe, J.B. (1957). Localization of the primary metabolic block produced by 2-deoxyglucose. *J Biol Chem* *224*, 963-969.
- Wiley, S.R., Schooley, K., Smolak, P.J., Din, W.S., Huang, C.P., Nicholl, J.K., Sutherland, G.R., Smith, T.D., Rauch, C., Smith, C.A., and et al. (1995). Identification and characterization of a new member of the TNF family that induces apoptosis. *Immunity* *3*, 673-682.
- Wilson, J.E. (2003). Isozymes of mammalian hexokinase: structure, subcellular localization and metabolic function. *J Exp Biol* *206*, 2049-2057.
- Wilson, S.M., Yip, R., Swing, D.A., O'Sullivan, T.N., Zhang, Y., Novak, E.K., Swank, R.T., Russell, L.B., Copeland, N.G., and Jenkins, N.A. (2000). A mutation in Rab27a causes the vesicle transport defects observed in ashen mice. *Proc Natl Acad Sci U S A* *97*, 7933-7938.
- Wisniewski, J.R., Hein, M.Y., Cox, J., and Mann, M. (2014). A "proteomic ruler" for protein copy number and concentration estimation without spike-in standards. *Mol Cell Proteomics* *13*, 3497-3506.
- Wolf, T., Jin, W., Zoppi, G., Vogel, I.A., Akhmedov, M., Bleck, C.K.E., Beltraminelli, T., Rieckmann, J.C., Ramirez, N.J., Benevento, M., Notarbartolo, S., Bumann, D., Meissner, F., Grimbacher, B., Mann, M., Lanzavecchia, A., Sallusto, F., Kwee, I., and Geiger, R. (2020). Dynamics in protein translation sustaining T cell preparedness. *Nat Immunol* *21*, 927-937.
- Wolter, K.G., Hsu, Y.T., Smith, C.L., Nechushtan, A., Xi, X.G., and Youle, R.J. (1997). Movement of Bax from the cytosol to mitochondria during apoptosis. *J Cell Biol* *139*, 1281-1292.
- Wong, Y.C., Ysselstein, D., and Krainc, D. (2018). Mitochondria-lysosome contacts regulate mitochondrial fission via RAB7 GTP hydrolysis. *Nature* *554*, 382-386.
- Wrobel, L., Topf, U., Bragoszewski, P., Wiese, S., Sztolszterer, M.E., Oeljeklaus, S., Varabyova, A., Lirski, M., Chroscicki, P., Mroczek, S., Januszewicz, E., Dziembowski, A., Koblowska, M., Warscheid, B., and Chacinska, A. (2015). Mistargeted mitochondrial proteins activate a proteostatic response in the cytosol. *Nature* *524*, 485-488.
- Wu, Z., Puigserver, P., Andersson, U., Zhang, C., Adelmant, G., Mootha, V., Troy, A., Cinti, S., Lowell, B., Scarpulla, R.C., and Spiegelman, B.M. (1999). Mechanisms controlling mitochondrial biogenesis and respiration through the thermogenic coactivator PGC-1. *Cell* *98*, 115-124.
- Yamada, T., Dawson, T.M., Yanagawa, T., Iijima, M., and Sesaki, H. (2019). SQSTM1/p62 promotes mitochondrial ubiquitination independently of PINK1 and PRKN/parkin in mitophagy. *Autophagy* *15*, 2012-2018.
- Yamada, T., Murata, D., Adachi, Y., Itoh, K., Kameoka, S., Igarashi, A., Kato, T., Araki, Y., Haganir, R.L., Dawson, T.M., Yanagawa, T., Okamoto, K., Iijima, M., and Sesaki, H. (2018). Mitochondrial Stasis Reveals p62-Mediated Ubiquitination in Parkin-Independent Mitophagy and Mitigates Nonalcoholic Fatty Liver Disease. *Cell Metab* *28*, 588-604 e585.

- Yamamoto, A., Tagawa, Y., Yoshimori, T., Moriyama, Y., Masaki, R., and Tashiro, Y. (1998). Bafilomycin A1 prevents maturation of autophagic vacuoles by inhibiting fusion between autophagosomes and lysosomes in rat hepatoma cell line, H-4-II-E cells. *Cell Struct Funct* *23*, 33-42.
- Yamano, K., and Youle, R.J. (2013). PINK1 is degraded through the N-end rule pathway. *Autophagy* *9*, 1758-1769.
- Ye, G.M., Chen, C., Huang, S., Han, D.D., Guo, J.H., Wan, B., and Yu, L. (2005). Cloning and characterization a novel human 1-acyl-sn-glycerol-3-phosphate acyltransferase gene AGPAT7. *DNA Seq* *16*, 386-390.
- Yi, J.S., Holbrook, B.C., Michalek, R.D., Laniewski, N.G., and Grayson, J.M. (2006). Electron transport complex I is required for CD8+ T cell function. *J Immunol* *177*, 852-862.
- Yonehara, S., Ishii, A., and Yonehara, M. (1989). A cell-killing monoclonal antibody (anti-Fas) to a cell surface antigen co-downregulated with the receptor of tumor necrosis factor. *J Exp Med* *169*, 1747-1756.
- Yoon, Y., Krueger, E.W., Oswald, B.J., and McNiven, M.A. (2003). The mitochondrial protein hFis1 regulates mitochondrial fission in mammalian cells through an interaction with the dynamin-like protein DLP1. *Mol Cell Biol* *23*, 5409-5420.
- Yu, Y.R., Imrichova, H., Wang, H., Chao, T., Xiao, Z., Gao, M., Rincon-Restrepo, M., Franco, F., Genolet, R., Cheng, W.C., Jandus, C., Coukos, G., Jiang, Y.F., Locasale, J.W., Zippelius, A., Liu, P.S., Tang, L., Bock, C., Vannini, N., and Ho, P.C. (2020). Disturbed mitochondrial dynamics in CD8(+) TILs reinforce T cell exhaustion. *Nat Immunol* *21*, 1540-1551.
- Yue, T., Zhan, X., Zhang, D., Jain, R., Wang, K.W., Choi, J.H., Misawa, T., Su, L., Quan, J., Hildebrand, S., Xu, D., Li, X., Turer, E., Sun, L., Moresco, E.M.Y., and Beutler, B. (2021). SLFN2 protection of tRNAs from stress-induced cleavage is essential for T cell-mediated immunity. *Science* *372*.
- Yue, W., Chen, Z., Liu, H., Yan, C., Chen, M., Feng, D., Yan, C., Wu, H., Du, L., Wang, Y., Liu, J., Huang, X., Xia, L., Liu, L., Wang, X., Jin, H., Wang, J., Song, Z., Hao, X., and Chen, Q. (2014). A small natural molecule promotes mitochondrial fusion through inhibition of the deubiquitinase USP30. *Cell Research* *24*, 482-496.
- Zeng, R., Cannon, J.L., Abraham, R.T., Way, M., Billadeau, D.D., Bubeck-Wardenberg, J., and Burkhardt, J.K. (2003). SLP-76 coordinates Nck-dependent Wiskott-Aldrich syndrome protein recruitment with Vav-1/Cdc42-dependent Wiskott-Aldrich syndrome protein activation at the T cell-APC contact site. *J Immunol* *171*, 1360-1368.
- Zhang, L., and Romero, P. (2018). Metabolic Control of CD8(+) T Cell Fate Decisions and Antitumor Immunity. *Trends Mol Med* *24*, 30-48.
- Zhang, N., and Bevan, M.J. (2011). CD8(+) T cells: foot soldiers of the immune system. *Immunity* *35*, 161-168.
- Zhang, W., Sloan-Lancaster, J., Kitchen, J., Tribble, R.P., and Samelson, L.E. (1998). LAT: the ZAP-70 tyrosine kinase substrate that links T cell receptor to cellular activation. *Cell* *92*, 83-92.
- Zhao, Q., Wang, J., Levichkin, I.V., Stasinopoulos, S., Ryan, M.T., and Hoogenraad, N.J. (2002). A mitochondrial specific stress response in mammalian cells. *EMBO J* *21*, 4411-4419.
- Zheng, L., Fisher, G., Miller, R.E., Peschon, J., Lynch, D.H., and Lenardo, M.J. (1995). Induction of apoptosis in mature T cells by tumour necrosis factor. *Nature* *377*, 348-351.
- Zorkau, M., Albus, C.A., Berlinguer-Palmini, R., Chrzanowska-Lightowlers, Z.M.A., and Lightowlers, R.N. (2021a). High-resolution imaging reveals compartmentalization of mitochondrial protein synthesis in cultured human cells. *Proc Natl Acad Sci U S A* *118*.
- Zorkau, M., Proctor-Kent, Y., Berlinguer-Palmini, R., Hamilton, A., Chrzanowska-Lightowlers, Z.M., and Lightowlers, R.N. (2021b). Visualizing Mitochondrial Ribosomal RNA and Mitochondrial Protein Synthesis in Human Cell Lines. *Methods Mol Biol* *2192*, 159-181.
- Zougman, A., Selby, P.J., and Banks, R.E. (2014). Suspension trapping (STrap) sample preparation method for bottom-up proteomics analysis. *Proteomics* *14*, 1006-1000.

zur Stadt, U., Rohr, J., Seifert, W., Koch, F., Grieve, S., Pagel, J., Strauss, J., Kasper, B., Nurnberg, G., Becker, C., Maul-Pavicic, A., Beutel, K., Janka, G., Griffiths, G., Ehl, S., and Hennies, H.C. (2009). Familial hemophagocytic lymphohistiocytosis type 5 (FHL-5) is caused by mutations in Munc18-2 and impaired binding to syntaxin 11. *Am J Hum Genet* *85*, 482-492.

zur Stadt, U., Schmidt, S., Kasper, B., Beutel, K., Diler, A.S., Henter, J.I., Kabisch, H., Schneppenheim, R., Nurnberg, P., Janka, G., and Hennies, H.C. (2005). Linkage of familial hemophagocytic lymphohistiocytosis (FHL) type-4 to chromosome 6q24 and identification of mutations in syntaxin 11. *Hum Mol Genet* *14*, 827-834.

Zweifach, A., and Lewis, R.S. (1993). Mitogen-regulated Ca<sup>2+</sup> current of T lymphocytes is activated by depletion of intracellular Ca<sup>2+</sup> stores. *Proceedings of the National Academy of Sciences of the United States of America* *90*, 6295-6299.

Zyryanova, A.F., Kashiwagi, K., Rato, C., Harding, H.P., Crespillo-Casado, A., Perera, L.A., Sakamoto, A., Nishimoto, M., Yonemochi, M., Shirouzu, M., Ito, T., and Ron, D. (2021). ISRIB Blunts the Integrated Stress Response by Allosterically Antagonising the Inhibitory Effect of Phosphorylated eIF2 on eIF2B. *Mol Cell* *81*, 88-103 e106.